Experimentally Simulating High Rate Deformation of Polymers & Composites

by

Michael James Kendall

Submitted to the Department of Engineering Science
in partial fulfillment of the requirements for the degree of

Doctor of Philosophy in Engineering Science
Mechanical Engineering, Applied Physics, & Solid Mechanics

at the

UNIVERSITY OF OXFORD
New College
Department of Engineering Science



Michaelmas 2013

Experimentally Simulating High Rate Deformation of Polymers & Composites

by

Michael James Kendall

in partial fulfillment of the
requirements for the degree of
DPhil in Engineering Science
Mechanical Engineering, Applied Physics, & Solid Mechanics
at the

UNIVERSITY OF OXFORD
Department of Engineering Science
New College
Supervised by Dr Clive R Siviour
Michaelmas 2013

Abstract

The research presented in this dissertation presents a methodology to experimentally predict and simulate the mechanical behavior of polymers under high strain rate deformation. Specifically, the interplay between the effects of temperature and strain rate on polymer behavior is examined and then used as a tool to help recreate the high rate mechanical response of several different polymers: ranging from rubbers to amorphous polymers to composites.

Multiple literature reviews are conducted and presented in this thesis, e.g. experimental mechanics test methods, high rate behavior, time-temperature equivalence, constitutive modeling, and temperature measurement methods.

In accordance with mechanical theory, an experimental and analytical protocol in rate- and temperature- dependence was applied to a range of PVC materials ranging in plasticizer contents. Further to this, these PVC materials were modeled with a rubbery model describing the network stress seen in polymer behavior, and an amorphous polymer model to describe PVC low to high rate responses to deformation. This modeling develops insights in the adiabatic nature of high rate response.

Time-temperature equivalence, and the temperature rise during adiabatic deformation, are studied and exploited in order to implement a proposed experimental method which simulates the high rate deformation of polymeric materials.

The development of an experimental methodology to simulate and predict high rate behavior is presented, applied, and expanded to a range of materials: amorphous polymers (e.g. PVC 20wt% plasticizer, PMMA, PC) and composites (e.g. polymer bonded explosive simulant). The work also presents and highlights the fact that micro to nano-scale imaging may be used in parallel with the simulation method in order to better understand high rate behavior.

Furthermore, in result of the studies conducted in this body of work, several novel techniques were developed, or improved upon, and applied to the current research (e.g. additions to time-temperature equivalence, temperature measurement methods at high, moderate, and low strain rates, and a method for measuring the high rate behavior of soft materials).

Acknowledgments

The research carried out in this thesis was sponsored by the Air Force Office of Scientific Research, Air Force Material Command, USAF. Dr Jennifer Jordan and Dr Jason Foley have helped me as sponsors, colleagues, and friends – I am so very grateful for their advice, help, collaboration, and stories during the past years.

Foremost, I must personally thank my supervisor Dr Clive Siviour of Pembroke College. It is his enthusiasm and passion for sincere science and mechanics which was the energy for my research. Originally, I contacted Dr Siviour from a faraway land in Los Angeles, California, with hopes to study under his esteemed guidance, and under the spires, prestige, and history of Oxford. Never did I imagine that he would grant me the opportunity after a 2 am video interview (10 am in England) with himself and Dr John Huber. My expectations have been far exceeded after being inducted into the 'Siviour Family,' and to be guided through my trials and tribulations in mechanics and a new country by Dr Siviour, I am truly grateful. Through my relations, I have been able to travel to and enjoy beautiful cities such as Freiberg, Germany, and Chicago, USA, and present my work to, and receive feedback from, several of the top scientists in the field. Furthermore, I have published parts of this work as a first author in several esteemed journals, and I am in the process of publishing more achievements from this thesis at the current moment. Most importantly, I conducted all of my research under the insightful guidance of the future leader of contemporary mechanics: Dr Clive Siviour.

During this project I have been blessed to have the support, thoughts, insights, and friendship of another mentor of mine in Oxford: Richard 'Dick' Froud. He has not only added large amounts of humor and enjoyment to each morning when stopping by his office or the ground-floor workshop, but he has also aided me with several discussions and ideas for a variety of advances within this research. Namely, the novel temperature measurement method, and the PZT gages for high rate behavior testing in soft (and difficult) materials, which would not have been at all possible without Dick. Dick, 'you're the man', as I would say back home. Richard Duffin, Neil, and all of the members of the workshop must also be thanked for their large amounts of help and patience with me and my constant need for new 'products', which always seemed to be asked for at the end of the day.

I have also been able to become a part of a larger network of scientists from being a part of the esteemed Solid Mechanics Group of the University of Oxford, home to the foundation of our research, Hooke's Law, and to so many other great minds with their own passions and interests in high rate mechanics, who have helped this research with insightful discussions and suggestions. Within this subset at the department, I cannot thank enough Dr Daniel Drodge, Dr Euan Wielewksi, and Dr Matthew Arthington, for their helpful discussions regarding my research. More specifically, Dr Daniel Drodge helped me design, and provided instrumental insight, in the novel SHPB soft material gages using PZT, while also providing several pieces of advice in writing my first journal papers, and lending me several helpful papers, and also inviting me to several relaxing and interesting coffee breaks in the afternoon. Not to mention several food, drink, and laughable memories in Germany and Illinois during the last two years. Dr Euan helped me thoroughly during my first visit, and has continued to remain close with me throughout my DPhil, constantly offering insightful advice and telling incredible stories, whether academic or beyond. My Oxford experience would not have been as rich without him.

In conducting quasi-static testing, I cannot thank Dr Igor Dyson enough for his friendly demeanor and sincerity in responses to my never-ending questions in physics or other interests. Further to this, his thorough help in learning to use equipment safely and

scientifically has led to great research and yours truly not injuring himself. In addition to this, I also must thank Kalin Dragnevski in his help with conducting ESEM experiments throughout my final year. For the majority of the DMTA testing presented in this research I must thank Nicholas Hawkins from the Zoology Department for helping me with DMTA equipment and testing of all materials presented in this thesis. Short notice never seemed to be a problem and I cannot thank Nick enough for that. In addition, Dr Heiko Schiffter and Thomas Healey at the Institute of Biomedical Engineering are thanked for their help in conducting additional DMTA testing in this thesis.

I am so thankful to have such great and hilarious friends in Oxford who have supported me and taught me so much during my time abroad here in England, encompassing such a wide variety of clubs and societies that I am so very blessed to be a part of: the New College Rugby Team (NCRFC); the Dinosaurs and la Duchesse; the New College Basketball Club, that is, the University Champions; the University of Oxford Basketball Club; all of my friends at New College in the MCR and other members – students, professors, and staff. I also must thank all of my friends back home in California, who now live all over the US and abroad – you guys always know how to make things fun, up, and interesting. All the Los Angeles team and all the boys in Malibu, the San Diego team, and Menudo – you guys are the best.

My mother, Susan, and my father, Prescott, were such a large source of encouragement and peace of mind during my PhD, or DPhil, that I cannot put into words how much I have to thank them. Their visits were some of my most memorable and best times in Oxford. I love you both so much. Mom, I would not have come here if it was not for your encouragement to attend Oxford, cancel all plans in New York, and venture outside of the US. My great aunt, Annamae or ‘Aunt Sis,’ has also been in my heart from the start to finish of this PhD, as well as my gorgeous grandmother, Mary Sue or ‘Grandma,’ miss you both so much. My older brothers who I look up to so much, Sean and Ryan, gave undying support, encouragement, hilarious jokes and stories, and insights through it all, and have been so incredibly important. So lucky to have you guys as brothers, I could not have done it without you both.

Contents

Abstract 3
Acknowledgments 5
Contents 7
1 Introduction 17
2 Review of Experimental Techniques at Different Strain Rates 23
2.1 Overview of testing techniques at different strain rates 23
2.2 Experimental Methodologies 27
2.2.1 Low Strain Rate: 10^{-3}➔10^{-1} s^{-1} 27
2.2.2 Medium rate testing 29
2.2.3 Hopkinson bar and high-rate behavior 30
2.2.4 Dynamic Mechanical & Thermal Analysis 39
2.2.5 Brazilian Testing 40
2.2.6 Environmental Scanning Electron Microscope 41
2.3 Polymers at High Rate 43
3 Rate Dependence of PVC & the Effects of Plasticizer 53
3.1 Introduction 53
3.2 Materials 55
3.3 Uniaxial Compression 56
3.3.1 Specimen Geometry 56
3.3.2 Experimental Method 58
3.3.3 Results and Analysis 59
3.4 Dynamic Mechanical and Thermal Analysis 74
3.4.1 Experimental Method 74
3.4.2 Results and Analysis 74
3.4.3 Discussion of DMTA and compressive results 79
3.5 Conclusions 87
4 Time-Temperature Equivalence 89
4.1 Early encounters 89
4.2 Discussion of the Application of Time-Temperature Superposition 96
4.3 Results and Discussion 98
4.3.1 WLF 103
4.3.2 Separation of α and β processes 104
4.3.3 Application and Discussion of Additional Materials 109
4.4 Conclusions 113

5 Simulation of High Rate Behavior....115
5.1 Introduction....115
5.2 Experimental method....121
5.2.1 Materials....121
5.2.2 Compression Testing....121
5.2.3 Simulating Adiabatic Conditions....123
5.3 Results and Discussion....126
5.4 Conclusions....132
6 Investigations and Applications in Amorphous Polymers PMMA & PC....133
6.1 Polymethyl methacrylate (PMMA)....136
6.1.1 Background....136
6.1.1 Materials....139
6.1.2 Results and Discussion....140
6.1.3 Experimental Simulation Model & Energies of Deformation....145
6.1.4 Conclusion....150
6.2 Polycarbonate....151
6.2.1 Background....151
6.2.2 Materials....153
6.2.3 Results and Discussion....153
6.2.3 Experimental Simulation Method....158
6.2.4 Conclusion....163
7 Simulating High Rate Composite Behavior in Tension & Compression:....165
Polymer Bonded Explosive Simulant....165
& Method for Soft Materials at High Rate....165
7.1 Background....167
7.2 Experiments....170
Compression Testing & Novel Piezoelectric SHPB Gage....171
Tension Testing via Brazilian Disc Tests....174
7.3 Results and Analysis....176
7.3.1 Dynamic Mechanical & Thermal Analysis....176
7.3.2 Compression Testing....179
7.3.4 Brazilian Testing on a Composite (PBS)....185
7.3.5 Predicting High Rate Composite Behavior in Tension....192
ESEM In-Situ Analysis....195
7.4 Conclusions....197
8 Constitutive Modeling....199
8.1 Introduction to Processes in Polymers....200

8.1.1 Structural makeup 200
8.1.2 Glass (α) and β transitions 201
8.1.3 Relation between microstructure and macroscopic response 203
8.2 Rubber Elastic Materials 204
8.2.1 Introduction to Modeling of Rubbery Polymers 204
8.2.2 Results and Analysis 209
8.3 Amorphous Polymers 217
8.3.1 Introduction to the Constitutive Modeling of Polymers 217
8.3.2 Model Application 229
Model vs. Experiment 237
Low, Medium, & High Strain Rates 237
Adiabatic Temperature Rise 241
8.4 Conclusions 243
9 Thermodynamic Investigations & 247
Novel Temperature Measurement Method 247
9.1 Background 248
9.2 Materials & Temperature Measurement Equipment 255
9.3 Experimental Setup 256
High Rate: PPVC-2 256
Moderate Rate: PMMA 257
9.4 Results and Discussion 258
High Rate 258
Moderate Rate 262
9.5 Conclusions 270
10 Concluding Remarks 271
Summary of Accomplishments 272
Rate & Temperature Dependence, & Time-Temperature Equivalence 272
Modeling & Temperature Measurement 272
Simulation & Prediction of High Rate Deformation 274
References 277

List of Figures

1-1 Stress wave propagation time-distance diagram 18
1-2 ESEM damage formation image 20
1-3 Summary of experimental simulation method 21

2-1 Division of strain rate regimes 24
2-2 Cam plastometer photograph 25
2-3 Compression and tension specimen examples 28
2-4 SHPB apparatus 31
2-5 SHPB strain gage signals 32
2-6 Force and velocity diagram for SHPB test 33
2-7 Force-time plot to confirm dynamic equilibrium 34
2-8 Brazilian test diagram 41
2-9 Bauwens-Crowet (1972) plot of yield stress against temperature 44
2-10 Bauwens-Crowet (1973) beta component of yield stress against temperature 44
2-11 Walley & Field (1994) PVC data 47
2-12 Cady et al. (2003) glass transition rate and temperature behavior 49
2-13 Siviour et al. (2005) peak stress with strain rate mapped onto temperature 51
2-14 Garg et al. (2008) experimentally measured temperature rises 52

3-1 Chemical structures PVC & DINP 54
3-2 Ringing observed in SHPB tests with 8 mm 57
3-3 Representative PVC rate dependent behavior 60
3-4 Representative PVC temperature behavior 61
3-5 Fractures and elastic recovery of PVC 63
3-6 High speed photographs of PVC 64
3-7 PPVC-2 rate dependent behavior 66
3-8 PPVC-2 temperature dependent behavior 67
3-9 PPVC-2 yield stress behavior with rate activated influences 68
3-10 PPVC-4 rate dependent behavior 69
3-11 PPVC-4 temperature dependent behavior 70
3-12 PPVC-6 rate dependent behavior 72
3-13 PPVC-6 temperature dependent behavior 73
3-14 PVC DMTA data 74
3-15 PPVC-2 DMTA data 75
3-16 PPVC-4 DMTA data 76
3-17 PPVC-6 DMTA data 77
3-18 PPVC-2 Low Temperature DMTA data 78
3-19 PPVC-4 Low Temperature DMTA data 78
3-20 PPVC-6 Low Temperature DMTA data 79
3-21 All PVC materials elastic modulus compared to yield stress 80
3-22 PVC Storage Modulus with material transitions 81
3-23 Yield stress log strain rate curve demonstrating material transitions 81
3-24 Beta transition temperature location with DMTA data 82
3-25 Theoretical Strain rate profiles 84
3-26 PPVC-2 strain rate profile comparison 85
3-27 PPVC-4 strain rate profile comparison 85

3-28 PPVC-6 strain rate profile comparison....86
3-29 Input bar and striker bar velocity profiles....87

4-1 Diagram for mapping parameter....90
4-2 PMMA yield as a function of temperature seen in Bauwens-Crowet et al., 1973....91
4-3 PC, PMMA, and PAI yield stress functions of temperature and strain rate....92
4-4 Williamson et al. (2008) time-temperature superposition....93
4-5 Furmanski et al. (2013) jump rate compression and time-temperature equivalence....95
4-6 Furmanski et al. (2013) comparison of time-temperature superposition methods....96
4-7 PVC time-temperature superposition....99
4-8 PPVC-2 time-temperature superposition....100
4-9 PPVC-4 time-temperature superposition....101
4-10 PPVC-6 time-temperature superposition....102
4-11 WLF equation applied to PPVC-2....104
4-12 PPVC-2 Low Temperature DMTA data....105
4-13 DSR method employed by Mullike and Boyce (2006)....105
4-14 PPVC-2 time-temperature superposition using DMTA data....107
4-15 PPVC-2 time-temperature superposition using DMTA data and beta transition....108
4-16 PPVC-2 time-temperature superposition using DMTA data and beta transition....108
4-17 PVC time-temperature superposition using DMTA data and beta transition....111

5-1 High rate post-yield behavior and temperature rise....116
5-2 Change from isothermal to adiabatic behavior in stress-strain response....118
5-3 Instron and temperature chamber/controls....123
5-4 Mapping technique schematic....124
5-5 Simulation of thermal softening diagram....126
5-6 Simulation test vs Low Temperature vs Medium Rate Test....127
5-7 PPVC-2 Temperature and rate behavior used for simulation method....128
5-8 Simulation of High Rate Behavior at all rates using PPVC-2....129
5-9 Simulation method with theoretical and input temperature rises....130

6-1 PMMA chemical structure....137
6-2 PC energies of deformation by Rudnev et al. (1991)....138
6-3 PC energies of deformation by Mulliken (2006)....138
6-4 PMMA DMTA data....140
6-5 PMMA stress strain behavior dependence on temperature....142
6-6 PMMA yield stress dependence on temperature....142
6-7 PMMA stress strain behavior dependence on strain rate....143
6-8 PMMA yield stress dependence on rate....143
6-9 Simulation of High Rate behavior using PMMA....144
6-10 PMMA experimentally measured temperature rise....148
6-11 PMMA energies of deformation....148
6-12 Simulation of high rate behavior using experimental temperature rise....149
6-13 PC chemical structure....152
6-14 PC DMTA data from Mulliken (2006)....153
6-15 PC stress-strain behavior as a function of temperature....155
6-16 PC yield stress dependence on temperature....155
6-17 PC stress-strain behavior as a function of strain rate....156
6-18 PC yield stress behavior as a function of strain rate....156
6-19 High rate PC behavior simulated with theoretical temperature rise....159

6-20 High rate PC behavior simulated with different beta values 160
6-21 High rate PC behavior simulated without any temperature rise 161
6-22 Comparison of PC temperature rises from literature and those used in testing 162

7-1 Awaji and Sato Brazilian test 168
7-2 Force time behavior of SHPB gages with soft material HTPB 171
7-3 Novel PZT strain gage SHPB setup 172
7-4 Dynamic equilibrium and transmitted wave comparisons of PZT gage 173
7-5 HTPB DMTA data 177
7-6 PBS DMTA data 177
7-7 HTPB stress strain temperature dependency 180
7-8 HTPB yield stress dependence on temperature 180
7-9 HTPB stress strain rate dependency using PZT gages 181
7-10 HTPB yield stress dependence on strain rate using PZT gages 181
7-11 PBS stress strain temperature dependency 182
7-12 PBS yield stress dependence on temperature 182
7-13 PBS stress strain rate dependency 183
7-14 PBS yield stress dependence on strain rate 183
7-15 Force time curves of PBS during high rate Brazilian testing 186
7-16 Tensile stress time curves of PBS during high rate Brazilian testing 186
7-17 High speed images during Brazil test 187
7-18 Strain calculation using DIC during high rate Brazilian testing 188
7-19 True strain results from DIC Brazilian test 188
7-20 PBS true stress-true strain in tension at high rate 190
7-21 High speed photos associated with preceding figure 190
7-22 Dynamic DIC image associated with figure 7-20 191
7-23 Simulation of high rate PBS behavior in compression 193
7-24 Simulation of high rate PBS behavior in tension 193
7-25 PBS stress-strain behavior in tension at low temperature 195
7-26 ESEM images corresponding to previous figure 196

8-1 PC storage modulus components 202
8-2 Arruda and Boyce (1993) comparison with Treloar (1955) 207
8-3 Shergold et al. (2006) fitting Ogden model to silicone rubber 208
8-4 Ogden model fits to all PVCs as function of temperature 211-212
8-5 Ogden model fits to all PVCs as function of strain rate 213
8-6 Shear moduli analysis in Ogden model 214
8-7 Haward Thackrary 1968 dashpot and spring model presentation 218
8-8 Roetling 1965 fits with Ree-Eyring model 220
8-9 Bauwens-Crowet et al. 1973 PMMA yield data model fits 221
8-10 Buckley and Jones model fits to PET 222
8-11 Richeton et al. 2007 yield stress fits 223
8-12 Rheological Mulliken & Boyce model 225
8-13 Mulliken & Boyce model fits to experimental data 225
8-14 Safari et al. 2013 PC experimental fits to DMTA data 226
8-15 Porter and Gould predictive model fits to experimental data 228
8-16 DMTA data broken into components 235
8-17 PVC elastic moduli fitted with a probability distribution 236
8-18 Mulliken Boyce model fit to all rates 238
8-19 Adiabatic temperature rise modeling with MB model 242

8-20 Comparison of low temperature response to high rate response 243

9-1 PMMA temperature rises by Chou et al. 1973 249
9-2 Rittel 1999 embedded thermocouple method 250
9-3 Arruda et al. 1995 IR temperature measurement setup 251
9-4 Collected literature on PMMA temperature rise at high rate 252
9-5 Collected literature on PC temperature rise at high rate 253
9-6 Thermocouple methods for testing 254
9-7 Novel temperature measurement method with Cu-Constantan sandwich 257
9-8 PPVC-2 temperature rise at high rate 259
9-9 Energies of deformation for PPVC-2 260
9-10 Sandwich thermocouple temperature measurement and response 261
9-11 PMMA temperature measurement with embedded thermocouple 262
9-12 PMMA IR temperature measurement 263
9-13 Photographs from previous figure 264
9-14 Experimentally measured temperature rise of PMMA 266
9-15 Energies of deformation – PMMA 266
9-16 PMMA behavior and temperature measurement with novel method 268
9-17 PMMA post-mortem photographs – sandwich versus embedded 268
9-18 PMMA experimental temperature rise compared to literature 269

List of Tables

2.1 Impedance properties of SHPB bar materials 38

3.1 Selected properties of unplasticized and plasticized PVC 54
3.2 Properties of PVCs used in thesis 55
3.3 Inertial contributions of test PVC materials 58

4.1 WLF constants used modeling 104
4.2 All PVC materials shift factors found from DMTA data 110

5.1 PPVC-2 Thermal properties 126

6.1 PMMA shift factors 140
6.2 PMMA thermal properties used for simulation method 142
6.3 PC shift factors 150
6.4 PC thermal properties used for simulation method 154

7.1 Calibration factors for PZT SHPB gages 172
7.2 Brazilian test parameters 174
7.3 HTPB and PBS shift factors 176

8.1 Ogden model parameters for all PVCs dependent on temperature 210
8.2 PPVC-6 Ogden model parameters dependent on rate 210
8.3 PVC parameters for DMTA model 236
8.4 PVC model parameters used for Mulliken Boyce modeling 245

Chapter 1

Introduction

The research presented in this dissertation aims to experimentally simulate and obtain a better understanding of the mechanical behavior of polymers under high strain rate deformation. Specifically, the interplay between the effects of temperature and strain rate on polymer behavior is examined and then used as a tool to help recreate the high rate mechanical response of several different polymers: ranging from rubbers to amorphous polymers to composites.

The mechanical properties of polymers are studied because of their widespread scientific and industrial importance, as seen in the automotive, aerospace, military, and medical industries. A considerable amount of research has been completed in both the impact behavior of polymers, and their sensitivity to variables such as temperature and strain rate. As high performance materials continue to be developed, there has been an increased demand for test methods capable of analyzing and comparing materials over a wide range of strain rates. The demand is particularly apparent in testing low impedance materials at high rates, for which there can be difficulties in obtaining dynamic stress equilibrium and thus reliable high rate data.

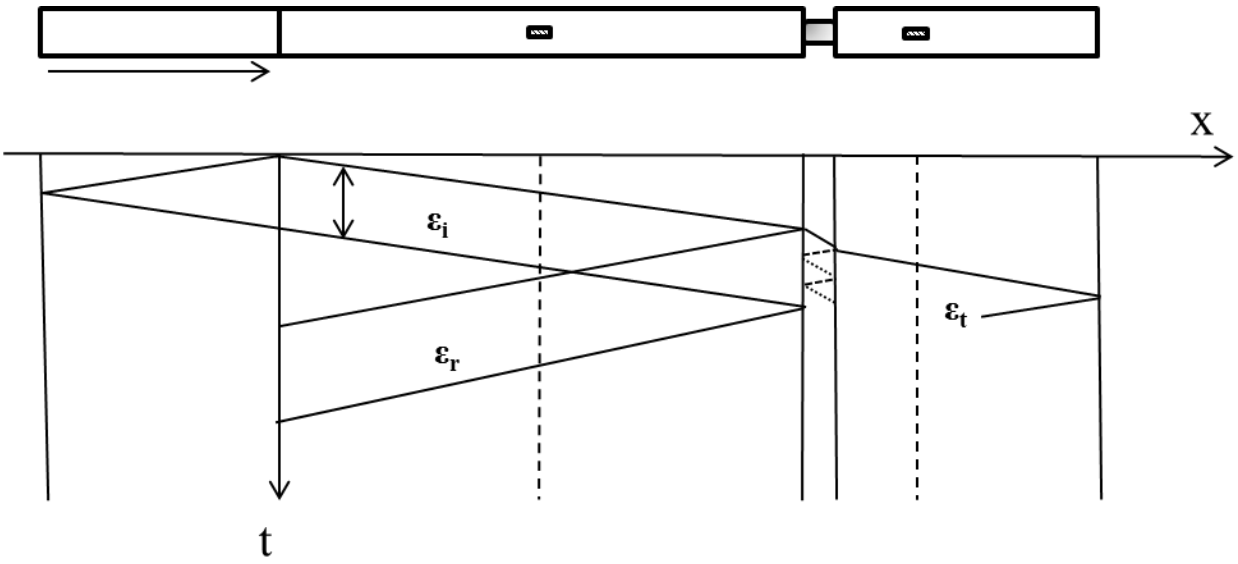


Figure 1-1: Time-distance diagram showing the stress waves propagating through space and time in a compression Split Hopkinson pressure bar (SHPB) arrangement. The specimen length is exaggerated to better illustrate the wave reverberation in the specimen. For more detail of this arrangement please refer to chapter 2 (section 2.3).

The high rate behavior of a range of polymers is well documented, and will be described further in chapter 2 (sections 2.4 – 2.6). In current experimental testing techniques, a specimen must reach mechanical equilibrium before the results of an experiment may be regarded as valid. The specimen is loaded from one end with a stress wave, which imposes a deformation rate on that end of the specimen. The wave oscillates a number of times within the specimen, each time increasing the specimen stress in a stepwise manner (figure 1-1). Eventually, enough oscillations occur so that the stress does not vary significantly with position in the specimen; the specimen is now in quasi-static equilibrium, although deformed at a high strain rate. Equilibrium is required because in the classical Hopkinson bar technique, only forces and velocities at the bar specimen interface are calculated, and thus average specimen properties are derived, and because, until equilibrium is achieved, the forces measured in the bars are not necessarily the same as those experienced by the specimen.

Although the difficulties of achieving specimen equilibrium are therefore obvious for materials with low sound speeds, composites can create similar difficulties in testing:

- Low impedance materials are frequently significant elements of composites
- Larger specimen volumes are often necessary to understand the constitutive response of a composite
- In-situ microscopic examination is required to fully understand damage formation

The complications in length scale and sound speed which generate difficulties in dynamic equilibrium, and the requirement of in-situ diagnostics create challenging obstacles when applying high rate testing to composite materials. Composites would similarly profit from an experimental simulation method in order to better understand high rate behavior.

As an example of a particulate composite, polymer bonded explosives (PBXs) typically use soft rubbers or polymers as a binder; the binder might only constitute 10% of the material, but has a large effect on the mechanical response, and in particular the rate and temperature dependence. Polymer bonded sugars (PBSs), seen in figure 1-2, are often used to simulate the response of PBXs in order to avoid several issues in contamination of experimental apparatus. The photographed composite uses a soft rubber as the polymer binder, hydroxyl-terminated polybutadiene (HTPB), in order to hold the sugar crystals. Biomaterials offer another example of composite materials with a wide range of length scales which provide similar challenges in high strain rate characterization. Biomaterials are typically very soft and have low impedance characteristics (e.g. spider-silk). These materials share the challenge of in-situ microscopic examination during deformation, and also the problem of achieving equilibrium, this time because of the relatively low sound speed in the material.

The current research project aims to achieve a better understanding of the interplay between temperature and strain rate using a model polymer: PVC. The ultimate goal is to be able to simulate (and even predict) high rate polymer response by performing experiments at

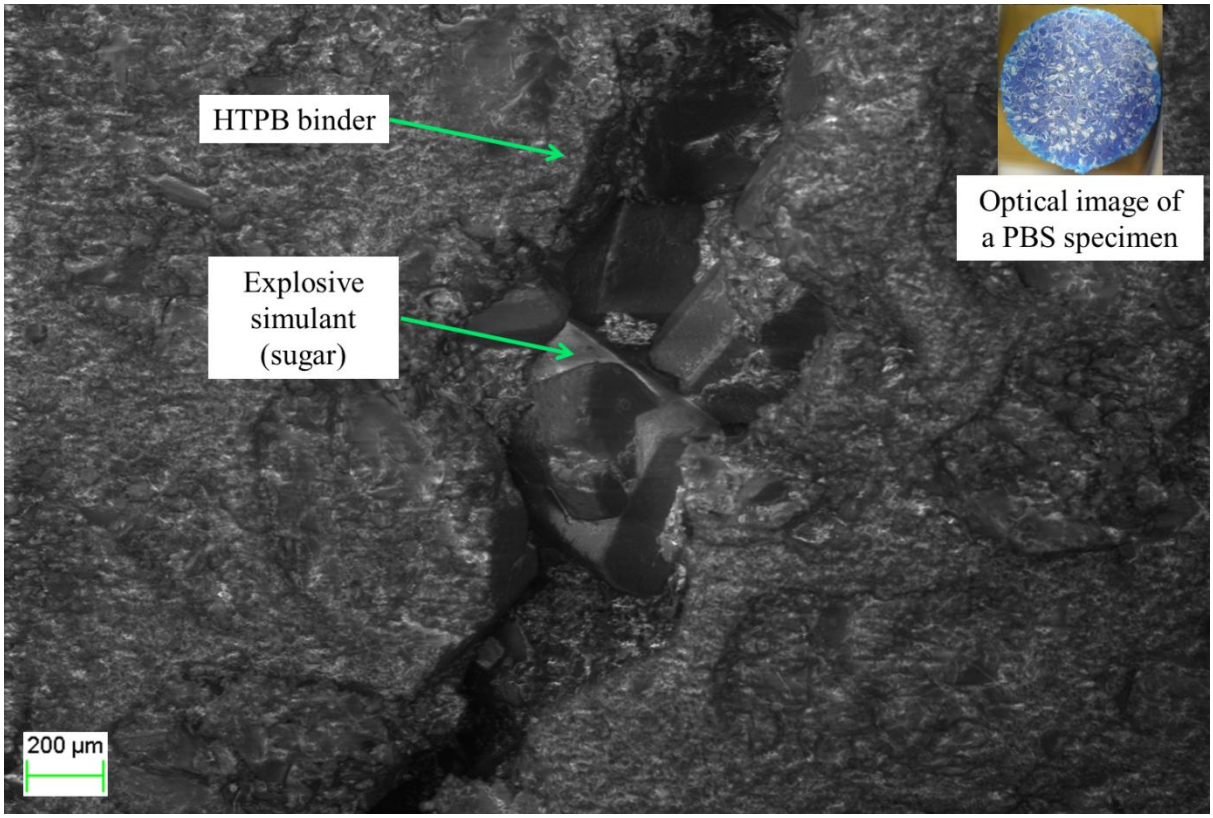


Figure 1-2: ESEM image showing damage formation on the surface of a polymer bonded sugar (PBS) after recovery from SHPB compression. A photograph of an undamaged PBS specimen (4 mm length x 8 mm diameter) is also shown.

low strain rates, summarized in figure 1-3 (please refer to chapter 5 for further detail). An experimental method such as this has the benefit of avoiding physical complications inherent in high rate testing while gathering critical constitutive information without the need for changing the material testing technique. The mapping methodology used by Siviour et al. (2005) will be used to advance our understanding of the relationship between temperature and strain rate in governing polymer mechanical behavior. By initially testing PVC specimens with different amounts of plasticizer, I am able to test a range of polymers: amorphous polymers to rubbery polymers. Namely, I am able to shift the transitions in the polymer and therefore observe more clearly the effects of these transitions on the rate and temperature dependence of the material. For example if, as documented in a large amount of literature, the β-transition is affecting high rate properties, and this transition is moved by modifying the amount of plasticizer, we can more readily see and analyze the changes which

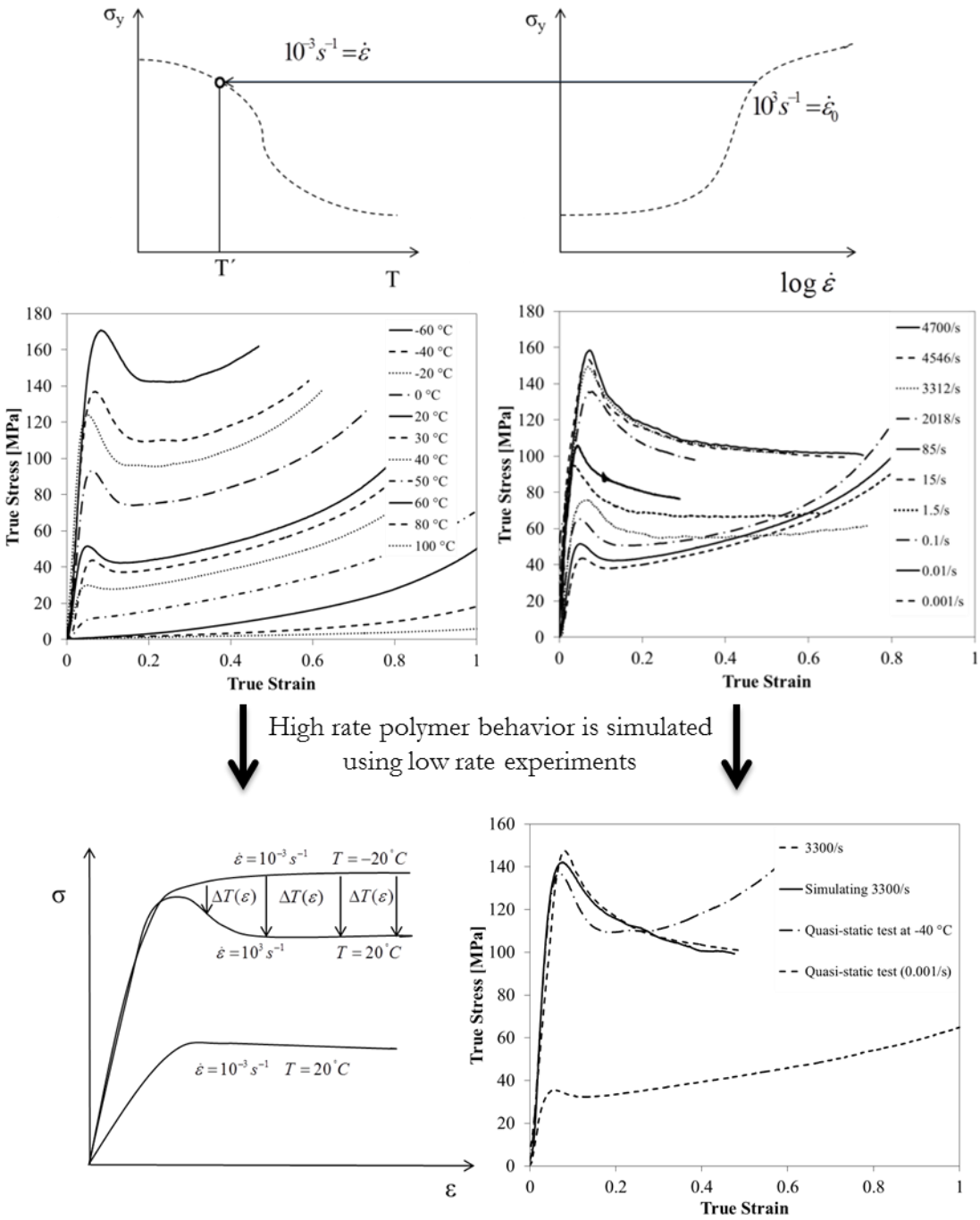


Figure 1-3: Summary of proposed experimental simulation method.

have occurred. While the effects of the β and α transitions on high rate behavior have been inferred using time-temperature equivalence, this is the first study which attempts to control this behavior, thus confirming previous observations.

Several soft materials, including rubbers, composites, and biological materials, are difficult to test at high rate, limiting knowledge in material properties. The lack of microscopic characterization apparatus that can be used at high rates limits our ability to perform critical experiments on composites or structured biological materials. Having created the experimental strategy to link the interplay between temperature and rate response, this method has then been applied to:

- Amorphous polymers
    - Poly(methyl methacrylate) (PMMA)
    - Polycarbonate (PC)
- Composite materials
    - Polymer bonded explosive simulant (PBS)

The work in the following chapters is conducted to create an experimental strategy to better understand the structural effects of these materials by using time-temperature superposition and other thermodynamic phenomena in order to simulate high rate loading (to large strains) through low rate experiments.

Chapter 2

Review of Experimental Techniques at Different Strain Rates

2.1 Overview of testing techniques at different strain rates

For impact applications it is essential to accurately characterize material behavior at different strain rates. Testing materials in uniform deformation under uniaxial stress, or one-dimensional wave propagation, ensures more straightforward analysis[1]. The standard range of strain rates for engineering applications usually varies from 10^{-5} s^{-1} in quasi-static loading to 10^{4} s^{-1} in dynamic loading. As presented in figure 2-1, these strain rate regimes are generally categorized as quasi-static (10^{-5} s^{-1} to 1 s^{-1}), medium rate (1 s^{-1} to 100 s^{-1}), and high rate (500 to 10^{4} s^{-1}). Understanding the behavior of amorphous polymers within a varied range of strain rates has several significant uses, ranging from military applications to medical devices inside the human body. Conventional servohydraulic and screw driven machines are used in most cases for testing at strain rates from quasi-static tests at 1 s^{-1} down to creep tests at 10^{-5} s^{-1}.

[1] In high rate testing the effects of inertia become important and also must be considered.

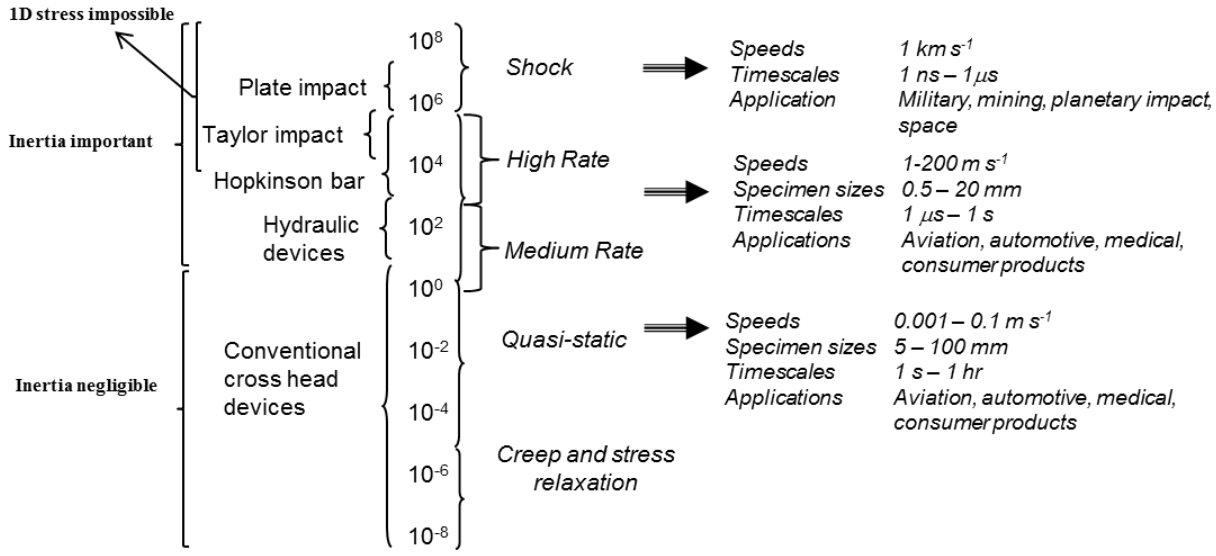


Figure 2-1: Approximate division of strain rate regimes (in s^{-1}), the experiments used to investigate material properties in these regimes, and selected applications. Specimen sizes are not given for plate impact, a technique that relies on wave propagation. Further information about the various techniques can be found in Field et al. (2004).

Mechanical testing machines have been available commercially since the mid-19th Century (Wade, 1856; Calvert & Johnson, 1859; Kirkaldy, 1862), and have gone through several evolutions, moving from purely mechanical machines to sophisticated electromechanical and servohydraulic systems with advanced electronics and computing. Microprocessors and other electronics have increased the accuracy and reliability of data gathered during experimentation. In order to achieve intermediate strain rates 1-100 s^{-1}, servohydraulic machines are typically used, in which a hydraulic pump and servohydraulic valves move an actuator piston (e.g. Richeton et al., 2006). The piston is attached to an end of the specimen that is controlled in order to perform compression, tension, or cyclic loading tests.

In investigating higher strain rates, the primary technique for testing is the split-Hopkinson bar, producing rates from 500 s^{-1} to 10^4 s^{-1} (this will be discussed in more detail later in this chapter). However, a number of other apparatus are also used. Delivering strain rates from 50 s^{-1} to 10^4 s^{-1}, the cam plastometer is often used in testing metals (Hockett & Lindsay, 1971; Baragar, 1987) and an image of the device is presented in figure 2-2.

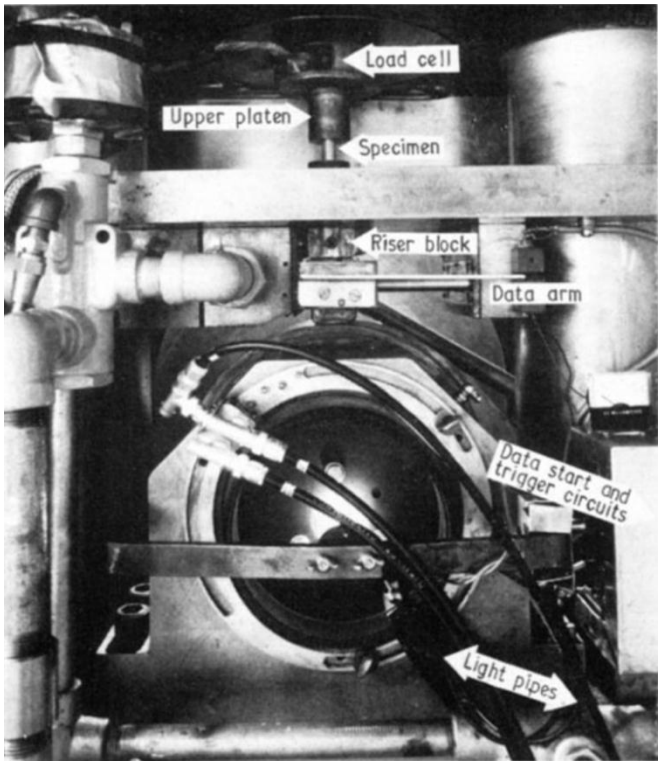


Figure 2-2: Cam plastometer press with the flywheel in the lower center of the photograph approaching the loading position (Hockett & Lindsay, 1971).

A cam is used to transfer load from a large flywheel in order to compress or extend a specimen. The inertia of the flywheel ensures that a constant strain rate is obtained. Cam plastometers are often large pieces of equipment, producing problems in balancing the cam, and other problems in providing effective amounts of strength with little deflection of the loading frame or drive train. Another method in the medium to high rate regime are drop tower compression tests, commonly known as the "drop weight test." This method uses a falling weight to apply a compressive load to the specimen, often generating high loads at medium strain rates, which are not as easily obtained with other methods. Roland et al. (2007) performed experiments studying the high strain rate behavior of polyurea, and concluded that the drop weight test gave advantages of a more uniform strain rate and the ability to ensure homogeneous strain. There has also been a lot of work in the Cavendish Laboratory, at the University of Cambridge, using a dropweight with transparent anvils (Field et al., 2004) to allow for effective photography of the specimen. For example, Cai and

colleagues (2008) used the drop-weight method to study polymer composites at rates of approximately 400 s^{-1}. A more direct flywheel method has also been used to test materials at high strain rates, where a rotating wheel with claws or noses stroke a yoke containing the test specimen (Foot et al., 1987). Furthermore, Al-Maliky and Parry (1996) tested polymers in tension by the expanding ring method, which involves placing a thin ring of polymer as a sliding fit around a hollow and thick-walled polymeric cylinder. The internal wall includes an exploding wire that generates a load via a blast wave. Al-Maliky and Parry were successful in obtaining data at strain rates up to 1.6×10^4 s^{-1} which they concluded compares favorably with the tensile split-Hopkinson bar which is limited to c.a. 1000 s^{-1} in tension due to effects of specimen inertia. A diversity of other test methods have been employed to study polymers at high strain rate, but none as recurrently or with as much achievement as split-Hopkinson pressure bar (SHPB) testing.

For even larger rates of strain, going above 10^5 s^{-1}, there are flat plate impact tests, often referred to as flyer plate methods. This method launches a flat flyer plate (carried in a sabot) at speeds of 500 to 2000 m s^{-1} against a stationary target plate supported by a spall ring, suppressing late-time radial tensile waves that could affect data measurement. These tests are frequently used to gather shock wave response data, equation of state data, and high rate yield data (Field et al., 2004).

2.2 Experimental Methodologies

This section presents an introduction to the testing techniques which were used in order to conduct the research presented in this thesis. Throughout this research, special attention is paid to polymer responses at high rates of deformation, and thus the subsequent section, 2.3, presents a literature review of this behavior.

2.2.1 Low Strain Rate: $10^{-3} \rightarrow 10^{-1}$ s^{-1}

For the purposes of this project, interest is in quasi-static mechanical tests performed at rates of strain from approximately 10^{-3} s^{-1} to 10^{-1} s^{-1} in tension or compression. Commercial screw-driven machines or hydraulic load frames are commonly used to achieve these lower rates of strain. Screw-driven machines are electromechanical devices that use an actuator screw threaded through a mobile crosshead. The screw is turned in both directions by an electric motor through a gear reduction system. The screws are rotated by a variable-control motor and power the moving crosshead up or down (Rinde & Hoge, 1971). Often a local fixture will be attached to the cross-head to improve anvil alignment. Extensometers are used to measure the changes in length of a specimen, allowing for the calculation of strain within the specimen. Extensometers range from clip-on extensometers that are attached on or near the specimen to non-contacting extensometers such as laser extensometers measuring strains greater than 1000% (Okereke et al., 2012). Temperature chambers are also commonly used to better understand materials response as a function of temperature. For example, the environmental chamber on the Oxford University Engineering Science Department's Instron testing machine can achieve temperatures from approximately -115 °C to +250 °C.

In compression testing, the right circular cylinder is the standard specimen geometry, figure 2-3. Typical length-to-diameter ratios are 1:3 or less, because longer specimens tend to lead to buckling instability or failure; however, it should be noted that measurements made

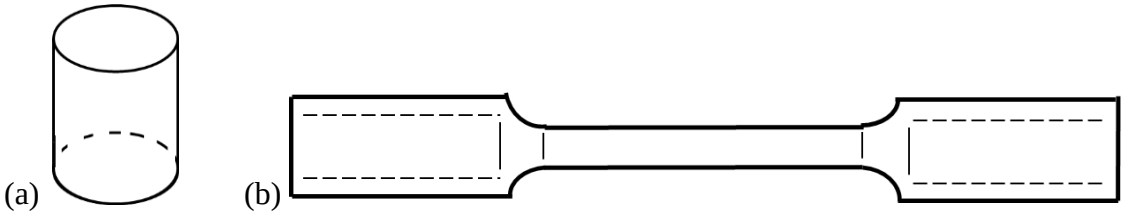


Figure 2-3: (a) Standard right cylindrical compression specimen and (b) a standard threaded tension specimen (dashed lines correspond to thread).

using very short specimens can suffer from the effects of friction at the specimen-platen interface. If there is excessive friction, a barrelling effect is observed, causing stress inhomogeneity such that the homogeneous deformation assumption is no longer sound. Therefore, such tests are not valid for the measurement of the bulk elastic and plastic properties of a material. In compression tests, lubrication of the specimen-platen interface is used to reduce platen-specimen friction and in order to mitigate the barrelling effect of the specimen. Paraffin wax has been shown to be an effective lubricant over a range of rates and temperatures (Trautmann et al., 2005). It is to be noted that because of the significant inertial effects at high rates (described in further detail in section 2.2.3), specimen dimensions in studies of rate dependence are often both shorter (*length/diameter* is 1 or less) and smaller (of the order of 10 mm or less) than would be ideally used in quasi static tests (Gorham, 1989).

In most quasi-static testing, the strain from the extensometer e_{gage} is converted to the nominal strain e of the specimen by taking into account the gage length l_{gage}, and the original specimen length l_0:

$$e = \frac{e_{gage} \times l_{gage}}{l_0} \tag{3.1}$$

The applied load is measured by a load cell in the cross-head. Measured applied loads are used to find the nominal stress [N/mm^2 or MPa] of the specimen by dividing the applied load by the original cross-sectional area of the sample. The nominal stress and nominal strain

values are then used to calculate the true stress and true strain of the specimen (assuming conservation of volume) by:

$$\varepsilon = \ln(e+1) \tag{3.2}$$

$$\sigma = s(e+1) \tag{3.3}$$

where ε is the true strain, s is the nominal strain, and σ is the true stress (Ashby & Jones, 2005). This same method is applied to the testing presented in the next chapter.

Typical tensile tests are performed using threaded tensile specimen geometry as seen in figure 2-3. To load the specimen, the threaded specimen is screwed into grips attached to each crosshead and the load is applied by moving the crossheads away from each other. Material factors, affecting accuracy and repeatability of testing, include specimen preparation (especially for brittle materials for which surface finish can be important) and specimen geometry: a long aspect ratio is preferred (Blumenthal et al., 2002).

2.2.2 Medium rate testing

Medium strain rate testing, as described previously, typically uses a hydraulic pump and servohydraulic valve setup to move an actuator piston that applies the desired loading rate (Zhao & Lampman, 2000). The servohydraulic machines are similar to conventional low rate testing but require higher crosshead velocities. For uniform strain rate, high machine stiffness is necessary. As strain rate increases, the measurement of load and displacement becomes more difficult due to problems such as load-cell ringing and adequate frequency response. Ringing of the load cell can be mitigated by selecting a load cell with a high vibrational frequency in order to ensure that its natural frequency is not excited. Another method is to dampen the impact that causes the specimen deformation with a thin layer of a deformable material place between impacting surfaces. In measuring the strain, several hydraulic test frames use linear variable differential transformers (LVDTs) and velocity transducers with good intrinsic frequency responses (Jordan et al., 2012). Corrections to the

reading must be taken into account when linking the signal to displacements within the specimen. Common causes for correction are displacements within the load frame and materials used for dampening signals. Noncontact methods of strain measurement are becoming more common with devices such as the laser interferometers and optical extensometers mentioned earlier (Kuhn, 2000).

2.2.3 Hopkinson bar and high-rate behavior

The split-Hopkinson pressure bar (SHPB) is the most widely used method for testing mechanical properties of materials in homogeneous deformation at high rates of strain. The set-up of the test is very different to the low rate and medium rate machines described previously. In particular, instead of assuming that the apparatus is in mechanical equilibrium, propagating waves in the apparatus are used to both deform the specimen and interrogate its response. The significance of the SHPB as an analysis instrument in the study of mechanical behavior of materials has grown in recent decades (Walley et al., 1991; Field et al., 1994) as finite element simulation capabilities in dynamic loading have created a requirement for accurate constitutive models and data for material response at high rates of deformation (Mulliken, 2006).

High strain rate testing methods have been developed since the pioneering work of John Hopkinson (J. Hopkinson, 1901) and later his son, Bertram Hopkinson (B. Hopkinson, 1905 & 1914) who first used long rods as waveguides for studying the impulse produced by explosive detonators. Based on these contributions and the work of Davies (1948), Kolsky (1949) invented the split-Hopkinson pressure bar, which allows the deformation of a sample of ductile material at a high strain rate, in a state of uniform uniaxial stress within the sample. The general theory of split-Hopkinson pressure bar testing has been well documented in the literature, e.g. Gray III (2000). Figure 2-4 shows a schematic diagram of a typical compressive SHPB apparatus. The experiment is started by firing a striker bar down the

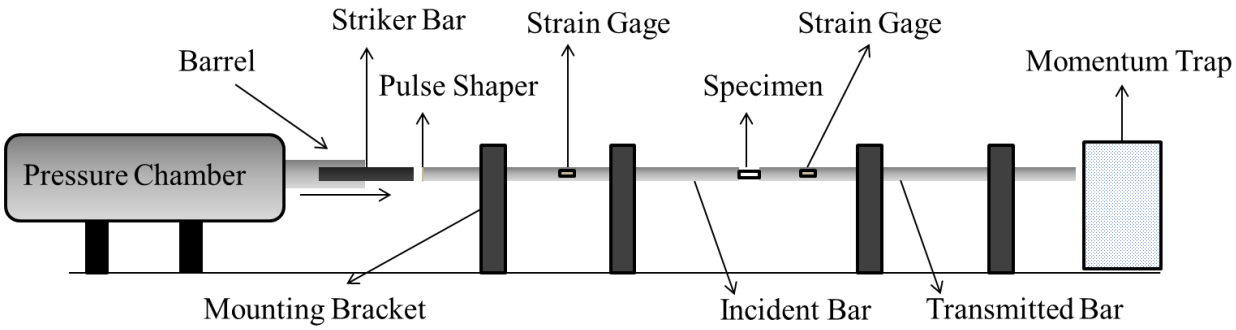


Figure 2-4: Schematic of a compression split-Hopkinson pressure bar.

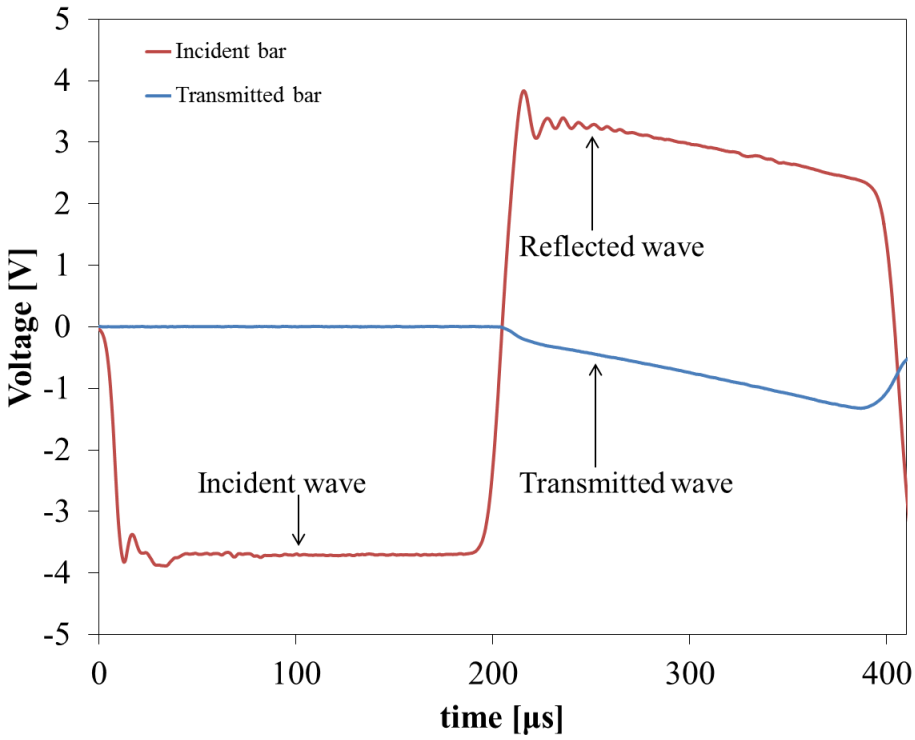


Figure 2-5: Strain gage signals from a representative SHPB test on a PVC specimen.

barrel by releasing high-pressure gas from the pressure chamber. The first pressure bar, the incident bar, impacted by the striker bar, creates an elastic compressive stress wave. The elastic wave travels down the length of the incident bar until it reaches the bar-specimen interface. An amount of the incident pulse is reflected back down the incident bar as a result of the difference of mechanical impedance at this interface, while the remaining portion of the pulse is transmitted through the specimen and into the second pressure bar, the

transmitted bar. Within the specimen, the wave reverberates, increasing the stress and deforming the material at a high rate of strain, ca. 10^3 s^{-1} to 10^4 s^{-1}. The incident, the reflected, and the transmitted stress pulses are recorded with strain gages attached to the pressure bars. These strain gages capture the resultant three pulses, consisting of a compressive input strain ε_i, tensile reflected strain ε_r, and compressive transmitted strain ε_t. Figure 2-5 is an example of these three pulses during a test on PVC.

The standard SHPB analysis is based on the assumption of one-dimensional wave propagation in the bars (Walley et al., 1991; Dioh et al., 1993; Field et al., 1994; Gray III & Blumenthal, 2000; Cady et al., 2003 Mulliken & Boyce, 2006; Okereke et al., 2012). One-dimensional assumption further simplifies the mathematics with little loss of accuracy in most SHPB applications. The general equation of wave motion in a slender rod is

$$\frac{\partial^2 u}{\partial x^2} = \frac{1}{c^2}\frac{\partial^2 u}{\partial t^2} \tag{2.1}$$

where u is the displacement in the x-direction, (along the axis of the pressure bar), t is time, and $c = \sqrt{E/\rho}$ is the acoustic longitudinal wave speed in a 1-D elastic medium, where ρ is the density and E is the elastic modulus. From elementary wave theory, the solution can be written as:

$$u = f(x - ct) + g(x + ct) \tag{2.2}$$

where f represents a wave traveling to the right, and g a wave traveling to the left. The 1-D strain, by definition, is given by $\varepsilon = \partial u/\partial x$ thus differentiating equation 2.2 with respect to x, the strain in the incident bar gives

$$\varepsilon = f' + g' = \varepsilon_i + \varepsilon_r \tag{2.3}$$

Differentiating equation 2.2 with respect to time and using equation 2.3, we have:

$$\dot{u} = c(-f' + g') = c(-\varepsilon_i + \varepsilon_r) \tag{2.4}$$

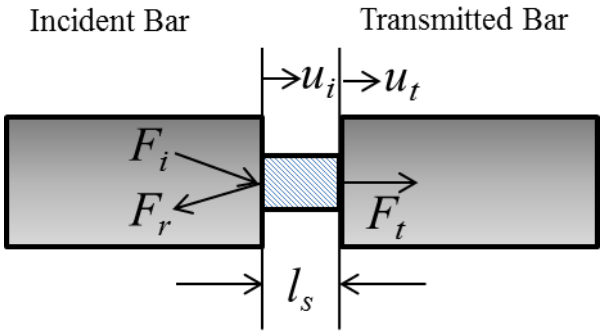


Figure 2-6: Expanded view of incident (input) bar/specimen/transmitted (output) bar region, where u_i and u_t are the incident bar and transmitted bar displacements, respectively.

where $\dot{u}$ is the time derivative of the displacement for the incident bar and c is the wavespeed of the bar material . The derivative of the displacement in the transmitted bar with respect to time gives:

$$\dot{u} = -c_b \varepsilon_t \tag{2.5}$$

Both equation 2.4 and 2.5 are true everywhere in the pressure bars. An expression for the strain rate $\dot{\varepsilon}$ in the specimen is found by taking the difference of two solutions – the solution specific for the rate of displacement at the end of the incident bar (equation 2.4) and one specific for the rate of displacement at the end of the transmitted bar (equation 2.5):

$$\dot{\varepsilon} = \frac{c}{l_s}\left(-\varepsilon_i + \varepsilon_r + \varepsilon_t\right) \tag{2.6}$$

where l_s is the length of the specimen. By definition, the forces in the two bars are:

$$F_1 = F_i + F_r = AE(\varepsilon_i + \varepsilon_r) \tag{2.7}$$

and

$$F_2 = F_t = AE\varepsilon_t \tag{2.8}$$

where E is the Young's modulus of the material, and A is the cross-sectional area of the pressure bars, as given schematically in figure 2-6. Stress equilibrium requires that the forces on the front and the back faces of the specimen be the same (e.g. F_1=F_2, from equations 2.7 & 2.8). When this assumption holds, the elastic bar strains that were measured also produce

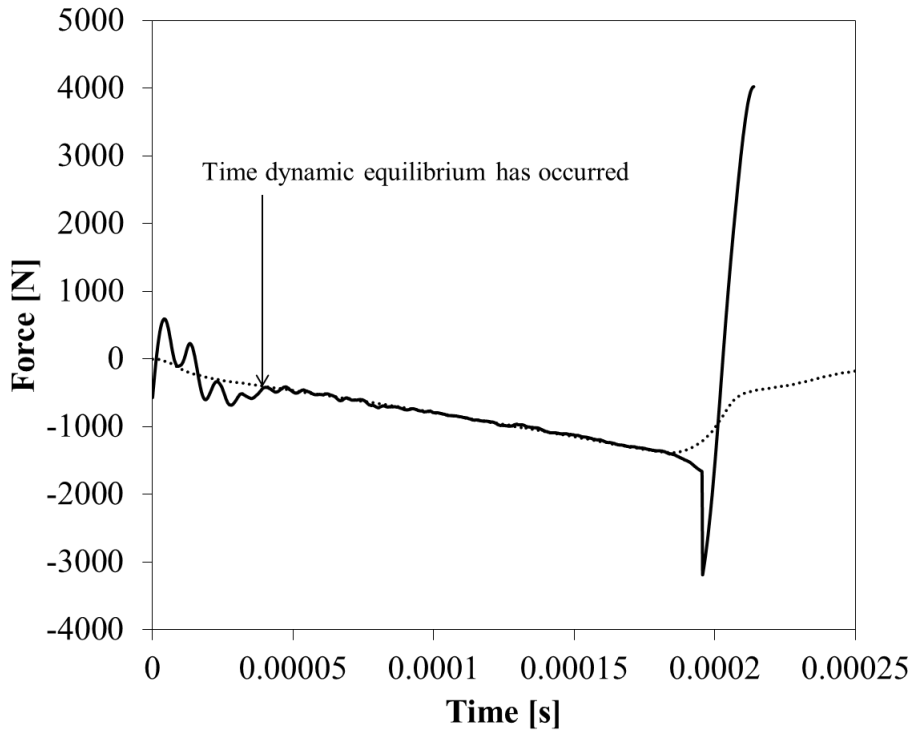


Figure 2-7: Force-time plot of $F_i + F_r$ (solid line) and F_t (dotted line) demonstrating the time dynamic equilibrium occurs in a PVC specimen at a strain rate of ~3000 s^{-1}.

expressions for the forces within the specimen and, in addition, the specimen behavior is representative of the bulk material. After some wave oscillation the specimen attains stress equilibrium and undergoes homogeneous deformation. If this is the case the two force equations corresponding to the two bars may be equated (see figure 2-7), and we see that:

$$F_t = F_i + F_r \tag{2.9}$$

Small specimen sizes are a necessity in order to ensure that this mechanical equilibrium is reached (see below for further explanation). With dynamic equilibrium, the final equation for specimen stress is simplified to:

$$\sigma = \frac{A_b E \varepsilon_t}{A_s} \tag{2.10}$$

A_b is the cross-sectional area of the bar, and A_s is the cross-sectional area of the specimen. The strain is found through numerical integration of equation 2.6. As seen in the equations above, and to be noted, the specimen stress is directly proportional to the transmitted pulse.

By altering the velocity and length of the striker bar, the magnitude and the duration of the input stress wave can be changed. At constant strain rate, the maximum strain that can be achieved in the specimen is directly proportional to the length of the striker bar utilized, *L*:

$$\varepsilon = 2\dot{\varepsilon}\frac{L}{c} \tag{2.11}$$

since the duration of the experiment is *2L/c*. A simple equation to provide an initial estimate of the strain rate is:

$$\dot{\varepsilon} = \frac{V}{l_s} \tag{2.12}$$

where V is the velocity of the striker bar, and l_s is the length of the specimen; this overestimates the rate because it does not account for the strength of the specimen, however, equations 2.11 and 2.12 provide good starting points for choosing test parameters to achieve an effective SHPB test (Gray III, 2000). Often, pulse-shaping techniques are used, placing a deformable material in between the striker bar and incident bar; the pulse shaper lengthens the rise time of the incident pulse to help reduce both the amount of strain accumulated and the time taken before stress equilibrium and homogeneous deformation of the specimen (Richeton et al., 2006). It also reduces ringing on the incident and reflected waves by filtering out high frequency components of the pulse (Chen et al., 1999; Quintavalla & Johnson, 2004).

In Hopkinson bar testing, the specimen geometry is very important because the specimen length determines the time to dynamic equilibrium, thus determining the validity of low-strain data. Furthermore, the strain rate (and hence maximum strain) is inversely proportional to the specimen length, and since the maximum speed of the striker bar is limited by the requirement that the input bar remains elastic, the shorter specimens must be used at higher rates. Additionally, specimen geometry must be chosen to mitigate buckling, frictional forces, and very importantly, inertial effects. Gorham (1989) has studied the

contributions of specimen geometry to inertial effects in detail, and in doing so, aiding the selection process of ideal specimen geometry to help mitigate these inertial effects and produce greater accuracy in measurement of material properties. He derived the following equation enabling the comparison of the inertial contribution to the measured flow stress and included the time variation of the specimen geometry:

$$P_2 = \sigma_y - \rho\left(\frac{r^2}{8} - \frac{h^2}{6}\right)\ddot{\varepsilon} + \rho\left(\frac{r^2}{16} - \frac{h^2}{6}\right)\dot{\varepsilon}^2 - \frac{\rho h \dot{v}}{2} \tag{2.13}$$

here P_2 is the pressure of the sample in contact with the transmitted bar, σ_y is the uniform (i.e. material) compressive yield stress, ρ is the specimen density, r and h are the instantaneous radius and height of the specimen, $\dot{\varepsilon}$ is the strain rate, $\ddot{\varepsilon}$ is the rate of change of the strain rate, and $\dot{v}$ is the rate of change of the transmitted end velocity. The sum of the last three terms is accepted as the inertial contribution of experiment. When compared to the stresses measured in an experiment, it is made clear whether the inertial contribution is negligible or significant (specimens are designed to ensure the former). Results of the inertial analysis by Gorham are presented in further detail in the high rate experimental methods and results, section 3.3.

A number of factors must be considered when designing a Hopkinson bar experiment, and several issues continue to rise in its application. There are particular difficulties that arise from studying lower impedance materials, which includes a wide range of polymers. Impedance in relation to a material (e.g. the acoustic impedance) is defined as:

$$Z = \sqrt{\rho E} = \rho c \tag{2.14}$$

and challenges for high rate testing on the split-Hopkinson bar include:

- Low wavespeeds in several polymeric materials (especially rubbers) results in larger amounts of time for the specimen to reach stress equilibrium, hence the data at small strains are sometimes unreliable.

- Rubbers (or ‘elastomers’) often necessitate testing to larger strains (by having higher elastic limits), thus increasing the duration of the experiment and requiring multi-point strain measurements with wave separation or longer apparatus (Siviour, 2011). This was confirmed by Shim & Mohr (2009) in their testing of polyurea with nylon input and output bars which introduced several cumulative errors into the data reduction. However, more recently, stress measurement techniques such as X-cut quartz crystals and optical methods have shown that excellent data may be obtained while avoiding the need for long bars or wave separation as shown by Chen et al. (2000), and Nie et al. (2009) while testing ultrasoft materials with an aluminum bar system.
- Supported loads are smaller, demanding large diameter specimens and sensitive strain gages. The smaller signals can cause difficulties in confirming specimen equilibrium.
- For very soft materials (i.e. silk and several other fibers) the intrinsic inertia may necessitate a large amount of force to accelerate the material to high deformation rates, which may not be possible with lower material strengths (Wu et al., 2002).

In particular, suitable bar materials must be selected (a comparison of properties of bar materials commonly used for testing are included in table 2.1). In choosing the correct bar material, desired characteristics include:

- High elastic limit - high strength for high strain rate capabilities
- Low attenuation. Signal loss in perfectly elastic materials is as near to zero as possible
- Small radial wave attenuation. Low Poisson ratio is desired
- Large thermal range over which elastic properties are constant
- Low interference potential – low coupling between bars and bar mounting bracket and high impedance with respect to air

Table 2.1: Comparison of the impedance properties of bar materials for split-Hopkinson pressure bar testing (Gray III, 2000).

	Elastic Modulus (E)	Wave impedance (ρ/c)	Impedance relative to steel $(\rho/c)_x/(\rho/c)$
Bar material	[GPa]	[kg s^{-1} m^{-2} x 10^{-6}]	%
Steel	212	40.8	100
Ti-6Al-4V	115	22.8	56
Aluminum	90	13.5	33
Magnesium	45	8.6	21
PMMA	4	2.2	5

In studying the high strain rate stress-strain response of low-impedance soft materials, one would additionally like a bar material to best match the mechanical impedance of the specimen being studied. The matching of bar material to specimen material is carried out with the aim of increasing the fraction of the incident force transmitted by the samples (a more detailed investigation in this subject is presented at the end of Chapter 3). Since low impedance materials also typically have low moduli, this also increases the force sensitivity of the system, making it easier to measure the transmitted stress. Several researchers have worked on quantifying how the nonlinear response of polymeric bars alters the classic SHPB data analysis. Such viscoelastic bars (frequently polymethyl methacrylate, 'PMMA'), exhibit wave attenuation and wave dispersion, along with having a non-linear elastic response, unlike metallic bars. As determined by Zhao et al. (1997), the geometrical dispersion in a viscoelastic SHPB setup is consistently non-negligible. These differences necessitate manipulations and corrections of measured strain pulses at positions along the pressure bars in order to perform correct analysis by SHPB (Labibes et al., 1994). Because of these obstacles, several other researches have utilized lower-impedance metallic bars to analyze several soft materials, such as aluminum (Wang & Arruda, 2001), magnesium (Shergold, 2006; Siviour, 2008), and titanium (Jordan et al., 2008) in order to achieve high resolution

data without complications in data reduction. An advantage of large transmission is that it is easier to calculate the force on the input face of the bar.

2.2.4 Dynamic Mechanical & Thermal Analysis

Dynamic mechanical and thermal analysis (DMTA) machines apply oscillating displacements with systematic variations of temperature (-100 °C to 200°C) and/or frequency (up to approximately 100 Hz) in order to study and characterize materials. In order to compare these data to those obtained in uniaxial experiments, the test frequency may be converted to a strain rate by examining one-quarter of a cycle in the sinusoidal load program. The time duration of this quarter cycle is known from the test frequency, and the strain amplitude achieved during this time can be approximated from the prescribed displacement amplitude and the known specimen gage length. The increase in strain over this time is approximated to be linear, and thus an average strain rate can be calculated:

$$\dot{\varepsilon} \approx \frac{\Delta\varepsilon}{\Delta t} = \frac{\frac{d_0}{l_g}}{\frac{1}{4}\frac{1}{\omega}} = \frac{4\omega d_0}{l_g} \tag{2.15}$$

Where d_0 is the displacement amplitude and l_g is the specimen gage length (Mulliken & Boyce, 2006). From DMTA testing and analysis, material transitions over small ranges in temperature can be identified. DMTA data are usually presented in terms of a storage modulus, loss modulus, and $\tan\delta$ (called the loss tangent; where δ is the phase angle or "phase lag"). The storage modulus is a measure of the elastic response of a material (equivalent to Young's modulus). The loss modulus is a measure of the viscous response of a material, namely, when the material does not give a perfectly elastic response. The dimensionless property, $\tan\delta$, is a ratio between the storage modulus and loss modulus; the term measures how the material absorbs or loses energy. DMTA data are often presented with $\tan\delta$ against temperature, with the peaks representing material transitions, allowing for

an unambiguous presentation of material transitions (i.e. melting point, glass transition, and β transition) (Gearing, 1999).

2.2.5 Brazilian Testing

Brazilian disc tests are used for tensile tests by loading a disc specimen using curved anvils and thus inducing a tensile stress along the axis of loading, while reducing the stress concentration at the specimen-anvil interface, and creating a 'splitting' of the sample. A diagram of the method is presented in figure 2-8. The flat anvil example (figure 2-8a) illustrates the premature failure resulting from high shear stresses that has been seen to occur, while the curved anvils present the desired tensile failure at the center of the disc specimen (figure 2-8b). The technique was originally developed by the Brazilian researchers Carneiro and Barcellos (1949), and expanded upon by Awaji and Sato (1979), for brittle samples such as marble. For this method, a tensile stress at the center of a specimen is described as:

$$\sigma = \frac{2P}{\pi D_s t_s}\left(1-\left(\frac{b}{R_s}\right)^2\right) \tag{2.16}$$

where P is the applied load, D_s and t_s the diameter and thickness of the specimen respectively, R_s is the radius of the specimen, and b is the contact width of the anvils. It has been shown by Awaji and Sato, and established by other others (Rae et al., 2002; Williamson et al., 2009; Grantham et al., 2004), that if the ratio b/R_s is greater than 0.27, then the tensile strength of the specimen is independent of b/R_s. Namely, a value of 0.27 is required in order to avoid the influence of the induced shear stresses (see figure 2-8a). Digital image correlation (DIC) is most often used as the (optical) strain measurement technique. A random speckle pattern is often used on the specimen with an acrylic paint in order to aid the DIC process. Grantham et al. (2004) applied Brazilian tests to composite materials at high rate using an explosive simulant (a polymer bonded sugar, or 'PBS') with the material of the

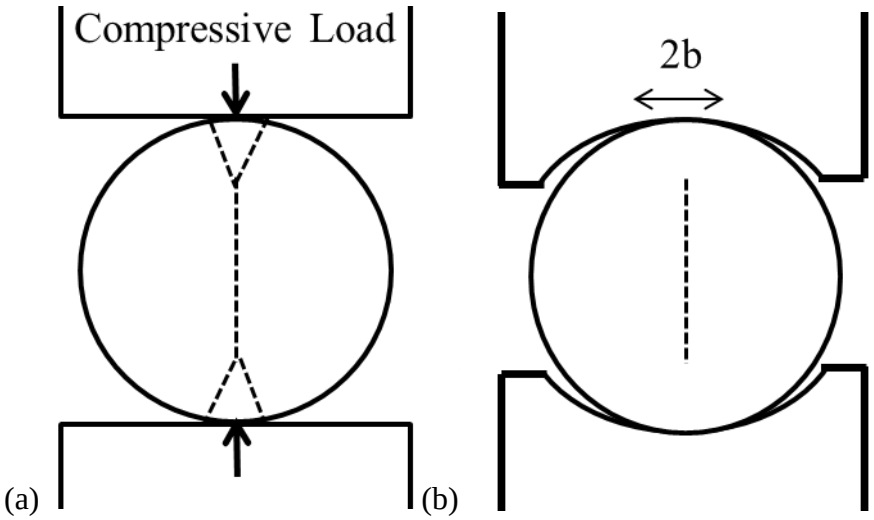


Figure 2-8: Brazilian test schematic diagram with (a) premature failure from flat anvils and (b) tensile failure from curved anvils, which has been presented in literature by e.g. Awaji & Sato (1979) testing graphite, and seen by the author of this thesis in testing polymer bonded explosive simulants (presented in Chapter 7).

rubber binder not mentioned in the paper (although a manufacturer name of 'PBS9501' was given). The group performed tensile tests (via Brazilian tests) in order to conclude with the several advantages of Brazilian testing as an effective high rate tensile test method over normal SHPB tensile testing, siting the simpler specimen geometry and thus specimen preparation. Williamson et al. (2009) investigated rate and temperature dependent behavior on a polymer bonded explosive (PBX) via Brazilian tests to find a log-linear relationship of 10 °C per decade strain rate. The authors also found that a transition from intergranular to transgranular failure occurred within the glass transition temperature region and below it. Gerlach et al. (2008) found Brazilian tests to be incompatible with their thermosetting resin system material RTM-6, which could be associated with the lack of brittleness of the material.

2.2.6 Environmental Scanning Electron Microscope

In investigating the high rate behaviour of polymers, Environmental Scanning Electron Microscopes (ESEMs) have often been used in studying the fracture behaviour of composites, typically involving a post-mortem analysis of specimens involved in moderate to

high rate deformation (Rae et al., 2002; Balzer et al., 2004; Drodge et al., 2010; Silva et al., 2011). Scanning electron microscopes are used in a wide variety of research across several disciplines. An ESEM allows for collecting electron micrograph images by using an electron beam and electromagnetic lenses to focus and direct the beam on the specimen surface. The small electron spot, or probe, is scanned over a small area and the beam electrons interact with the specimen surface layer and produce various signals that are collected by detectors. These detectors then output an image that corresponds to the respective pixel matrix retrieved from the specimen surface. There is opportunity for in-situ ESEM analysis during low rate experiments (which is presented in Chapter 7 of this thesis). Time-temperature equivalence (presented in Chapter 4 of this thesis) would be a starting point to achieve the necessary mechanical behaviour to understand high rate behaviour via in-situ microscopic diagnostics.

2.3 Polymers at High Rate

Taylor (1946; 1958) and Volterra (1948) performed the first split Hopkinson bar tests on polymers and explosives, with Kolsky following (1949), and Chou, Robertson, and Rainey (1973) being the first to produce a significant set of SHPB data and examine the behavior of different polymers over a wide range of strain rates (10^{-4} s^{-1} to 10^{3} s^{-1}). Within their study, Chou et al. examined the rate-dependent yield and compressive stress-strain behavior of polymethyl methacrylate (PMMA) and cellulose acetate butyrate (CAB), with the highest rates being performed on a split-Hopkinson pressure bar apparatus. The authors observed an increase in strain rate sensitivity of yield stress at higher rates of strain. A temperature rise in the specimen (measured by thermocouples) was also noted at higher rates, which was credited to an adiabatic thermodynamic condition, while also linking the heat created to an increase in the amount of strain softening at high strain rates.

During the late 1960s to early 1970s there was a large amount of work conducted by Bauwens in studying the yield stress behavior of polymers, specifically in the glass transition region, and a secondary transition region, known as the β-transition, in which he observed the heightened sensitivity of yield stress in the lower temperature regime, as seen in figure 2-9 at approximately -85 °C. Bauwens (1972) tested polycarbonate (PC) under uniaxial compression at a constant strain rate over a wide range of temperatures from -120 to 120 °C, as well as tension from -140 to 20°C, describing the yield behaviour as two different flow processes as seen in figure 2-9, illustrating the variation in engineering yield stress across a wide range of temperatures (-150 to 200 °C). These data were shown to fit the Ree-Eyring model (see chapter 8 for more detail) with nearly perfect agreement between model and experiment. Furthermore, in 1973, Bauwens-Crowet investigated PMMA and proposed a yield criterion, which she used to build a master curve spanning strain rates from 10^{-4} s^{-1} to 10^{6} s^{-1} and a temperature range of -20 to 100°C . The prediction of yield behavior “for any

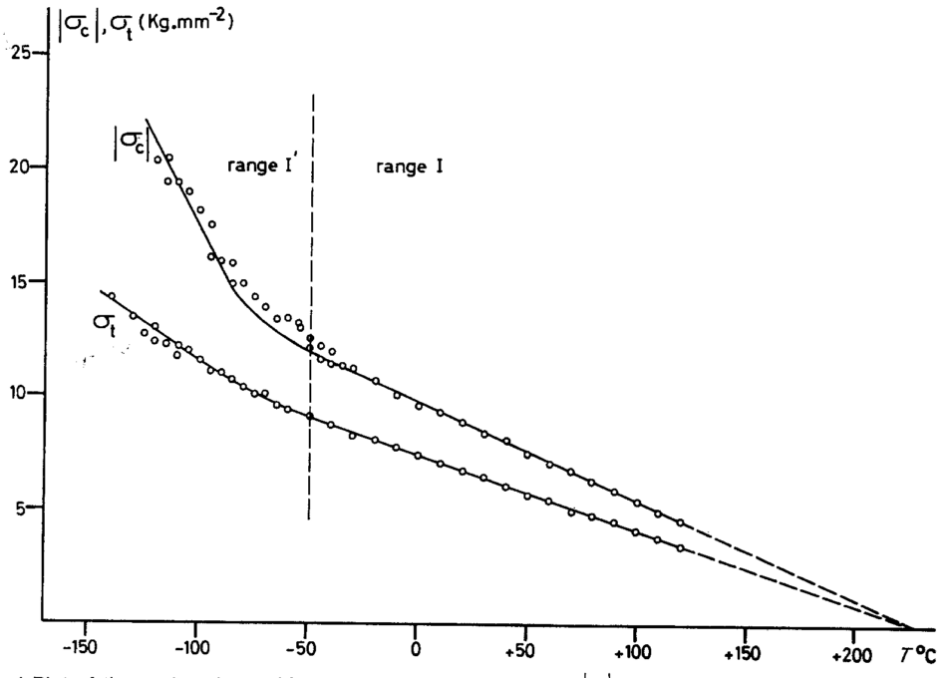


Figure 2-9: Plot of the engineering yield stress in uniaxial compression $|\sigma_c|$ and in tensile tests σ_t versus temperature at a constant strain rate of 4.16 x 10^{-3} s^{-1}. Data has been fit with the Ree-Eyring model. (Bauwens-Crowet et al., 1972).

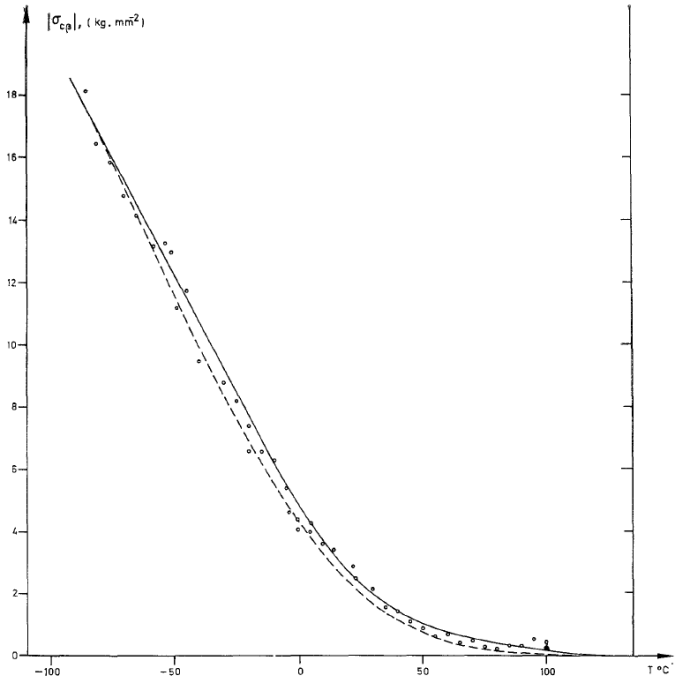


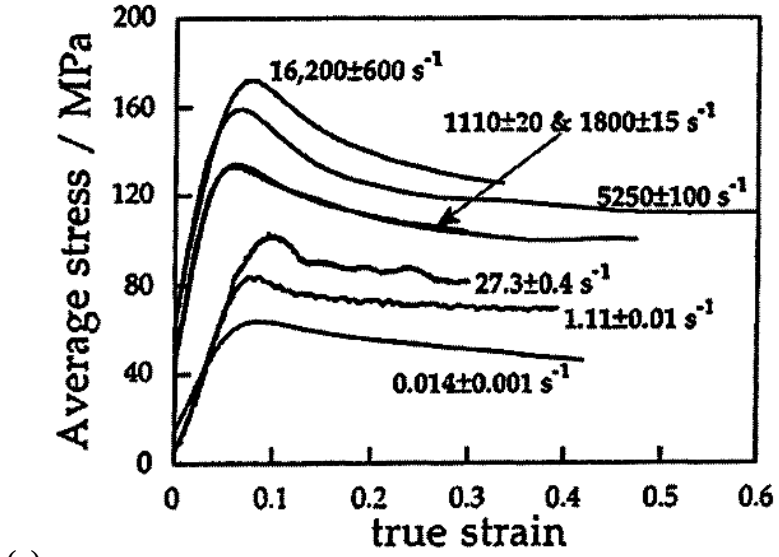
Figure 2-10: β component of the compression yield stress as a function of temperature at constant strain rate of deformation. (Bauwens-Crowet, 1973).

state of stress, or value of temperature and strain rate in the glassy range" was possible using a temperature time-superposition formula, along with empirical data gathered from the same range of temperatures on the master curve and from testing at strain rates ranging from 10^{-4} to 10^{0} s^{-1}. By testing at these strain rates Bauwens-Crowet was able to use the same testing machine, and avoid the issues of including data from different apparatuses, which consist of friction, inertia, and specimen equilibrium. Bauwens-Crowet's investigation corroborated evidence found in the previously mentioned studies of PC, in looking at the heightened sensitivity at higher strain rates while analyzing yield behavior. Bauwens-Crowet deduced a bilinear relationship in the yield stress to strain rate relationship, demonstrating an increase in strength at high strain rates and/or low temperatures. She also highlighted the similarity between the polymers' molecular processes within the high strain rate regime and at low temperatures, specifically the molecular secondary relaxation process, known as the β-transition. Figure 2-10 presents the β component of the compression yield stress as a function of temperature at constant strain-rate.

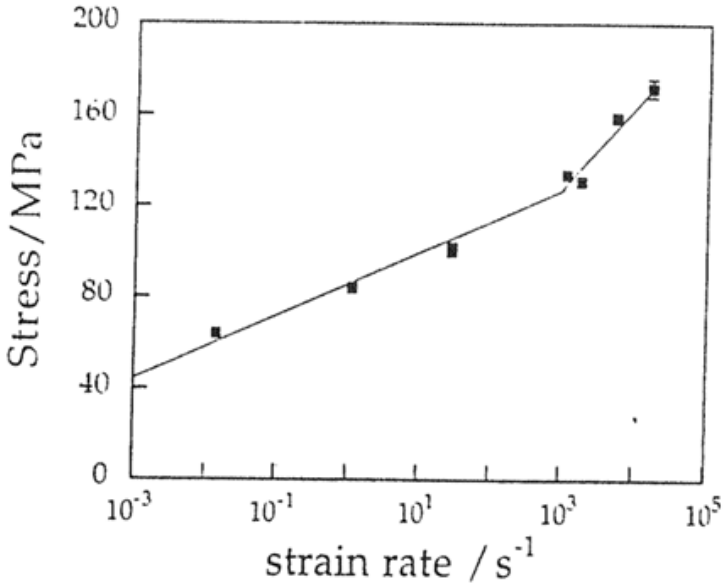
Rietsch and Bouette (1990) continued Bauwens's work while testing materials under compression at high-rate, to confirm and further document the secondary transition in the yield behaviour of PC. They were the first to attempt this with an SHPB system. The authors tested PC in uniaxial compression at temperatures ranging from -40 °C to 60 °C, and strain rates from 150 s^{-1} to 3000 s^{-1} on a SHPB system, and from 10^{-4} s^{-1} to 10 s^{-1} on a servo-hydraulic machine. Their data revealed a clear transition in the rate-dependent yield behaviour of PC for all of the temperatures tested. The transition appeared to occur at approximately 100 s^{-1} at room temperature. They fitted their data to Bauwens's temperature-dependent data, finding a good agreement between the two. Any slight discrepancies in data that were observed were attributed to the different manufacturers of the PC used (perhaps leading to differences in the molecular weight of the PC). The basis for the β-transition was

interpreted as the same molecular relaxation process in PC that Bauwens had concluded previously.

Walley and Field (1989, 1991, 1994) studied several polymers, focusing on rate-dependent behaviour. The tests were conducted at strain rates ranging from 10^{-2} s^{-1} to 10^{4} s^{-1}, using four different apparatus, including a direct-impact Hopkinson bar for strain rates above 10^{3} s^{-1}. Some examples of the stress-strain curves and a maximum stress as a function of strain rate curve produced from their investigation of PVC are shown in figure 2-11. Identifying and attempting to eliminate sources of error, they carefully studied the effects of friction and inertia in their compression tests, utilizing the expression given by Gorham (1989) and high-speed photography (used for measuring diametral expansion and thus used to determine the strain) in their analysis. While combining data from tests in the different strain rate regimes, they found that acrylonitrile-butadiene styrene (ABS), poly(ethylene terephthalate) (PET), polypropylene (PP), polyvinyl chloride (PVC), and poly(vinylidene fluoride) (PVDF) all showed an increase in the sensitivity of yield stress at high strain rates. The other materials were placed into two other categories: one being a linear relationship, with no change at higher strain rates, while the other group consisted of materials in which the yield stress began to decrease at and above a strain rate of approximately 10^{3} s^{-1}. The decrease in maximum stress at high rates was an unexpected occurrence that was seen specifically in nylon 66, polycarbonate (PC), polyetheretherketone (PEEK), and polyethersulphone (PES). Materials such as PC and nylon 66 were included in other studies such as Rietsch and Bouette (1990) and Chou et al. (1973), and neither found any decrease in yield stress in the range of strain rates tested, but rather found an increased rate sensitivity of yield in the high rate regime. Further studies by Siviour (2005) have attributed the different observations to the possibility of these studies not going to high enough strain rates for the grade of polymer they used, after these drops in yield stress were validated for nylon 66 and



(a)



(b)

Figure 2-11: (a) Compressive stress-strain behavior of PVC at seven different strain rates and (b) maximum stress as a function of strain rate for PVC. Data was obtained from four different apparatus: an Instron mechanical testing machine, a hydraulic mechanical testing machine, and two Direct Impact Hopkinson Bars (differing in bar diameter) (Walley & Field, 1994).

PEEK by Al-Maliky et al. (1998) using an expanding ring technique, and Hamdan and Swallowe (1996 & 1996) using a modified striker bar launch system (a cross-bow) within their split-Hopkinson bar.

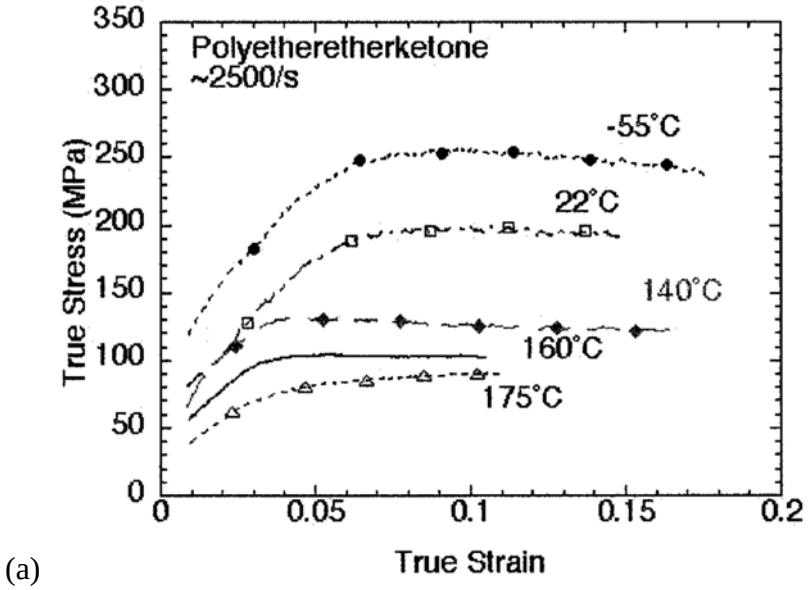
These studies revealed a bilinear behavior occurring before the drop in yield stress – thus an increased rate sensitivity of yield within the high rate regime and then a decrease that

followed with still further rate increases. It is likely that Walley and Field missed out the very narrow range of rates in which the increase in yield stress is observed. Supporting their conclusions with X-ray diffraction studies, Al-Maliky (1998) attributed the observed processes to be an increasing cystallinity of the samples or the introduction of a further activated rate process, and it would therefore appear that whatever process causes the crystallinity to increase $>10^2$ s^{-1} can no longer operate at rates $>10^4$ s^{-1}.

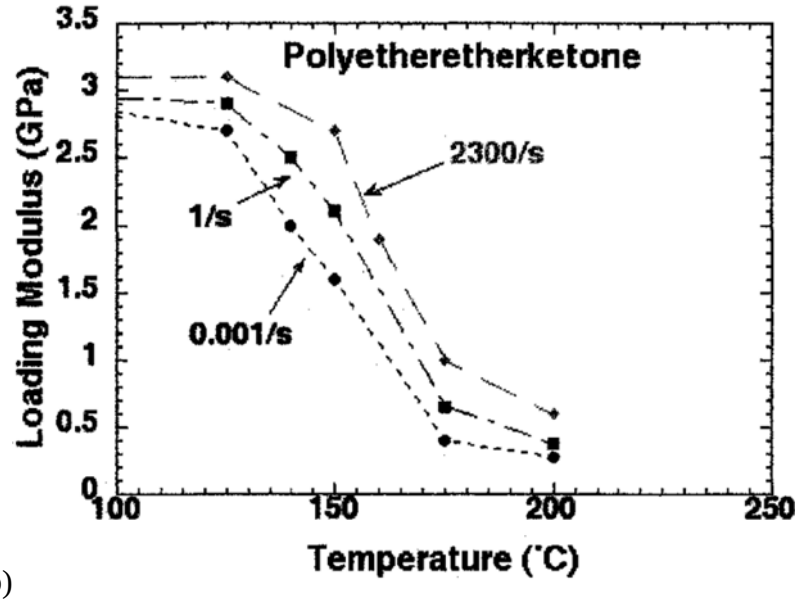
In contrast, Dioh et al. (1993 & 1994) argued that increases in rate sensitivity are due to specimen size effects in the Hopkinson bar and showed that the effect is reduced for smaller specimen thicknesses. Hamdan and Swallow (1996 and 1996), and Swallowe and Fernandez agreed with Al-Maliky in his conclusions regarding the increase or decrease in crystallinity. Swallowe and Lee (2003) later presented data for PET demonstrating that the increase in crystallinity develops late enough into the deformation to not be able to contribute to the flow and yield stress, saying that the activation volume changes perhaps play a role.

Cady et al. (2003) studied the mechanical response of several polymers under dynamic loading (using a SHPB) over a range of temperatures (-55°C to 300°C) and strain rates in order to present a comprehensive study on the relationship between temperature, strain rate, and the initial slope of the stress-strain curve known as the 'loading modulus,' or 'elastic modulus'[2]. The authors were able to locate the glass-transition temperature (T_g) at different strain rates from the fact that the elastic modulus drops significantly over the temperature range centered about T_g (presented in figure 2-12). Furthermore, the shift in T_g with strain rate was observed for the polymer PEEK, in moving from approximately 145 °C at 10^{-3} s^{-1} to approximately 160°C at 2200 s^{-1}. The authors furthered evidence for the fact that yield stress, flow stress, and loading modulus increase with increasing strain rate or

[2] However, it is generally accepted that elastic modulus cannot be derived for Hopkinson bar experiments because the specimen is not in mechanical equilibrium.



(a)



(b)

Figure 2-12: (a) Compressive stress-strain behavior of PEEK at five different temperatures tested at 2500 s^{-1} and (b) the rate dependency of loading modulus as a function of temperature demonstrating the shift in T_g seen in PEEK at different strain rates. Cady et al. (2003).

decreasing temperature for several polymers – making the qualitative equivalence between temperature and strain rate clear and stating explicitly that, "low temperature/low strain rate tests can be used to simulate higher temperature/higher strain rate tests" in making a reference to how these sorts of materials may be modeled. Richeton (2005) added to this relationship with his experimental findings in uniaxial compression of PC, PMMA, and polyamideimide (PAI), as well as furthering the development of understanding the

"secondary transition by linking the yield behavior to the energy associated to the β mechanical loss peak."

Further developing temperature- and rate-dependent research in polymers, Siviour et al. (2005) investigated PC (a glassy polymer) and PVDF (a semi-crystalline polymer), and expanded on studies previously conducted at Cambridge. In researching the temperature-dependent behavior, experiments were conducted across a wide range of strain rates (10^{-4} s^{-1} and 10^{4} s^{-1}) and a wide range of temperatures (-50 °C to 150 °C). Siviour related temperature and strain rate by using a simple mapping equation:

$$T - T_0 = D\left(\log\frac{\dot{\varepsilon}_0}{\dot{\varepsilon}}\right) \tag{2.17}$$

where D is a mapping parameter that quantifies the interaction between rate and temperature and maps from a temperature T to a new temperature T_0, and mapping the strain rate $\dot{\varepsilon}_0$ to a new strain rate $\dot{\varepsilon}$ (i.e. a set of data would be comprised of room temperature experiments at T_0 = 21°C while varying strain rate, and a set of data would consist of experiments at a strain rate of $\dot{\varepsilon}_0$ =1000 s^{-1} while varying temperature). This mapping aided conclusions regarding the increase in rate sensitivity being due to the β-transition (a material property) moving to room temperature at high strain rates for PC. This was done by relating the increased sensitivity to high strain rate to an equivalent increase at low temperature. Siviour et al. presented strong evidence of the temperature and strain rate relationship with respect to the yield stress, or "peak stress," by plotting a variation of peak stress with temperature and also the variation of peak stress with strain rate mapped onto temperature, seen clearly in figure 2-13. Room temperature data illustrated that PC exhibited an increase in rate sensitivity of yield in the high rate regime, as compared to the low-rate tests. In constant rate testing ($\dot{\varepsilon}_0$ = 5500±500 s^{-1}), a similar transition was seen in the temperature-dependent yield behavior

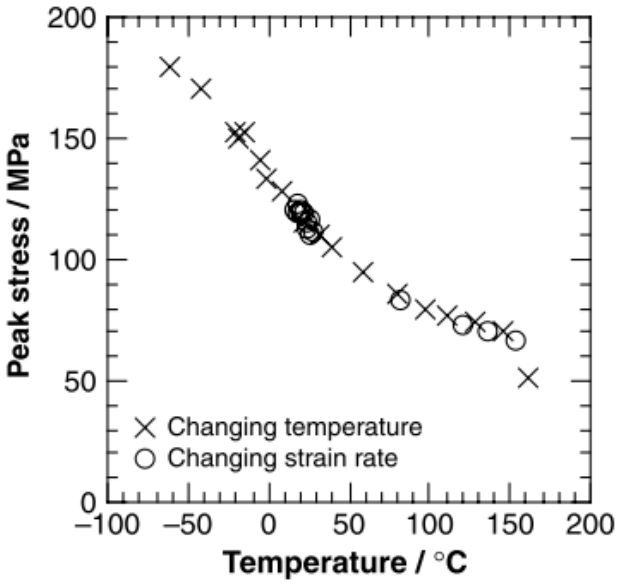


Figure 2-13: Comparison of the variation of peak stress with temperature, and the variation of peak stress with strain rate mapped onto temperature of PC. (Siviour et al, 2005).

located at approximately 40°C. Through the extrapolation of dynamic mechanical and thermal analysis (DMTA) data (explained previously in section 2.2.4), both of these yield transitions were found to occur under the same strain rate conditions/temperature conditions as the viscoelastic β-transition.

Mulliken and Boyce et al. (2006 & 2008), researched PC in uniaxial compression at high rates (greater than 1000 s^{-1}) on a SHPB apparatus and compared the data to tests performed at low strain rate (0.5 s^{-1}), while analyzing the specimen temperature as a function of strain with an infrared (IR) detector system. In 2008 (Garg et al.), they not only confirmed the presence of an additional energy barrier to yield at higher strain rates (greater than 100 s^{-1} for PC - as previously seen in Rietsch and Bouette, 1990), or the 'β-transition regime', but also measured temperature rise as a function of inelastic strain in order to better understand thermal softening issues in polymers. Results from PC experiments are presented in figure 2-14.

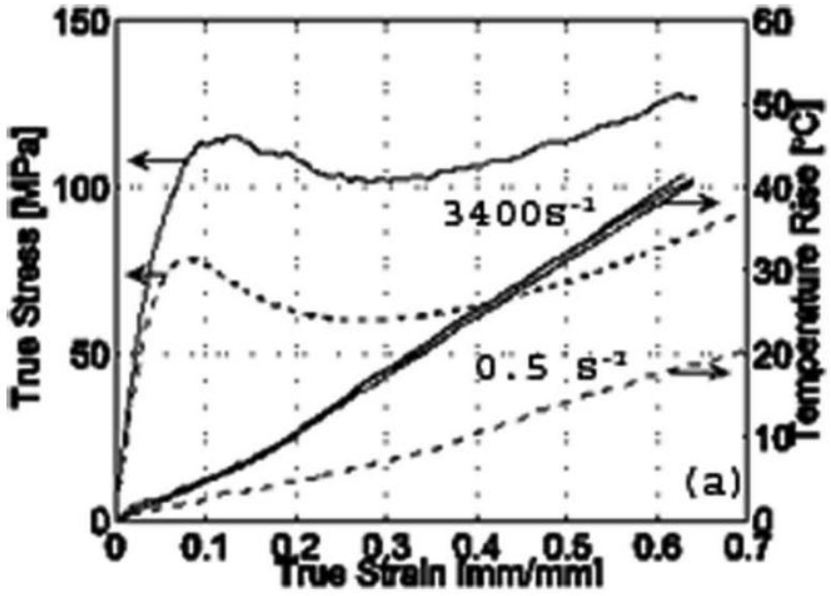


Figure 2-14: PC true stress-true strain behavior accompanied with the experimentally measured temperature rises at 3400 and 0.5 s^{-1} rates of deformation. Garg et al. (2008).

More recently, multiple papers in polymers used for composite systems and polymer-based composite materials have been studied while using a split-Hopkinson pressure bar as the primary form of dynamic testing with the use of high speed cameras. Gerlach et al. (2008) investigated a very brittle material, thermosetting resin RTM-6, up to strain rates of 10^4 s^{-1}. Testing was conducted on both a steel compression SHPB system and a tension SHPB system. The authors were able to develop a novel pulse shaping technique for their tensile SHPB experiments in the form of a pre-loading bar which sits at the end of the incident bar. Koerber et al. (2010) tested a unidirectional carbon-epoxy prepreg system HexPly IM7-8552, or an 'intermediate-modulus fibre and toughened resin system' on a compression SHPB system to examine in-plane shear properties. Both groups used photography in directly measuring strain of their specimens (and additionally for fracture angles in Koerber's work), and pulse shaping techniques to achieve dynamic equilibrium in investigating the respective and challenging materials.

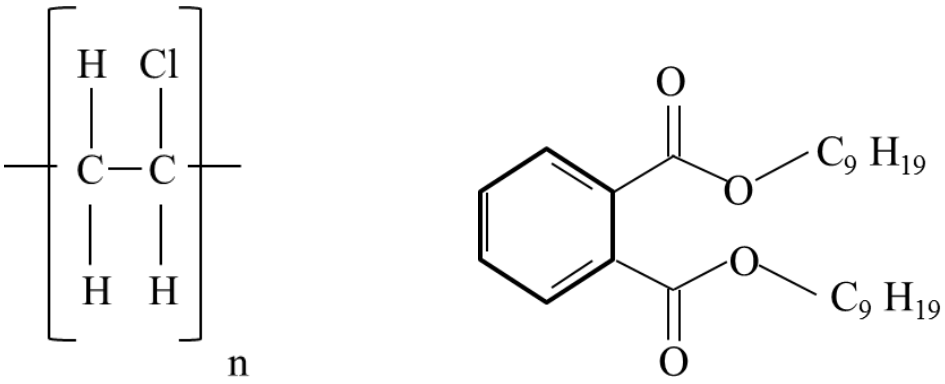
Chapter 3

Rate Dependence of PVC & the Effects of Plasticizer

Four different PVC materials varying in plasticizer content were studied. Adjusting the plasticizer content allows the temperature at which the α-transition (glass transition) and β-transition occur to be moved in order to better examine the interplay of temperature and strain rate dependence in the material. This chapter includes work presented in Kendall and Siviour (2013) in the journal Polymer, and work from Kendall and Siviour (2012) presented at a Dymat Conference in Freiberg, Germany.

3.1 Introduction

The mechanical properties of polymers are studied because of their widespread scientific and industrial importance, as seen in the automotive, aerospace, military, and medical industries. Most polymers (including PVC and its plasticized counterparts) exhibit time dependent mechanical behavior, as evidenced by rate-dependent elastic moduli, yield strength and post-yield behavior. This rate and temperature sensitivity is seen to change in different temperature and rate regimes (with sensitivity increasing at higher rates of strain) depending on different molecular mobility mechanisms being activated. In several polymers, the sensitivity is understood to increase at higher rates and/or lower temperatures because of a lack of secondary molecular mobility (β-motions), which causes increased strength and



(a) (b)

Figure 3-1: Chemical structure of (a) poly(vinyl chloride) and (b) diisononyl phthalate.

Table 3.1: Selected properties of unplasticized PVC and plasticized PVC (Titow, 1984 and Soong et al., 2006).

Property	Unplasticized PVC	Plasticized PVC
Density [g cm^{-3}]	1.3–1.45	1.1–1.35
Tensile strength at yield [MPa]	31–60	10–25
Young's modulus [MPa]	2500	250
Glass Transition Temperature[°C]	82.4	-20
Melting Point [°C]	100-260	40-50
Thermal conductivity [W m^{-1} K^{-1}]	0.14–0.28	0.14–0.17

stiffness (Bauwens et al., 1969; Walley & Field, 1994; Porter & Gould 2009). Alternatively, the increased strength in more rubbery or elastomeric polymers is accounted for by the change in molecular mobility during the glass transition (or α-transition). These transitions are usually seen within polymers at lower temperatures, but can be shifted in temperature by changes in strain rate, as the transition increases in temperature with increasing strain rate (Bauwens-Crowet, 1973; Siviour et al. 2006; Soong et al., 2006).

The capability to alter these molecular-level transitions through the incorporation of additives (i.e. plasticizers) offers new opportunities to understand the mechanical properties of polymers. In many applications in which poly(vinyl chloride) (PVC) is used (figure 3-1a), it is blended with a plasticizer based on an phthalate ester compound, such as diisononyl phthalate (DINP) (figure 3-1b). The plasticizer is used to enhance ductility and decrease properties such as the yield stress and stiffness. By changing the amount of plasticizer the

temperature- and rate-dependence are potentially changed, allowing one to better analyze and compare the mechanisms that govern these dependencies. Thus materials such as PVC have the potential to offer great insight into understanding the interplay between temperature and rate dependence of polymers. Selected properties of unplasticized PVC and plasticized PVC are listed in table 3.1.

This chapter describes a combination of experimental and analytical research which were conducted with attention to the extensive theory and understanding that has been established in the literature, and discussed in Chapter 2. A wide range of experimental investigations were pursued in studying the rate and temperature dependence of PVC, with the goal to establish an experimental strategy to better understand interplay between temperature and strain rate in the PVC materials tested so that high rate tests can be better understood, or even avoided.

3.2 Materials

Table 3.2: The four PVC materials chosen for the investigation presented with the amount of plasticizer in parts per hundred resin (phr).

Resin	Label in text	Amount of Plasticizer [wt%]	Measured Density [g·cm^{-3}]
DGA166-09	PVC	0	1.429
264-01PC	PPVC-2	20	1.317
264-03PC	PPVC-4	40	1.263
264-05PC	PPVC-6	60	1.214

Four different PVCs with the same base polymer were chosen for this research and were manufactured and supplied by Solvin. As seen in table 3.2, the four PVCs examined range from an unplasticized form, ‘PVC,’ listed at the top, to the most plasticized form, ‘PPVC-6,’ listed at the bottom, with a high plasticizer level of 60 wt%. DINP was used as the

plasticizing agent. The PVC came as pressed plates with dimensions of 11.5 x 20 cm and a thickness of 2.5 mm. These plates were machined to the specified specimen geometries.

3.3 Uniaxial Compression

3.3.1 Specimen Geometry

All specimens were right circular cylinders with the axis of the specimen in the loading direction perpendicular to the plane of the plate. Previous work has suggested that length-to-diameter ratios of 1:2 or less are required in the testing of low-impedance materials at high rates in order to achieve equilibrium. This geometric ratio has demonstrated optimal results in minimizing the effects of axial, radial, and tangential inertia in the specimen, and wave propagation in high rate testing (Davies & Hunter, 1963; Gorham, 1989).

The specimen length was fixed by the 2.5 mm thickness of the plates, and diameters of 5 mm and 8 mm were initially used. During the initial testing of PVC and PPVC-6, both specimen sizes were used at all rates in order to allow for a more straightforward comparison between rates. All specimens were lubricated on both faces with a thin layer of petroleum jelly, which has shown a reduction of friction to a negligible value within experimental error over a wide range of temperatures (Trautmann et al., 2005), and little to no barrelling was observed. During SHPB testing, a thin layer of petroleum jelly was used on the impact side of the incident bar for pulse shaping the incident pulse. The thin layer of petroleum jelly has a distinct effect on reducing the characteristic high-frequency Pochhammer-Chree (Pochhammer, 1876 & Chree, 1889) oscillations associated with the propagation of the stress pulse, and increases the rise time of the incident pulse (softens sharpness of pulse), which assists in establishing stress equilibrium (Richeton et al., 2006). Dynamic equilibrium was achieved before yield in all tests, due to pulse shaping and the short specimen length.

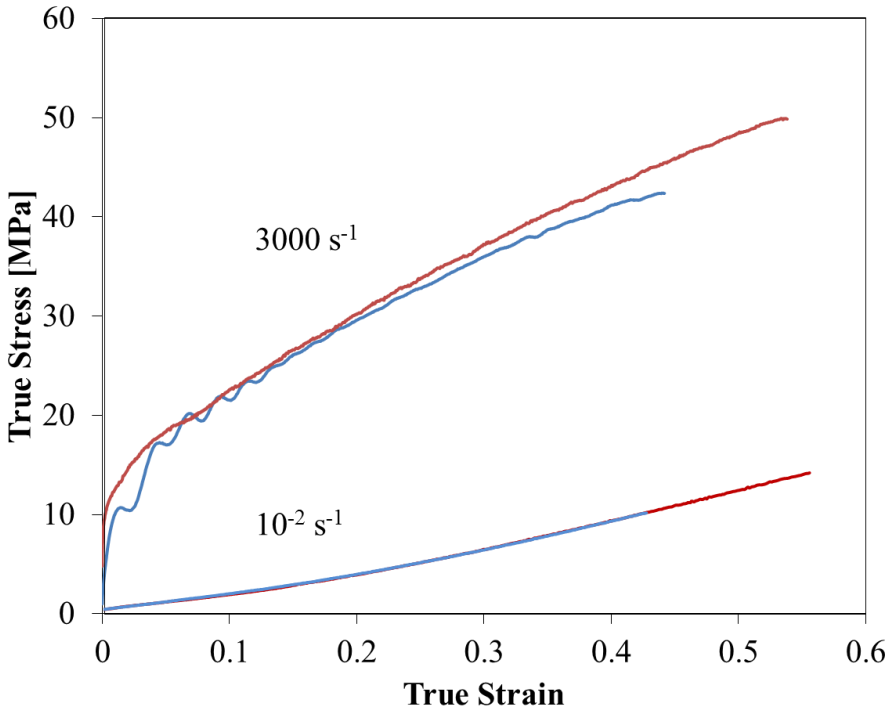


Figure 3-2: PPVC-6 true stress-true strain response at 10^{-2} s^{-1} and 3000 s^{-1} using 5 mm (red lines) and 8 mm (blue lines) diameter specimens. Ringing is observed in the true stress-true strain response at 3000 s^{-1} of the 8 mm specimen.

During low rate tests, both specimen sizes (PVC & PPVC-6) demonstrated nearly identical material responses to deformation. The only observed differences were in the amount of strain to which the specimen could be loaded, because the 8 mm specimen is stronger and the maximum load was determined by the capacity of the load cell used. In high rate tests, however, an undesirable amount of ringing was observed in the results from the 8 mm specimens as compared to the 5 mm specimens, as seen in figure 3-2. This is thought to be due to increased radial inertia, or dispersion, in the 8 mm specimen. The 8 mm specimens were therefore discontinued.

Inertial contributions and room temperature flow stresses for each material (using 5 mm diameter specimens) are compared in table 3.3. These values were calculated using the equation of Gorham (1989), equation 2.13, which is discussed in greater detail in section 2.4. It is shown that inertial contributions are negligible compared to the room temperature strength of each material tested (all PPVCs and PVC).

Table 3.3: Inertial contributions of each material compared to the room temperature (20 °C) flow stresses at the highest rates tested.

Material	Strain Rate [s^{-1}]	20 °C Flow Stress [MPa]	Inertial Contribution [kPa]	Negligible contribution?
PVC	6300	155	100	Yes
PPVC-2	7550	140	68	Yes
PPVC-4	14000	65	24	Yes
PPVC-6	13500	26	16	Yes

3.3.2 Experimental Method

Uniaxial compression tests were performed over rates ranging from 10^{-3} s^{-1} to 14000 s^{-1}. Tests at 10^{-3}, 10^{-2}, and 10^{-1} s^{-1} were performed using an Instron testing machine. Force measurements were taken from the load cell and displacement measurements from a clip gage extensometer attached to the loading platens. Quasi-static experiments were conducted over the temperature range -115 to +100 °C using a standard Instron environmental chamber. Temperature readings from the environmental chamber were confirmed by the use of thermocouples attached to the platens adjacent to the specimen-platen interface. When the environmental chamber is used, its size necessitated a very long set of anvils between the cross-head and specimen, which at times caused problems with anvil alignment. In order to correct this, a local fixture was added for better alignment. The Instron mechanical machine's output consists of 4 parameters: time in seconds, displacement of the cross-head in millimeters, load measured by a load cell in Newtons, and the measured strain from an extensometer attached to the platens.

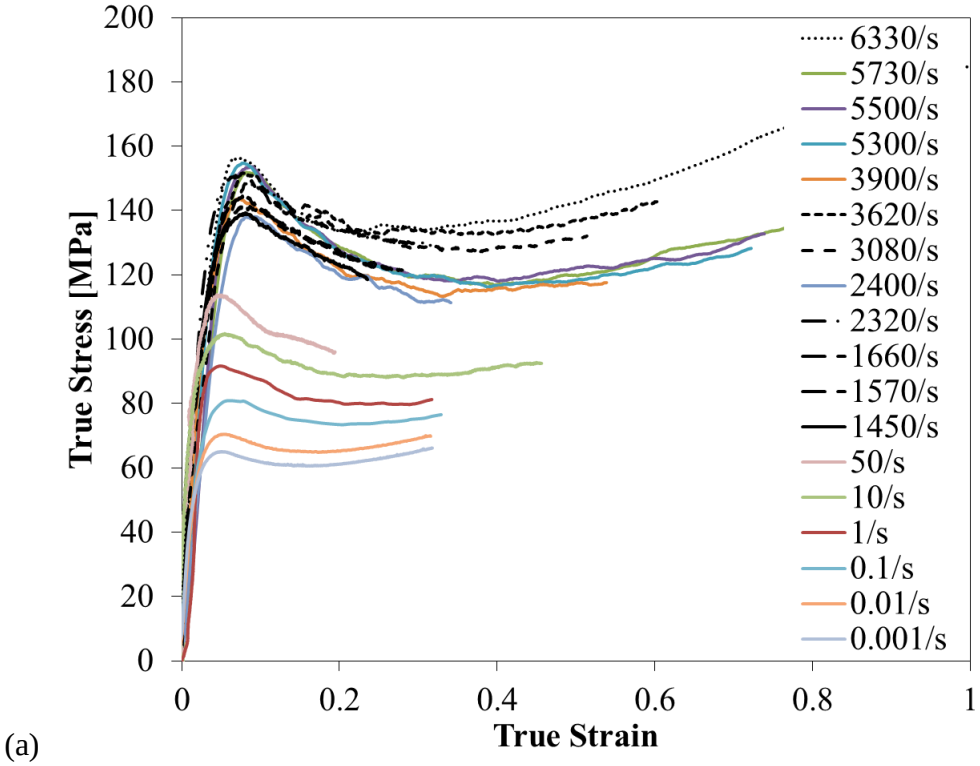
Experiments at rates ranging from 1 s^{-1} to 100 s^{-1} were conducted on a custom-built hydraulic load frame. Linear variable differential transformers (LVDTs) were used to measure the displacements of the anvils, and a strain gauge based load cell measured the

force supported by the specimen. These data were used to calculate the stress-strain relationship in the sample.

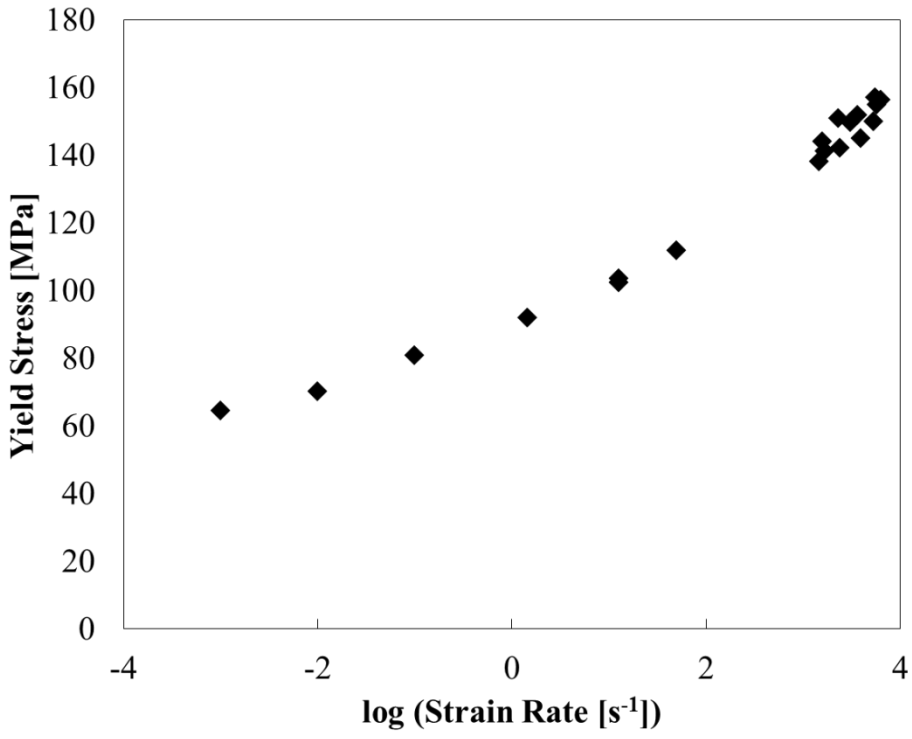
High rate tests were performed from 550 s^{-1} to 14000 s^{-1} on a split-Hopkinson pressure bar (SHPB) apparatus using magnesium alloy (AZM), titanium alloy (Ti-6Al-4V), and steel bars. The striker bar, incident bar, and transmitted bars all had diameters 12.7 mm, with lengths of 0.5 m, 1.0 m, and 0.5 m, respectively. The strain gauges were placed 0.5 m from the specimen-bar interface on the incident bar and 50 mm from the specimen-bar interface on the transmitted bar. The standard analysis described in chapter 2 was used to calculate stress-strain curves, and dynamic equilibrium was confirmed after each test by calculating force-time profiles for both specimen-bar interfaces.

3.3.3 Results and Analysis

Figures 3-3 through 3-11 summarize the rate dependent (at 20°C) and temperature dependent (at 10^{-2} s^{-1}) response of each material tested. The figures provide a summary of the representative low to medium to high rate responses of each material. Each material shows a distinct response to rate and temperature. In this study the yield stress is recognized as the peak stress that the polymer reaches around yield: the intrinsic yield described by Bowden (1973), and this approach will be used in the current research. With more rubbery materials it is the true stress taken at 5% true strain, which is approximately where polymers often yield when below their glass transition temperature.

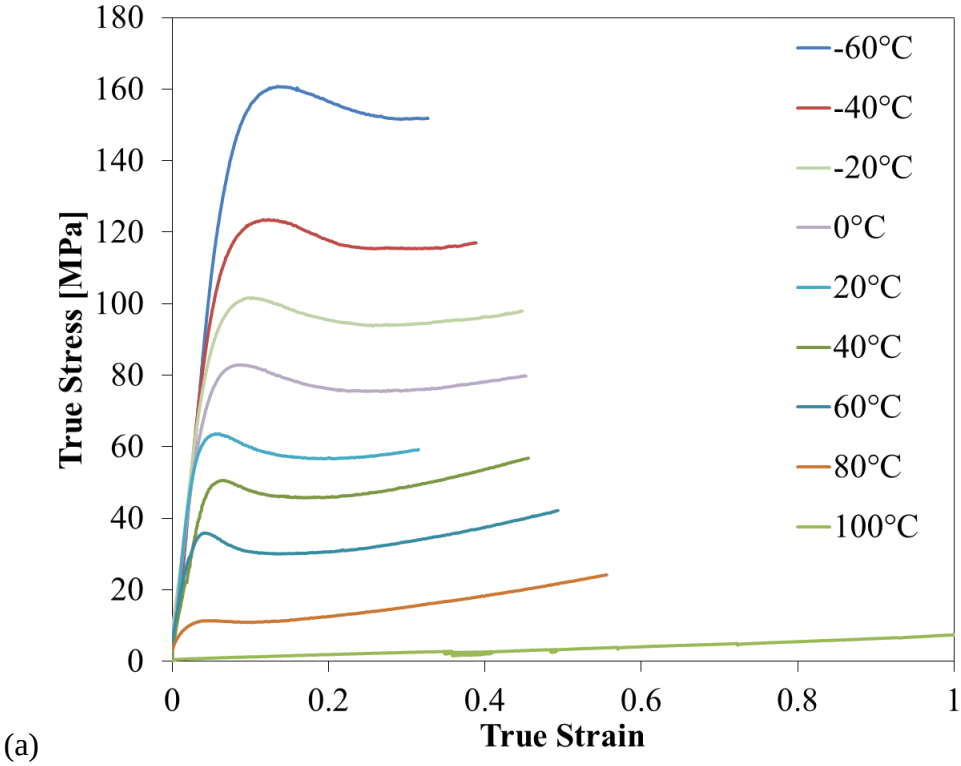


(a)

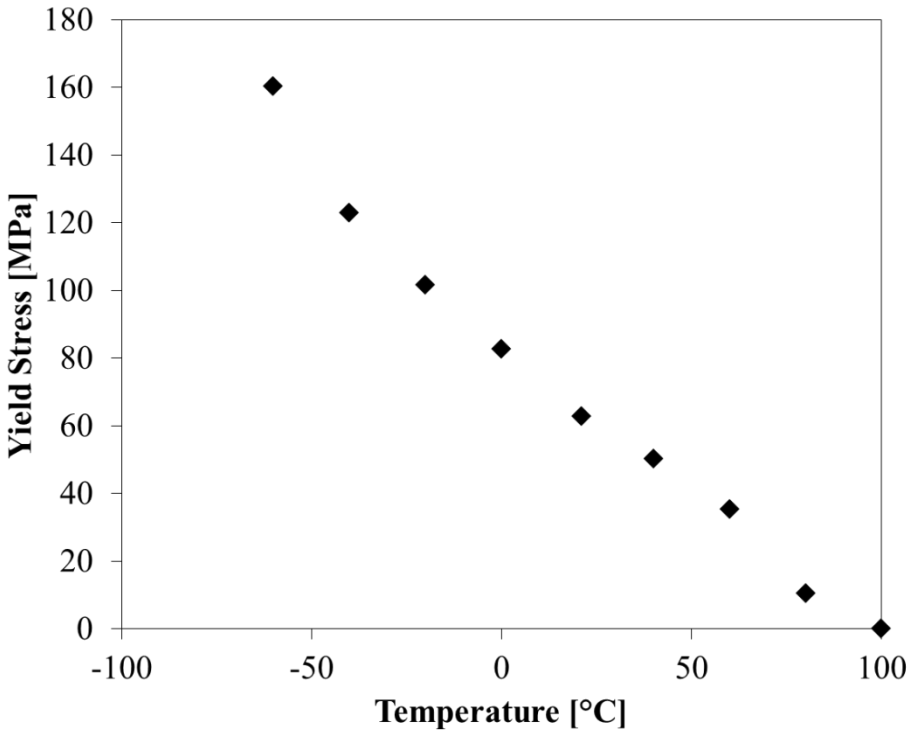


(b)

Figure 3-3: Representative behavior of PVC. (a) True stress-true strain response in uniaxial compression over all rates tested at 20 °C and (b) the true yield stress as a function of strain rate over a logarithmic scale.



(a)



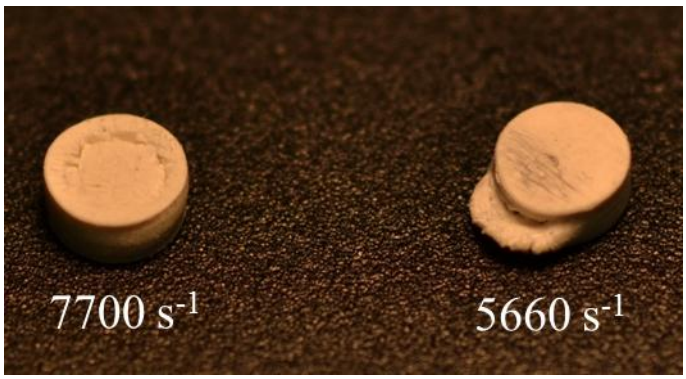
(b)

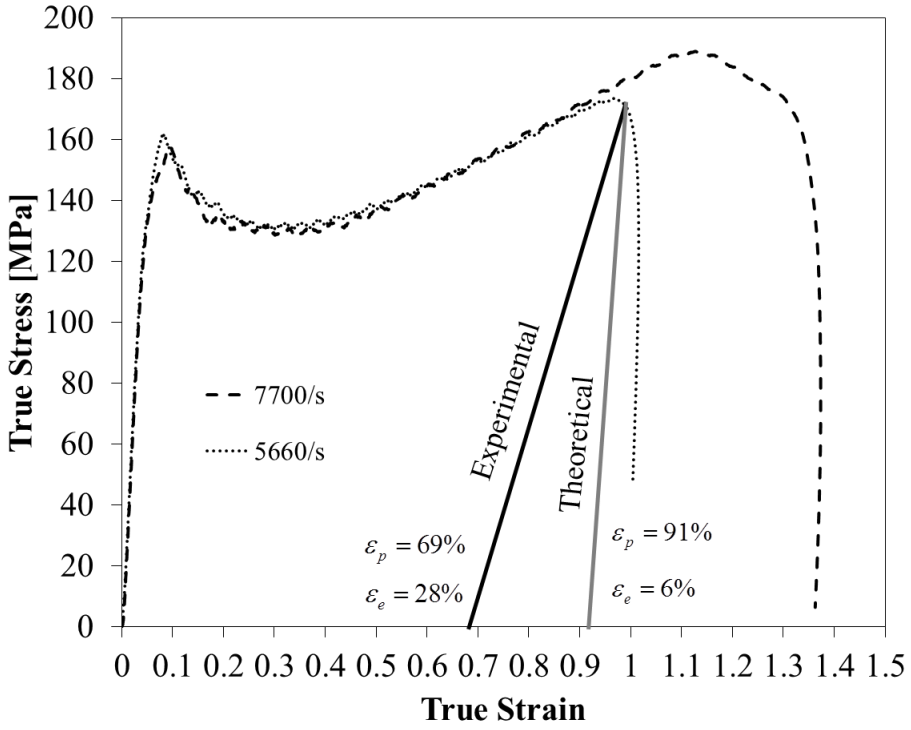
Figure 3-4: Representative behavior of PVC. (a) True stress-true strain response in uniaxial compression over all temperatures tested at 10^{-2} s^{-1} and (b) the true yield stress as a function of strain rate over a temperature scale in degrees Celsius.

The PVC material demonstrates a response to uniaxial deformation consistent with that seen in previous literature (discussed in Chapter 2) in both its temperature dependent and rate dependent responses. Its glassy polymer response is characterized by initial linear visco-elasticity, a non-linear shift to yield, strain softening, and following with strain hardening (presented in figures 3-3a and 3-4a). Within the rate-dependent yield data (figure 3-3b), PVC exhibits an approximately linear dependence in the low to medium rate regime and transitions to a second linear dependence in the high rate regime. The slope of the second linearity in the high rate regime is steeper and corresponds to a material transition which has a combined effect of the β transition and α transition. These transitions become clear upon analyzing DMTA data which will be presented in the following section. In the temperature dependent data this slope increase (reading right to left) of the second linearity can be seen at approximately -50 °C.

Force-time comparison confirmed the stress equilibrium required for homogeneous deformation in each high rate test conducted. Uniquely amongst the materials tested (during post-mortem analysis of test specimens), PVC specimens were observed to form fractures during high rate testing on the SHPB – these fractures occurred at rates higher than 2400 s^{-1} but their formation was not observed to affect the stress-strain response. From both the stress-strain behavior and the stress equilibrium confirmation, these fractures were assumed to occur during the inevitable reloading of the specimen that occurs after the test is completed during SHPB testing. Examples of these fractures are presented in figure 3-5. High speed photography demonstrated that the imprints seen in both 7700 and 5660 s^{-1} testing are a result of specimen expansion to a diameter larger than the bar, allowing for a plastic imprint on the specimen surface and/or an artifact at the side of the specimen. Alongside this analysis, the theoretical elastic recovery was in testing PVC was investigated. The results of this investigation are summarized in figures 3-5 and 3-6.

(a)

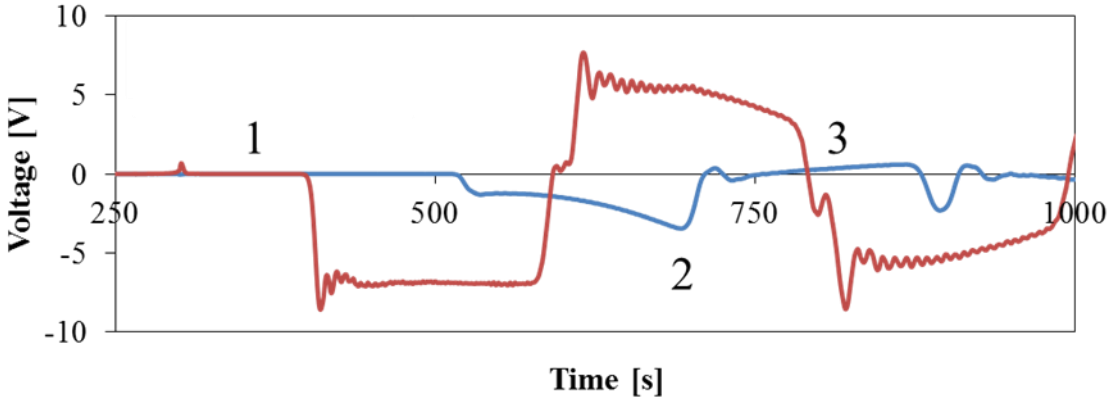




(b)

Figure 3-5: (a) Post-mortem photographs of PVC specimens with observed fractures and the (b) true stress-true strain behaviors of the respective specimens presenting a comparison between observed and theoretical elastic recoveries during testing.

(a)



(b)

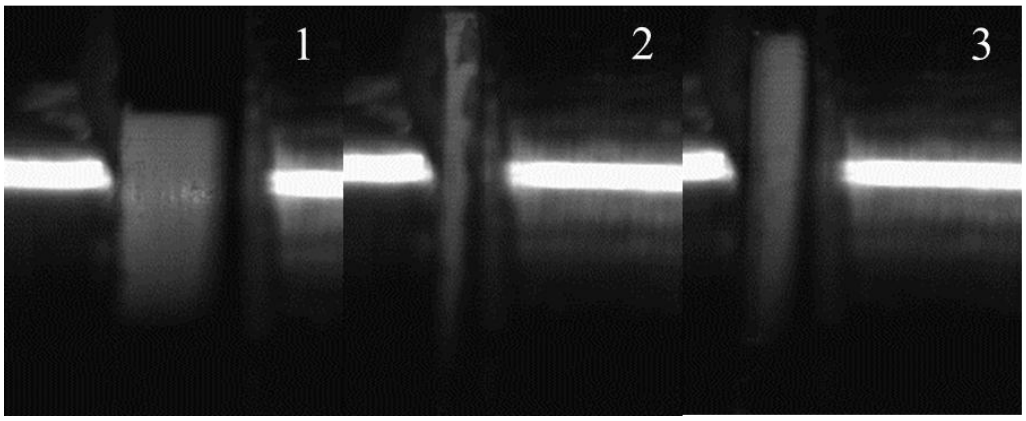
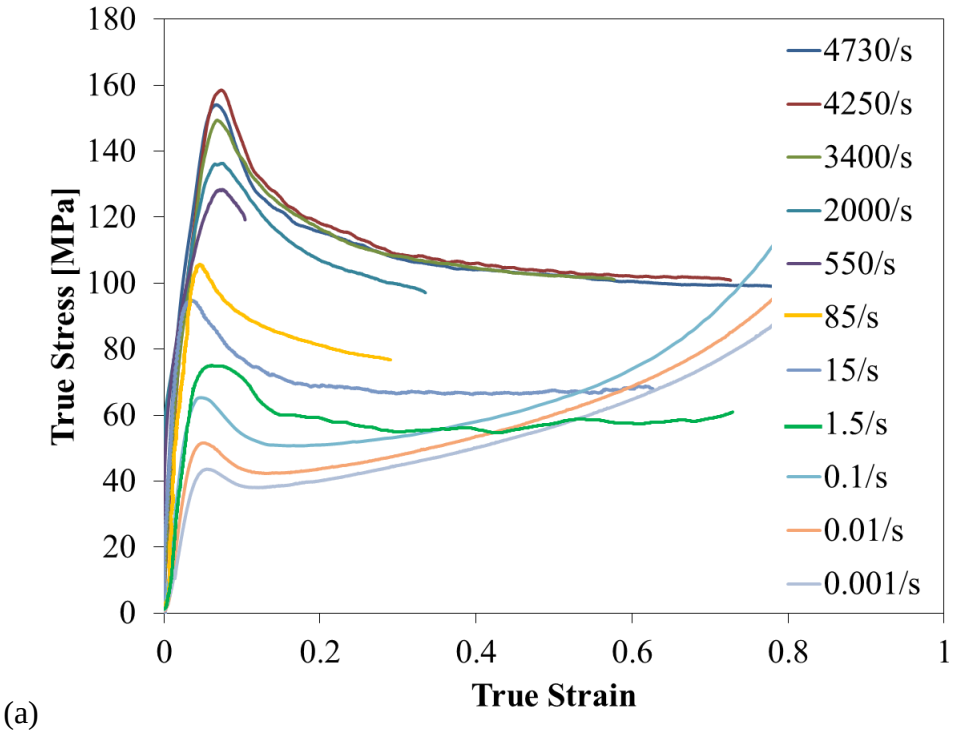


Figure 3-6: (a) Voltage-time plot displaying the input signal (red) and output signal (blue), and (b) respective high speed photographs of a 5660 s^{-1} test which demonstrates the observed unloading and reloading during SHPB experiments. The unloading was used to measure the experimental elastic recovery, which is presented analytically in figure 3-5.

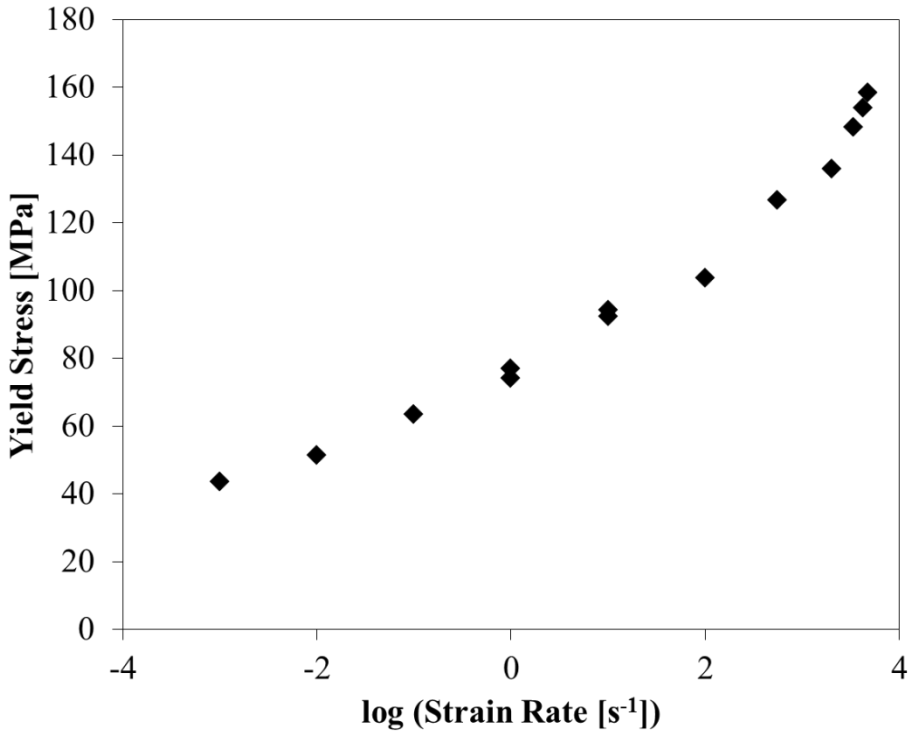
Furthermore, true strain rates were either near constant or varied very little during testing. This is understood to be a result of the closeness of the wave impedance of the bar material and the specimen material, as well as the velocity of the striker bar during testing. These relations are investigated further at the end of this chapter.

The behavior of PPVC-2 in uniaxial compression is summarized in figure 3-7a and 3-8a. The addition of plasticizer (20 wt% for PPVC-2) allows for an increase in strain softening. For example in the highest rate of loading, the yield is *ca.* 160 MPa, dropping to 105 MPa after softening, a drop of 55 MPa compared to 25 MPa in PVC. PPVC-2 also exhibits strong rate dependence, with much less post-yield softening at low rates when compared to medium and high rate responses. Soong et al. (2006) blended a 20 wt% dioctyl phthalate (DOP, Sigma-Aldrich) plasticizer with PVC (PPVC-2), and unlike the results presented here, the authors found an increase in strain hardening compared to (unplasticized) PVC as strain rate increased in value. The increase in strain softening is investigated via multiple temperature measurement methods in Chapter 9, these findings indicate that the softening may be due to adiabatic (or at least non-isothermal) conditions during high rate testing. This observation will be further explored in Chapters 6 and 9.

During deformation a fraction of work is converted into heat. The rate determines the amount of time available for the heat to escape the specimen, where an appropriately high rate would not allow any of the heat to escape the specimen during the time scale of testing (approximately 150 μs) allowing for the PPVC-2 to experience thermal strain softening. This increase in strain softening with increasing rate of deformation has also been seen in PMMA by Arruda et al. (1995). The strain softening of PPVC-2 being more significant in that of PVC emphasizes that the flow stress of PPVC-2 is more sensitive to temperature and strain rate than that of PVC. The temperature dependent data of PPVC-2 are in contrast to the rate dependent data, the isothermal quasi-static behavior demonstrates an increase in the gradient of strain hardening with decreasing temperature, while the rate dependent data demonstrates large amounts of thermal strain softening at these same true strain values. Additionally, when compared to PVC, the shape of the yield is much sharper in the temperature- dependent true

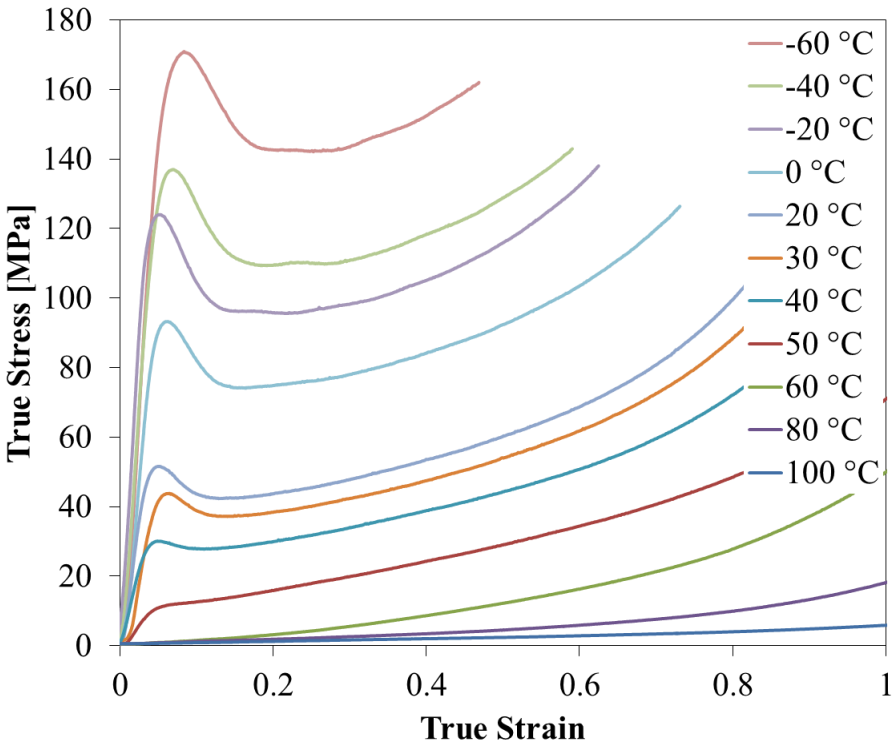


(a)

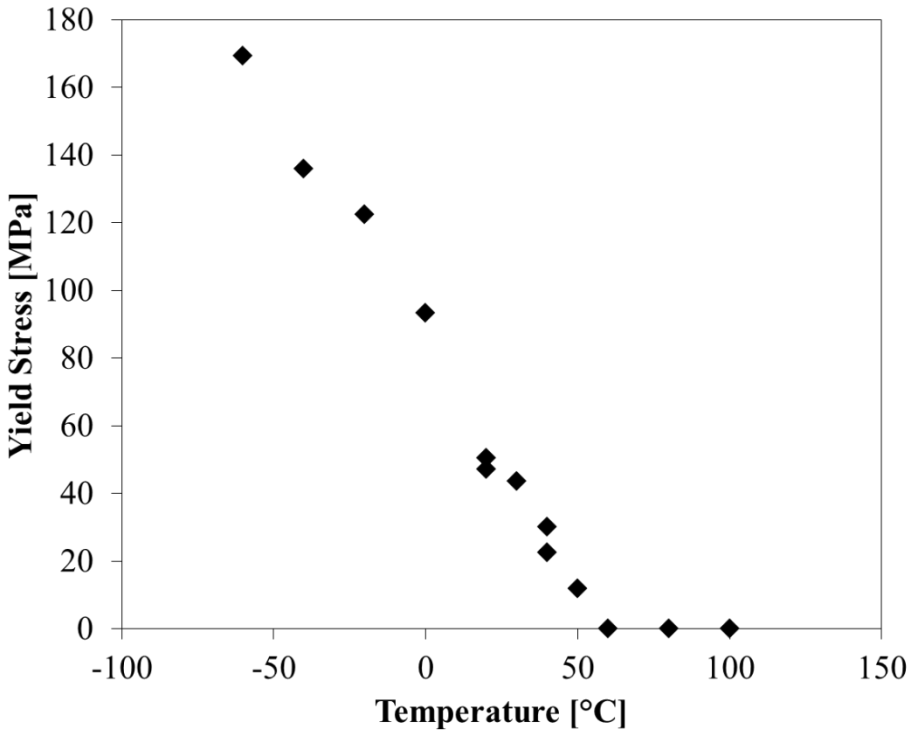


(b)

Figure 3-7: Representative behavior of PPVC-2. (a) True stress-true strain response in uniaxial compression over all rates tested at 20 °C and (b) the true yield stress as a function of strain rate over a logarithmic scale.



(a)



(b)

Figure 3-8: Representative behavior of PPVC-2. (a) True stress-true strain response in uniaxial compression over all temperatures tested at 10^{-2} s^{-1} and (b) the true yield stress as a function of strain rate over a temperature scale in degrees Celsius.

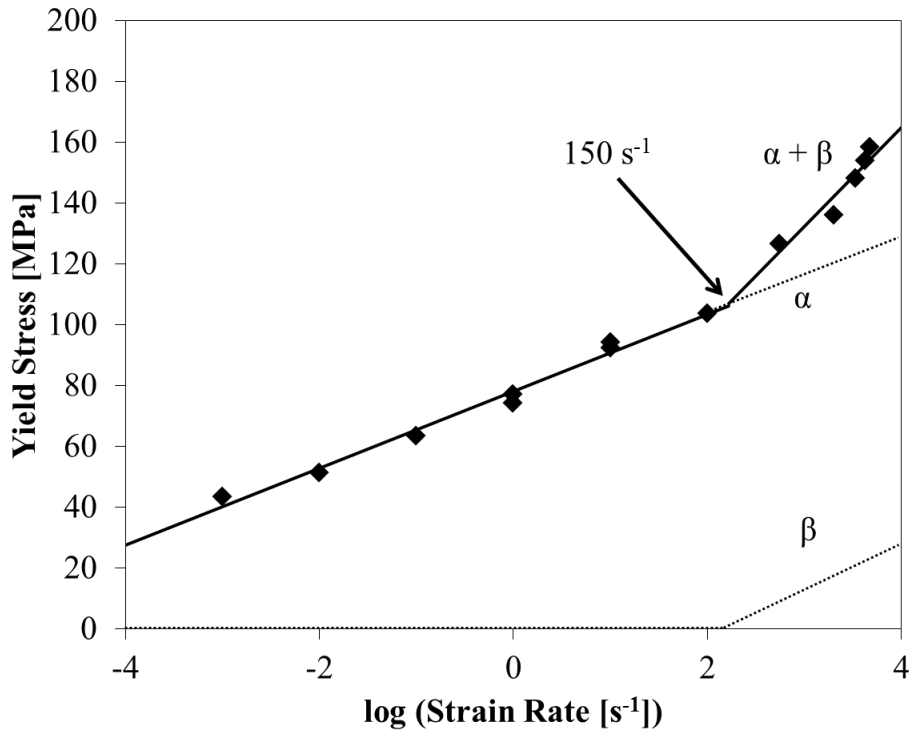
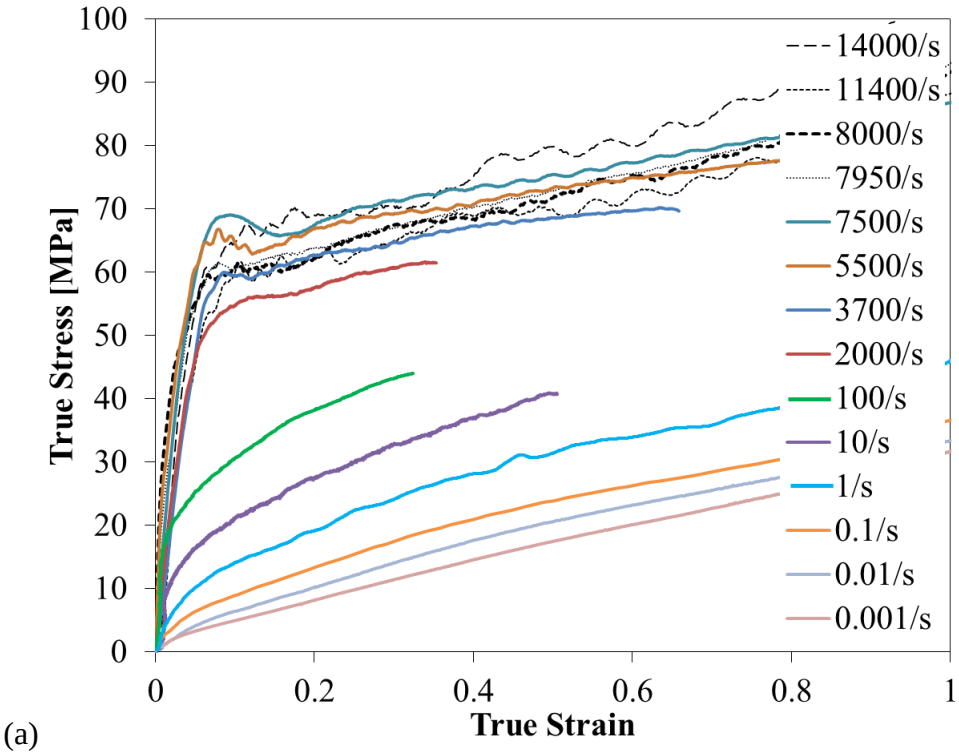


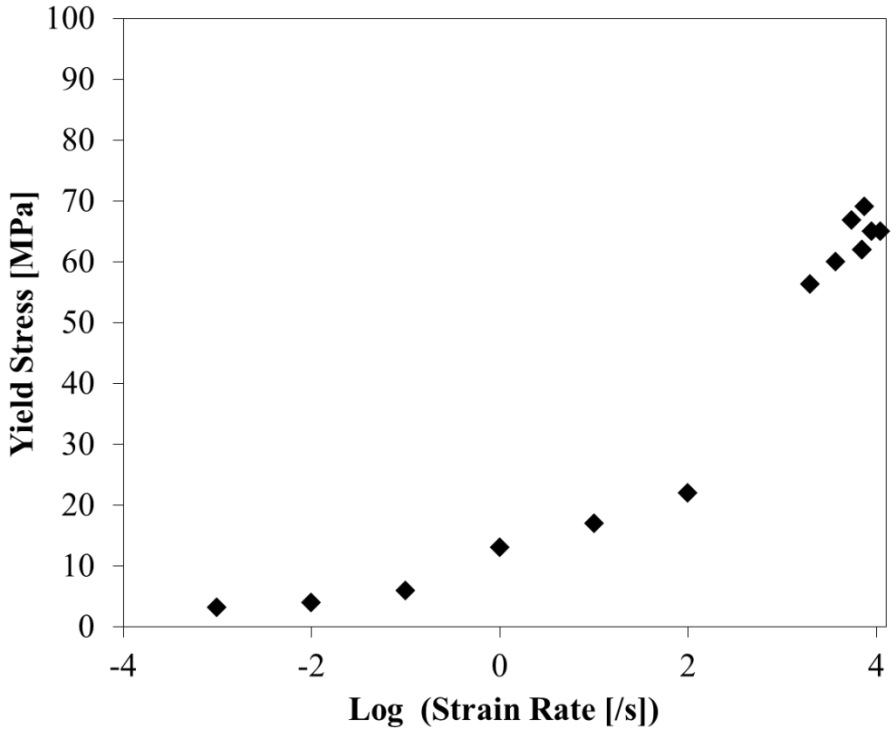
Figure 3-9: True yield stress of PPVC-2 as a function of strain rate over a logarithmic scale presenting the influences of two different rate activated processes (α and β). All tests were conducted at 20 °C.

stress-true strain response of PPVC-2, compared with a much broader yield in PVC data. This sharpness is an additional illustration of the greater sensitivity of the flow stress of that of the plasticized PPVC-2 compared to PVC. This analysis of flow stress will be explored further in Chapters 5, 6, and 9, and is similar to the analyses of Richeton et al. (2006) when comparing amorphous polymers (e.g. PC & PMMA).

The yield stress dependence upon strain rate and temperature of PPVC-2 is shown in figure 3-7b and 3-8b. The rate dependent data illustrates a transition in material response at approximately 150 s^{-1}, which is demonstrated in figure 3-9. The transition is understood to correspond with the addition of the β transition (or a lack of β motions) to the previously single activated process (α) and is more subtly seen in the temperature dependent data at -50 °C, and the DMTA data in the following section.

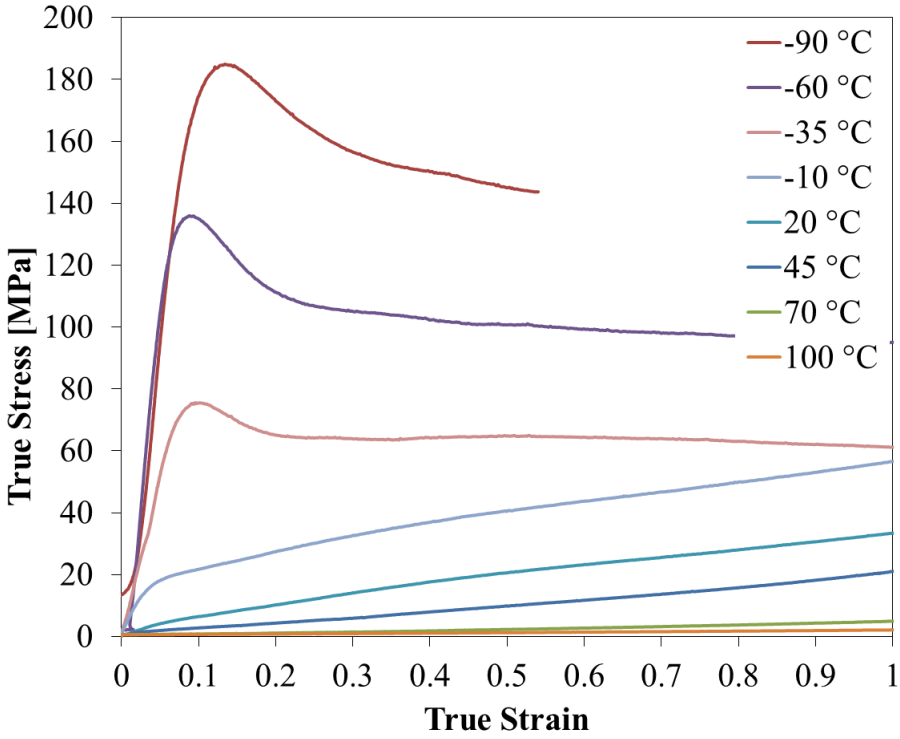


(a)

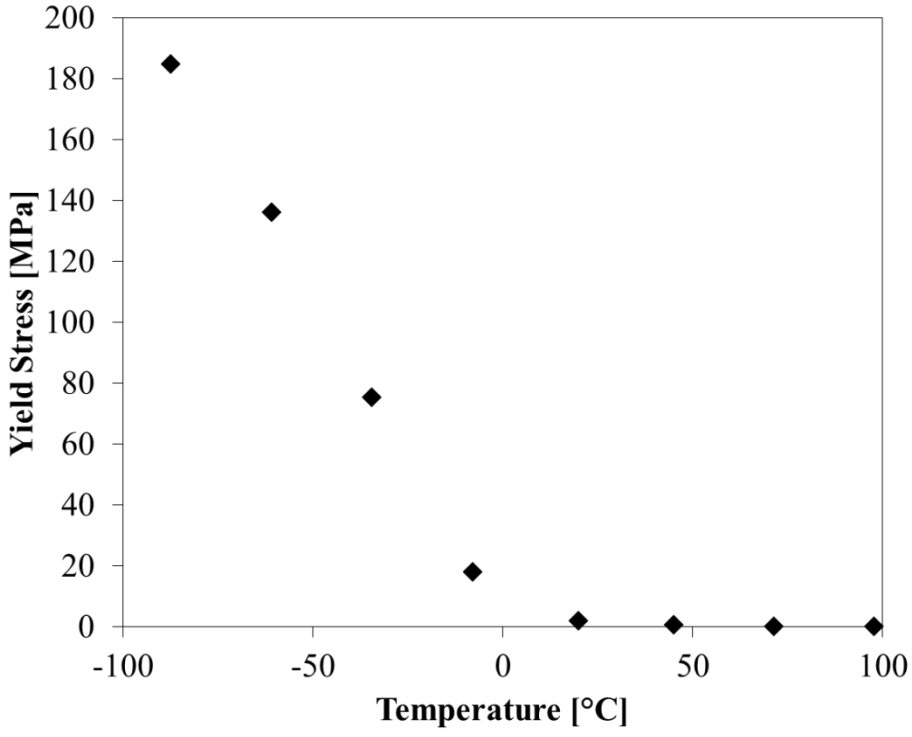


(b)

Figure 3-10: Representative behavior of PPVC-4. (a) True stress-true strain response in uniaxial compression over all rates tested at 20 °C and (b) the true yield stress as a function of strain rate over a logarithmic scale (yield is determined by the maximum stress at 10% true strain for this material).



(a)



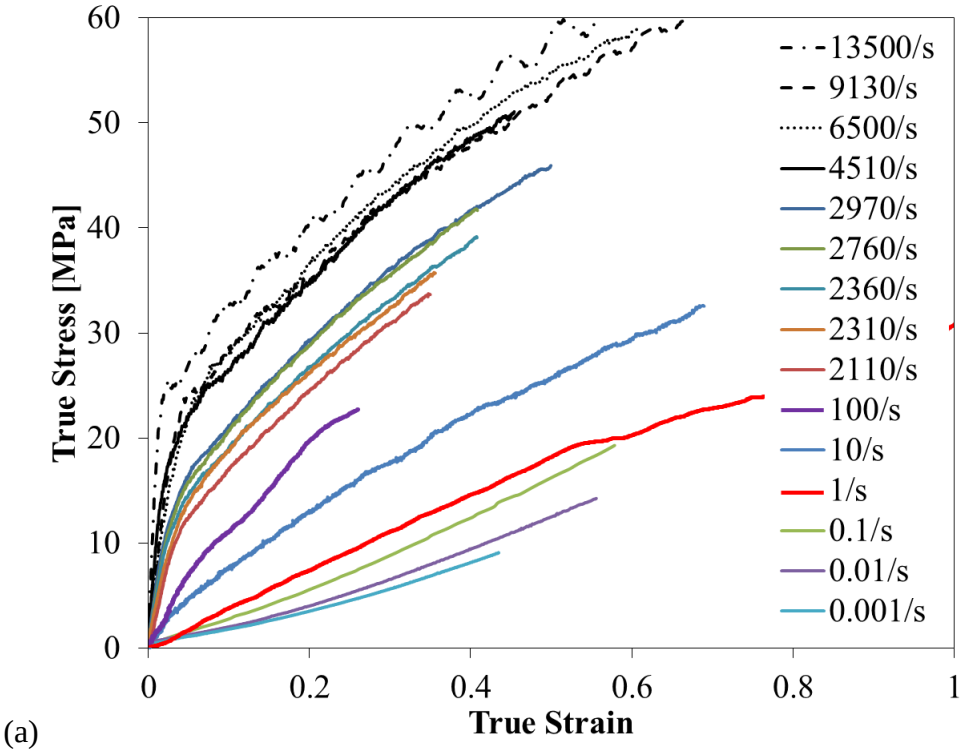
(b)

Figure 3-11: Representative behavior of PPVC-4. (a) True stress-true strain response in uniaxial compression over all temperatures tested at 10^{-2} s^{-1} and (b) the true yield stress as a function of strain rate over a temperature scale in °C.

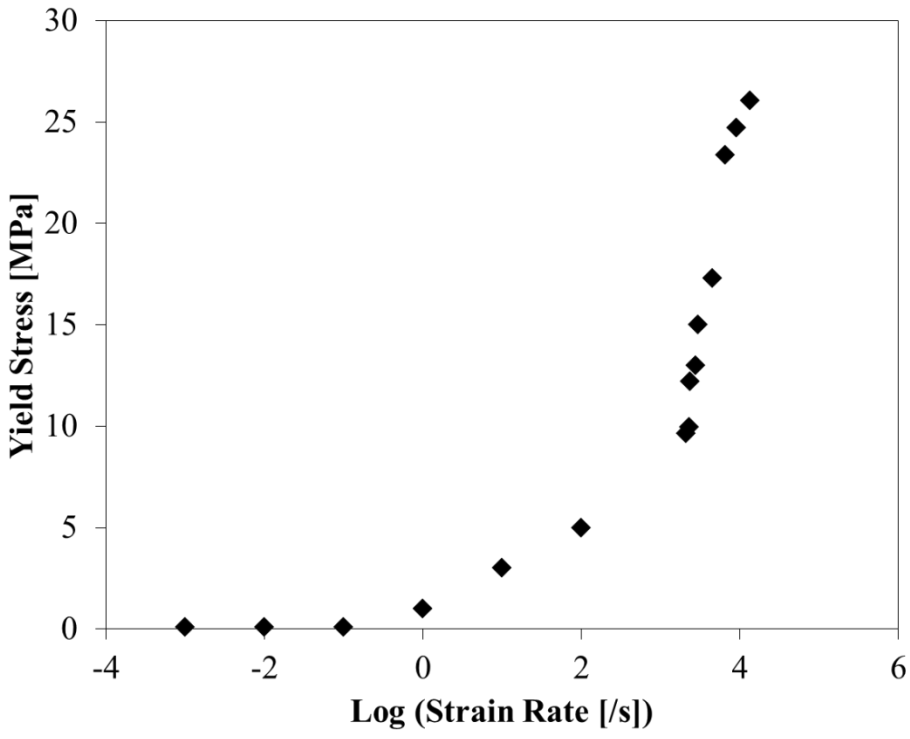
PPVC-4 and PPVC-6 present similar responses to each other which are summarized in figures 3-10 – 3-13. Both have glass transition temperatures well-below room temperature. The glass transition of PPVC-4 is observed in the temperature dependent yield data (figure 3-11b) at approximately 0 °C, while the glass transition of PPVC-6 is recognizable at -30 °C (figure 3-13b). Both of these material transition temperatures have been confirmed by DMTA data (section 3.4). These transitions are also visible in the stress-strain responses in both the temperature dependent and rate dependent data.

PPVC-4 displays glassy polymer behavior in both its temperature and rate dependent stress-strain responses. Interestingly, the rate dependent response of PPVC-4 presents strain-hardening, versus an absence of strain hardening in the temperature dependent response up to the plastic strain tested. More specifically, this behavior is seen in figure 3-10a and 3-11a, when comparing high strain rates (2000 – 14000 s^{-1}) to low temperature data at -35 °C where similar stresses are reached in both sets of data.

The stress-strain temperature dependent behavior of PPVC-6 (figure 3-13b), like PPVC-4 in figure 3-11b, presents three regions, and two material transitions, in its behavior moving from a rubbery response at room temperature (and above) and going through a leathery response up until its glass transition temperature (at -30 °C) where a glassy polymer response is seen in the shape of the yield and post-yield strain softening and subsequent strain hardening. The response of PPVC-4 presents several similarities to that of PPVC-6, although differences are seen in the glassy response at high rates in the rate dependent stress-strain data of PPVC-4 versus the leathery-glassy response at high rates in the rate dependency of PPVC-6, illuminating key differences from the slight increase in DINP-plasticizer content. The PPVC-6 rate dependent stress-strain behavior between 100 and 1770 s^{-1} presents a transition from a leathery response to a response that combines the leathery response and the

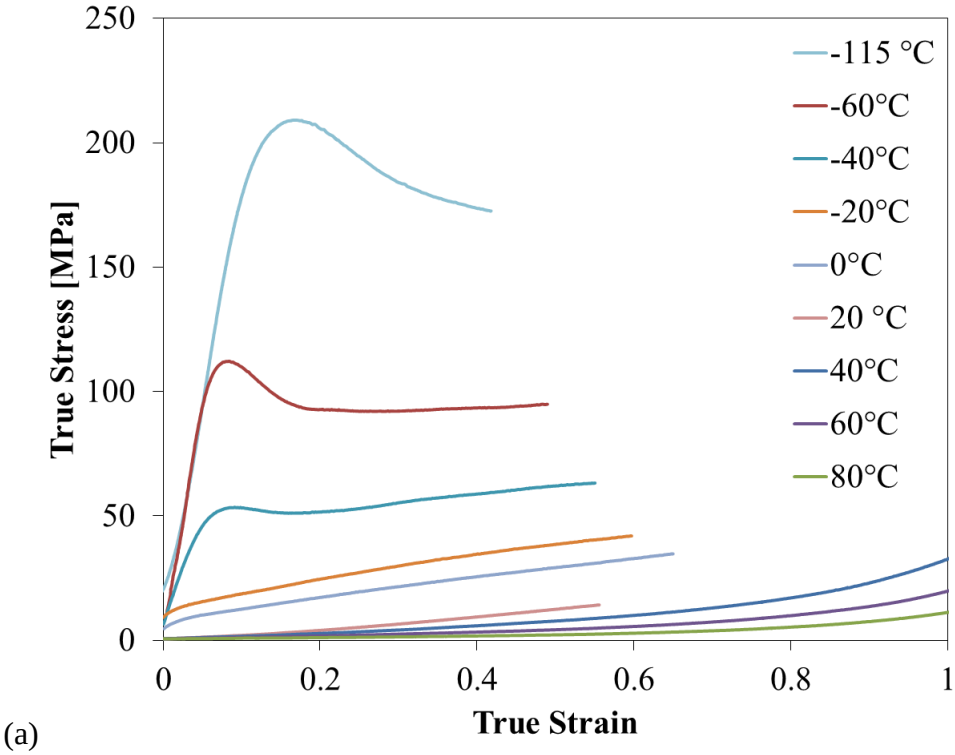


(a)

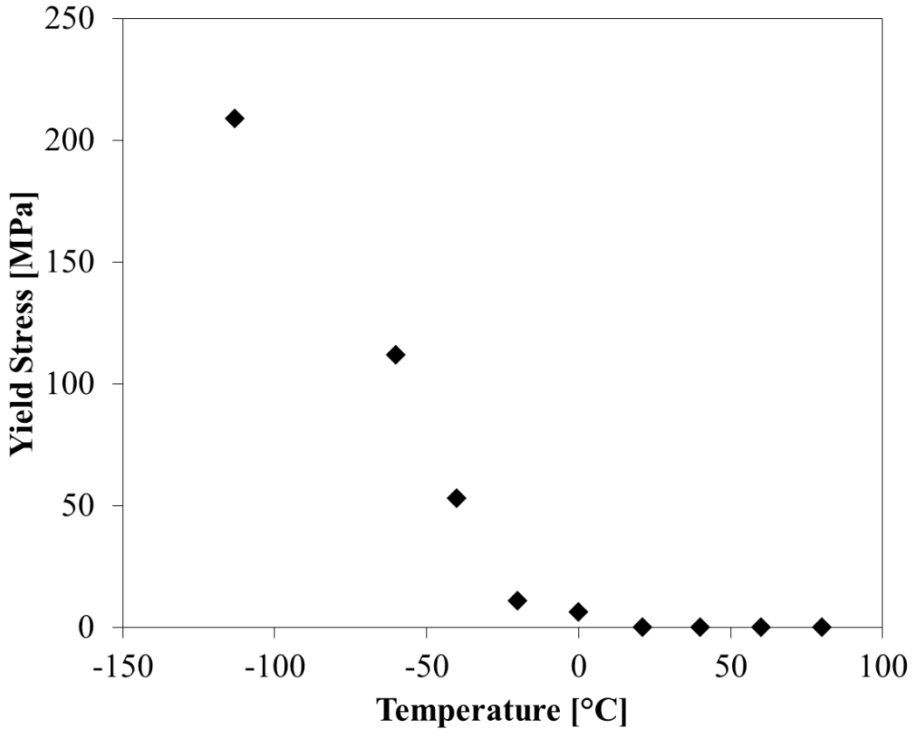


(b)

Figure 3-12: Representative behavior of PPVC-6. (a) True stress-true strain response in uniaxial compression over all rates tested at 20 °C and (b) the true yield stress as a function of strain rate over a logarithmic scale (yield is determined by the maximum stress at 5% true strain for this material).



(a)



(b)

Figure 3-13: Representative behavior of PPVC-6. (a) True stress-true strain response in uniaxial compression over all temperatures tested at 10^{-2} s^{-1} and (b) the true yield stress as a function of strain rate over a temperature scale in degrees Celsius.

glassy response – a glassy polymer yield with post-yield strain softening is not visible. It is worth noting the similarity of the PPVC-6 stress-strain response at -20 °C and the high rate responses of PPVC-6 centered at 2000 s^{-1}, connections such as these highlight interplay between temperature and strain rate which will be exploited and used as the foundation for a proposed simulation method presented in subsequent chapters (5, 6, and 7).

3.4 Dynamic Mechanical and Thermal Analysis

3.4.1 Experimental Method

Dynamic Mechanical and Thermal Analysis (DMTA) testing was conducted at the Department of Zoology and the Institute of Biomedical Engineering at the University of Oxford in order to understand the rate and temperature dependence of the molecular mobility transitions. These experiments were carried out on a TA Instruments Q800 DMTA. The rectangular specimens had dimensions of 2.5 mm height, 10 mm width, and 35 mm length, and were used in the dual-cantilever mode of the DMTA machine with a set amplitude of 20 μm. Tests were performed at temperatures ranging from -150 to 100°C. Testing was conducted at frequencies of 1, 10, and 100 Hz, with the exception of the data presented towards the end of the next section using unplasticized PVC material (in which 0.1, 1, and 10 Hz were used) in order to investigate the methodology of locating the β transition within DMTA and uniaxial compression.

3.4.2 Results and Analysis

Characteristic storage and loss modulus curves for all tested frequencies are shown in figures 3-14 – 3-17, for PVC – PPVC-6 respectively. The test frequencies are converted to their approximate strain rates using equation 2.15 from section 2.2.4.

In figure 3-14, the PVC loss modulus has two large peaks corresponding to two material transitions: the α and the β transitions. PVC has a clear and relatively sharp glass (α)

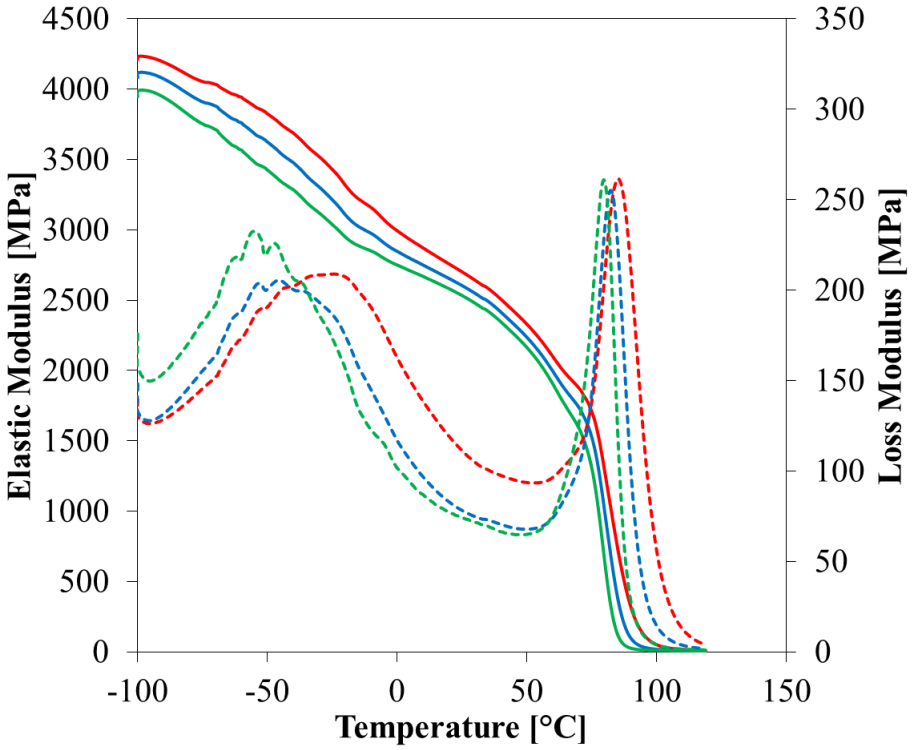


Figure 3-14: PVC elastic modulus (solid lines) and loss modulus (dashed lines) curves at 0.035 s^{-1} (1 Hz – green), 0.35 s^{-1} (10 Hz – blue), and 3.5 s^{-1} (100 Hz – red). β transitions and α transitions are centered respectively at approximately -45 °C and 82 °C. These transitions correspond to the loss modulus peaks at these temperatures.

transition centered at 82 °C which agrees with literature on neat (or 'unplasticized') PVC (table 3.1 and Wang & Arruda, 2001). The α transition is visible in the storage modulus data with a drop in modulus from 2000 MPa to a very small value. In figures 3-15 – 3-17, this transition is seen to shift to lower temperatures with increasing amounts of plasticizer. PPVC-2 has an α-peak located at 45 °C, PPVC-4 at 0 °C, and PPVC-6 at -20 °C. The loss modulus peak corresponding to this transition also broadens with the addition of plasticizer: for PVC it begins at 60 °C and ends just above 100 °C, spanning 40 °C, while PPVC-6 spans up to 100 °C (PPVC-4 also spans 100 °C, and PPVC-2 spans roughly 80 °C). This transition is understood as constrained translations and rotations of large segments of the polymer main chains – this agrees with the addition of a chemical structure such as DINP (figure 3-1b), the plasticizing agent, which is considered to create more 'free volume' in the unplasticized PVC

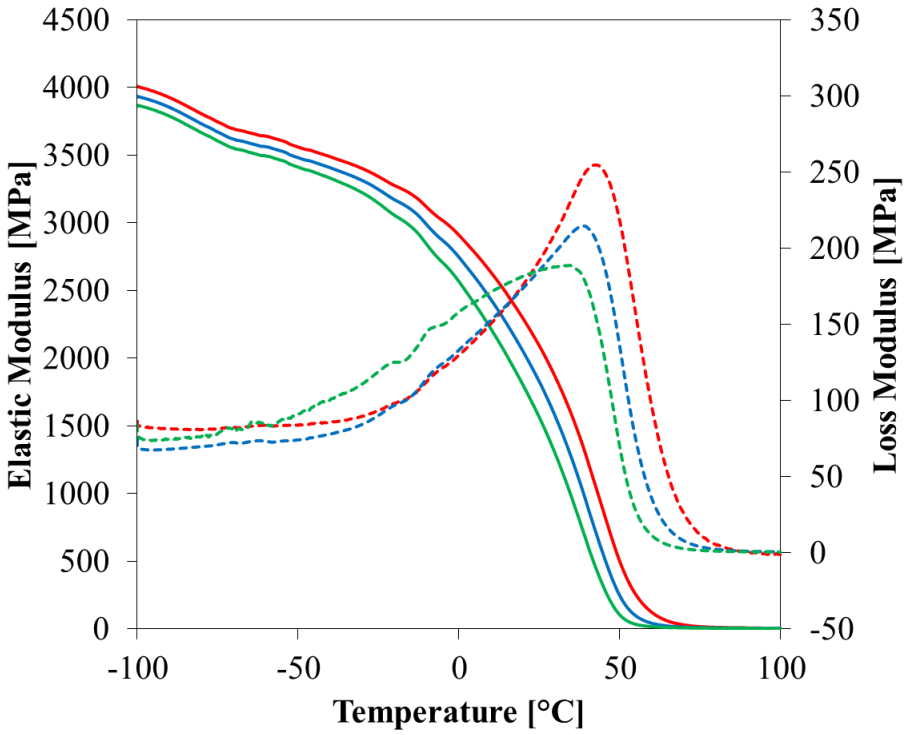


Figure 3-15: PPVC-2 elastic modulus (solid lines) and loss modulus (dashed lines) curves at 0.035 s^{-1} (1 Hz – green), 0.35 s^{-1} (10 Hz – blue), and 3.5 s^{-1} (100 Hz – red). The α transition is centered at ~ 45 °C.

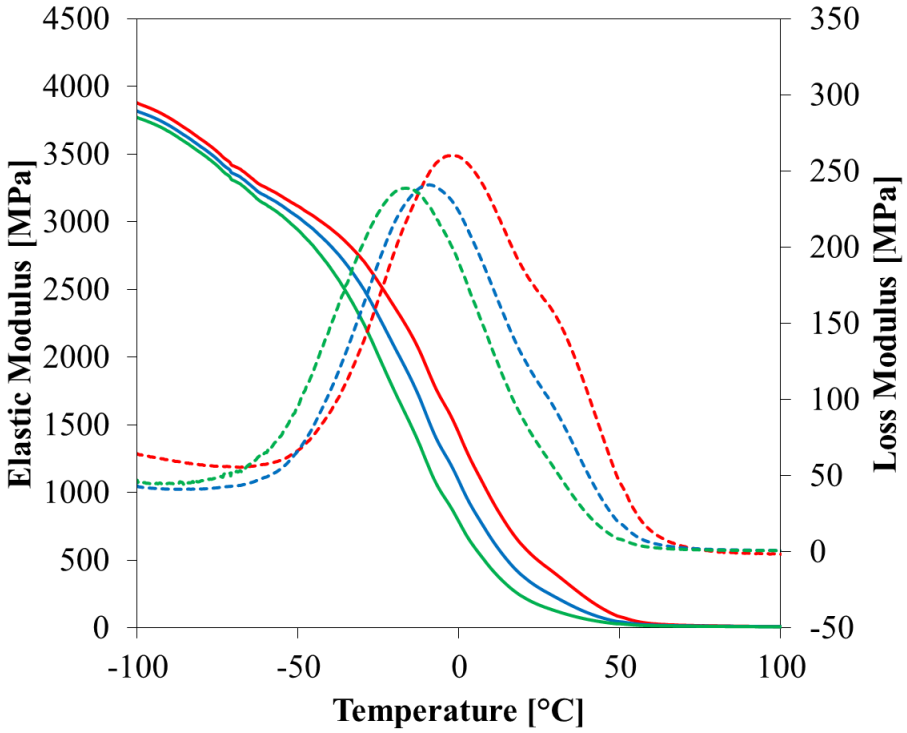


Figure 3-16: PPVC-4 elastic modulus (solid lines) and loss modulus (dashed lines) curves at 0.035 s^{-1} (1 Hz – green), 0.35 s^{-1} (10 Hz – blue), and 3.5 s^{-1} (100 Hz – red). The α transition is centered at ~ 0 °C.

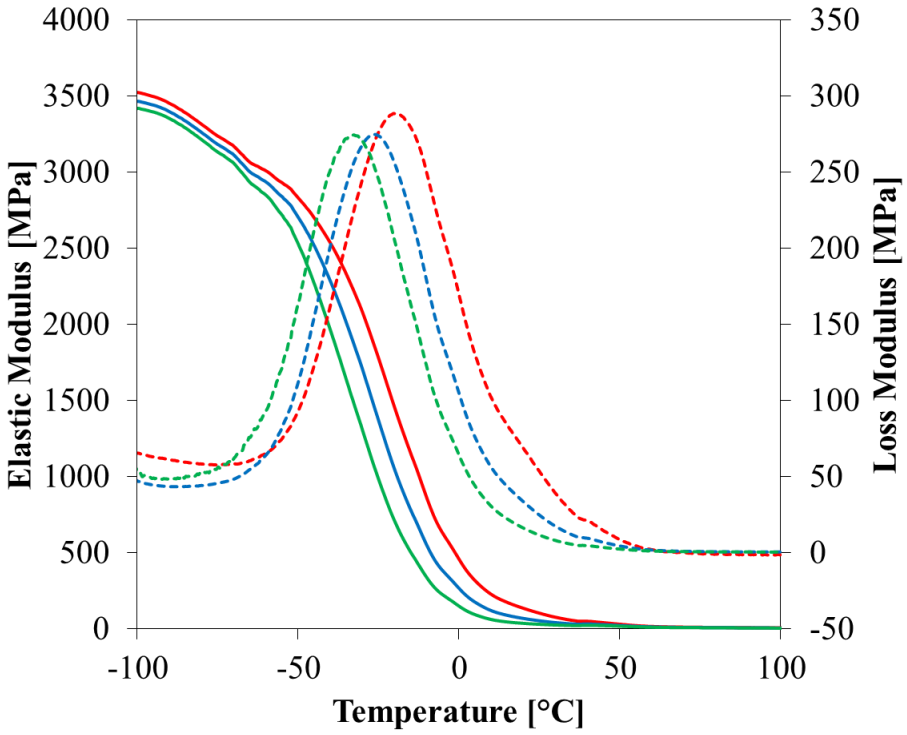


Figure 3-17: PPVC-6 elastic modulus (solid lines) and loss modulus (dashed lines) curves at 0.035 s^{-1} (1 Hz – green), 0.35 s^{-1} (10 Hz – blue), and 3.5 s^{-1} (100 Hz – red). The α transition is centered at approximately -20 °C.

(which has a relatively simple chemical structure that would take much more energy to rotate/translate main chain segments with the smaller amount of free volume) (Bicerano, 2002).

The loss modulus peak relating to the β transition is within the -100 °C range with the unplasticized PVC as seen in figure 3-14, although for the plasticized PPVCs, this is not the case. In the PVC curve, the β-peak, at approximately -45 °C, overlaps slightly with the peak corresponding to the glass transition, although there is enough spacing for the effect of the two transitions to be observed in the storage modulus response. There is a slight bend in the loss modulus curve for each of the PPVC curves (figures 3-15 – 3-17) observed at -100 °C which corresponds to the beginning of the β transition. In order to locate the β-peak and better understand the movement of the peak corresponding to increases in plasticizer content, additional DMTA tests ranging from -150 to 30 °C were conducted (figures 3-18 – 3-21).

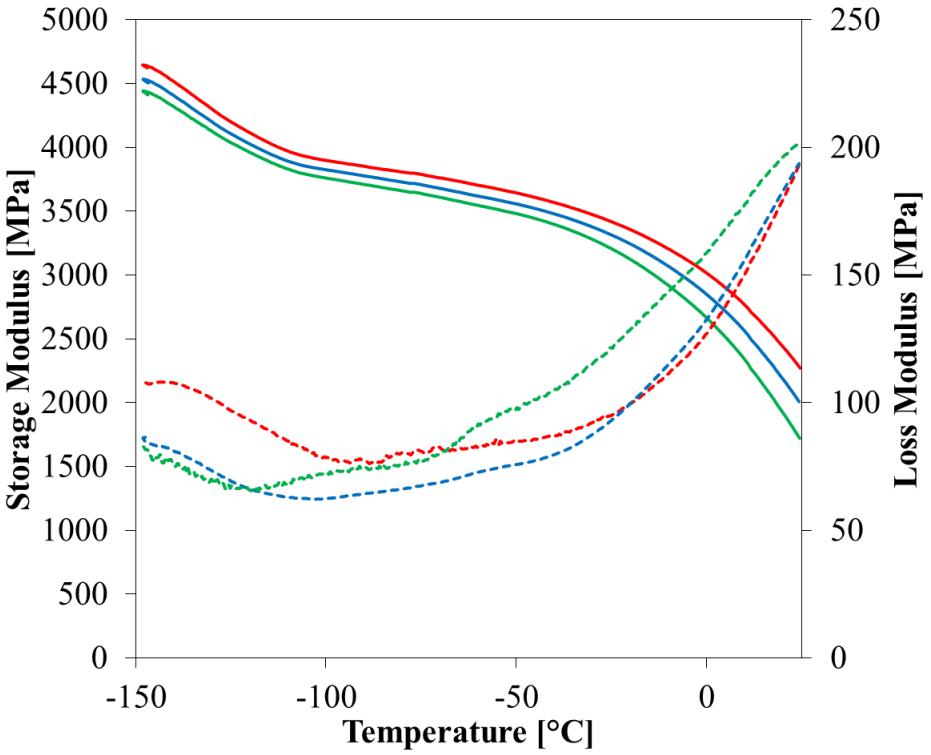


Figure 3-18: PPVC-2 elastic modulus and loss modulus curves at 0.035 s^{-1} (1 Hz – green), 0.35 s^{-1} (10 Hz – blue), and 3.5 s^{-1} (100 Hz – red). β transitions and α transitions are centered respectively at approximately -150 °C and 45 °C.

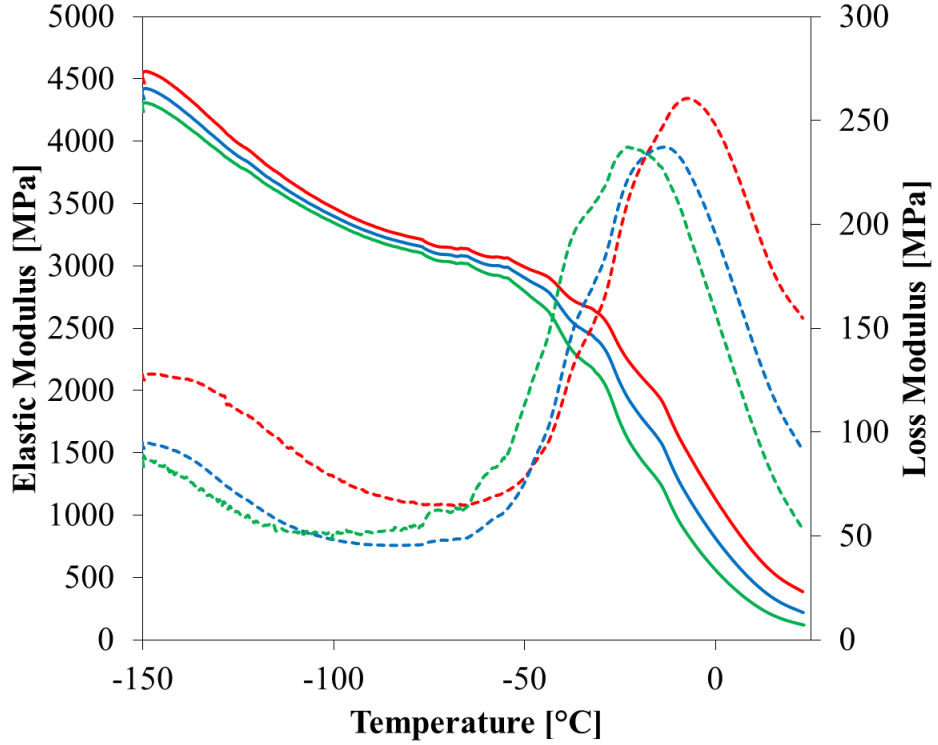


Figure 3-19: PPVC-4 elastic modulus and loss modulus curves at 0.035 s^{-1} (1 Hz – green), 0.35 s^{-1} (10 Hz – blue), and 3.5 s^{-1} (100 Hz – red). β transitions and α transitions are centered respectively at approximately -150 °C and 0 °C.

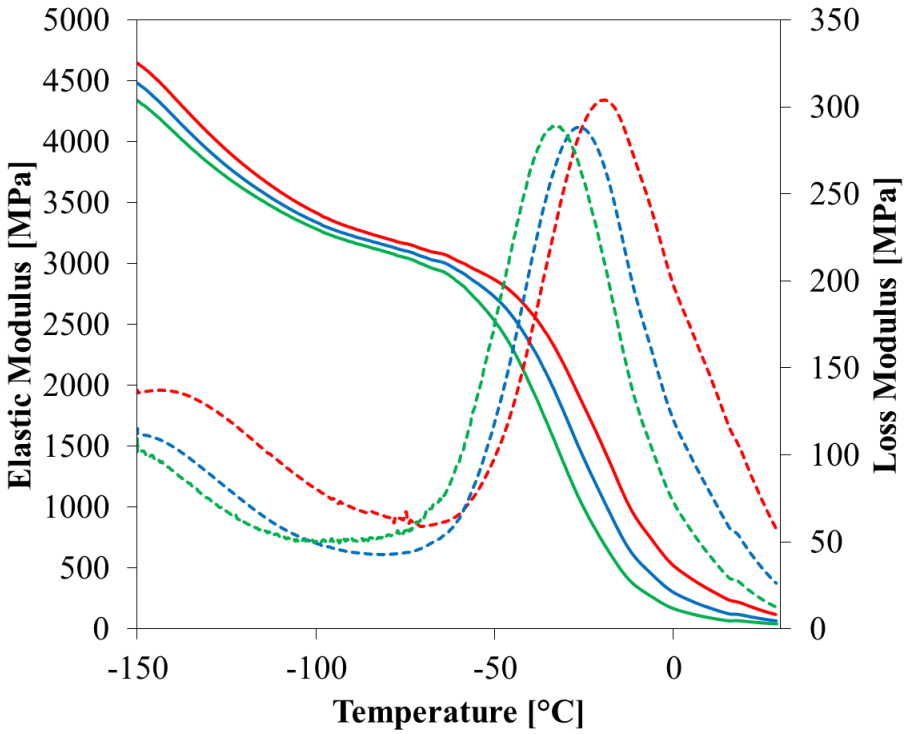


Figure 3-20: PPVC-6 elastic modulus and loss modulus curves at 0.035 s^{-1} (1 Hz – green), 0.35 s^{-1} (10 Hz – blue), and 3.5 s^{-1} (100 Hz – red). β transitions and α transitions are centered respectively at approximately -150 °C and -20 °C.

With the addition of plasticizer, a much more distinct beta transition, distinct from the alpha transition, is seen not only in the loss modulus but even more clearly in the storage modulus when comparing PPVCs to PVC (previously presented in figure 3-14). To quantify this separation, we see that neat PVC has a separation between α-peak and β-peaks of approximately 125 °C versus 195 °C for PPVC-2, 150 °C for PPVC-4, and 130 °C for PPVC-6. Interestingly, the beta transition appears to be in the same temperature location (~ -150 °C) regardless of the amount of plasticizer added to PVC. These results will be investigated further in the following chapter.

3.4.3 Discussion of DMTA and compressive results

Figure 3-21 presents the similarities in yield stress of the temperature dependent quasi-static (10^{-2} s^{-1}) data and the rate and temperature dependent elastic modulus data from DMTA testing by superimposing the two sets of curves. These data present clear similarities between

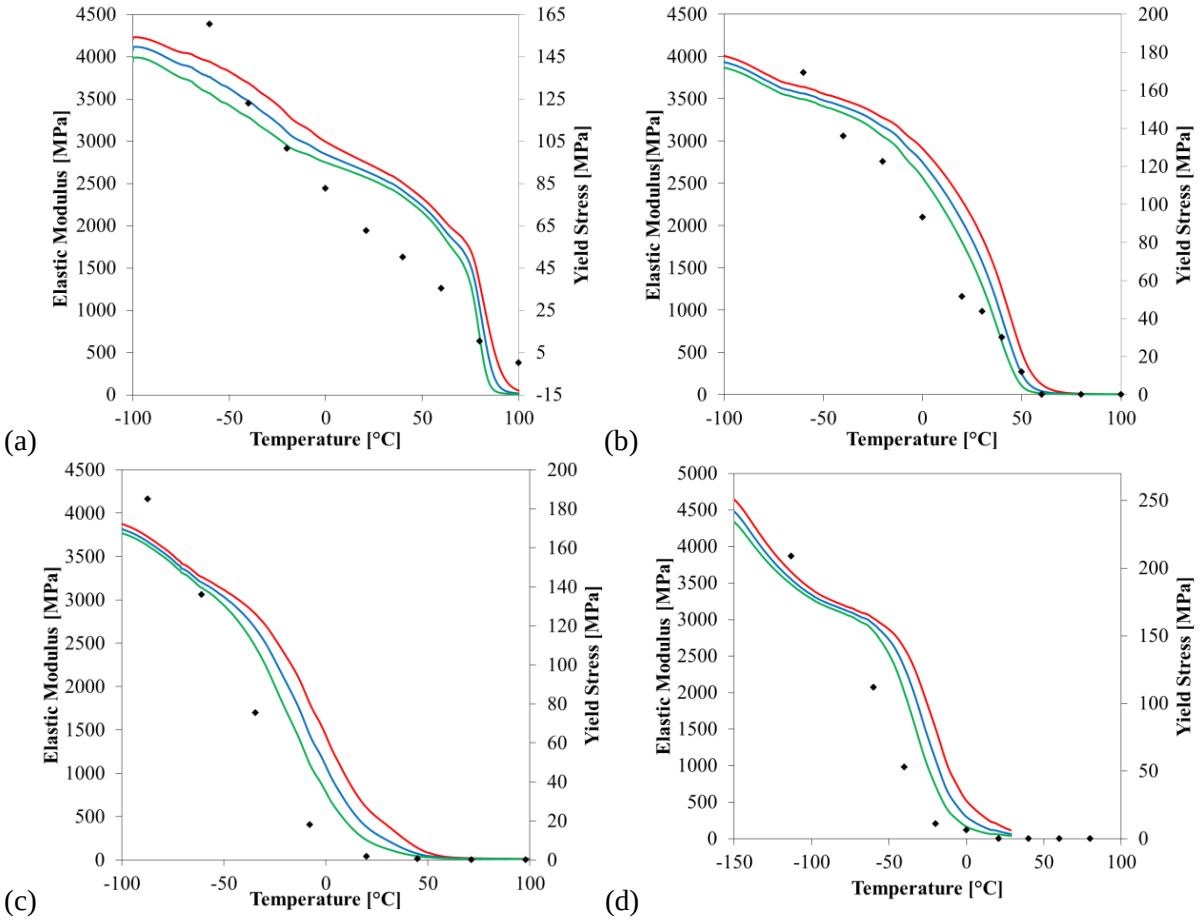


Figure 3-21: PVC (a), PPVC-2 (b), PPVC-4 (c), and PPVC-6 (d) with yield stress data superimposed onto elastic modulus data at 0.035 s^{-1} (1 Hz – green), 0.35 s^{-1} (10 Hz – blue), and 3.5 s^{-1} (100 Hz – red).

the increases in elastic modulus (from DMTA data) and yield stress (from compression data) with decreasing temperature. The minor differences in temperature values for alpha and beta transitions (comparing yield data versus modulus data) are attributed to the broadness of these transitions (seen in loss modulus behavior).

The dependence of PVC and PPVC(-2, -4, -6)'s yield strength upon strain rate and temperature are summarized in section 3.3.3. These curves make clear the material transitions which occur at high strain rate/low temperature (both α and β in PVC). A comparison of these data and DMTA data is useful in predicting the transitions and the rate at which they occur. PVC's yield stress dependence upon temperature is very similar to the shape of the curve produced in DMTA when measuring the dependence of the storage modulus with respect to

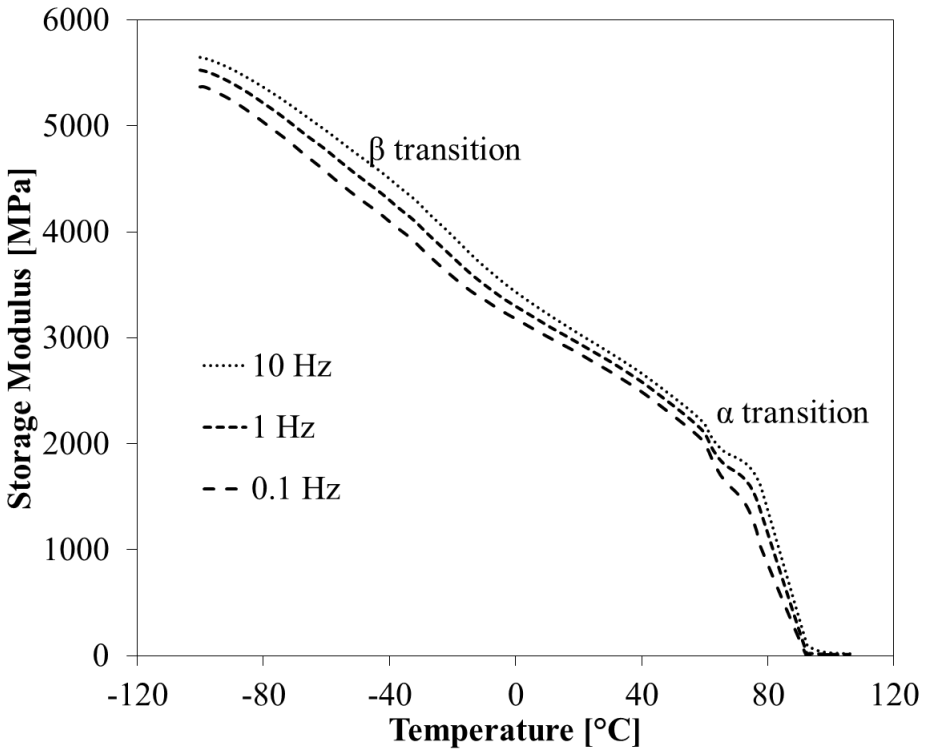


Figure 3-22: DMTA storage modulus curves for PVC: temperature dependence of the storage modulus at 10, 1, and 0.1 Hz.

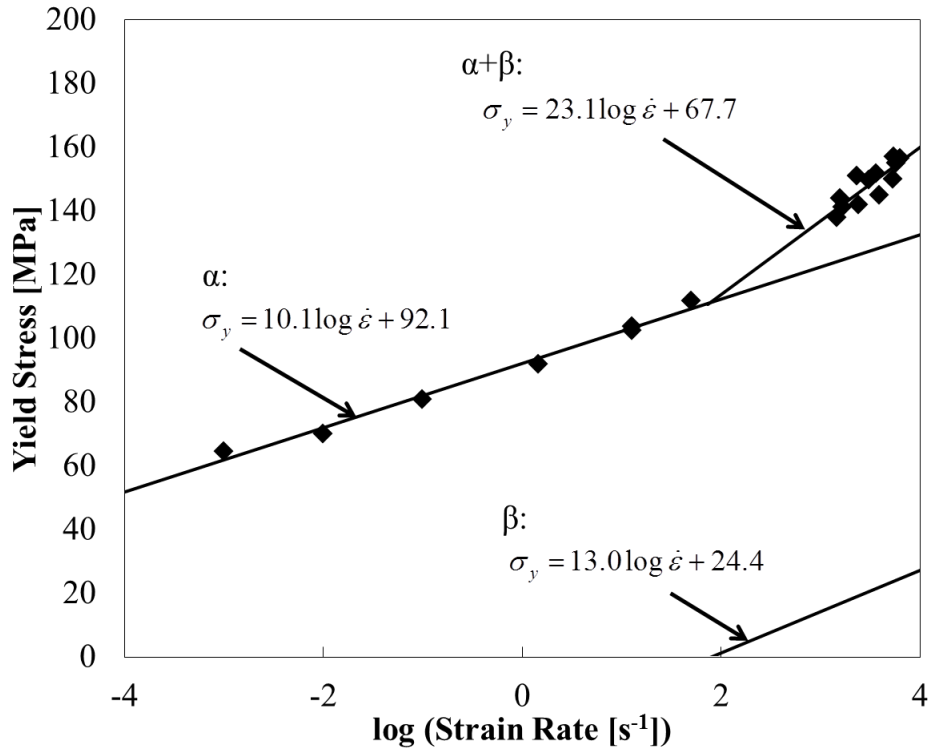


Figure 3-23: PVC true yield stress data split into components. Above the strain rate at the (β) transition, or ~80 s^{-1}, it is assumed that the α and β process contribute to the resistance to plastic deformation; below the transition, only α contributes. Trendlines are fitted to locate the location of this transition.

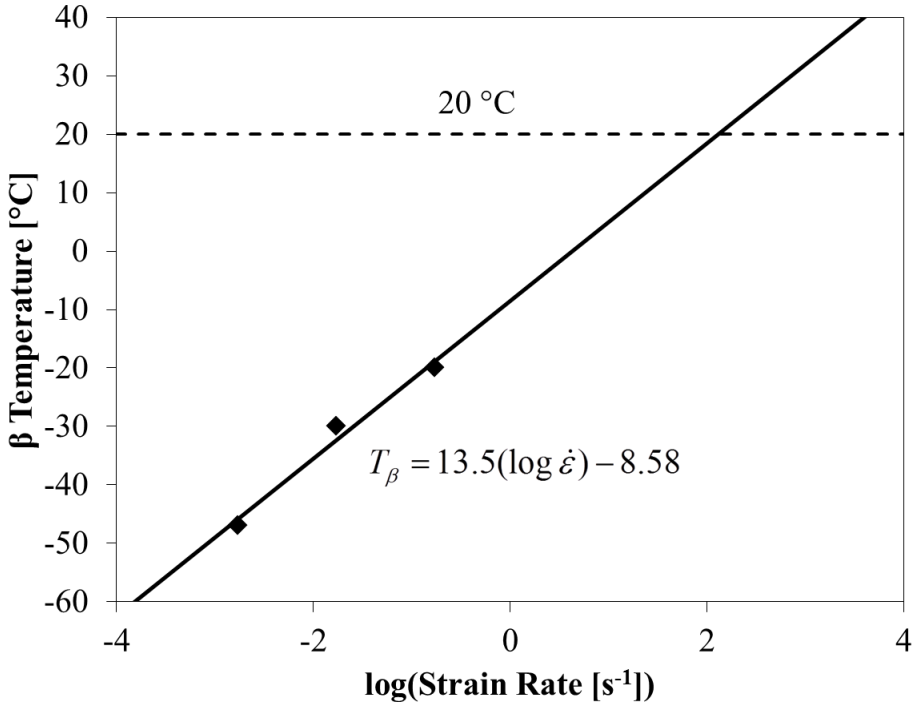


Figure 3-24: β transition temperature as a function of strain rate. The three data points on the left are from DMTA data, the line is fitted to these data and extrapolated to 20 °C to produce the intersection-point of interest on the right.

temperature (figure 3-21a) illustrating the consistency of and confirming the α and β transitions in the uniaxial compression data and the DMTA data.

From time-temperature equivalence we are able to predict the strain rate at which the β transition begins to affect the results from room temperature testing on PVC – seen as the point at which the polymer's strength has an increase in sensitivity to strain rate (figure 3-23). By assuming the β transition temperature increases linearly with the logarithm of strain rate, a line fitted to the locations of the beta transition temperatures in DMTA testing is extrapolated to predict the location of the strain rate (at room temperature) at which the transition occurs. The beta transition temperatures obtained from the DMTA data are indicated in figure 3-24. The three frequencies are converted to approximate strain rates using equation 2.16 in section 2.7. The presented behavior shows the dependence of the β transition temperature on strain

rate and extrapolates the dependence seen in the DMTA data up to room temperature, or equivalently, high strain rates.

The prediction of the beta transition is analogous to the linear mapping technique presented in the previous chapter (section 2.6, equation 2.15). The beta transition seen on the DMTA results is shifted up to room temperature by increments of the change in temperature of the beta transition 5°C per decade of strain rate for PVC (the methodology for this is described in additional detail in the next chapter). By calculating this shift, the strain rate at which the beta transition is expected to occur at room temperature is found. This was compared with the value of strain rate that would be found by a bilinear fit to the yield stress versus log strain rate curve and calculating where the two lines intersect. The DMTA shifting method produced a value of 2.1 for the logarithm of strain rate, or roughly 125 s^{-1}. With reference to figure 3-23, we observe that the intersection of the lines fitted to the yield stress data on the same material is 1.9 corresponding to approximately 80 s^{-1}. There is therefore very close agreement between the values from the two methods.

Strain Rate Profiles – Effects of Different Bar Materials

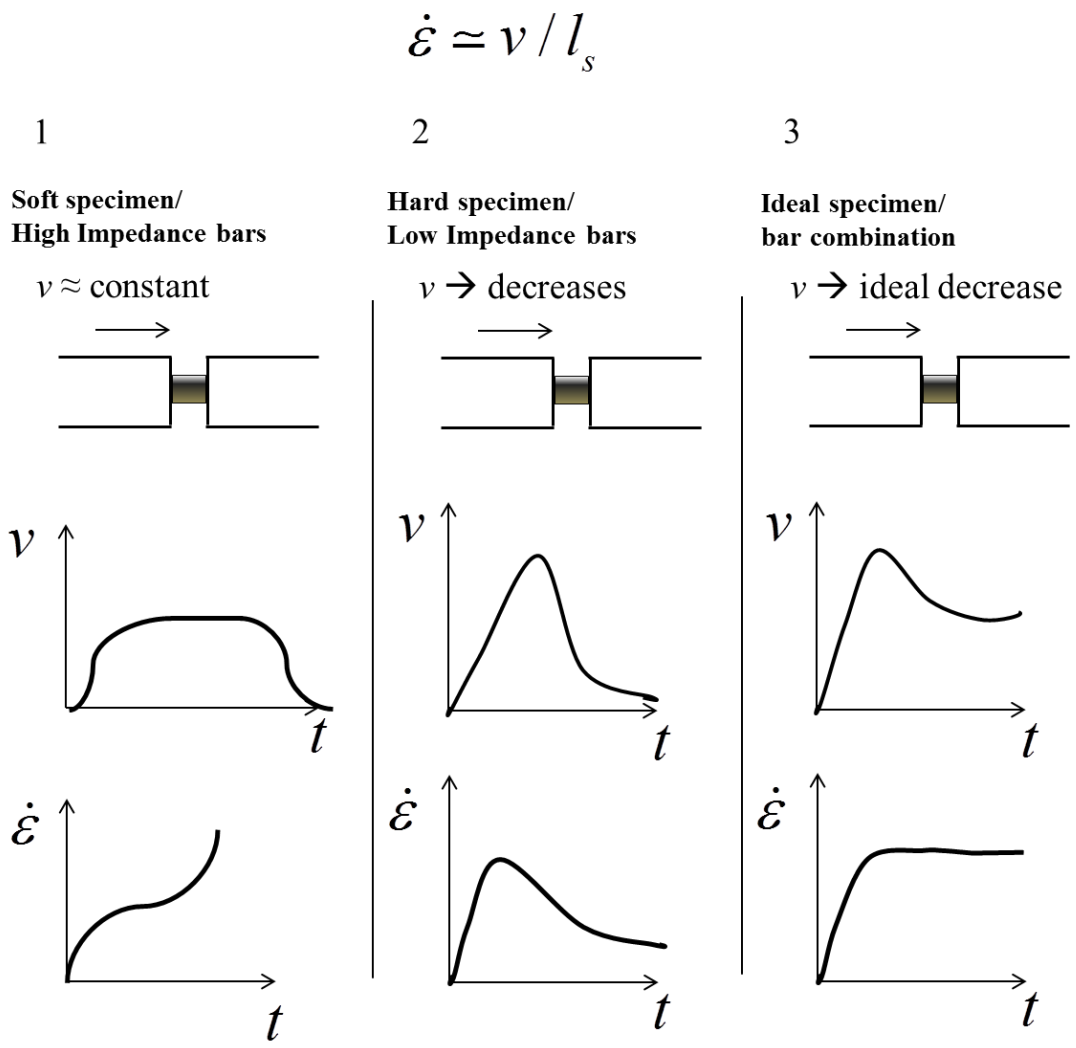


Figure 3-25: Theoretical velocity profiles and true strain rate profiles dependent upon the relative strength of the specimen material compared to the bar material.The same theoretical bar material and striker bar velocity are used in each example. v is the input bar velocity, t is the time during testing, and l_s is the instantaneous specimen length.

Figure 3-25 summarizes the theoretical velocity and true strain rate profiles seen in polymer testing. For example, when a very hard material is tested, the input bar of the SHPB in contact with the test specimen slows down a large amount during testing. Alternatively, for a soft material, the bar stays at a constant velocity during testing but because of the change in specimen length during testing (seen in the true strain rate equation at the top of the figure) it is made clear that the true strain rate increases during testing: a shrinking specimen length

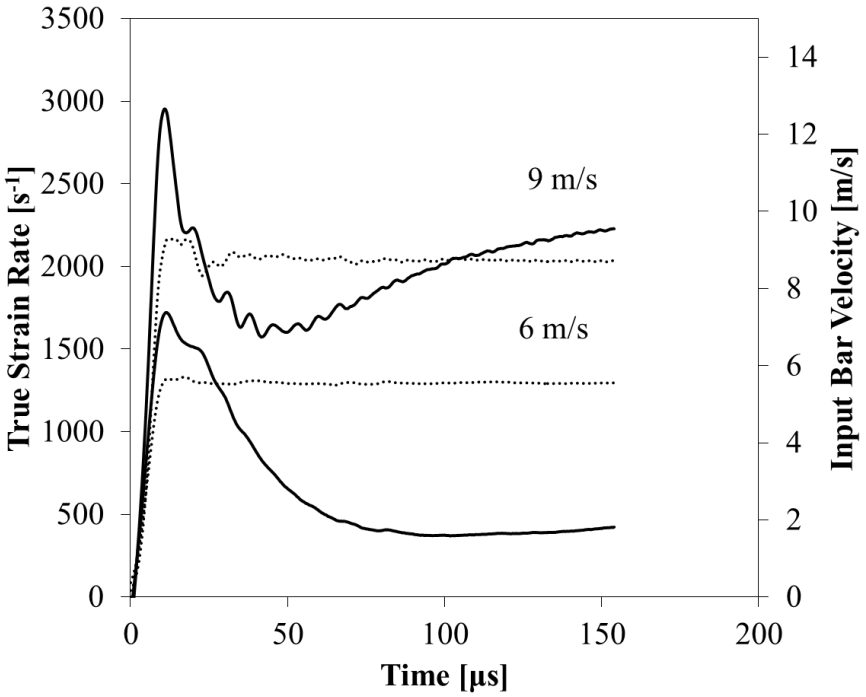


Figure 3-26: Near constant Mg alloy (AZM) input bar velocities profile (dotted lines) are presented at 6 and 9 m s^{-1} in conjunction with the resultant true strain rate profiles of PPVC-2 (solid lines).

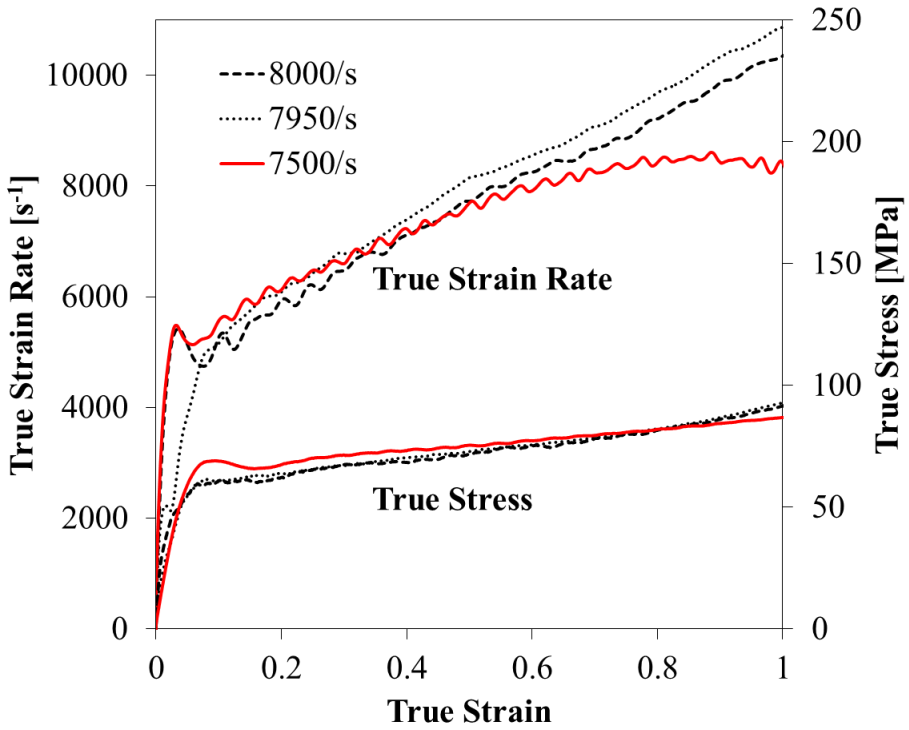


Figure 3-27: True strain rate behavior of PPVC-4 undergoing high rate deformation via SHPB. One strain rate with Mg alloy bars (red) and two strain rates with Ti alloy bars (black) are superimposed for comparison between bars, and relating this to any changes in true stress-true strain behavior.

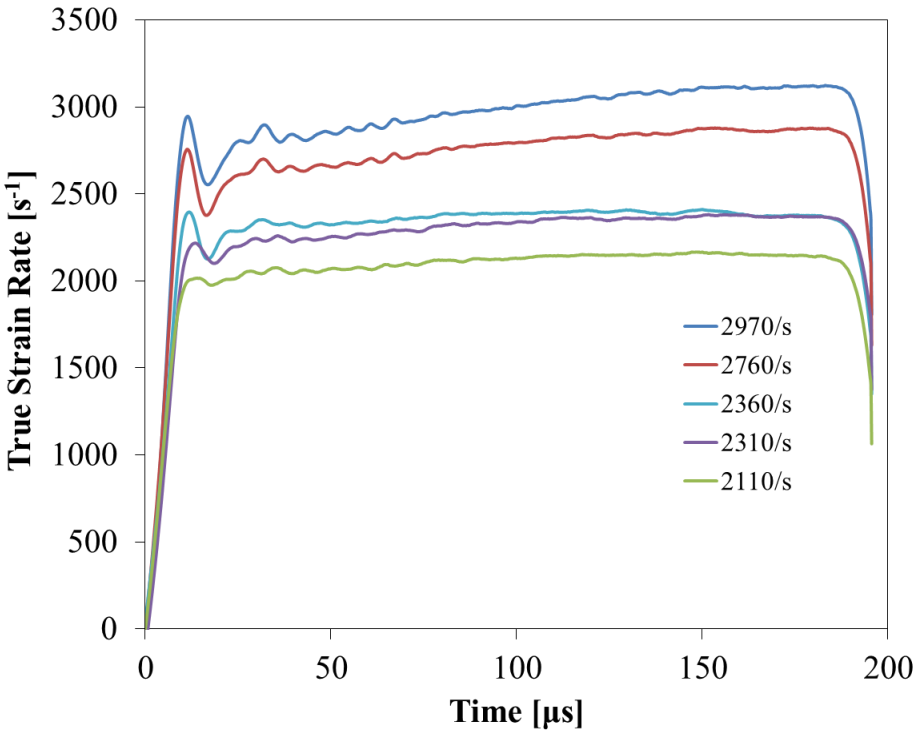


Figure 3-28: PPVC-6 displaying nearly constant strain rate with Mg alloy SHPB bars at strain rates ranging from 2000 to 3000 s^{-1}.

with a constant bar velocity. These profiles are not only dependent upon the strength of the specimen, but are also dependent upon the bar material, thus an optimal specimen length change and bar velocity must be achieved in order to obtain a constant strain rate in SHPB testing.

Figures 3-26 – 3-28 follow the theoretical behavior previously presented, with the experimental behavior seen during the testing conducted on PVC materials in this chapter. Figure 3-26 represents the hard specimen/low impedance bars example, figure 3-27 is representative of soft specimen/high impedance bars in PPVC-4's behavior to Ti alloy bars (while demonstrating improvement in strain rate profile when moving to the lower impedance bars of Mg alloy), and figure 3-28 represents the ideal specimen/bar combination in high rate testing. This material has a similar enough impedance to the SHPB bar material (magnesium in this case, see table 2-1 in the previous chapter). This behavior is additionally helped by the

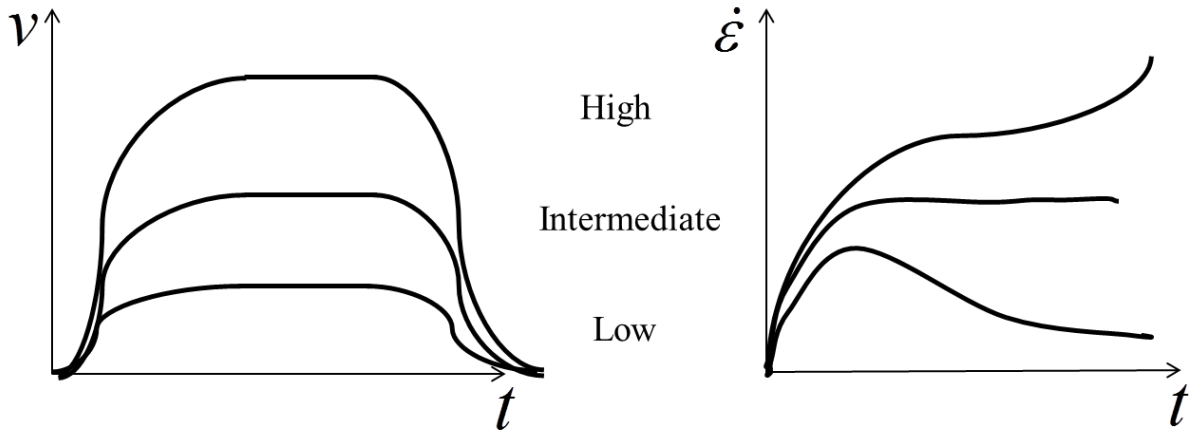


Figure 3-29: Input bar and striker bar velocity profile is constant at different test velocities, and causes different true strain rate profiles as a result.

fact the material is being tested at moderate rates on the SHPB (centred around 2000 s^{-t}, or a ~5 m s^{-1} bar velocity) – this additional factor in the complexity of obtaining constant strain rate profiles is presented in figure 3-29. In this case, during intermediate rates, the SHPB performs at an effectively constant strain rate. As the rate of deformation is increased, the strain rate profile becomes less constant because of two factors: as the velocity of the input bar is increasing, the length of the specimen is also decreasing to smaller values during testing. Magnesium's low wave impedance make it a strong candidate for testing soft materials, such as PPVC-4 and PPVC-6, but is less convincing in testing stronger materials (e.g. PPVC-2, presented in figure 3-26).

3.5 Conclusions

Four PVCs with different plasticizer levels have been characterized through uniaxial compression experiments over a broad range of strain rates and temperatures.

Reloading being the cause of the post-mortem fractures in PVC at high strain rates was proven and investigated via high speed analysis. A supplementary investigation, within the former study was also carried out in order to confirm the accuracy of the theoretical

elastic strain recovery in PVC tests. The experimental elastic recovery was shown to be almost five times the theoretical elastic recovery.

Moreover, DMTA characterization has been performed on all materials – with further analysis of DMTA data performed in the next chapter. In each material, the effects of polymer transitions on rate dependence are clear – the glass transition in each of the materials, and the β transition in the unplasticized and most plasticized (PPVC-6). In the unplasticized PVC, DMTA data were successfully extrapolated to predict the strain rate at which the β transition begins to affect the rate dependence of the material. Superimposition of elastic modulus curves from DMTA testing and yield stress dependence upon temperature curves help confirm the robust interplay of temperature and rate dependences of several different types of polymer (whether an amorphous polymer such as PVC, or a rubber such as PPVC-6). Additionally, what constitutes a constant strain rate profile, and/or not constant profile was investigated at the end of this chapter; in order to better understand the driving parameters of strain rate behavior, both theoretical and experimental strain rate behaviors were presented, compared, and analyzed.

Chapter 4

Time-Temperature Equivalence

Models involved in predicting the time-temperature equivalence of polymers have been studied. These models have been applied to our data, and in result, a novel model of time-temperature equivalence has been developed and is presented here.

4.1 Early encounters

Several models have attempted to capture large strain time-temperature equivalence in amorphous polymers, which are commonly obtained via an adaptation of the Ree-Eyring multi-process rate activated approach (as seen earlier in describing constitutive polymer models) (e.g. Richeton et al., 2006; Bauwens-Crowet et al., 1973; Glasstone et al., 1941). A demonstration of equivalent stress states as a function of strain rate and temperature is presented in figure 4-1. In this figure, similar to that seen in Furmanski et al. (2013), parameter *D* relates the strain rate and temperature sensitivities during deformation in units of temperature per decade of strain rate (or strain rate on a logarithmic scale). The equation involving *D* is presented in the next section in equation 4.3.

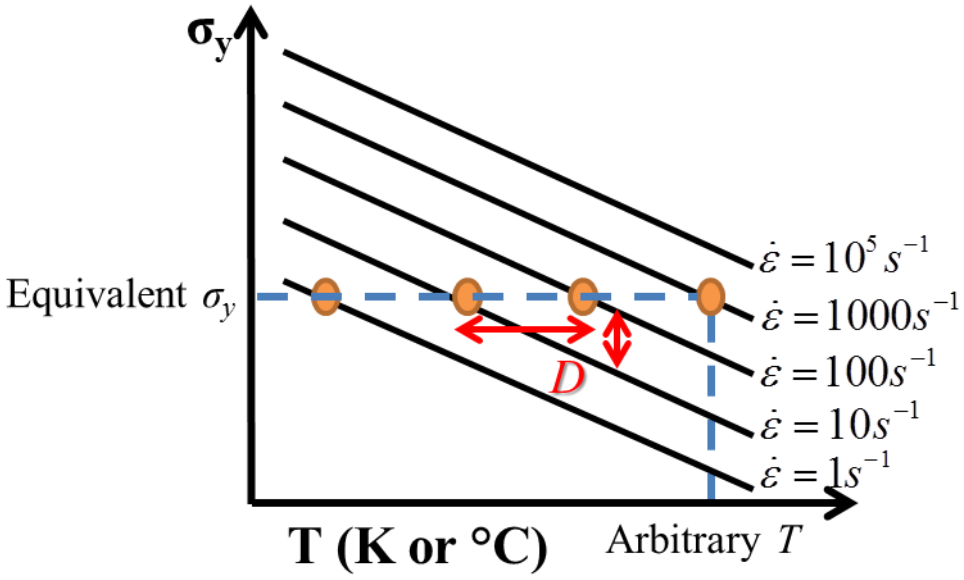


Figure 4-1: Yield stress dependence on absolute temperature of an arbitrary polymer, with multiple strain rates shown to obey a linear time-temperature superposition. An equivalent yield stress is found corresponding to a chosen temperature.

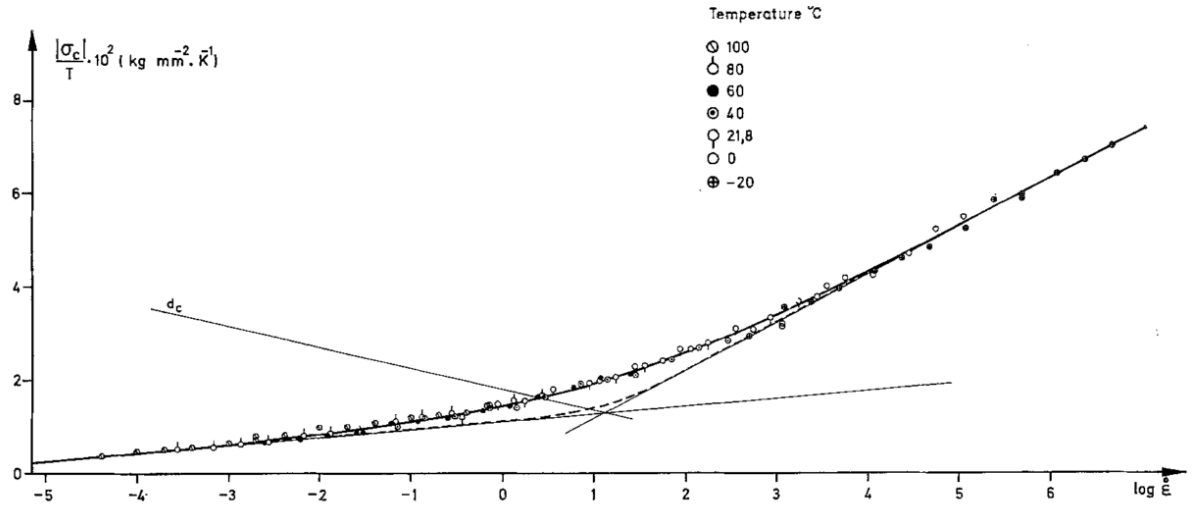


Figure 4-2: PMMA yield data as a function of temperature mapped onto strain rate yield data to create master curves at 100 °C in uniaxial compression. The dashed curve is calculated from the Ree-Eyring equation (please refer to section 8.3.1). (Bauwens-Crowet et al., 1973).

Bauwens-Crowet (1973) and partners are understood to be the first to describe large strain behavior and yield stress, over a wide range of temperatures and strain rates, using a time-temperature equivalence method. The group achieved a master curve of superposed rate and temperature dependent data, presented in figure 4-2. The master curve spanned strain

rates from below 10^{-4} s^{-1} up to 10^{6} s^{-1}, derived from experimental data spanning 10^{-4} to 10^{0} $s^{-1}$and temperatures -20 to 100 °C.

Richeton and contemporaries (2006) carried out uniaxial compression stress-strain tests on three amorphous polymers, including PC, PMMA, and polyamideimide (PAI), at temperatures ranging from -40 to 180 °C and strain rates ranging from 0.0001 s^{-1} to 5000 s^{-1}. Presented in figure 4-3, the Richeton-Ahzi cooperative model was used to fit experimental time-temperature superposition data, as well as to validate the rate/temperature superposition principle for the reduced yield stress. The Richeton-Ahzi model differentiates from the two-process Ree-Eyring model (seen in figure 4-2, and described in greater detail in a modeling section of this thesis, 8.3.1), in that below 10^{-3} s^{-1}, the cooperative model predicts an approximately constant yield stress independent of strain rate, while the Ree-Eyring model calculates that the yield stress will continue to decrease with decreasing rate.

Siviour, Walley, Proud, and Field (2005 & 2006) were the first since Bauwens-Crowet and partners to investigate time-temperature equivalence beyond a small strain window. PC and polyvinyldifluoride (PVDF) were investigated over a wide range of strain rates (10^{-4} to 10^{4} s^{-1}) at constant temperature (room temperature), and a wide range of temperatures (-50 to 150 °C) at constant strain rate (10^{3} s^{-1}). The authors proposed an empirical formula (referring forward to equation 4.3 in section 4.2, and further described in section 2.6) for mapping the yield (or 'peak') stress dependence on temperature to the dependence on strain rate, which agreed well with experimental data (seen previously in section 2.3, figure 2-13) and comparisons in literature. The formula employed a linear inter-dependence of temperature and strain rate, using a reference strain rate and reference temperature as experimental constants, as well as the experimentally determined mapping parameter *D*. The parameter *D* has been termed the temperature-strain-rate equivalence parameter by other authors who have used the formula while conducting

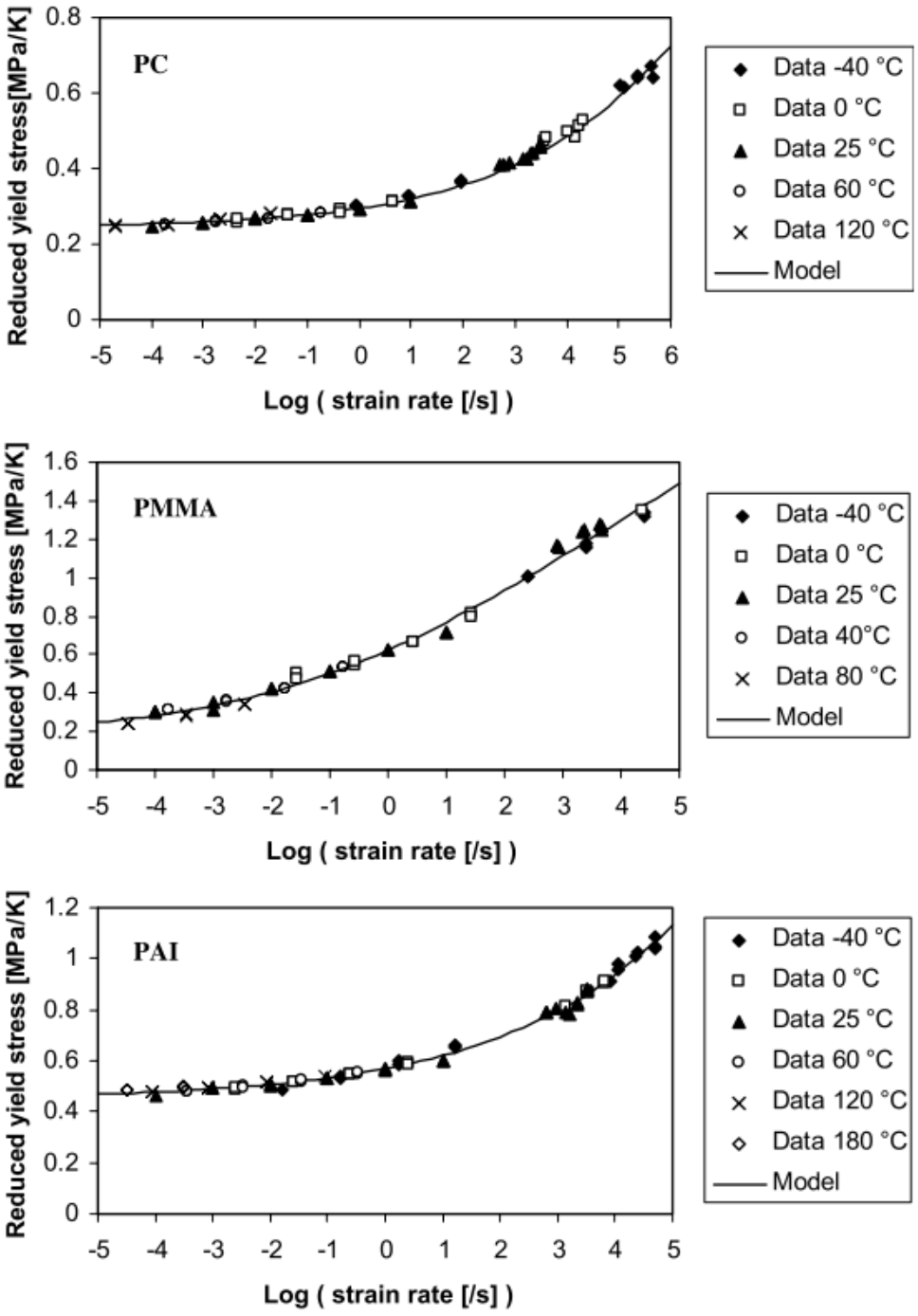


Figure 4-3: PC, PMMA, and PAI yield data as a function of temperature mapped onto strain rate yield data to create master curves at 25 °C in uniaxial compression. (Richeton et al., 2006). Note: Reduced yield stress is often used when analyzing a range of temperature dependent data sets conducted at different strain rates.

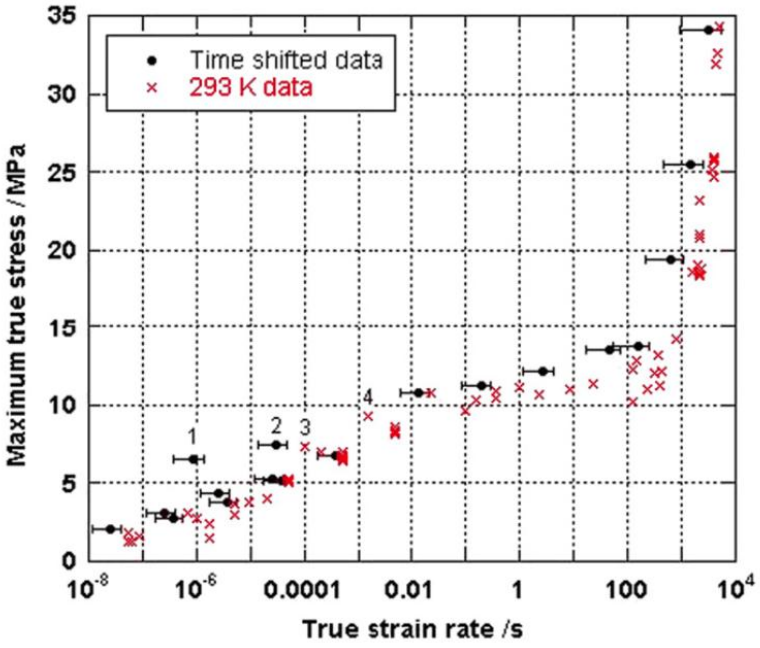


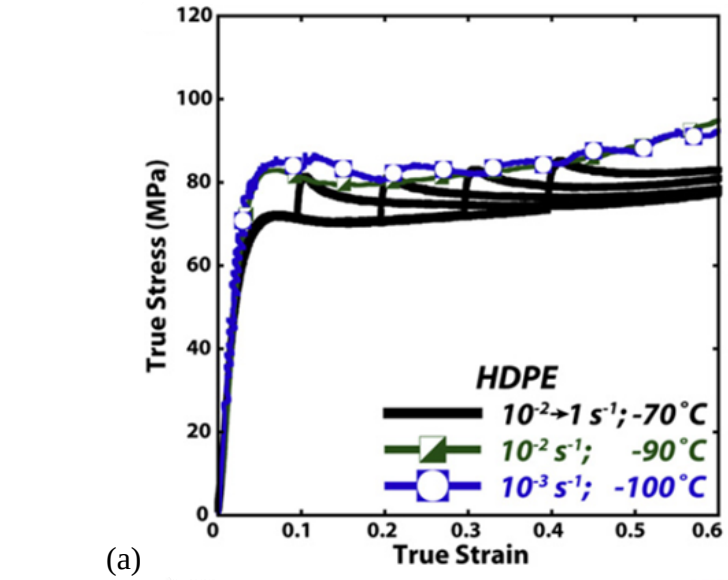
Figure 4-4: Williamson et al. (2008) application of time-temperature superposition principle. It is noted that data points 1-4 are of lower aspect ratio than the neighboring data in this area.

additional investigations (*e.g.* Furmanski et al., 2013), and relates the strain rate and temperature sensitivities during deformation. This parameter can be found from the rate sensitivity seen in DMTA data, or alternatively via temperature dependent and rate dependent data and interpolation. Siviour's formula was able to capture several changes in deformation mechanisms during changes in yield stress, including the inflection in data which involves the glass transition (being seen at equivalent temperatures/strain rates) in both PC and PVDF, and inflection which is understood as the beginning of the β transition in PC.

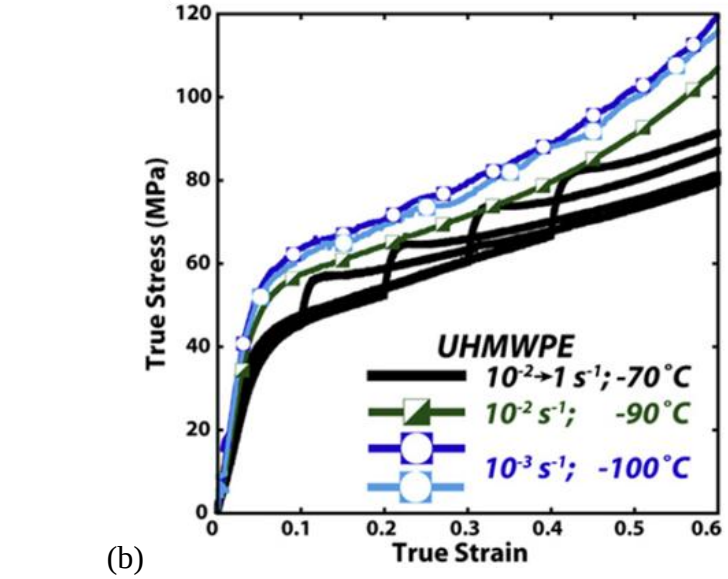
Other authors have applied the Siviour and colleagues (2005) formula to PTFE (Jordan et al., 2007) and high-density polyethylene (HDPE), ultra-high molecular weight polyethylene (UHMWPE), and cross-linked polyethylene (PEX) (Brown et al., 2007). Both found that the formula gave good agreement between their temperature dependent and rate dependent yield stress data. Williamson et al. (2008 & 2009) were able to successfully implement the linear time-temperature superposition formula to composites such as polymer bonded explosives (PBXs), finding that a *D* parameter of -13.1 K/decade of strain rate fit

their data sets, as seen in figure 4-4. These different works presented the wide agreement of time-temperature superposition in a range of dissimilar polymers via the single-parameter empirical model.

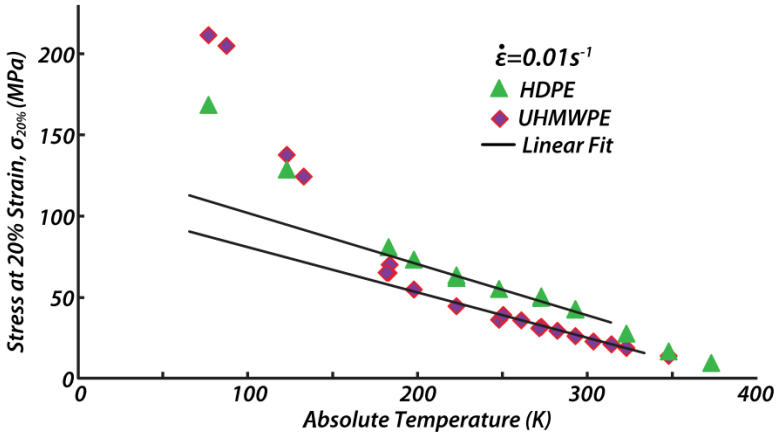
Cady et al. (2003) mentioned the possibility of simulating the high rate response of polymers by low rate/low temperature tests. An investigation such as this would experimentally apply the phenomena described by the WLF and Siviour formulas in time-temperature superposition. More recently, Furmanski et al. (2012 & 2013) found a linear empirical formulation of time-temperature equivalence in HDPE while investigating HDPE and UHMWPE, while using jump-rate compression tests to investigate isothermal high rate response with the absence of adiabatic heating. An overview of some of their significant results is presented in figure 4-5.



(a)



(b)



(c)

Figure 4-5: Stress-strain curves with strain rate jumps from 0.01 → 1 s^{-1} for (a) HDPE and (b) UHMWPE at -70 °C, and (c) flow stress at 20% strain as a function of temperature for both materials at 0.01 s^{-1}. The linear fits are used to display the inflection to nonlinear temperature dependence. The departure from linearity at lower temperatures is also seen in b) the -90 and -100 °C curves not being captured by the -70 °C strain rate jumps. (Furmanski et al., 2013).

4.2 Discussion of the Application of Time-Temperature Superposition

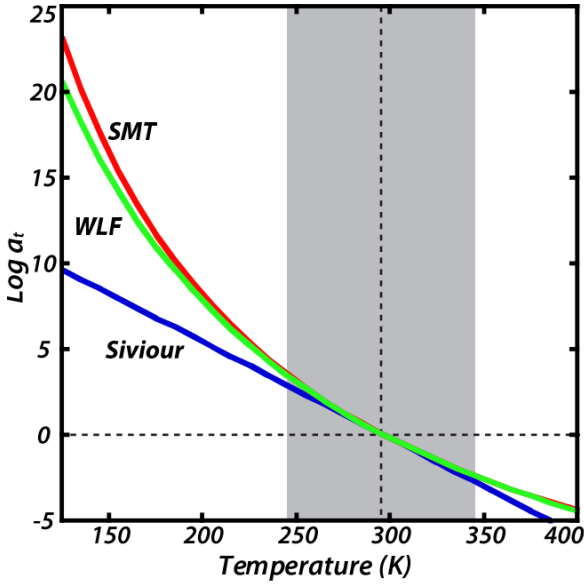


Figure 4-6: An arbitrary plotting of the Site Model Theory (SMT), Williams, Landel, and Ferry (WLF), and Siviour shift factors for time-temperature equivalence over a range of temperatures (Furmanski et al., 2013).

Certain uncertainties arise in the range of applicability of the methods of time-temperature superposition for polymers, especially seen at lower temperatures. Some well-known models in time-temperature superposition are shown in figure 4-6, presenting a comparison of Glasstone's Site Model Theory (SMT) (1941), Williams, Landel, and Ferry (WLF) model, and Siviour's time-temperature equivalency model. Building from the work of Eyring (1935, 1936, & 1955) with a modification to Eyring's stress-activation formulation, SMT has a constant activation energy and the shift factor a_T can be written as

$$\log(a_T) = \log\left(\frac{\dot{\varepsilon}_a}{\dot{\varepsilon}_b}\right) = \frac{-\Delta H}{R}\left(\frac{1}{T_b} - \frac{1}{T_a}\right) \tag{4.1}$$

where $\dot{\varepsilon}_a$ and $\dot{\varepsilon}_b$ are two strain rates of attention with the corresponding temperatures T_a and T_b (Kelvin), R is the gas constant, and ΔH is the activation energy. The empirical WLF model

(which is only valid in the T_g +100°C region, and described in section 8.1.3) shift factor a_T is written as

$$\log\left(a_T\right) = \log\left(\frac{\dot{\varepsilon}}{\dot{\varepsilon}_{T_g}}\right) = -C_1 \frac{T - T_g}{C_2 + (T - T_g)} \tag{4.2}$$

where $\dot{\varepsilon}$ and $\dot{\varepsilon}_{T_g}$ are two strain rates of attention with the corresponding temperatures T and T_g, and C_1 and C_2 are experimentally fitted constants. For a comparison of the shift factor a_T, Siviour's formula (presented in section 3.4.3, equation 3.2) can be rewritten as

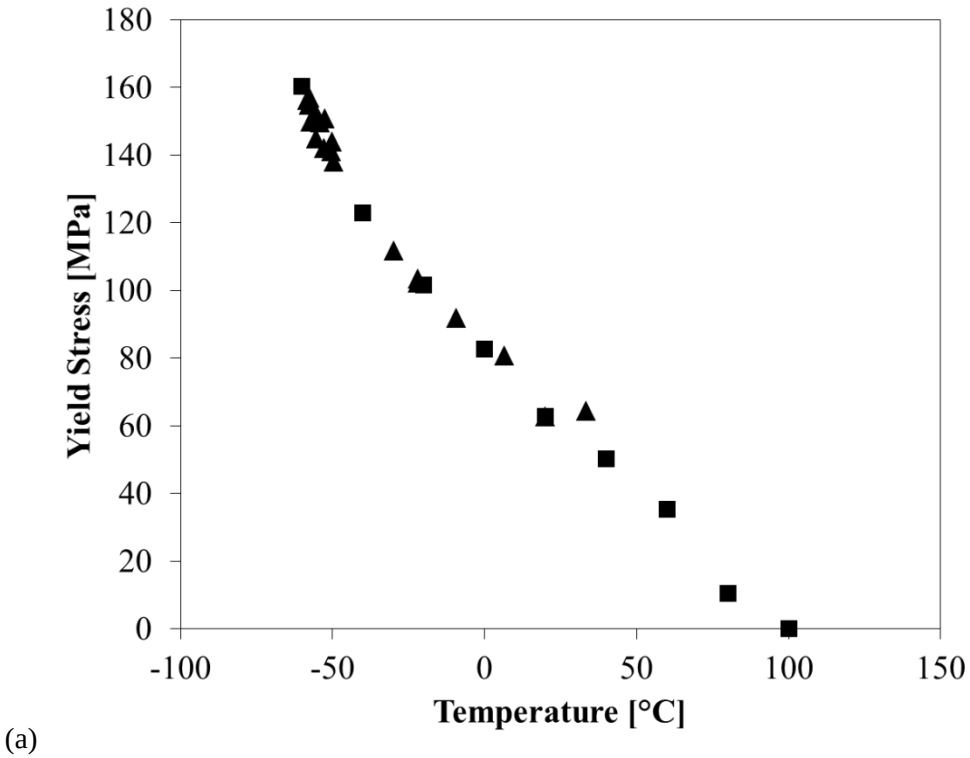
$$\log\left(a_T\right) = \log\left(\frac{\dot{\varepsilon}_0}{\dot{\varepsilon}}\right) = \frac{1}{D}\left(T - T_0\right) \tag{4.3}$$

Figure 4-6 presents a clear deviation from the SMT and WLF models from Siviour and colleagues' linear formulation at lower temperatures. Although, the shift factor used in the equation 4.3 has a maximum divergence of ~15% at the T_g +100°C region (shaded in grey), and looks to be an approximation that works well over this window and has advantages in its simplicity over the two other equations (4.1 and 4.2). SMT and WLF models also diverge from one another at much lower temperatures, beginning noticeably at 200 K. As described earlier, Siviour's equation has been shown to capture several data sets, yet here we see the formula has trouble extending past the commonly tested temperature regimes (<173K or below -100 °C). In looking closer at these temperatures with regards to time-temperature superposition of most amorphous polymers, it is realized that below these commonly tested temperatures lies a temperature regime which relates to $>10^5$ s^{-1} strain rates which are unlikely to happen in most practical applications, making the study mainly academic. Rates this high would have to consider shock wave and compressibility phenomena to accurately predict such deformation (if going to large strains) (Furmanski et al., 2013) which are beyond the scope of this research.

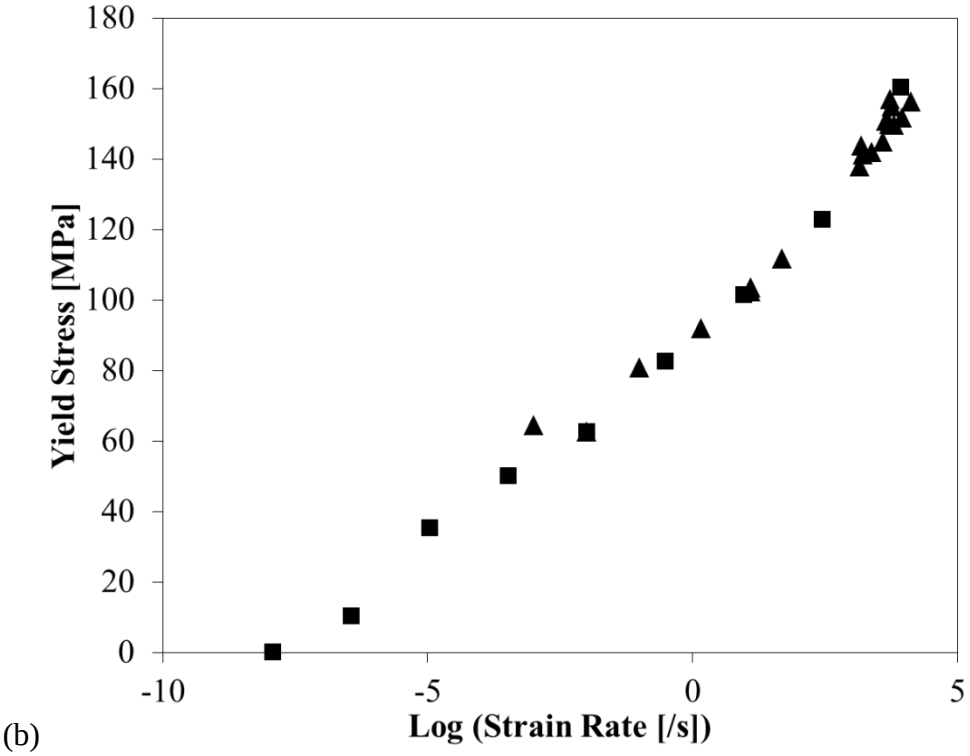
Additional critiques of the Siviour and coauthors (2005) model have been offered from Furmanski and authors (2013), who observe a limitation of the model being that it only has a single point of stress at a particular strain to generate the time-temperature equivalency. Furmanski and colleagues made the argument that there is a need for a relation to the full deformation response, in order to capture the full stress-strain curve at multiple distinct points (or 'equivalent states'). Capturing the entire response of a polymer along the stress-strain curve was noted as a critical step to modeling the correct thermomechanical constitutive behavior of the material. More practically speaking, a point-to-point relation to the entire deformation response would be needed if "equivalent controlled laboratory-generated stress-strain curves are to be used in place of measurements made at extreme equivalent states that are experimentally inaccessible" (Furmanksi et al., 2013). These were key criticisms which added to the encouragement to pursue the simulation method presented in the following chapter (5), where the true stress-true strain response of high rate loading is experimentally simulated via low rate/low temperature tests.

4.3 Results and Discussion

Presented below in figures 4-7 – 4-10 are the time temperature equivalence yield data fitted with the Siviour et al. (2005) method (equation 4.10). Each mapping parameter was fitted manually and gave very good agreement between rate and temperature equivalence for all PVC materials (PVC, PPVC-2, 4, and 6). The rate or temperature dependent data is converted to an equivalent test temperature or rate test using different mapping parameters or 'temperature-strain rate equivalence factors' for each material.

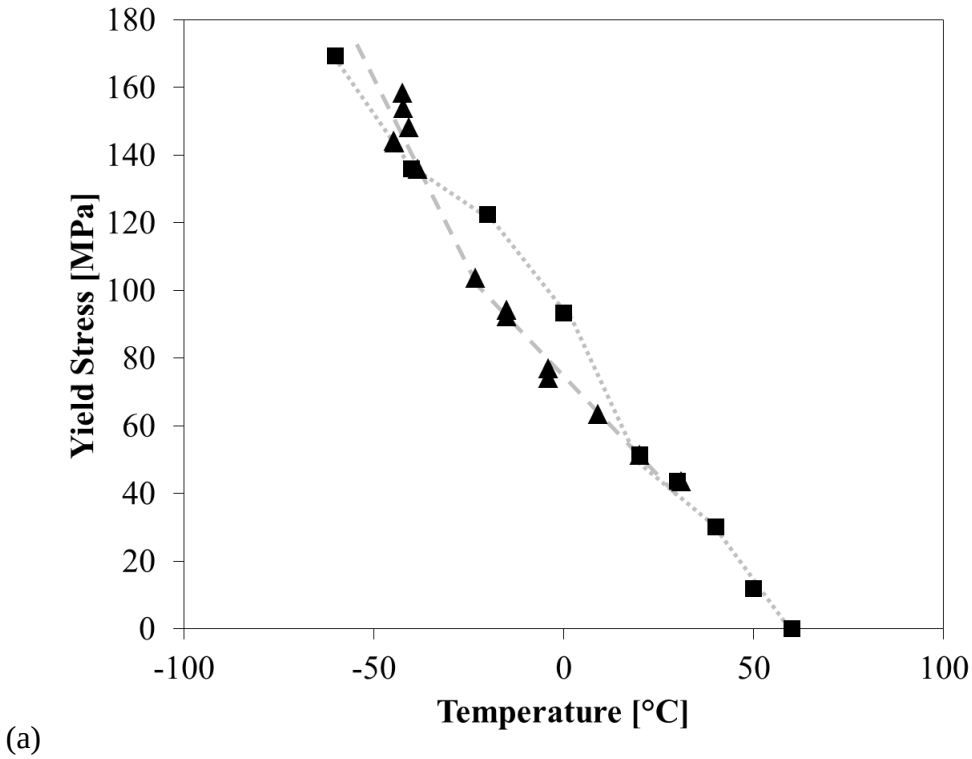


(a)

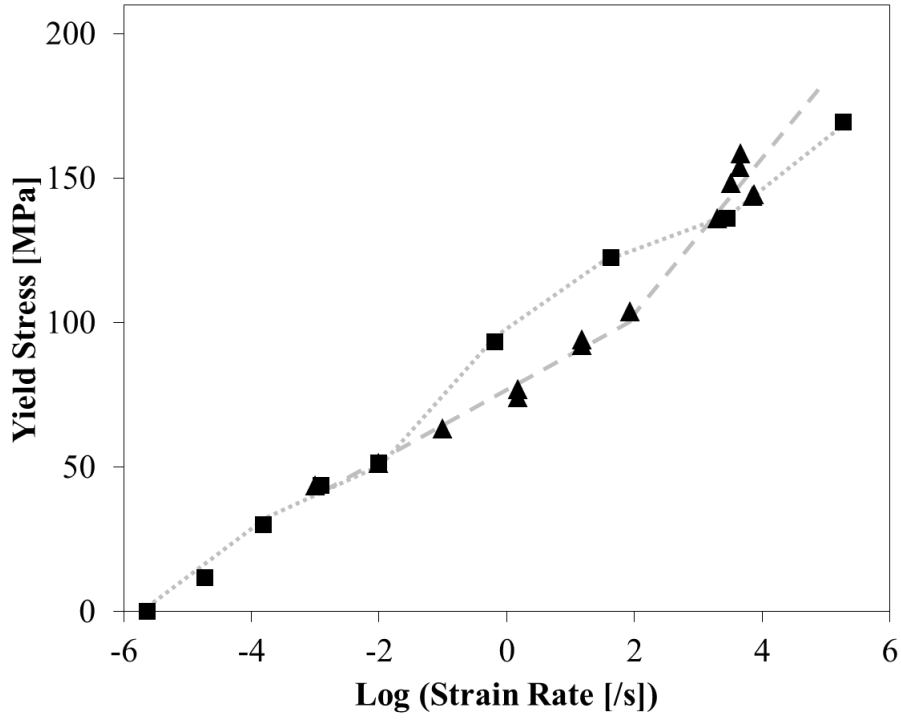


(b)

Figure 4-7: PVC yield stresses where (a) temperature data (squares) is mapped onto strain rate data (triangles) and (b) strain rate data is mapped onto temperature data using D = 13.5 °C/decade $\dot{\varepsilon}$ from equation 4.3.

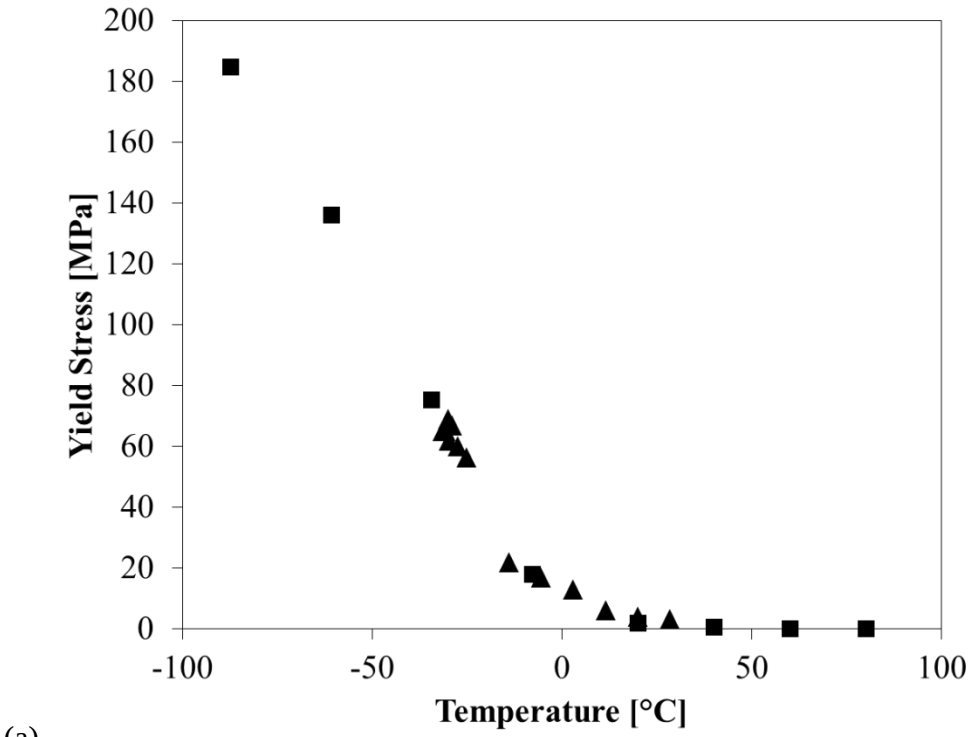


(a)

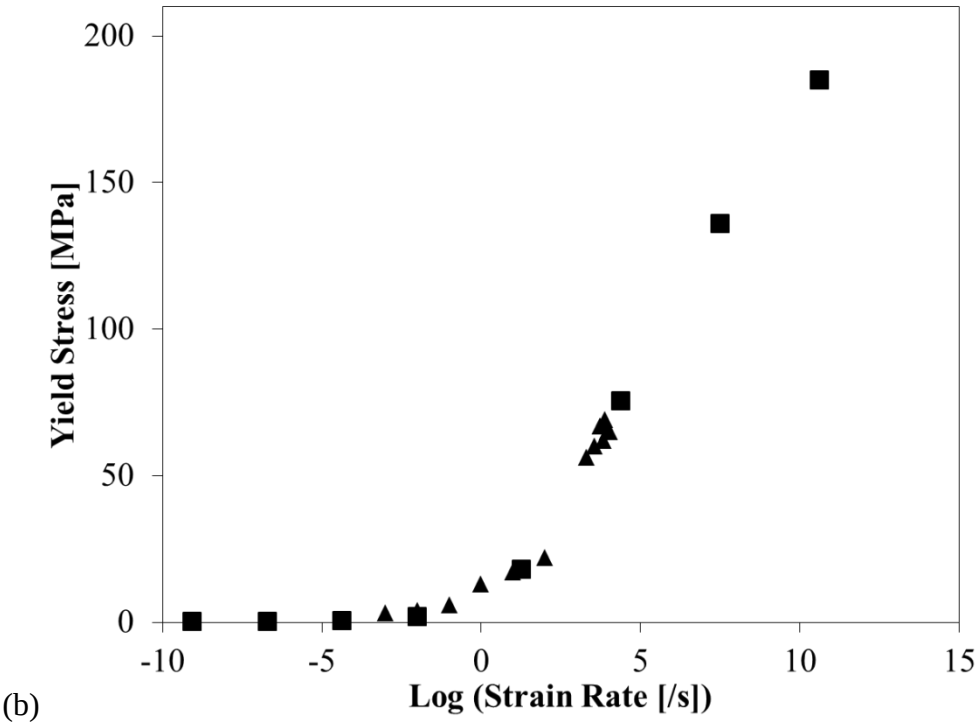


(b)

Figure 4-8: PPVC-2 yield stresses where (a) temperature data (squares) is mapped onto strain rate data (triangles) and (b) strain rate data is mapped onto temperature data using D = 11 °C/decade $\dot{\varepsilon}$. The dashed lines (strain rate data) and dotted lines (temperature data) are used to help present the subtleties of the two different sets of data. This data is described in greater detail in the next section below.

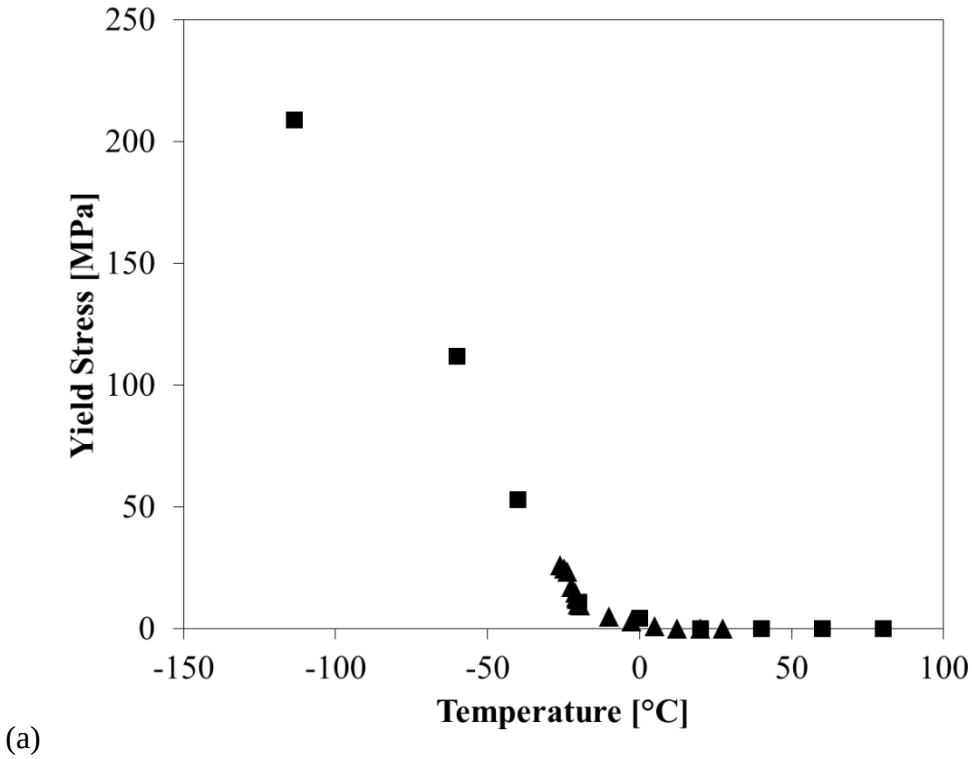


(a)

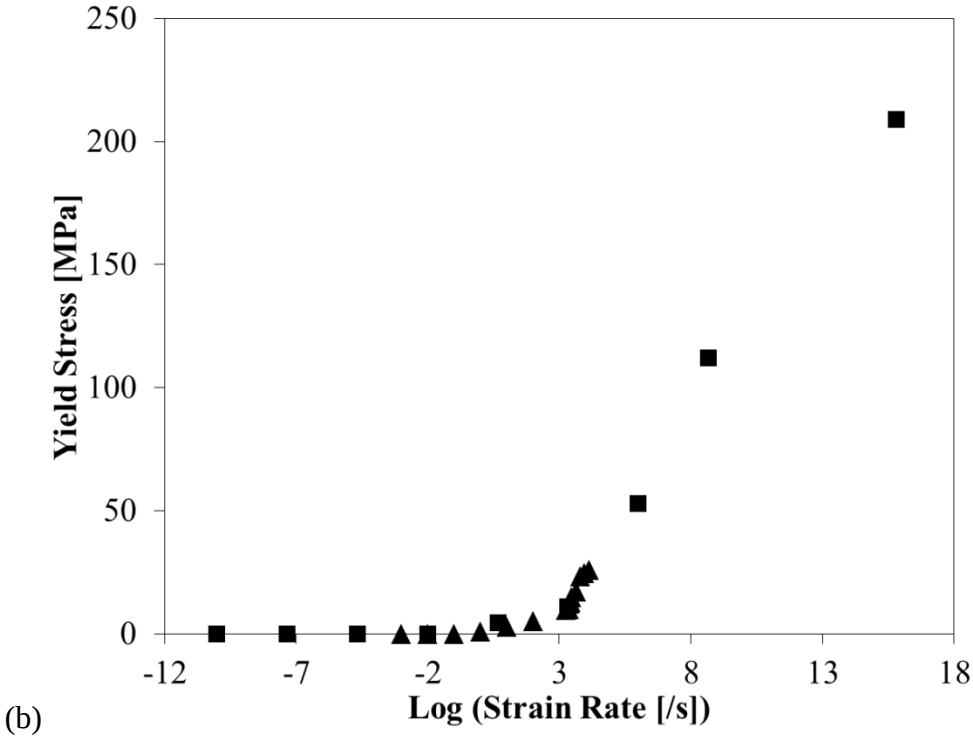


(b)

Figure 4-9: PPVC-4 yield stresses where (a) temperature data (squares) is mapped onto strain rate data (triangles) and (b) strain rate data is mapped onto temperature data using D = 8.5 °C/decade $\dot{\varepsilon}$.



(a)



(b)

Figure 4-10: PPVC-6 yield stresses where (a) temperature data (squares) is mapped onto strain rate data (triangles) and (b) strain rate data is mapped onto temperature data using D = 7.5 °C/decade $\dot{\varepsilon}$.

Due to relatively weaker superposition results of PPVC-2 (figure 4-8), the time-temperature equivalence method was further improved upon in order to better understand the time temperature behavior of this material.

4.3.1 WLF

The Williams-Landel-Ferry (WLF) model is an empirical formula (equation 4.2, and described earlier in section 7.1.3) which employs two empirically fitted constants (C_1 and C_2) in order to fit small strain data (see table 4.1). The formula has been very effective in predicting small-strain deformation for a modest temperature range of T_g to T_g +100 °C in several amorphous polymers with hardly any or no changes to the coefficients in the model (Williams et al., 1955). Critiques of the WLF formula in viscoelastic studies often include the model's limitation to the low strain regime and its difficulties in predicting large strain deformations.

In order to use the WLF model with temperature and rate dependent true yield stress data, equation 4.2 must be applied to both sets of data. In order to compare the two sets of data on the same axes, a frequency dependency was employed:

$$\log f' = \log a_T + \log \dot{\varepsilon} \tag{4.4}$$

where f' is the equivalent frequency. In order to compare the two sets of data with additional temperature and rate data, the model was also employed with DMTA data. The implementation was conducted once again with equation 4.2, using the range of temperatures tested, and a frequency dependency was used again in order to compare data with more certainty:

$$\log f' = \log a_T + \log f_{DMTA} \tag{4.5}$$

where f_{DMTA} is the DMTA test frequency. The final implementation of the model involved the elastic modulus (E) of the DMTA data being compared on a separate axis to the true yield

Table 4.1: PPVC-2 experimentally derived constants for WLF formula

	PPVC-2
C_1	-30
C_2	200
T_s [K]	311

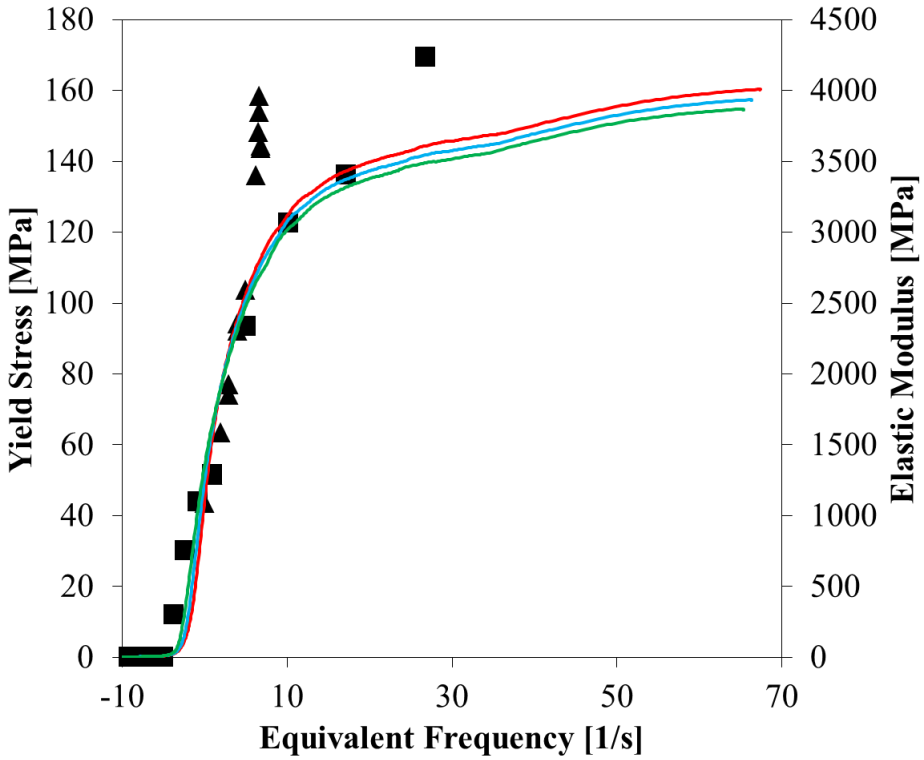


Figure 4-11: PPVC-2 yield stress data and storage modulus data dependent upon frequency data modeled with the WLF formula equation 4.9. Temperature dependent true yield stress data (squares); rate dependent true yield stress data (triangles); DMTA elastic modulus data at 0.035 s^{-1} (green), 0.35 s^{-1} (blue), and 3.5 s^{-1} (red). The analytical method presented in this figure is that of Nielsen (1962), where the independent variable is manipulated to be frequency (instead of temperature).

stress given from the temperature and rate dependent data. The result of this is presented in figure 4-11. Both constants C_1 and C_2 (table 4.1) were fitted manually with the experimental data shown. The reference temperature, T_s, was chosen as the glass transition temperature.

4.3.2 Separation of α and β processes

The DMTA results for PPVC-2 were further investigated for a better understanding of the interplay between temperature and rate. After the WLF equation ineffectively captured the

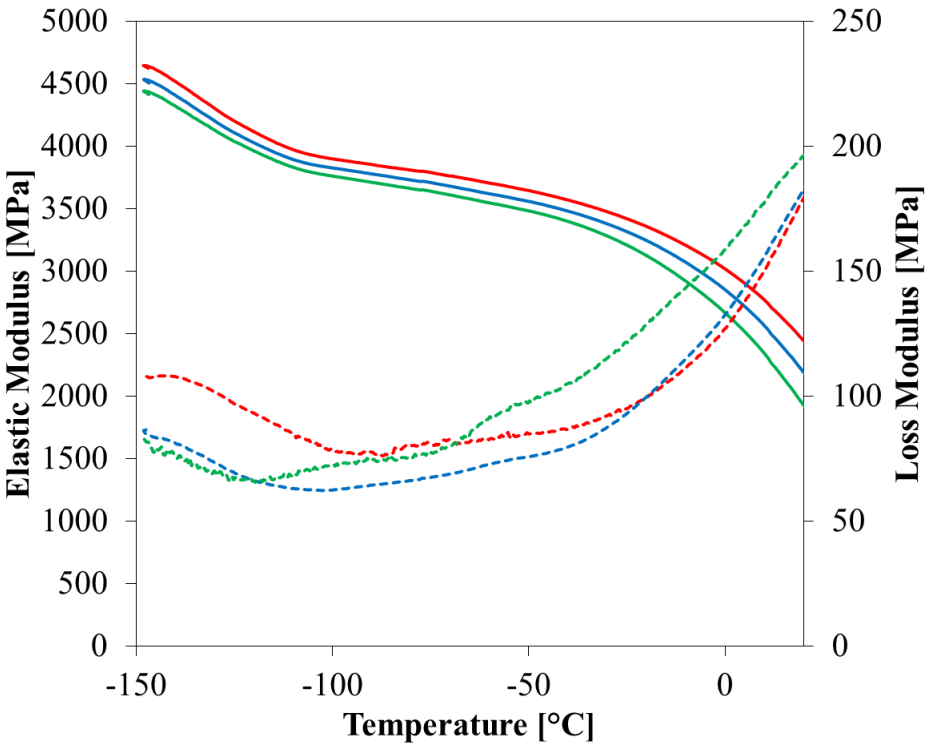


Figure 4-12: PPVC-2 elastic modulus and loss modulus curves at 0.035 s^{-1} (1 Hz – green), 0.35 s^{-1} (10 Hz – blue), and 3.5 s^{-1} (100 Hz – red). β transition is centered at approximately -150 °C. Note: this figure is repeated from the last chapter for reference.

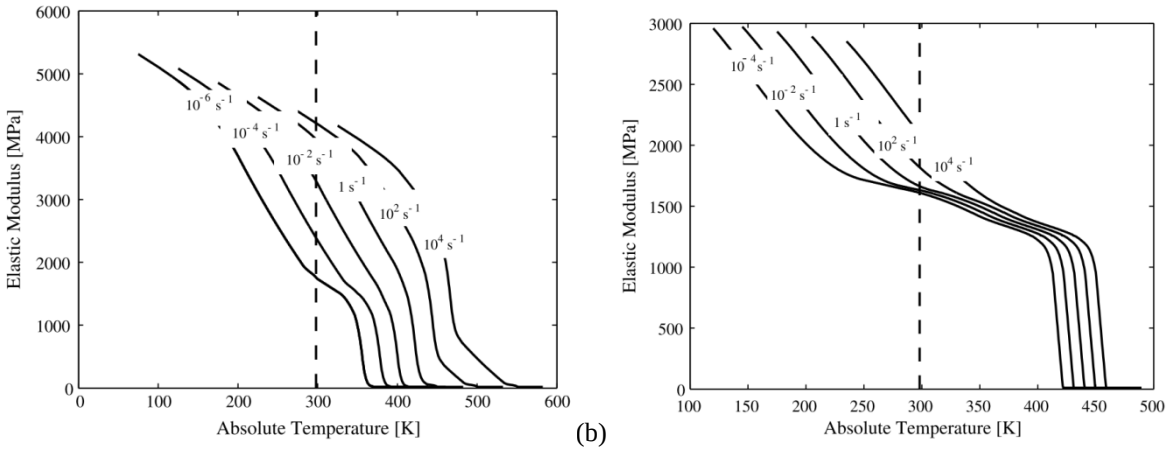
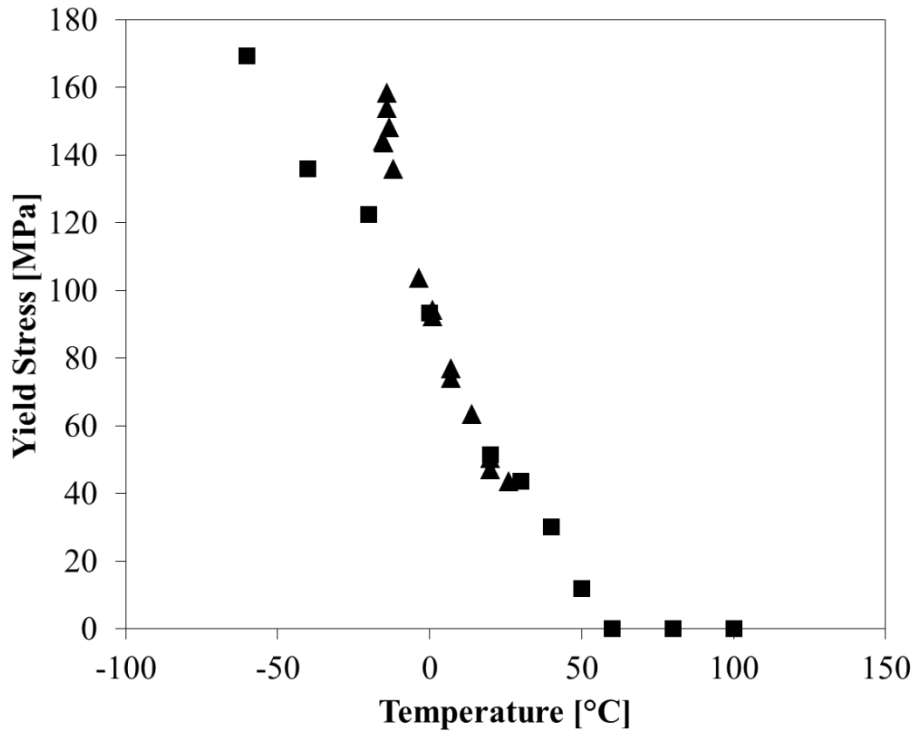


Figure 4-13: Deconstruct-Shift-Reconstruct (DSR) method implemented by Mulliken & Boyce (2006) which presents the PC elastic modulus at five strain rates: 10^{-4} s^{-1} to 10^{4} s^{-1}. The vertical dashed line represents a room temperature of (298 K).

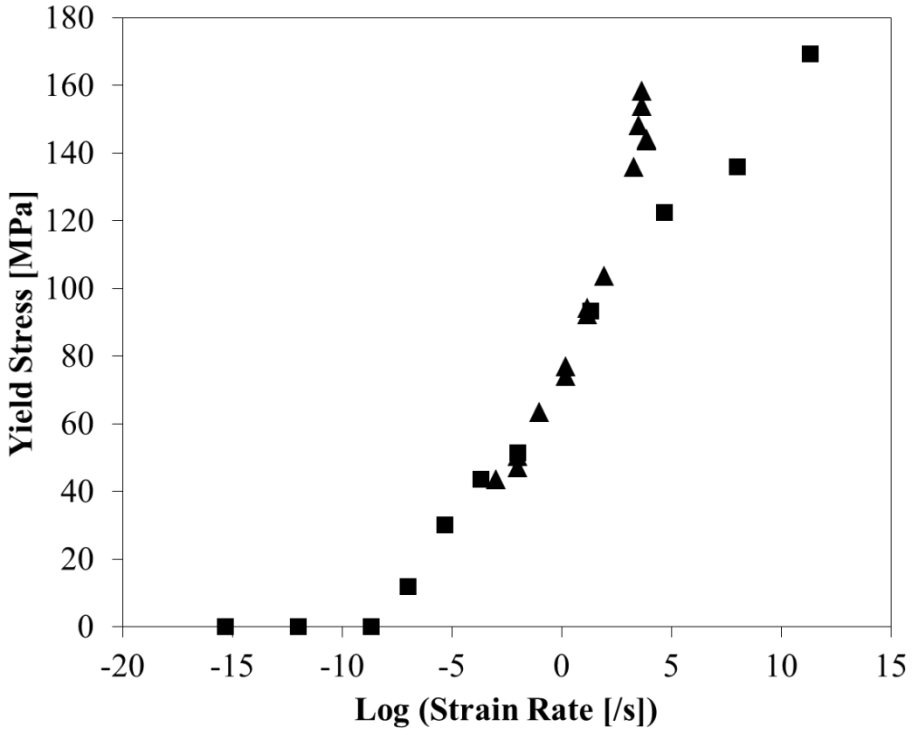
time temperature behavior of PPVC-2, leading to the linear equivalence formula developed by Siviour and co-authors (2005) being further investigated (referring forward to equation 4.10). Low temperature (-150 °C) DMTA data (presented in section 3.4.2) were used to find an experimentally determined shift factor of 6 °C/decade $\dot{\varepsilon}$ to fit PPVC-2 data with the Siviour et al. methodology[3]. Using DMTA data (figure 4-12) to find experimentally determined shift factors[4] gives a different perspective on the time-temperature equivalence approach in place: frequently the shift factor is found from fitting the two sets of data. The result of the shift factor found from DMTA data is presented in figure 4-14. Using the DMTA shift factor noticeably improves the fit of the low to moderate rate (10^{-3} to 85 s^{-1}) and moderate to high temperature data (0 to 100 °C).

There is exceptional agreement through moderate rate data (up to 85 s^{-1}, or up to the equivalent temperature of -5 °C), with a slight separation from the linear inter-dependence of the data sets at higher rates (>1000 s^{-1}, or < -10 °C) from the influence of the β transition. This departure can be attributed to the β transition having a different rate, or frequency, dependence than the temperature dependent yield stress data and elastic modulus data. As seen from the DSR data of two amorphous polymers (PC and PMMA) in figure 4-13, the elastic modulus (analogous to the true yield stress in time-temperature shifting) takes a different shape as the rate is increased. The β transition has a different rate dependence compared to the α transition (which can also be realized from the different shift factors for the two transitions). Thus, the β transition can be observed at a high rate (e.g. 2000 s^{-1} at room temperature, 20 °C) but not until very low temperatures at low rates (e.g. the 10^{-2} s^{-1} strain rate used for temperature dependent compression data). For example, a temperature such as -140 °C at a rate of 0.035 s^{-1} is the location of the β transition, or peak of the red loss modulus curve in figure 4-12, thus the β transition does not occur until this low a temperature

[3] Additional detail in DMTA shift factors is presented in the following section when using all PVC materials.
[4] This method has been used for locating shift factors in constitutive modeling (presented later in Chapter 8), but is often not employed in time-temperature equivalence calculations.



(a)



(b)

Figure 4-14: PPVC-2 yield stresses where strain rate data (triangles) is mapped onto temperature dependent data (squares) and (b) temperature data (squares) is mapped onto strain rate (triangles) data using D = 6 °C/decade $\dot{\varepsilon}$.

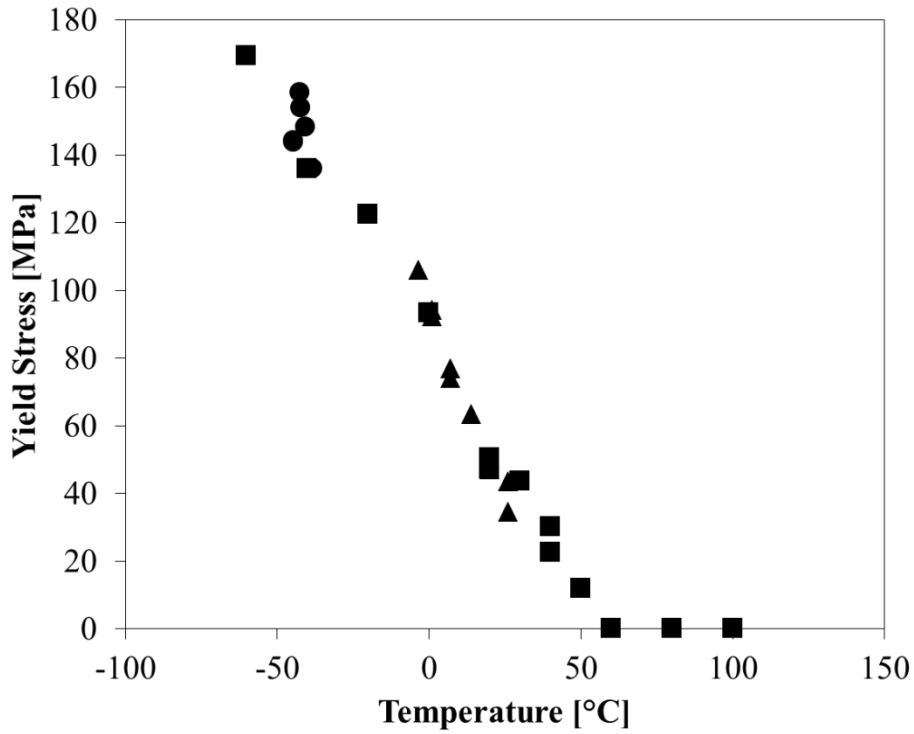


Figure 4-15: PPVC-2 strain rate data (triangles and circles) mapped onto temperature data (squares). Using D_α = 6.0 °C/decade $\dot{\varepsilon}$ (triangles) from equation 4.6 for low to moderate strain rates (0.001 to 85 s^{-1}) and using D_β = 13.0 °C/decade $\dot{\varepsilon}$ (circles) for high strain rates (2018 to 7554 s^{-1}) where β influences were confirmed by DMTA data.

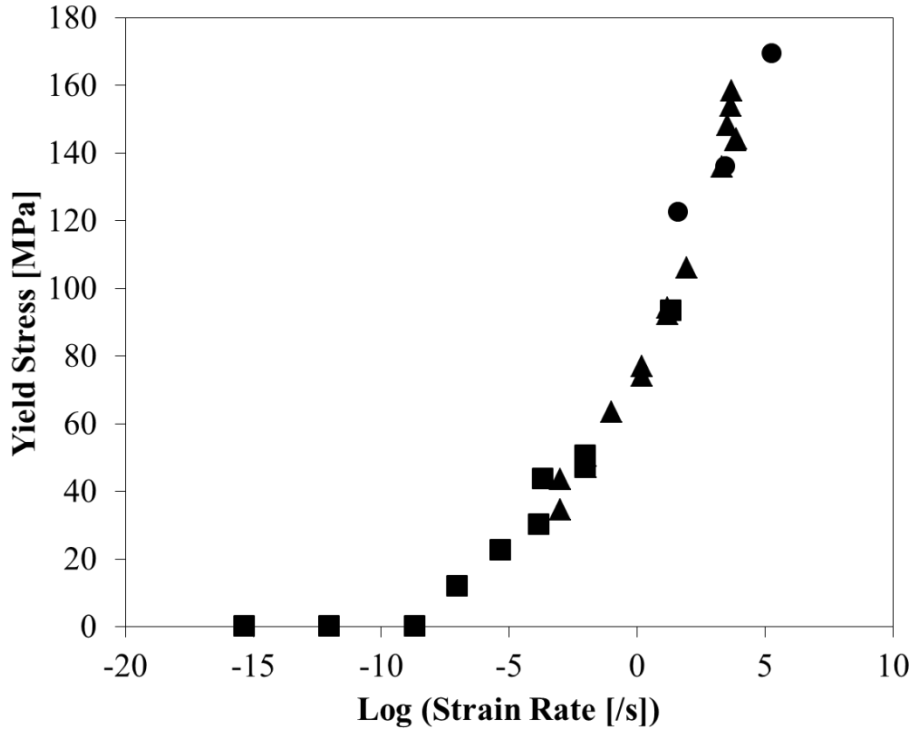


Figure 4-16: PPVC-2 temperature data (squares and circles) mapped onto strain rate data (triangles). Using D_α = 6.0 °C/decade $\dot{\varepsilon}$ (squares) from equation 4.6 for low to moderate strain rates (0.001 to 85 s^{-1}) and using D_β = 13.0 °C/decade $\dot{\varepsilon}$ (circles) for high strain rates (2018 to 7554 s^{-1}) where β influences were confirmed by DMTA data.

in the quasi-static data and would not be seen in the material response until at approximately < -100 °C.

The β influence in the high rate response becomes clear when using the β shift factor, a larger D_β value found from the DMTA-confirmed β transition (13.0 °C/decade $\dot{\varepsilon}$), for the high rate or low temperature PPVC-2 data. The DMTA-confirmed α transition (6 °C / decade $\dot{\varepsilon}$) is also used (figures 4-15 and 4-16).

This time-temperature equivalent methodology to describe the data is given as:

$$T - T_0 = D_\alpha \left(\log \frac{\dot{\varepsilon}_0}{\dot{\varepsilon}} \right) \tag{4.6}$$

$$T - T_0 = D_\beta \left(\log \frac{\dot{\varepsilon}_0}{\dot{\varepsilon}} \right) \tag{4.7}$$

and the results of which are presented in figures 4-15 and 4-16. These different values capitalize on the β transition and α transition having different temperature-strain rate equivalence factors. The use of the experimentally determined shift factors shows exceptional agreement in time-temperature equivalence of the yield stress data. This good, and very interesting, agreement highlights the fact that several processes involved in determining an amorphous polymer's elastic modulus and yield stress are shared, or overlap, with one another. Furthermore, this presents a new addition to the methodologies of time-temperature equivalence and offers opportunities in standardization, automation, and a more scientific method for finding shift factors (D_α and D_β) for time-temperature equivalence.

4.3.3 Application and Discussion of Additional Materials

In order to confirm the validity and strength of the proposed method in the previous section, the methodology was applied to the three other PVC based materials.

After examining table 4.2, the values of experimentally fitted shift factors are defined by whether the material has an above or sub-ambient alpha transition temperature. In the

Table 4.2: PVC and all PPVCs' shift values[5] [K/decade strain rate] found experimentally from DMTA data compared to shift values found from an experimental fit to data.

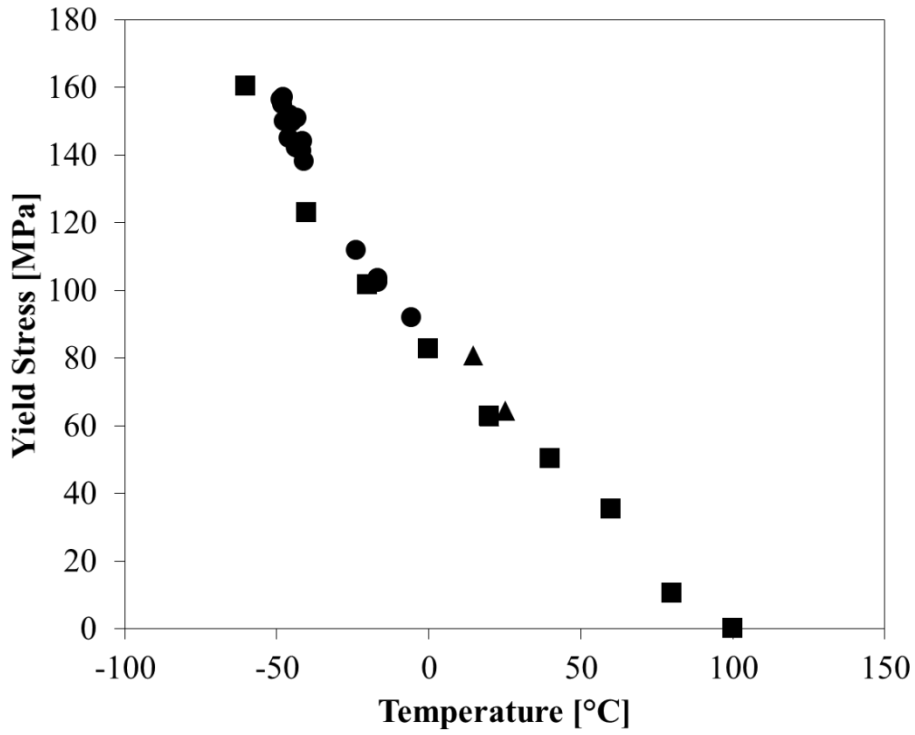
	D_α	D_β	D
Material	DMTA	DMTA	Experimental Fit
PVC	5.4	11.8	13.5
PPVC-2	6.0	13.0	11.0
PPVC-4	7.6	16.8	8.5
PPVC-6	7.7	17.3	7.5

cases of materials with glass transition temperatures above room temperature (the more 'glassy polymers'), the shift factor *D*, is defined by the β transition, and the α transition appears to define the effectiveness of the shift factor if this same transition lies below ambient temperature.

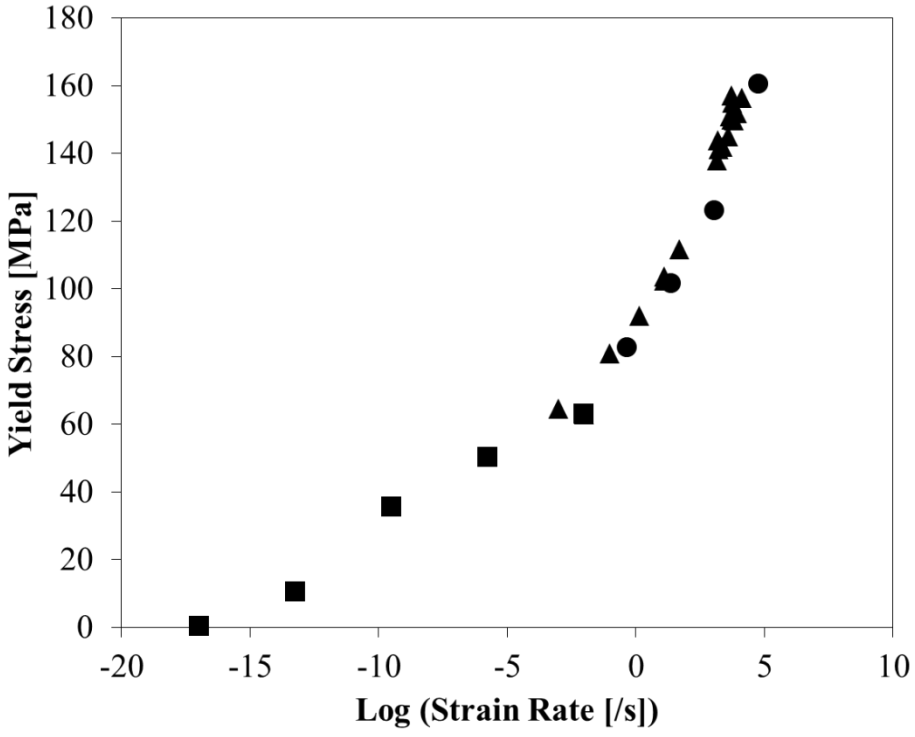
In addition, upon examining the measured shift factor values for the alpha and beta transitions, it is noted that D_β is much larger than D_α. Macroscopically this difference demonstrates the higher rate sensitivity of the beta transition compared to the alpha transition. On the molecular scale, there is a difference between the amount of energy that is necessary to stop the movement associated with the much smaller and more localized scale polymer chain (and/or side groups attached to them) motion, β-motions, versus the larger and cooperative chain motion associated with the glass transition, α-motions (Bicerano, 2002).

The table also presents trends in plasticizer wt%, which clearly affects the behavior of the polymers. Firstly, the addition of plasticizer increases both shift factors (α and β), or increases the sensitivity of the location of the transitions to the rate of deformation. Namely, the more plasticizer added to (or rubbery behavior of) a polymer, the polymer needs higher

[5] tanδ or loss modulus peaks may be used to find the temperature locations of the material transitions (α and β). These values are also used to find the shift factors (D_α and D_β). Differences in this thesis are typically ~1 °C/decade strain rate when using tanδ rather than the loss modulus. Loss modulus peaks were used in all cases in this thesis.



(a)



(b)

Figure 4-17: PVC (a) strain rate data (triangles and circles) mapped onto temperature data (squares) and (b) temperature data (squares and circles) mapped onto strain rate data (triangles). Using D_α = 5.35 °C/decade $\dot{\varepsilon}$ (squares) for low strain rates (0.001 to 0.1 s^{-1}) and using D_β = 11.80 °C/decade $\dot{\varepsilon}$ (circles) for moderate to high strain rates (1 to 6330 s^{-1}) where β influences were confirmed by DMTA data.

rates of deformation to observe the shift of the beta transition to room temperature. More specifically, to stop the polymer chain or side group motion which occurs on a much more localized scale or 'intramolecular skeletal modes of vibration' (Porter & Gould, 2009), a much shorter time scale of deformation is required. The shift factor of materials determines the rate dependence of the material and how easily these transitions are seen in material response at ambient temperature.

By examining the DMTA curves of the PVC materials, the beta transition appears to shift to a much lower temperature once plasticizer is added (in this case 20 wt%). Interestingly, regardless of the amount of plasticizer added (e.g. 20 wt% for PPVC-2 vs 60 wt% for PPVC-6), the beta transition stays in approximately the same position at the lowest rate (0.035 s^{-1} or 1 Hz): the amount of plasticizer does not shift the approximate location of the β transition, even though the α transition shifts to a lower temperature once plasticizer is added (as expected). Thus, the addition of more phenyl rings (or DINP), which is understood to create additional free volume in the material (Hill, 1950; Hasan & Boyce, 1995; Soong et al., 2006), does not affect the location of the beta transition. Thus, the beta transition must include more than just the behavior of phenyl rings (i.e. a π-flip), if making comparisons to materials such as PC with and/or without additives (e.g. Bicerano, 2002), and therefore there must be some intra- or intermolecular cooperativity included.

The dual-process time-temperature superposition method (via DMTA shift values) was also applied to PVC[6] which is presented in figure 4-17, demonstrating a very good agreement in the new addition to time-temperature equivalence methodologies.

[6] The formula was not applied to PPVC-4 or PPVC-6, as the temperatures and strain rates tested did not reach the β transitions of either material. Furthermore, the experimentally fitted shift values (data which only included α processes) agreed well with the D_α found from DMTA data.

4.4 Conclusions

The literature involved in time-temperature equivalence was investigated. Additionally, the nature of three different time-temperature equivalence methods was explored over a large temperature range, which gave a useful insight into the ease and accuracy of each method (Siviour, SMT, and WLF). It was concluded that the Siviour formula had the most straightforward implementation and met the necessary requirements for the temperature and rates used in this study – the formula successfully described three of the four (PVC, PPVC-4, and PPVC-6) materials behaviors. Furthermore, the accuracy of two different time-temperature equivalence methods (Siviour and WLF) was investigated using PPVC-2 – the study demonstrated that neither methodology accurately described the behavior of PPVC-2, particularly the high rate behavior. Lastly, building upon the linear formulation of time-temperature equivalence (Siviour et al, 2005), a new component to the methodologies of time-temperature equivalence was created to separate the β and α influences in high rate and low temperature data, emphasizing the alternative for finding shift factors (D_α and D_β) experimentally via DMTA data, and a better understanding of the driving factors in time-temperature equivalence were better understood by better describing amorphous and rubbery polymer time-temperature behavior.

Chapter 5

Simulation of High Rate Behavior

Polymers are frequently used in applications in which they may be exposed to high rate or impact loading, and there is a growing industrial importance in understanding what constitutes their mechanical behavior. This chapter describes research that has been performed to better understand and predict the dependence on strain rate of mechanical properties such as yield and flow stress, by investigating the relationship between rate dependence and temperature dependence. In particular, the mechanical behavior of poly(vinyl chloride) with 20wt% plasticizer has been studied at strain rates from 0.001 to 4700 s^{-1} and temperatures from -60 to +80 °C. In this chapter, a novel experimental method is presented in which the effects of modulus, yield, and post-yield behavior (e.g. figure 5-1) seen at high strain rates of deformation are simulated at quasi-static rates of deformation.

This chapter includes data presented in Kendall and Siviour (2013) published in Polymer journal.

5.1 Introduction

As high performance materials continue to be developed, there has been an increased demand for test methods capable of analyzing and comparing materials over a wide range of strain rates. The demand is particularly apparent in testing low impedance materials at high rates, for which there can be difficulties in obtaining dynamic stress equilibrium.

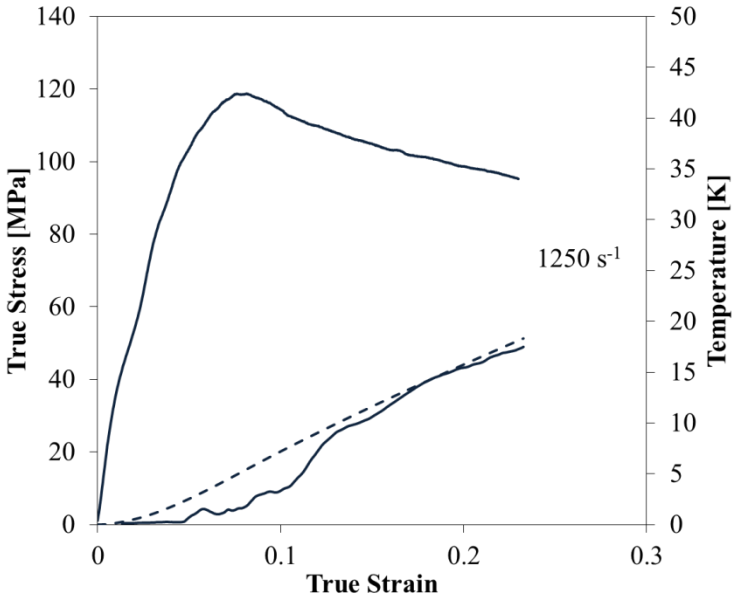


Figure 5-1: Example of high rate post-yield behavior: Temperature rise observed (solid line in lower half of figure) during testing due to the adiabatic nature of testing at 1250 s^{-1} and the ~100% conversion of plastic work being converted to heat during temperature measurement experiments presented in Chapter 9 of this thesis. Note: Dashed line is the theoretical temperature rise calculated from the true stress-true strain behavior (solid line).

A large amount of literature has been produced describing investigations of the rate dependence of polymers. Chou et al. (1973) were some of the first to examine the structural performance of polymers over a wide range of strain rates (10^{-4} s^{-1} to 10^{3} s^{-1}), looking at cellulose acetate butyrate, nylon 66, polymethyl methacrylate (PMMA), and polypropylene on a Split Hopkinson Bar (SHPB) apparatus and a medium rate testing machine. Examination of the mechanical strength, or yield stress, dependence upon the logarithm of strain rate showed that the polymers were more sensitive to increases in strain rate under high rate loading than they were under quasi-static.

Polymers are very sensitive to both temperature and strain rate. In several polymers, the sensitivity is understood to increase at lower temperatures and/or higher rates of strain because of a lack of secondary mobility (β motions), which causes increased strength and stiffness. Alternatively, the increased strength in more rubbery or elastomeric polymers is accounted for by the change in molecular mobility during the glass transition (or α transition).

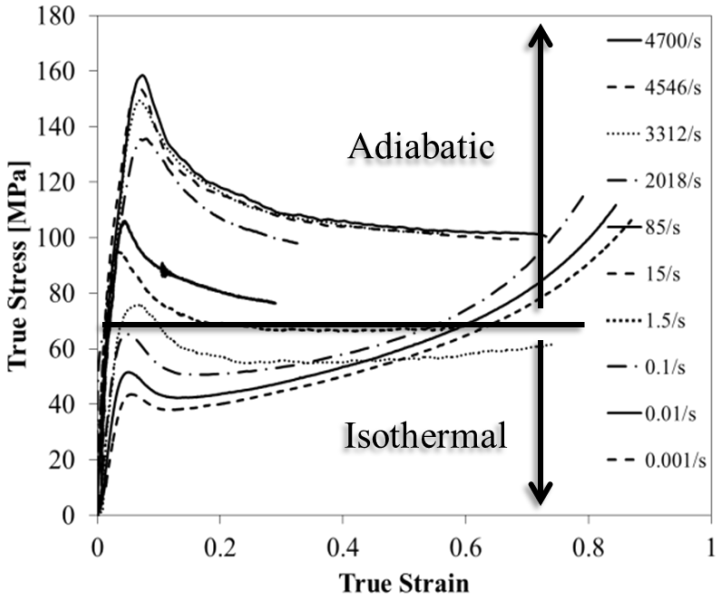


Figure 5-2: The observed change in true stress-true strain post-yield behavior understood to be the transition from isothermal to adiabatic conditions; seen here with PPVC-2 between 10^{-1} s^{-1} and 1.5 s^{-1}.

In many cases, these transitions are observed in polymers at low temperatures, but can be shifted in temperature by changes in strain rate: the transition temperature increases with increasing rate. This phenomenon was observed in PVC by Bauwens in 1969, where the effect was captured via the Ree-Eyring theory of non-Newtonian flow. Similarly, attempts to connect the effects of temperature and strain rate via time-temperature superposition have been investigated using the well-known WLF equation (Williams et al., 1955), or a linear time-temperature equivalence mapping (Siviour et al., 2005; Brown et al., 2007, Williamson et al., 2008). In experimentally unifying these phenomena, Cady et al. (2003) mentioned the possibility of simulating high rate response of polymers by low rate/low temperature tests, and more recently, Furmanski et al. (2012 & 2013) found a linear empirical formulation of time-temperature equivalence in HDPE, while using jump-rate compression tests to investigate isothermal high rate response with the absence of adiabatic heating.

The change from isothermal to adiabatic conditions (figure 5-2) as the strain rate increases is an important feature of high rate deformation and post-yield behavior, which

must be considered alongside the temperature dependence of yield stress when considering changes in material behavior as a function of strain rate.

Important studies involving the measurement of temperature rise in specimens during high rate deformation have been conducted by a number of authors. A notable achievement was by Chou et al. (1973), who showed that the temperature rise in specimens increases significantly after yield. Furthermore, Arruda et al. (1995) presented visible increases in strain softening with increases in strain rate, coupled with corresponding temperature measurements using infrared detectors. Rittel (1999), and later Regev and Rittel (2007), used thermocouples to measure the temperature rise in specimens undergoing high rate deformation and later confirmed the accuracy of this method via infrared techniques. Additionally, Garg et al. (2008) used infrared techniques to measure the temperature rise of PC undergoing high rate deformation. Good agreement was observed between the experimentally measured temperature rise and the 'theoretical' rise obtained by assuming that 100% of the mechanical work is converted to heat, and adiabatic conditions prevail. Hillmansen et al. (2000 & 2001) studied plastic work being converted to heat by studying high density polyethylene (HDPE) and found, similarly, that the plastic work at large strains was approximately 100 % converted to heat.

By combining an understanding of temperature dependence with an appreciation of adiabatic conditions, there is an opportunity to better understand and capitalize on the analogous effects of temperature and strain rate in polymers. This is particularly timely considering the several obstacles of high rate testing, especially when the materials of interest are soft (e.g. rubbers and biomaterials), or have large representative volume elements, requiring large specimens (composites). An important consideration when measuring high rate properties of materials, especially those with a low sound speed, is the well-described requirement for a specimen to reach mechanical equilibrium before the results of an

experiment may be regarded as valid (Gray III, 2000). The specimen is loaded from one end with a stress wave, which imposes a deformation rate on that end of the specimen. The wave oscillates a number of times within the specimen, each time increasing the specimen stress in a stepwise manner. Eventually, enough oscillations occur so that the stress does not vary significantly with position in the specimen; the specimen is now in quasi-static equilibrium, although deformed at a high strain rate. Equilibrium is required because in the classical Hopkinson bar technique, only forces and velocities at the bar specimen interface are calculated, and thus average specimen properties are derived, and because, until equilibrium is achieved, the forces measured in the bars are not necessarily the same as those experienced by the specimen, and the quasi-static assumption is not valid.

Although the difficulties of achieving specimen equilibrium are therefore obvious for materials with low sound speeds, composites create similar difficulties in testing, and would similarly profit from an experimental simulation method in order to better understand high rate behavior. Composites often have a polymer, or soft material, as a filler, such as 3D fibre reinforced polymers (Thiruppukuzhi et al., 1998) and polymer bonded explosives (Drodge et al., 2010). Modern 3D reinforced fibre composites can have complex deformation behaviors (Gerlach et al., 2012). Experimental determination of these behaviors is complicated by the fact that the characteristic length of the polymer filler may be on the order of a 100 μm length scale, while the damage formation is on a 1-10 μm length scale and the repeat units in the weave are on 10-100 mm length scales. This means that large specimens are desirable to have a suitable representative volume element, but in-situ microscopic examination is required to fully understand damage formation. Both of these requirements are difficult to meet in a high strain rate experiment. As an example of a particulate composite, polymer bonded explosives (PBXs) typically use soft rubbers or polymers as a binder; the binder might only constitute 10% of the material, but has a large effect on the mechanical response,

and in particular the rate and temperature dependence. Biomaterials provide another example of composite materials with a wide range of length scales which provide similar challenges in high strain rate characterization. These materials share the challenge of in-situ microscopic examination during deformation, and also the problem of achieving equilibrium, this time because of the relatively low sound speed in the material.

This chapter presents data obtained using a novel experimental method that aims to predict and experimentally simulate the stress-strain response expected in a polymer, by performing a low rate experiment at reduced temperatures. A key development is to simulate not only the increase in modulus and yield stress, by reducing the temperature at the start of the experiment, but also the effects of adiabatic heating by increasing appropriately the temperature as the experiment progresses. The opportunity to predict or simulate high rate loading not only avoids several obstacles of high rate testing, such as dynamic equilibrium, but also allows for microscopic investigation on much smaller length scales through the use of electron and optical microscopy, especially in composite materials in which one component exhibits rate and temperature dependence while the other does not. In addition, future development of the technique to increase its fidelity beyond that presented in this chapter may provide an opportunity to better understand the mechanisms of high rate deformation, especially the conversion of work to either heat or to structural changes in the material.

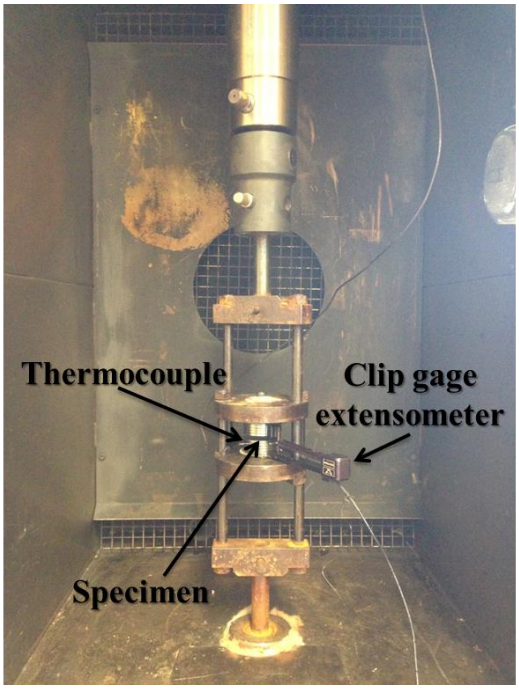
5.2 Experimental method

5.2.1 Materials

Low, medium, and high rate compression tests were conducted with PPVC-2 specimens of 2.5 mm length and 5 mm diameter. PPVC-2 has a low plasticizer level of 20wt%. The PPVC-2 came as pressed plates with dimensions of 11.5 x 20 cm and a thickness of 2.5 mm. These plates were machined to the specified specimen geometry, such that the axis of the specimen in the loading direction was perpendicular to the plane of the plate. All specimens were lubricated with a thin layer of petroleum jelly (Trautmann et al., 2005), and there was no observable barreling during the experiments.

5.2.2 Compression Testing

Uniaxial compression tests were performed over rates ranging from 10^{-3} s^{-1} to 4700 s^{-1}. Quasi-static tests at 10^{-3}, 10^{-2}, and 10^{-1} s^{-1} were performed using an Instron testing machine. Force measurements were taken from the load cell and displacement measurements from a clip gage extensometer attached to the loading platens. Quasi-static experiments were conducted over the temperature range -60 to 100 °C using a standard Instron environmental chamber. Here temperature readings from the environmental chamber were confirmed by the use of thermocouples attached to the platens adjacent to the specimen-platen interface. Temperatures were recorded with a National Instruments USB thermocouple reader. The colder temperatures were obtained using liquid nitrogen, with a standard tank attachment to the environmental chamber. To note, the equipment described in this paragraph was the setup used for the experimental simulation descried throughout and presented in this chapter, presented in figure 5-3. During the simulation experiment, the temperature was controlled manually via the temperature controller presented in figure 5-3b.

(a) 

(b) 

Figure 5-3: a) Quasi-static testing machine by Instron with custom-built compression rig and surrounding temperature chamber (50 cm length x 40 cm width x 66 cm height) used for low rate dependency, temperature dependency, and simulation experiments. The b) temperature control was used to make temperature adjustments during simulation tests.

Experiments at rates ranging from 1.5 s^{-1} to 85 s^{-1} were conducted on a custom-built hydraulic load frame. Linear variable differential transformers (LVDTs) were used to measure the displacements of the anvils, and a strain gauge based load cell measured the force supported by the specimen. These data were used to calculate the stress-strain relationship in the sample.

High rate testing was performed at rates ranging from 2018 to 7554 s^{-1} at 3300 s^{-1} on a split-Hopkinson pressure bar (SHPB) apparatus using magnesium alloy (AZM) bars for 2018 to 4700 s^{-1} tests and titanium alloy (Ti-6Al-4V) bars for 7221 and 7554 s^{-1} tests. The striker bar, incident bar, and transmitted bars all had diameters 12.6 mm, with lengths of 0.5 m, 1.0 m, and 0.5 m, respectively. The strain gauges were placed 0.5 m from the specimen-bar interface on the incident bar and 50 mm from the specimen-bar interface on the transmitted bar.

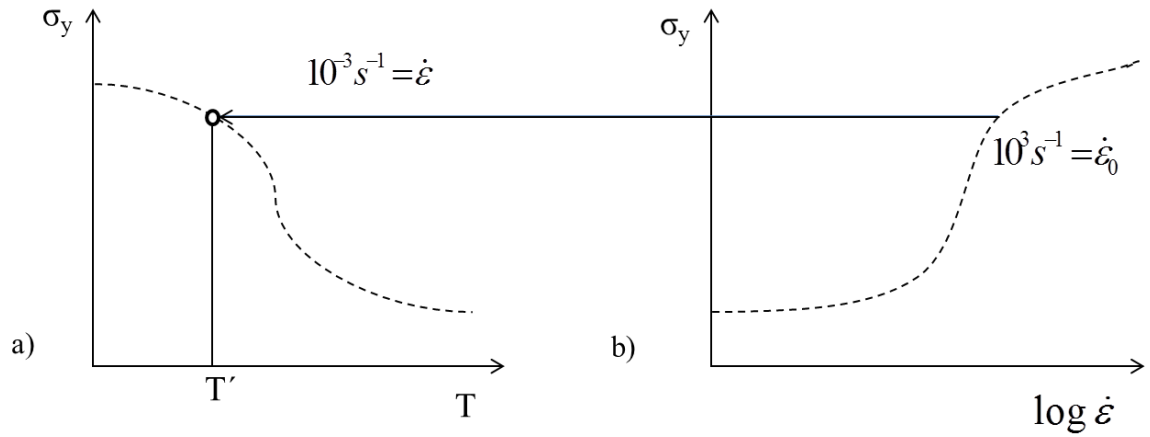


Figure 5-4: Schematic diagram of yield stress dependence upon a) temperature and b) strain rate, indicative of the process used to determine the initial temperature of testing in order to simulate the modulus and yield stress of a higher rate response.

Dynamic equilibrium was confirmed after each test by calculating force-time profiles for both specimen-bar interfaces.

5.2.3 Simulating Adiabatic Conditions

In order to simulate a given strain rate, $\dot{\varepsilon}_0$, an initial temperature *T'* was calculated using a mapping technique that compared the dependence of yield stress on temperature at a fixed rate to the dependence on strain rate at room temperature, this is illustrated in figure 5-2. The mapping is based on the same linear time-temperature equivalence method which has been successfully applied in previous papers (Siviour et al., 2005, Brown et al., 2007, Williamson et al., 2008; Jordan et al., 2008; Furmanski et al., 2013):

$$(T'-T)=D[\log\dot{\varepsilon}-\log\dot{\varepsilon}_0] \tag{5.1}$$

where *D* is a constant quantifies the relationship between temperature- and rate-sensitivity of the material, or the PPVC-2. Theoretically, the constant, *D*, can also be calculated from the time-related shift between frequencies from Dynamic Mechanical and Thermal Analysis (DMTA), however this was not done in the current study.

In order to complete the simulation process, the effects of adiabatic heating were then included. The rate at which the system is expected to behave adiabatically can be calculated from the size of the specimen and the thermal diffusivity of the specimen material using the three equations 5.2(a), (b) and (c). Firstly the thermal diffusivity is calculated from the conductivity, *k*, density, ρ, and specific heat capacity, *C*, using equation 5.2(a), alternatively the diffusivity can be found in a number of books. Secondly, the relationship in 5.2(b) is used to relate a characteristic timescale for thermal diffusion, *t*, to a characteristic length-scale μ_t. If μ_t is the length of the specimen, the characteristic timescale thus derived can be converted to a strain rate using equation 5.2(c).

$$\begin{aligned} &\text{(a)}\ \ \alpha = k \big/ \rho C \\ &\text{(b)}\ \ \mu_t = 2\sqrt{\alpha t} \\ &\text{(c)}\ \ \dot{\varepsilon} = 1/t \end{aligned} \qquad (5.2)$$

Although this is only an approximate calculation, the fact that material response is usually dependent on log($\dot{\varepsilon}$), means that in practice, when considering rate dependence of material properties, it is only necessary to have an order of magnitude estimate of the transition strain rate from essentially isothermal to essentially adiabatic conditions.

In terms of specimen response, specimen heating is understood to start at the onset of plastic deformation, which in practice can be taken to be the either the start of yielding, or the point of peak stress during yield. This assumption is supported by experimental results, where the temperature rise in polymers during high rate deformation was measured via infrared techniques (Arruda and Boyce, 1995; Regev and Rittel, 2007; Garg et al., 2008). Moreover, the experimental data presented in these papers support the assumption that that 100% of the post-yield work put into deforming the specimen is converted to heat, so that the equation:

$$\Delta T(\varepsilon) = \frac{\beta_T}{\rho C} \int_{\varepsilon_y}^{\varepsilon} \sigma d\varepsilon \qquad (3)$$

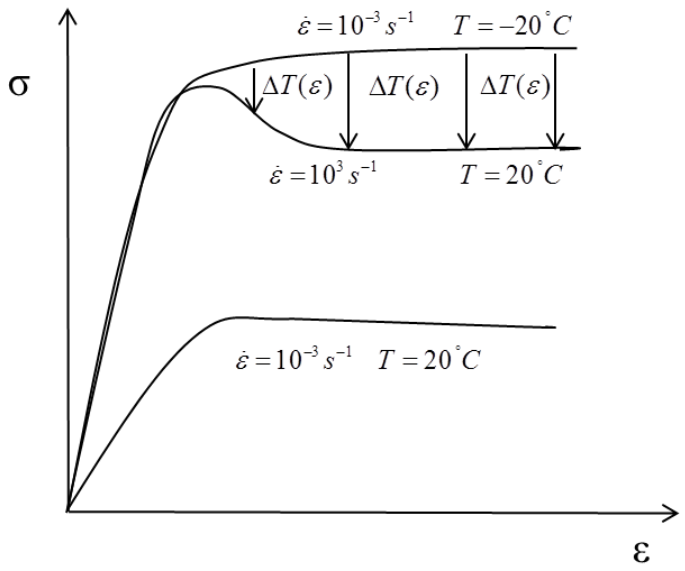


Figure 5-5: Change in temperature necessary to recreate the adiabatic heating which occurs at higher rates. The diagram includes the 10^{-3} s^{-1} strain rate which was used for the experimental work, and the room temperature during testing, 20 °C.

Table 5.1: PPVC-2 thermal properties used for the proposed simulation method

PPVC-2		
Heat capacity	880	J kg^{-1} K^{-1}
Density	1317	kg m^{-3}
Thermal diffusivity	0.08	mm^2 s^{-1}

can be used to find the temperature increase as a function of strain, where C is the heat capacity of the specimen, ρ is the density, and β_T is the so-called beta factor, or fraction of work converted to heat. The area of the stress-strain curve was numerically integrated via the trapezium rule and the result of this integral is converted to a temperature rise using $\beta = 1$.

The adiabatic temperature rise was simulated in the low rate experiments using the environmental chamber, with the temperature rise being regulated manually in increments of 0.01% strain. The method, including the hypothesized end result, is outlined in figure 5-5. The concept is further demonstrated experimentally in figure 5-6, by comparing the stress-strain response of PPVC-2 at 0 °C and 10^{-3} s^{-1} to an experiment at 15 s^{-1} and room temperature. Here, the reduction in initial temperature in the lower rate experiment matches

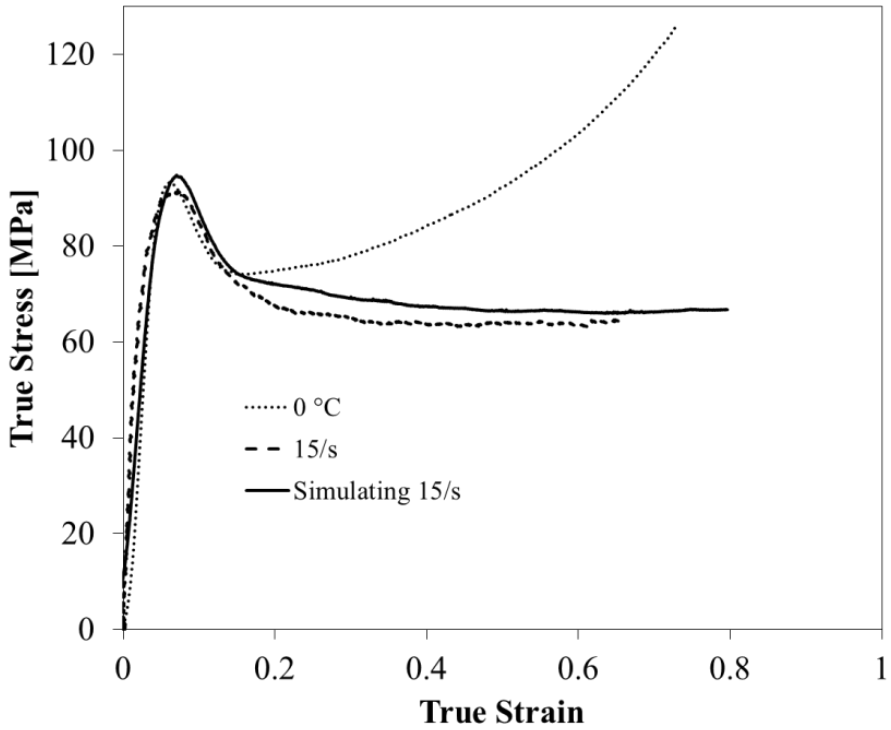


Figure 5-6: A comparison of PPVC-2 specimen response at 15 s^{-1} at room temperature, 10^{-3} s^{-1} at 0 °C which gives a similar yield to the 15 s^{-1} response, and a 10^{-3} s^{-1} response (starting from 0 °C) with adiabatic conditions simulated in order to capture the detail of the 15 s^{-1} response.

the yield stress in the higher rate, but not the post-yield response. To simulate the post-yield response, a 0 °C test was conducted in which the adiabatic heating within the specimen was simulated from the onset of plastic deformation onwards, resulting in a good agreement between the 15 s^{-1} response and the 10^{-3} s^{-1} simulation.

5.3 Results and Discussion

Initial experiments were performed to evaluate the response of the PVC to loading over a range of strain rates and temperatures (figure 5-7). When comparing the curves at different strain rates (figure 5-7b), there appears to be a clear transition between those experiments (at

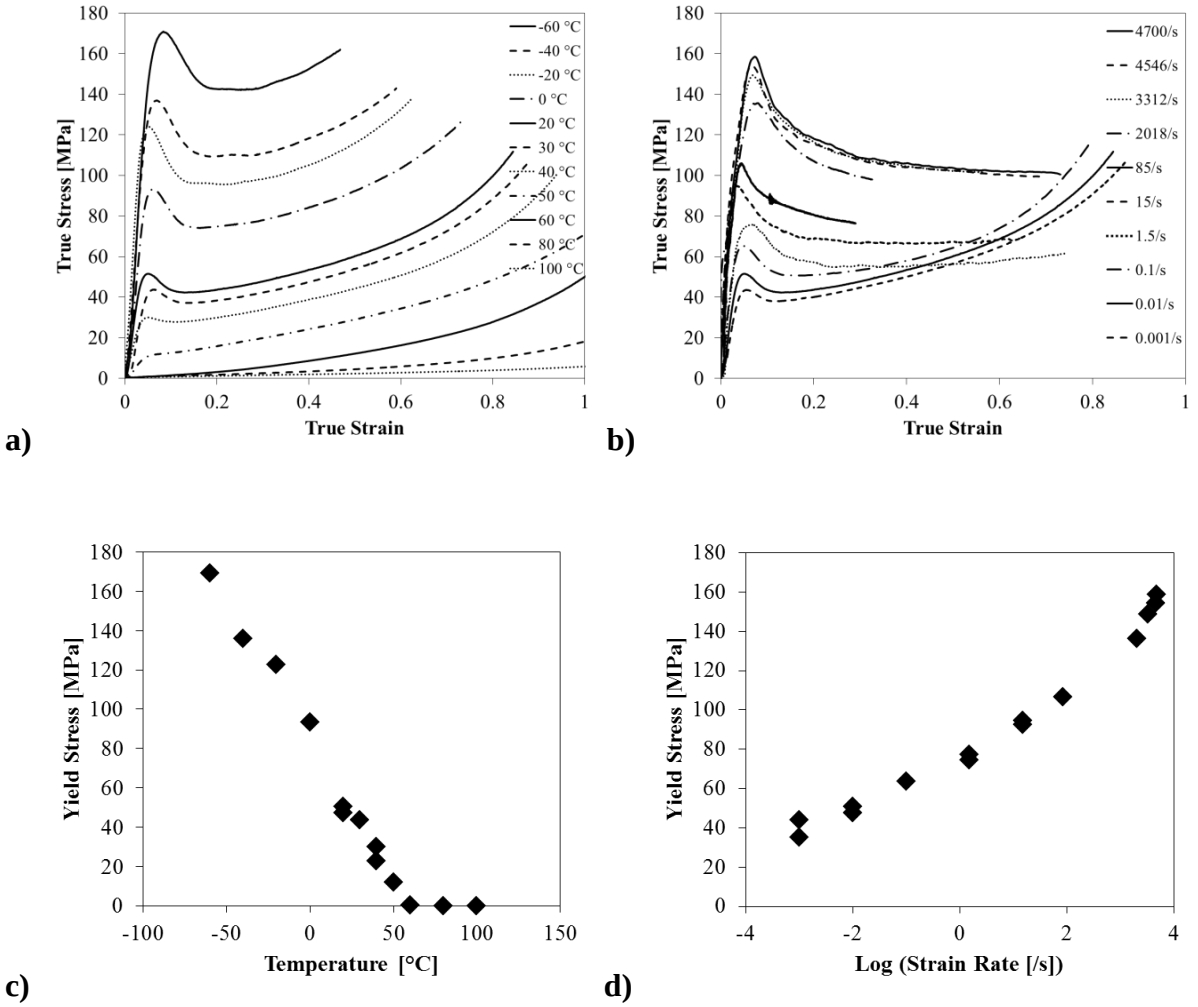


Figure 5-7: a) PPVC-2 stress-strain behavior in uniaxial compression over a range of temperatures. All tests were performed at a strain rate of 10^{-2} $s^{-1}$and b) PPVC-2 stress-strain behavior in uniaxial compression at room temperature over a range of strain rates. c) PPVC-2 yield stress dependence on temperature and d) the logarithm of strain rate.

rates of 0.1 s^{-1} and below) in which post-yields strain hardening is significant, and those (at rates of 1 s^{-1} and above) in which this hardening is not observed. Values of k=0.1510 W m^{-1} K^{-1}, ρ=1.41 g cm^{-3}, and C=1 J g^{-1} K^{-1} (Matthews, 1996), were used in order to calculate the strain rate in which the transition from isothermal to adiabatic heating takes place in PPVC-2. Equation 2 shows that the strain rate at which the adiabatic heating would become significant is of the order 0.3 s^{-1}. The data presented, therefore, are consistent with adiabatic heating playing a role in the reduction of strain hardening observed at higher rates of strain.

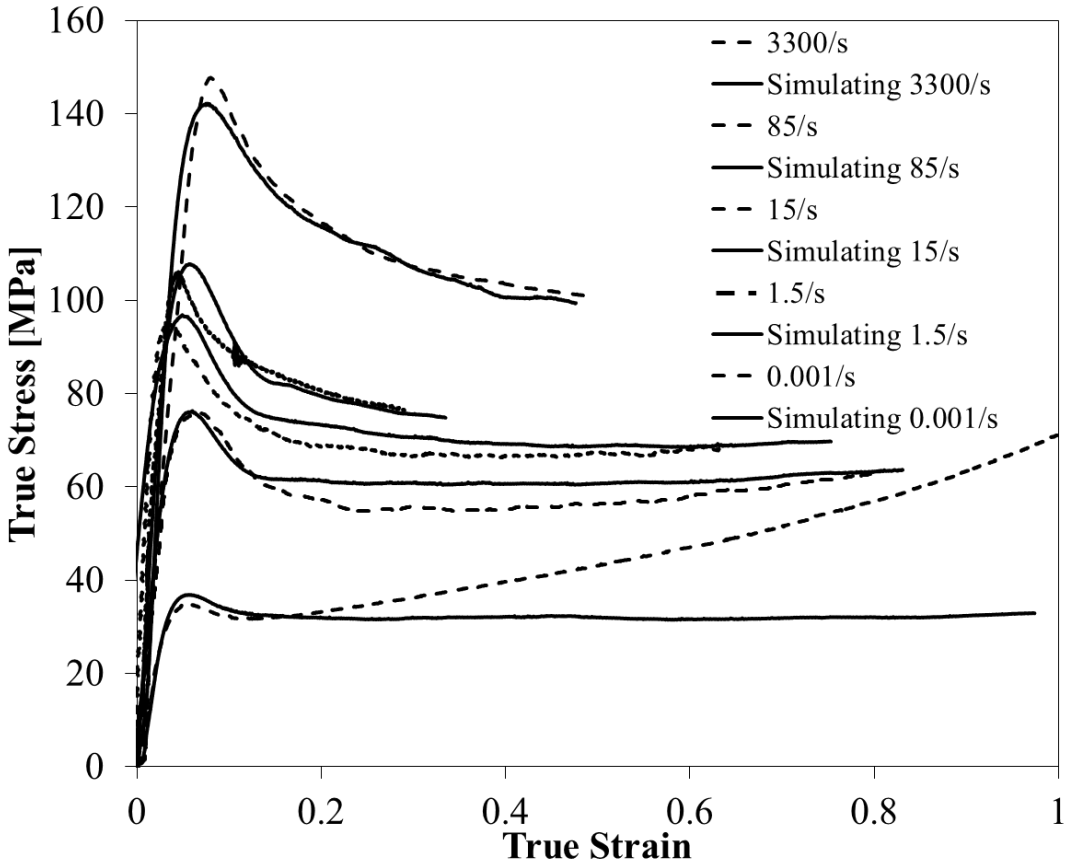


Figure 5-8: PPVC-2's response to 0.001 s^{-1} to 3300 s^{-1} strain rates and these same strain rates simulated via the simulating adiabatic conditions (SAC) method. The 0.001 s^{-1} response is shown to highlight the shift in material response from an isothermal to an adiabatic response.

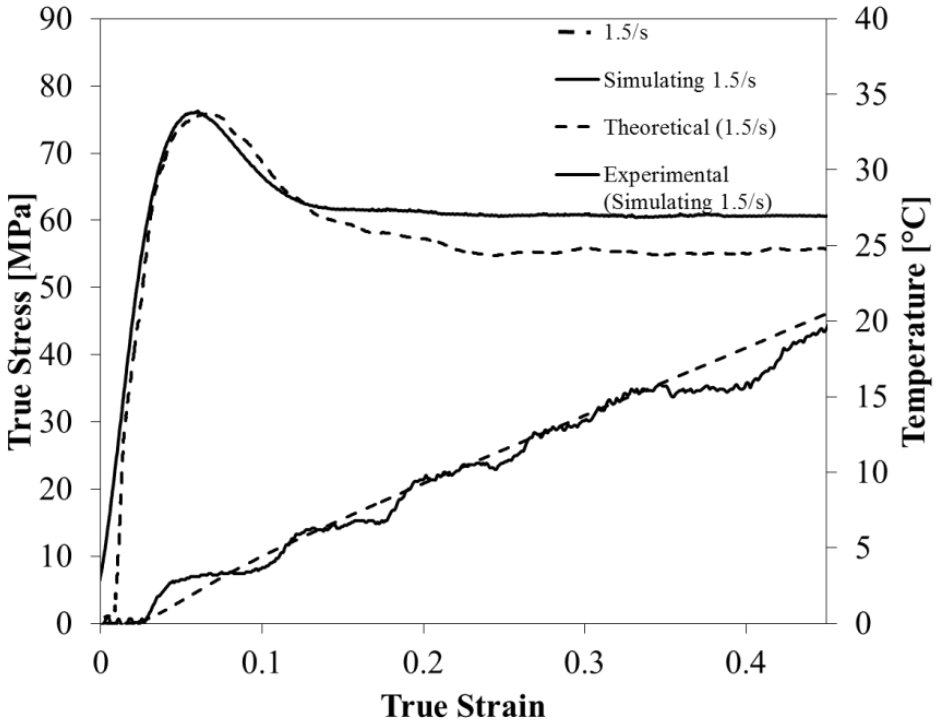


Figure 5-9: Experimental temperature rise of PPVC during a simulation experiment compared to the calculated theoretical temperature rise. The corresponding stress-strain behavior of a 1.5 s^{-1} response and the simulated response at 10^{-3} s^{-1} is shown.

It is also instructive to plot the rate and temperature dependencies of yield stress (figure 5-7c & d). Previous research (Siviour et al., 2005; Mulliken et al., 2006) has shown that the small increase in rate sensitivity at higher strain rates is due to the beta transition in the polymer. The data in figure 5-7 was used to obtain the required information to implement the simulation technique.

As described in section 5.2.3, initial temperatures were chosen to match the yield stress of the rate to be simulated, while temperature profiles were obtained by integrating the stress-strain curve. The experimental data thus obtained are shown in figure 5-8. Here each set of room temperature data is accompanied by the Simulating Adiabatic Conditions curve (SAC), which was obtained by performing an experiment at 0.001 s^{-1} with the appropriate temperature profiling – note that for completeness an additional SAC curve was obtained at

0.001 s^{-1} even though this does not represent a physically plausible loading condition. This curve also emphasizes the clear transition between isothermal and adiabatic conditions – the simulation method manages to capture the yield, but the theoretical temperature rise causes a clear deviation from experiment and simulation method. At lower strain rates, such as 0.001 s^{-1} and 1.5 s^{-1}, there appears to be very good agreement between the yield behavior of the simulation method and experiment. At higher rates of strain, such as 15 s^{-1} and 85 s^{-1}, there seems to be a relative decrease in agreement in the yield behavior, where the experimental curves are seen to have much sharper yields (spanning ~2% true strain) versus the simulation method yield (which spans ~5% true strain). At 3300 s^{-1} the yield behavior is captured very well, demonstrating very good agreement and almost complete overlap of pre-yield, and post-yield behavior, which is accompanied by a slight divergence in yield stress (observed in the simulation technique) of just under 5 MPa. The post-yield strain softening demonstrates very good overlap, or agreement, in the moderate rate behavior at 85 s^{-1} as well.

The responses at 15 s^{-1} and 1.5 s^{-1} both present similar post-yield behavior, one where the post-yield flow stress is seen to stay above the experiment. This separation between data sets at 15 s^{-1} is approximately 2 MPa at 20%, and decreases to an overlap in responses at higher strains. At these higher strains, strain hardening is observed in both simulation and experiment, with experiment strain hardening beginning at approximately 60% true strain. At 1.5 s^{-1} the separation between simulation and experiment is approximately 5 MPa in true stress immediately after the completion of yield and strain softening, at the beginning of the subsequent flow stress which occurs at ~55 MPa in experiment and 60 MPa in simulation. These curves do not overlap until approximately 80% true strain. The moderate rate experiment reveals the strain hardening caused by the network back stress, and the simulation experiment continues with its flow stress. This flow stress is caused by the heat input (or temperature profile) which masks any strain hardening which would be observed at these

higher strains – the strain hardening appears to begin at ~80% true strain in PPVC-2. The good agreement between the SAC stress-strain curves and experimental curves up until large strains indicates that this is a promising technique for predicting, simulating and understanding high rate behavior.

There are a number of possible causes for the discrepancies observed in both the yield and post-yield behavior. Experimentally, it is difficult to achieve a well-controlled temperature profile in the specimens, due to the thermal inertia in the temperature chamber. Figure 5-9 shows a typical profile obtained: a smooth 'theoretical' temperature rise is compared to the slightly wavy experimental temperature input used during the experiments. In addition, although care was taken to measure the temperature in a number of locations close to the specimen, the specimen may not be in thermal equilibrium with the platens or the surrounding air in the chamber. More positively, the differences may be the result of mechanical behavior of the polymer that has not been accounted for in the simple models used in this chapter. As the strain rate changes the mechanical processes that govern the observed response are likely to change, especially as the influence of the beta transition changes. In addition, the processes that govern post-yield behavior may not have the same temperature dependence as those that govern yield. Finally, the discrepancies might result from inadequacy in the assumption that all of the work done on the specimen is converted to heat: the beta factor, β_T, may not be 1. It is hoped that in future work, with suitable technical improvements to the heating control, experiments with suitable fidelity will allow the behavior to be explored in more detail, giving better understanding of the mechanisms that govern high strain rate response.

5.4 Conclusions

The data presented in this chapter show that it is possible to experimentally simulate the high strain rate response of a polymer by performing low strain rate experiments with suitable temperature profiles. The key development was not only to modify the initial temperature in order to simulate the change in yield stress, but also to capture the post-yield behavior by simulating adiabatic heating in the specimen. The straightforward, yet effective approach, offers significant opportunities in better understanding the high rate behavior in a large number of materials. In particular, this technique offers the possibility of better characterizing the behavior of composite materials in which one component is rate sensitive, and to perform experiments on these materials using in-situ diagnostics (e.g. SEM imaging, X-Ray tomography) that cannot be applied to high rate experiments. Further to these immediate opportunities, the simulation of adiabatic conditions as a function of strain offers the potential to develop further insights into the effects of temperature rises in high rate deformation, and highlights the connection between a polymer's temperature-dependent and rate-dependent behavior. Experiments presented in the following chapters of this thesis allow us to develop a stronger understanding of the mechanisms that underlie the constitutive behavior of several polymers, which contribute to an improved understanding of prediction methods and constitutive model developments.

Chapter 6

Investigations and Applications in Amorphous Polymers PMMA & PC

This chapter includes work presented in Kendall and Siviour (2013c) to be published in The Royal Society.

Introduction

In the fourth chapter of the thesis, it was proposed that the yield stress dependence upon strain rate could be described in terms of multiple rate activated processes. Principally, it was hypothesized that the restriction of β-motions, or small-scale secondary molecular mobilities, affected the agreement of time-temperature superposition data. This theory was then applied to two representative amorphous polymers, (unplasticized) PVC and PPVC-2. This hypothesis was supported with a description of the experimental procedure of the rate and temperature conditions at which the effects of this secondary transition could be seen. Temperature and rate dependence data were used to locate the β transition and the time- and temperature-dependent shift factor associated with this transition. The two separate shift factors which pertained to two distinct transitions in molecular mobility (α and β) of each

material were applied to temperature and rate dependent yield stress data via superposition to confirm the parity of temperature and rate in amorphous polymer behavior. More recently, in the fifth chapter of this thesis, a new experimental model was proposed in an effort to describe the observed behaviors in a way that corresponds with thermodynamic and molecular theory. It was suggested that the elastic, yield, and post-yield amorphous polymer behavior at moderate to high strain rates may be captured by low temperature quasi static behavior, with a subsequent temperature rise to capture the post-yield strain softening understood to be caused by adiabatic heating at higher rates of strain. An experimental simulation method was presented and successfully applied to the rate dependent behavior of a prototypical amorphous polymer PPVC-2 (PVC with 20wt% DINP plasticizer).

In this chapter, investigations of the applicability and generality of the experimental and theoretical methods of the experimental technique are conducted with two exemplary amorphous polymers: PMMA and PC. Special attention is paid to high rates of deformation and the adiabatic temperature rise which occurs at these high rates of deformation.

Experimental Design

In experimental apparatus and methods used in this chapter are as described in Chapter 3 (for standard characterization) used to study PVC, PPVC-2, PPVC-4, and PPVC-6, and Chapter 5 (for simulation method) used to investigate PPVC-2. The PC DMTA data is referenced from literature (Mulliken, 2006). Titanium (Ti-6Al-4V) SHPB bars were used for high rate testing ($\sim 10^3$ s^{-1} rates of deformation)

Dynamic Mechanical and Thermal Analysis

Dynamic mechanical and thermal analysis (DMTA) testing with a TA Instruments Q800 was performed on PMMA in single cantilever configuration at 1, 10, and 100 Hz over the temperature range -150 °C to +150 °C. Rectangular samples were 60 mm long x 12.5 mm wide x 2.5 mm thick.

Temperature measurement of PMMA during deformation

In order to further validate the simulation method, temperature measurements were conducted during testing of PMMA at a rate of 0.1 s^{-1}. These temperature measurements were carried out via a novel temperature measurement design (using thermocouples) explained in detail in Chapter 9 of this thesis. In this method a flat and circular T-type thermocouple (with an 8 mm diameter) was placed between two 4 mm length x 8 mm diameter PMMA specimens. This temperature measurement method not only produced more accurate temperature measurement results, but had less effect on the material deformation: in other test methods thermocouple have been embedded into the side of a specimen which has been seen to cause differences when compared to unmodified specimens, such as atypical true stress-true strain behavior and premature brittle failure.

6.1 Polymethyl methacrylate (PMMA)

6.1.1 Background

The mechanical properties of amorphous polymers have become increasingly important as their breadth of application has been seen in the aerospace and defense, electronics, and medical industries (which has been described in more detail in the second and third chapter of this thesis). PMMA is prominent in many engineering applications and a large amount of literature has been focused on the strain rate and temperature dependence of PMMA (Chou et al., 1973; Bauwens-Crowet, 1973; Hasan et al., 1993; Lee & Swallowe, 2006; Mulliken et al., 2006; Richeton et al., 2006; Rittel et al., 2008). Similar to other amorphous polymers, PMMA has shown a clear interplay between rate and temperature dependence while exhibiting increases in yield strength and elastic modulus with increasing strain rate and decreasing temperature. PMMA presents interesting material behavior as the β transition is seen in effect at much lower strain rates (i.e. 10^{-2} s^{-1}) while still at room temperature (~20 °C) (which is shown in DMTA data later in this chapter, figure 6-4).

As described in earlier chapters of this thesis, the α transition for amorphous polymers is a result of larger scale polymer chain motion. PMMA's β transition was initially investigated by Illers, Kilina, and Kosfeld (1961) who did not have enough data to conclude upon the molecular origins of the β transition, however they did find from nuclear magnetic resonance (NMR) data that the entire ester side group is unable to move at temperatures below -196 °C. In work following this, involving dielectric and DMTA techniques, the β transition has been attributed to the molecular motion of the ester side group along the main polymer chain (a restriction of motion at higher strain rates/lower temperatures) (Heijboer, 1964; Bicerano, 2002). Furthermore, at temperatures below (or rates above) the β transition, PMMA demonstrates brittle failure (Richeton et al., 2006). A more in depth study of the

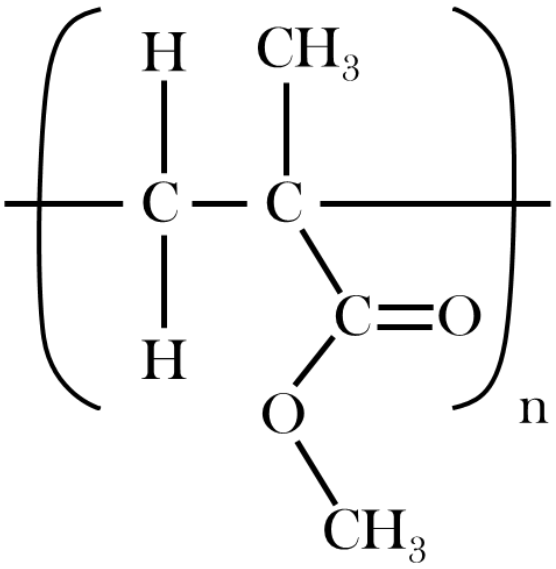


Figure 6-1: Poly(methyl methacrylate) chemical structure

developments in the understanding of mechanisms (e.g. yield and strain softening) of polymers have been described in previous chapters (2, 3, and 5).

Several studies have been conducted in order to study and quantify the storage and release (in heat) of mechanical work in polymers during deformation. As mentioned earlier in Chapter 5, total work of deformation is calculated from the stress-strain response, with the heat released (or 'heat of deformation') being calculated via measured temperature rises (including calorimetry chamber techniques measuring slight changes in air pressure calculated by development of heat in the chamber), and the internal (or 'stored') energy being calculated by the difference between the work done on the specimen and the measured heat according to the first law of thermodynamics. Characteristic experimental results of Rudnev et al. (1991) and Mulliken et al. (2006) with an amorphous polymer (PC) are presented in figures 6-2 and 6-3. Studies similar to this have garnered similar results (i.e. Arruda et al., 1995; Garg et al., 2009), in that 45 and 100% of the work of inelastic deformation is dissipated as heat for amorphous polymers. This thesis will investigate the energies of deformation of PMMA under moderate rate loading.

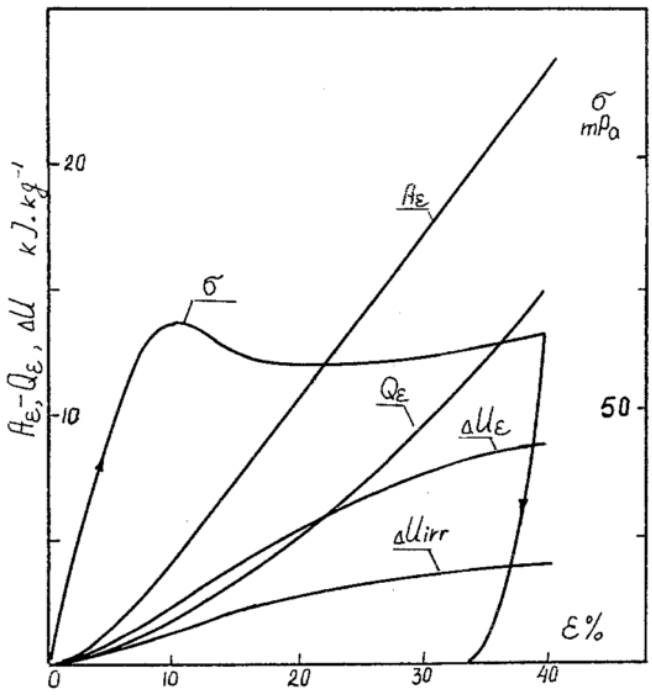


Figure 6-2: PC energies of deformation at 10^{-2} s^{-1} (298 K) strain rate in uniaxial compression calculated by calorimetry experiments during deformation: total work (A_ε), heat of deformation (Q_ε), and internal or 'stored' energy (ΔU_ε), and internal energy not recovered upon unloading (ΔU_{irr}). Rudnev et al. (1991).

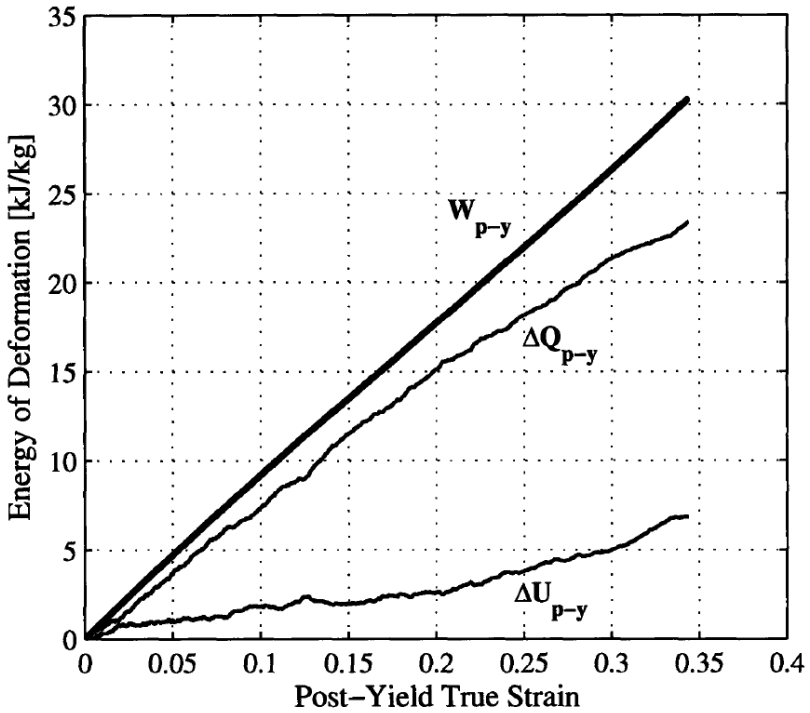


Figure 6-3: PC post-yield energies of deformation at 2550 s^{-1} (298 K) strain rate in compression: total work (W_{p-y}), heat of deformation (ΔQ_{p-y}), and internal or 'stored' energy (ΔU_{p-y}). Calculated via stress-strain and temperature rise data using infrared (IR) techniques (Mulliken et al., 2006).

6.1.1 Materials

All PMMA temperature and rate dependent tests in uniaxial compression, and in DMTA testing, were conducted on cylindrical PMMA samples machined from 25.4 mm diameter extruded rod. Samples for quasi-static compression testing were 8 mm diameter x 8 mm long, and those for dynamic compression testing were 8 mm diameter x 3.5 mm long.

6.1.2 Results and Discussion

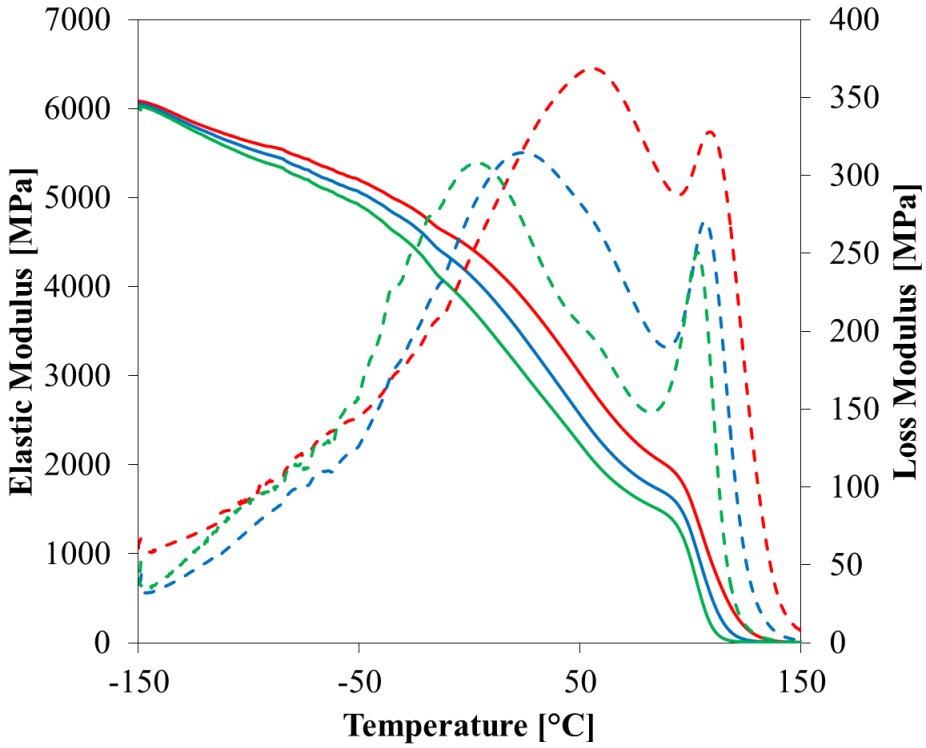


Figure 6-4: PMMA storage modulus and loss modulus as a function of temperature at 1 Hz (~0.035 s^{-1}), 10 Hz (~0.35 s^{-1}), and 100 Hz (~3.5 s^{-1}).

Table 6.1: Shift factors of PMMA viscoelastic transitions

	D_α [°C/decade strain rate]	D_β [°C/decade strain rate]
PMMA	5	25

PMMA DMTA test results are summarized in figure 6-4. PMMA presents interesting time- and temperature- dependent behavior in that at ~0.035, 0.35, and 3.5 s^{-1} the β transition is seen at room temperature (~20 °C) which is not typically seen in low rate amorphous polymer behavior – the loss modulus[7] peaks of these β transitions occur at approximately 0, 25, and 50 °C, respectively. The highest frequency data, 50 °C transition, presents an interesting case where α and β transitions begin to coalesce at such high rates. The larger rate

[7] tanδ or loss modulus peaks may be used to find the temperature locations of the material transitions (α and β). These values are also used to find the shift factors (D_α and D_β). Differences in this thesis are typically ~1 °C/decade strain rate when using tanδ rather than the loss modulus. Loss modulus peaks were used in all cases in this thesis.

sensitivity of the β transition is consistent with other amorphous polymers in this thesis, PVC and PPVC-2, presented in Chapter 3. The α transition is seen to occur at ~90, 95, and 100 °C, demonstrating a shift factor of approximately 5 °C/decade strain rate versus a 25 °C/decade strain rate shift factor for the β transition. The α shift factor in this thesis is approximately 5 °C/decade strain rate lower than that found in literature (5 vs. 10 °C/decade strain rate), while the β shift factor is the same as previous studies (Mulliken et al., 2006).

During low to moderate rate compression testing, all PMMA specimens deformed in a ductile manner at all tested temperatures (figures 6-5) until -60 °C which saw brittle failure at ~35% true strain, and -87 °C which saw brittle failure just after the maximum stress during yield at ~10% true strain. In rate dependent testing, specimens performed in a ductile manner until ~50 % true strain (figures 6-7), with the exception of high rate testing (2500 s^{-1}) where failure was seen at what appears to be the beginning of yielding at ~7% true strain. The nature of deformation of was confirmed from post-mortem analysis of the test specimens, with little to no barreling observed in PMMA.

The results of all uniaxial compression testing of PMMA are summarized in figures 6-5 – 6-8. Figure 6-5 presents representative true stress-true strain curves for PMMA along all of the tested temperatures. In this example, PMMA is shown to have different behavior at each of the tested temperatures. Starting at 40 °C and moving to lower test temperatures, we see the shape of the yield stress broadening and strain softening occurring through larger strains. This behavior is caused from more sites along the polymer chain overcoming the resistance to rotation with increasing strain. The increase in yield stress with lower temperatures is caused by the individual polymer chain segments on the local and larger scales having to overcome resistance to rotation and move cooperatively (Bicerano, 2002) – both the α and β transitions are showcased in this low temperature behavior. As mentioned

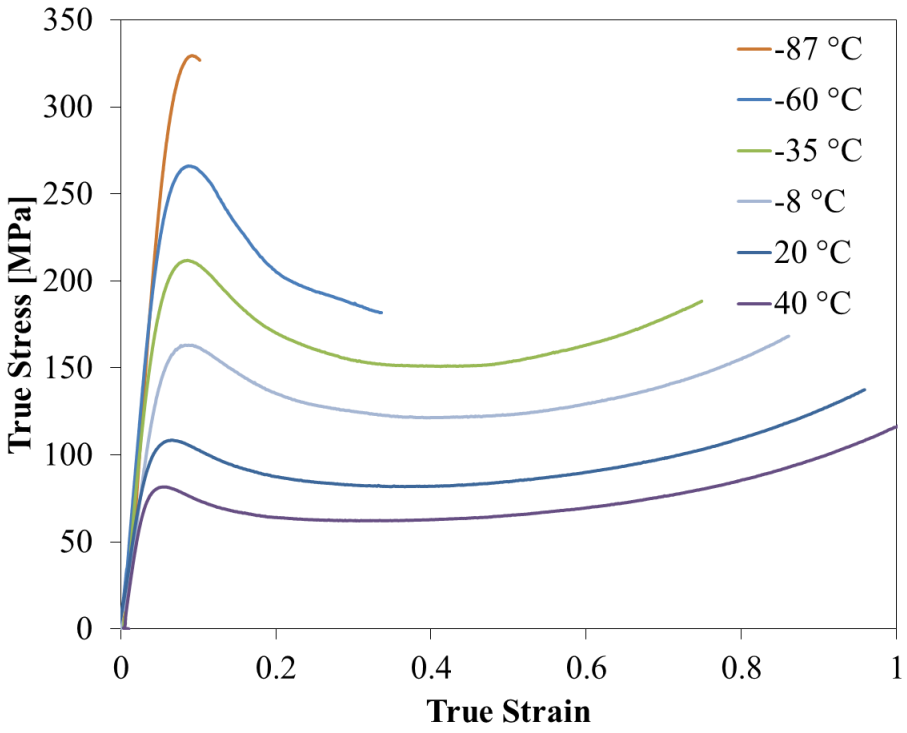


Figure 6-5: PMMA true stress-true strain behavior as a function of temperature (-87 – 40 °C) at a rate of 10^{-2} s^{-1}.

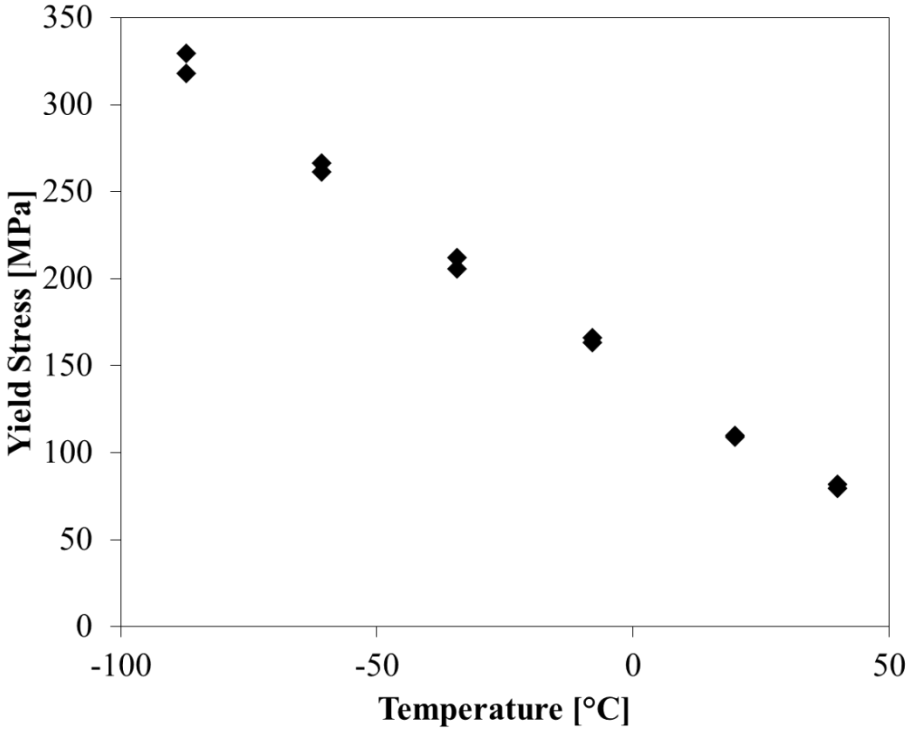


Figure 6-6: PMMA yield stress behavior as a function of temperature (-87 – 40 °C).

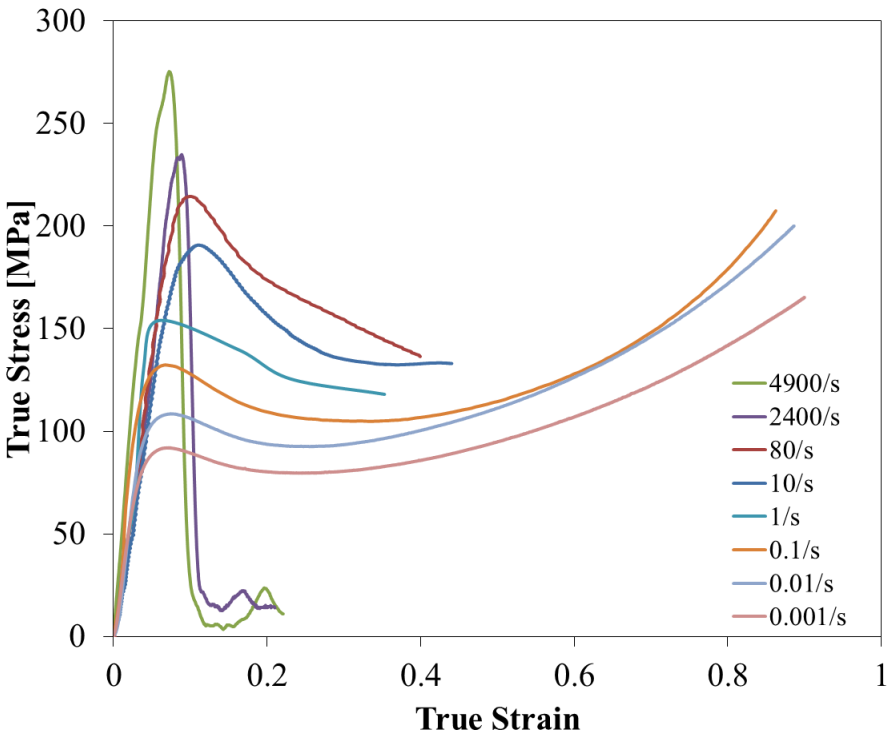


Figure 6-7: PMMA true stress-true strain behavior as a function of strain rate (5 x 10^{-4} s^{-1} – 2500 s^{-1}).

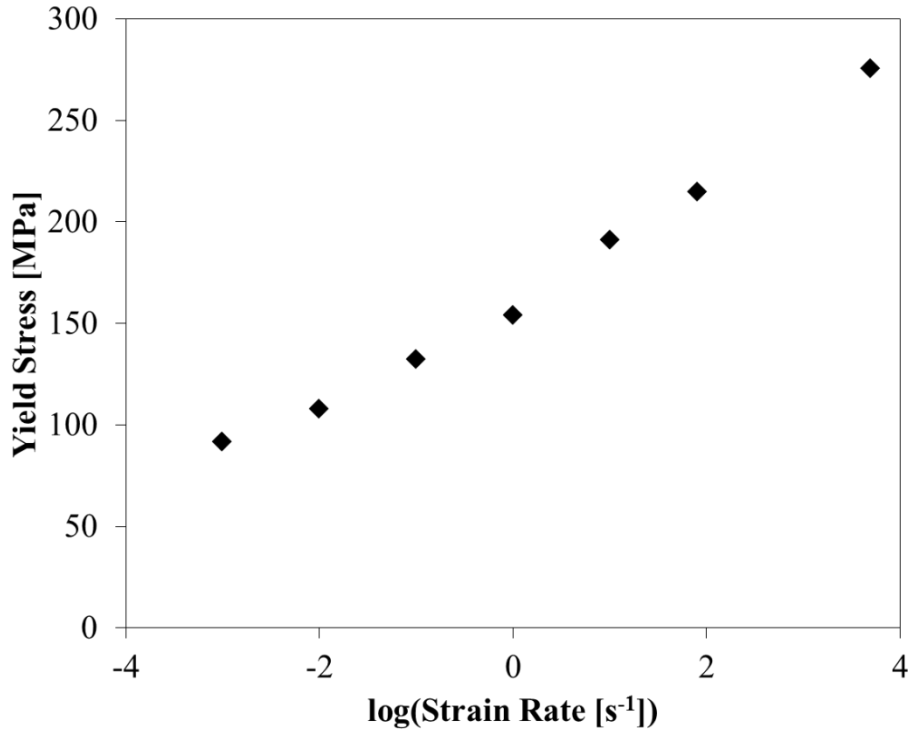


Figure 6-8: PMMA yield stress behavior as a function of strain rate (5 x 10^{-4} s^{-1} – 4900 s^{-1}).

earlier, brittle failure is seen to occur during -60 and -85 °C tests conducted at 10^{-2} s^{-1} rate of strain (at ~35% and ~ 10% true strain, respectively). This behavior is mirrored by the true stress-true strain curves for PMMA along all tested strain rates (figure 6-7). Starting at 5×10^{-4} s^{-1} and moving to higher rates of deformation, we see a similar behavior to the temperature dependent behavior with a broadening of the yield and strain softening. In these cases the strain softening is more pronounced, caused by thermal softening which occurs when the material does not have enough time to for heat transfer during the time scale of the tests (this is seen in PMMA behavior from rates as low as 0.1 s^{-1} going upwards to 2500 s^{-1}). Brittle failure is observed only in high rate testing, seen at 2500 s^{-1}. PMMA yield stress behavior appears to be relatively linear in both temperature- and rate-dependent data (figures 6-6 & 6-8). This is to be expected with the α and β temperatures being so close to one another in temperature at the strain rates tested in this study.

6.1.3 Experimental Simulation Model & Energies of Deformation

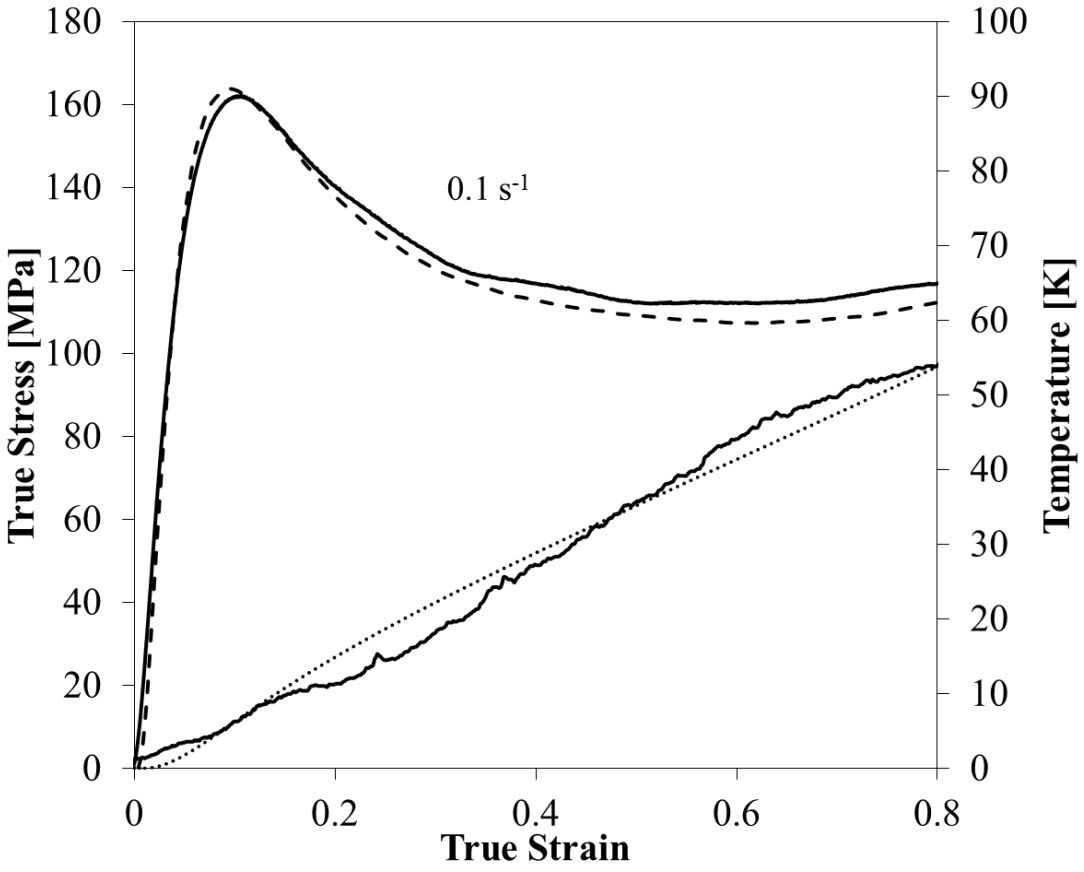


Figure 6-9: PMMA true stress-true strain behavior in uniaxial compression at 0.1 s^{-1} (at 20 °C): experiment (dashed line) with its theoretical temperature rise from the model (dotted line) below, and experimental simulation model (solid line) and its temperature input during testing (solid line) in the lower half of the figure.

Table 6.2: Thermal properties used for simulation method implementation and analysis

PMMA		
Heat capacity	1470	J kg^{-1} K^{-1}
Density	1190	kg m^{-3}
Thermal diffusivity	0.11	mm^2 s^{-1}

Using the experimental data presented above, the experimental simulation method described in Chapter 5 was extended to capture PMMA behavior. The technique has already been shown to capture PPVC-2 over representative true stress-true strain behavior from its rate dependent response.

In this particular case, the experimental simulation model is applied to PMMA to predict the true-stress and true-strain behavior up to a large true strain of 80%. The result of a simulation test recreating PMMA behavior at a 0.1 s^{-1} rate of deformation is presented in figure 6-9 (using the density and heat capacity presented in table 6.2). This rate was chosen because it represents the lowest rate at which adiabatic heating is visible in the true stress-true strain rate dependent response (figure 6-7), starting from the lowest rate and increasing in value. This was also confirmed numerically using the thermal diffusivity equation (presented in Chapter 5), calculating a ~0.07 s^{-1} characteristic strain rate for adiabatic heating in PMMA. A simulation was conducted at a strain rate of 10^{-3} s^{-1} and a starting temperature of -7.25 °C, which was calculated from rate dependent shift factors calculated from rate-dependent and temperature-dependent data[8]. The theoretical temperature gradient was chosen in assuming (as previously in Chapter 5) that 100% of the plastic work (per unit volume) was converted into heat during deformation. There is very good agreement between the experimental

[8] D = 15.25 °C/strain rate which is approximately the average of the two DMTA found shift factors relating to the α and β transitions (15 °C/strain rate) – this agrees with the overlap of α and β loss modulus peaks seen in figure 6-4.

simulation model and experiment. Slight differences at strains of 30% and above are seen on the order of ~1-3.5 MPa, which can be attributed to natural variation in the results.

In order to validate the temperature gradient applied in the experimental model, the temperature rise in PMMA during a 0.1 s^{-1} test was experimentally measured (via a novel T-type thermocouple wafer methodology described in detail in Chapter 9). The results of this are presented in figure 6-10 with the experimentally measured and theoretically calculated temperature rises compared to each other. These curves result in gradients of approximately 0.68 K/% true strain (theoretical) and 0.52 K/% true strain (experimental). This comparison was then extended to studying the energies of deformation during a 0.1 s^{-1} rate of uniaxial compression (figure 6-11). Approximately 76% of the work was converted into heat (commonly the 'β-factor') during 0.1 s^{-1} testing. This value is consistent with the 45-100% range seen in literature (please refer to section 6.1.1). It is noted that at 0.1 s^{-1} the experiment is only slightly above the rate of ~0.07 s^{-1} which was calculated as the characteristic strain rate for adiabatic heating to occur. Looking at figure 6-11, the internal energy (or 'stored energy') plateaus with increasing strain, staying between ~15-19 kJ kg^{-1} from 30% true strain until the end of testing; this is consistent with previous observations in amorphous polymers (see figures 6-2 & 6-3 in section 6.1.1).

This experimentally measured temperature rise was subsequently applied to the experimental simulation method (presented in figure 6-12). Simulation with the experimental temperature rise offers a less accurate result when compared to the simulation which assumed that 100% conversion of plastic work to heat. The overall work of deformation per unit volume has increased (seen by the increased area under the true stress-true strain curve), causing the simulated percentage of work converted to heat to decrease by approximately ~2.5 % in the experimental simulation test (compared to the total work and heat of deformation values seen in figure 6-11).

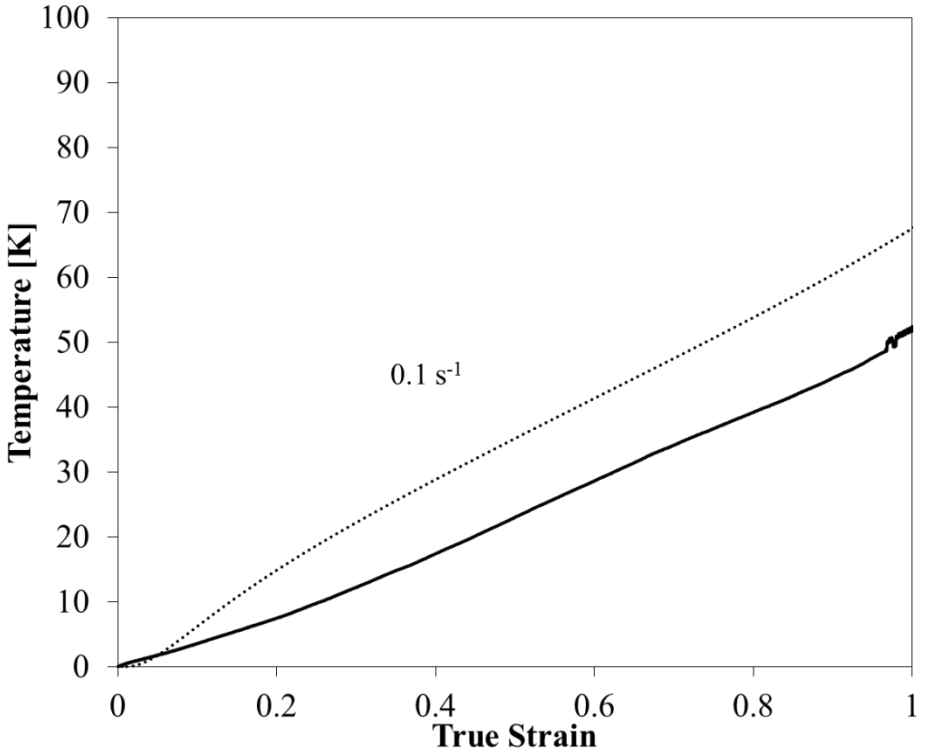


Figure 6-10: PMMA experimentally measured temperature rise (solid line) and theoretical temperature rise (dotted lines) during uniaxial compression at 0.1 s^{-1}.

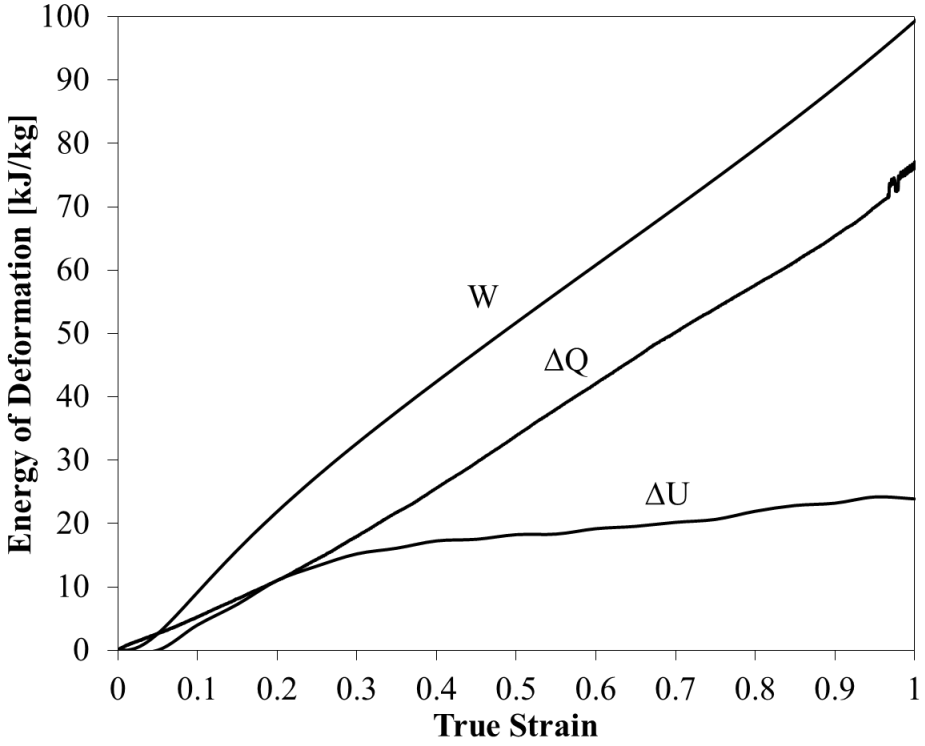


Figure 6-11: PMMA energies of deformation at 0.1 s^{-1} strain rate in uniaxial compression: total work (W), heat of deformation (ΔQ), and internal or 'stored' energy (ΔU). Mechanical work and heat of deformation during testing are calculated from the theoretical and experimentally measured temperature rises in figure 6-10; internal energy is calculated as the difference between the two.

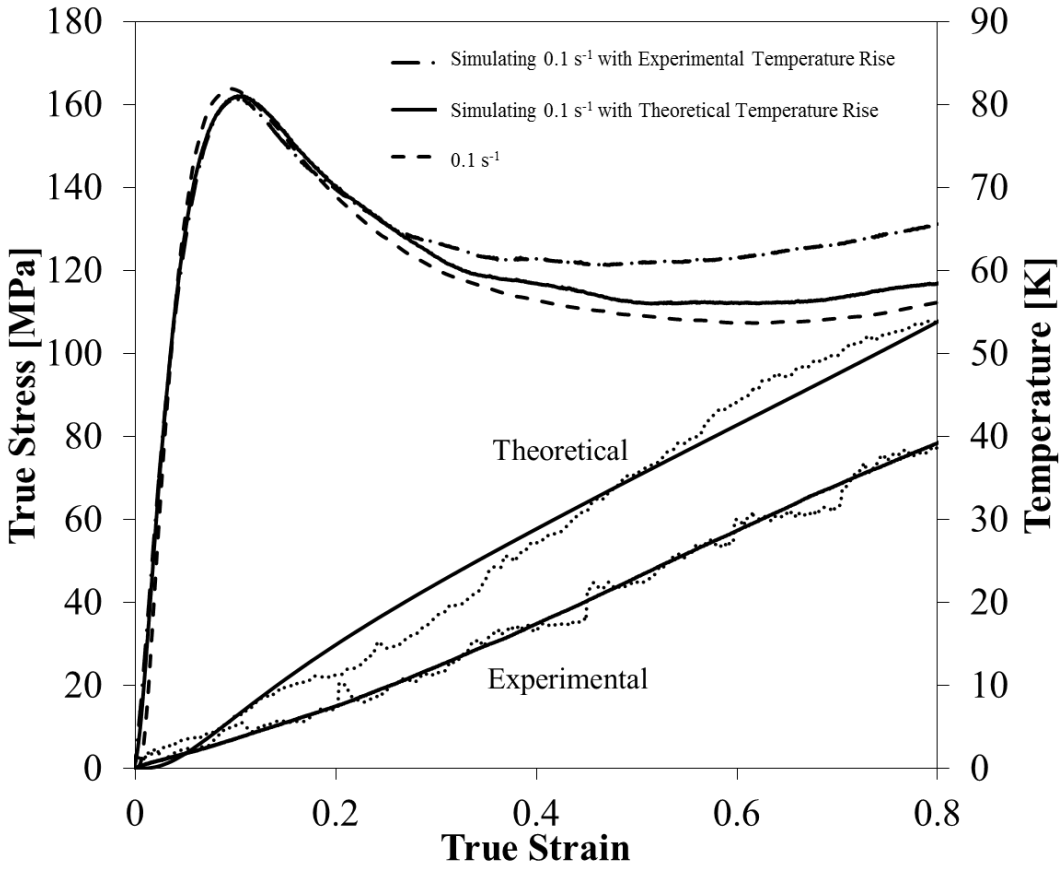


Figure 6-12: PMMA true stress-true strain behavior in uniaxial compression at 0.1 s^{-1}: experiment compared with the experimental simulation model using an experimentally measured temperature rise versus a theoretical temperature rise (assuming that 100% of the work is converted to heat during deformation). The temperature curves in the lower half of the plot present the theoretical and experimentally measured temperature rises during deformation (solid lines) compared with the temperature input used during the implementation of the experimental simulation model (dotted lines).

This difference in true stress-true strain behavior is attributed to a strain rate-driven strain softening which is not caused by heat – a certain amount of work which is converted into heat contributes to strain softening in unison with a certain amount of internal energy (or a certain remainder of the work of deformation) which also contributes to strain softening. This observation illustrates that a majority of the strain softening seen in the true stress-true strain behavior is indeed caused by the heat of deformation, ΔQ, but the remainder of the

strain softening is caused by a material characteristic seen only in higher rates of deformation, which is not accommodated for at the rate of deformation of the simulation experiments (10^{-3} s^{-1}).

6.1.4 Conclusion

The temperature- and rate-dependent behavior of PMMA was studied via uniaxial compression and DMTA testing. Rate-dependent true stress-true strain behavior showed effects of adiabatic heating at 0.1 s^{-1}; this agreed well with the characteristic strain rate at which PMMA experiments with this sample size would be expected to e adiabatic: ~0.07 s^{-1}. The experimental method presented in the fifth chapter was then applied to PMMA behavior at 0.1 s^{-1} rate of deformation with very good agreement between experimental versus model results. A novel temperature measurement method was then used to obtain the experimental temperature rise of the specimen at 0.1 s^{-1}. These data were compared with the temperature rise expected in adiabatic conditions and further analyzed to study the energies of deformation of PMMA at the experimental strain rate. Lastly, the experimentally measured temperature gradient was then applied to PMMA with the experimental simulation method; this garnered poorer agreement between experiment and model. The worse agreement was understood to be a contribution of non-heat induced strain softening which occurs at higher rates of strain; this additional contribution in strain softening is made up for by using a theoretical temperature gradient (or heat of deformation) equivalent to the total work of deformation gradient (felt by a PMMA specimen at 0.1 s^{-1}) when conducting a simulation test, thus facilitating the very good agreement between results.

6.2 Polycarbonate

6.2.1 Background

Polycarbonate (PC) (figure 6-13), like PMMA, is very prominent in engineering applications, making it a suitable material for this investigation, and has been investigated in a large amount of literature in experimental and constitutive modeling work attempting to better understand and predict its constitutive behavior (Bauwens-Crowet, 1973; Siviour et al., 2005; Richeton et al., 2005; Mulliken & Boyce, 2006; Jordan et al., 2012), and its temperature rise at high rates of deformation (Li & Lambros, 2001; Lerch et al., 2003; Regev & Rittel, 2007; Garg et al., 2008). Literature data on the temperature rise of PC at high rates of deformation are presented alongside the temperature measurement investigations conducted in Chapter 9; these data are also presented later in section 6.2.3 when compared with experimental values used in this chapter. The differences in temperature gradients by each author may be attributed to several issues: differences in base-polymer of PC, differences in test strain rate, temperature measurement methods – IR versus thermocouples, and the initial true strain which the author associates with the initial measured temperature rise.

Similar to other amorphous polymers, PC has shown a clear interplay between rate and temperature dependence while exhibiting increases in yield strength and elastic modulus with increasing strain rate and decreasing temperature. PC presents interesting material behavior, which contrasts PMMA and PVC, in that it has shown to increase in strain-hardening (or decrease in strain-softening) with increasing strain rate, despite the increase in temperature associated with adiabatic heating. This is shown in the rate-dependent compression data presented later in this chapter, figure 6-18.

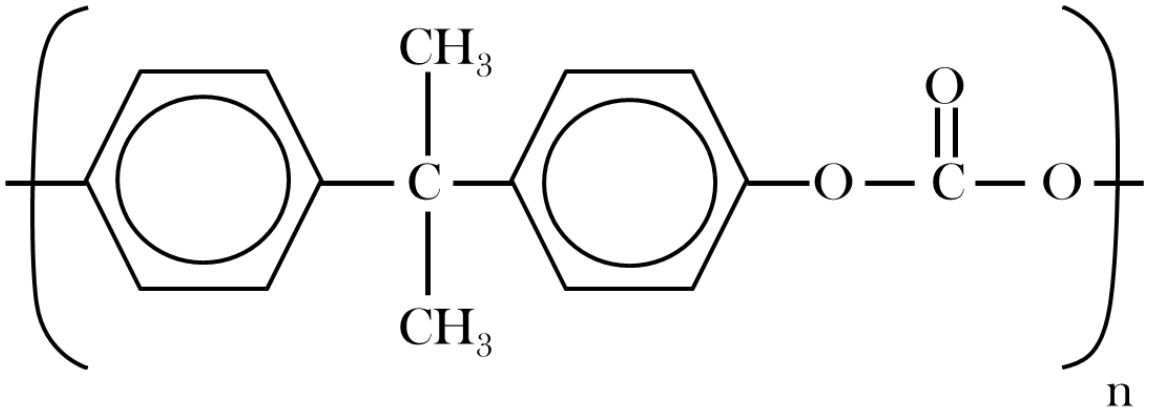


Figure 6-13: Bisphenol A polycarbonate (traditional PC) chemical structure

Yee and colleagues (Jho & Yee, 1991; Xiao & Yee, 1992), Floudas et al. (1993), and Monnerie et al. (2005), have all studied the molecular mobility involved with β motions[9], effects of which are seen at high rates of deformation and low temperatures, and are thought to cause increases in modulus and yield stress. It has been shown by Yee et al. that variations of polycarbonate (e.g. tetramethylbisphenol-A polycarbonate, TMBPA-PC, block copolymers), exhibit the same secondary transitions seen by the 'traditional' PC in figure 6-13 (with the requirement of a minimum number, 7, of adjacent monomer units). Floudas et al. tested other variants of PC and concluded that β motions are constituted by phenyl ring π-flips and a certain amount of intermolecular or intramolecular cooperativity Monnerie et al. suggested that local scale vibrations of the phenyl rings, with a minimum amount of intermolecular activity, is the cause of β motions. Thus, unlike the case of PMMA, there is not a general consensus regarding β motions in PC. It is worth noting that after looking at a variety of amorphous polymers, each has different types of β-motions (i.e. backbone versus side-group).

[9] α motions are generally agreed as large scale chain motion for PC – more specifically, phenyl π-flips which induce motion on the same chain, intramolecular motion, and neighboring chains, intermolecular motion.

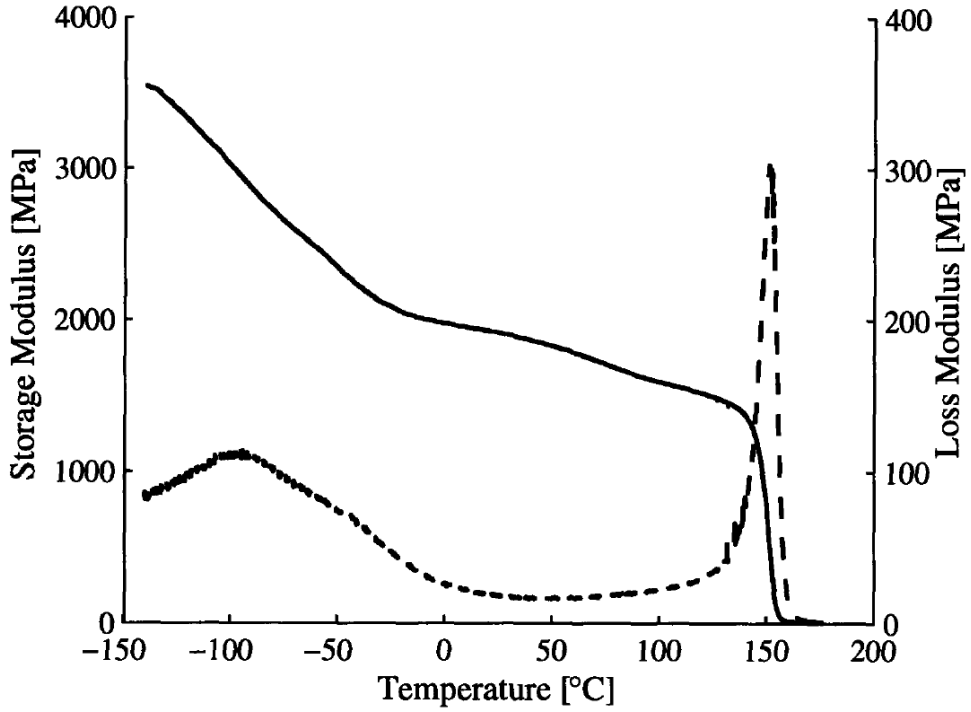


Figure 6-14: PC storage modulus (solid line) and loss modulus (dashed line) curves with respect to temperature at 1 Hz frequency (or 3.2 x 10^{-3} s^{-1}). The loss modulus curve presents peaks at approximately -95 and 150 °C which correspond to the β and α transitions (Mulliken & Boyce, 2006).

6.2.2 Materials

All PC temperature and rate dependent tests, in uniaxial compression were conducted on samples machined from extruded rod. Samples for quasi-static and dynamic compression testing were right cylinders 5 mm diameter x 2.5 mm height.

6.2.3 Results and Discussion

PC DMTA test results from Mulliken (2006) are summarized in figure 6-14. PC presents interesting time- and temperature- dependent storage modulus behavior, moving from high temperature to low temperature, in that at ~0.0035 s^{-1} the β transition is very pronounced, rising approximately 1500 MPa from the glass transition region. PC also presents a distinct contrast from the PMMA, this is readily seen in the distinctiveness and separation of the loss modulus peaks. The α peak is at approximately 150 °C, with the β peak being separated

Table 6.3: Shift factors of PC viscoelastic transitions (Mulliken, 2006)

	D_α [°C/decade strain rate]	D_β [°C/decade strain rate]
PC	4.7	15.3

almost 250 °C, thus allowing the transitions to be distinct from one another (unlike the PMMA α and β peak overlap seen earlier in section 6.1.2, figure 6-4). The DMTA data from literature (Mulliken, 2006), also presents new shift factors (table 6.3) – the sensitivity to high strain rates of deformation affected by the relatively low β shift factor (when compared to PMMA), 15 °C/decade strain rate. In contrast to PMMA – PC is much less sensitive to increases in strain rate at higher rates or lower temperatures, although at higher temperatures and lower strain rates the dependences are more similar because of the similarity of the α shift factor (both ~5 °C / decade of strain rate).

The uniaxial compression true stress-true strain behavior of PC is presented in figures 6-15 and 6-17. The true stress-true strain behavior of PC is characterized by strain hardening at higher strains, with its clear decrease in strain softening and increase in strain hardening with increasing strain rate and decreasing temperature. The temperature dependent data (figure 6-15) demonstrates the beginning of the β transition at approximately -20 °C, seen in the near constant increase in elastic modulus and yield stress (figure 6-16) while decreasing temperature. The rate dependent true stress-true strain data (figure 6-17) mirrors the temperature dependent data in increases in strain hardening (with increases in strain rate). In the yield stress data (figure 6-18), we observe the β transition come into effect at higher strain rates (1175 – 6300 s^{-1}), and calculate this increase in elastic modulus and yield stress to occur at a rate of approximately 260 s^{-1}. As mentioned in the previous section, the behavior of PC at higher rates is interesting in that, unlike other amorphous polymers (e.g. PMMA), at higher rates when β-motions are restricted, the intrinsic strain softening of PC seems to decrease.

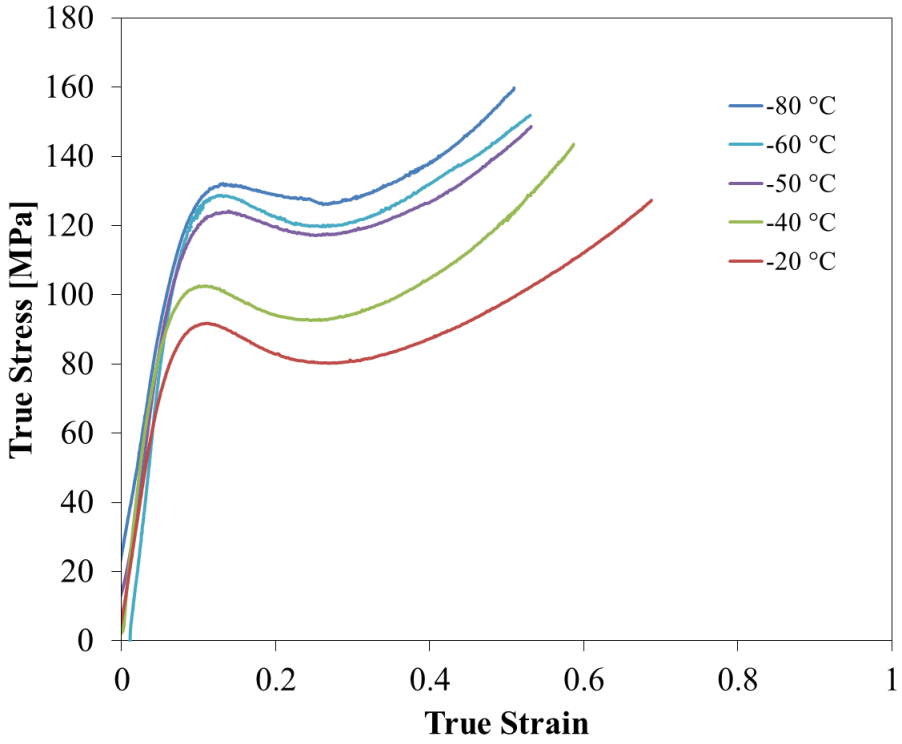


Figure 6-15: PC true stress-true strain behavior as a function of temperature (-80 to -20 °C) at a rate of 10^{-2} s^{-1}. The influence of the β transition is present in all responses assuming PC properties are consistent with figure 6-14.

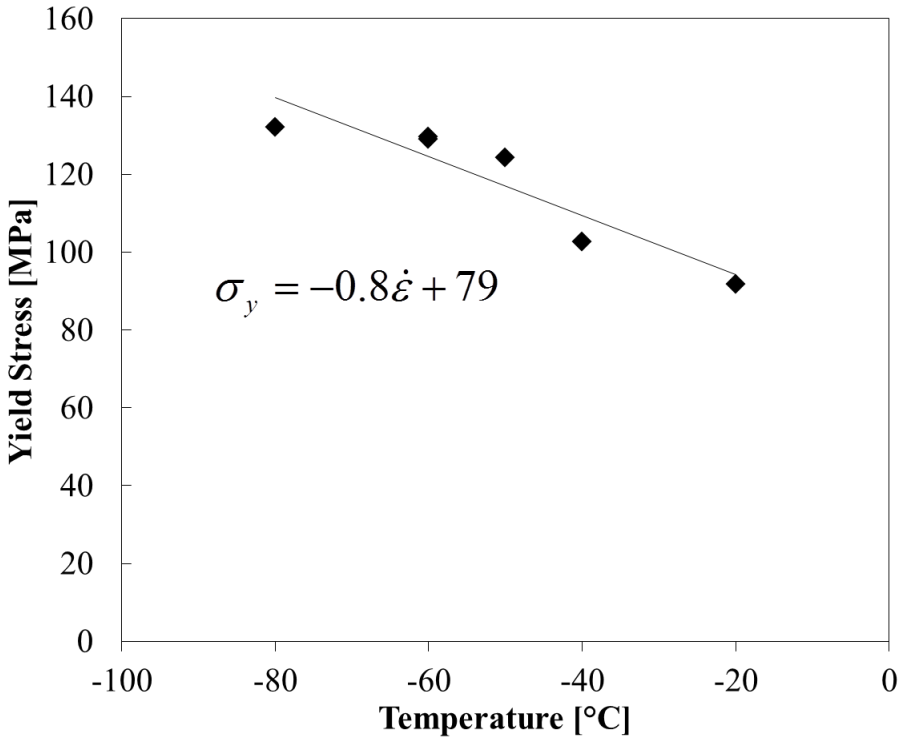


Figure 6-16: PC yield stress behavior as a function of temperature (-80 to -20 °C).

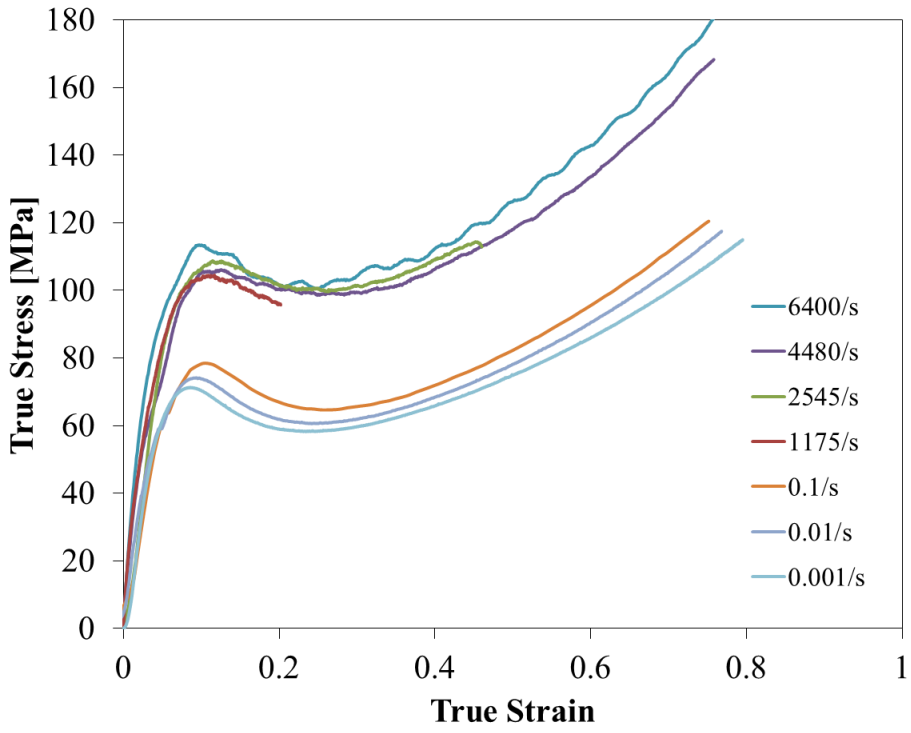


Figure 6-17: PC true stress-true strain behavior as a function of strain rate (10^{-3} s^{-1} – 6400 s^{-1}).

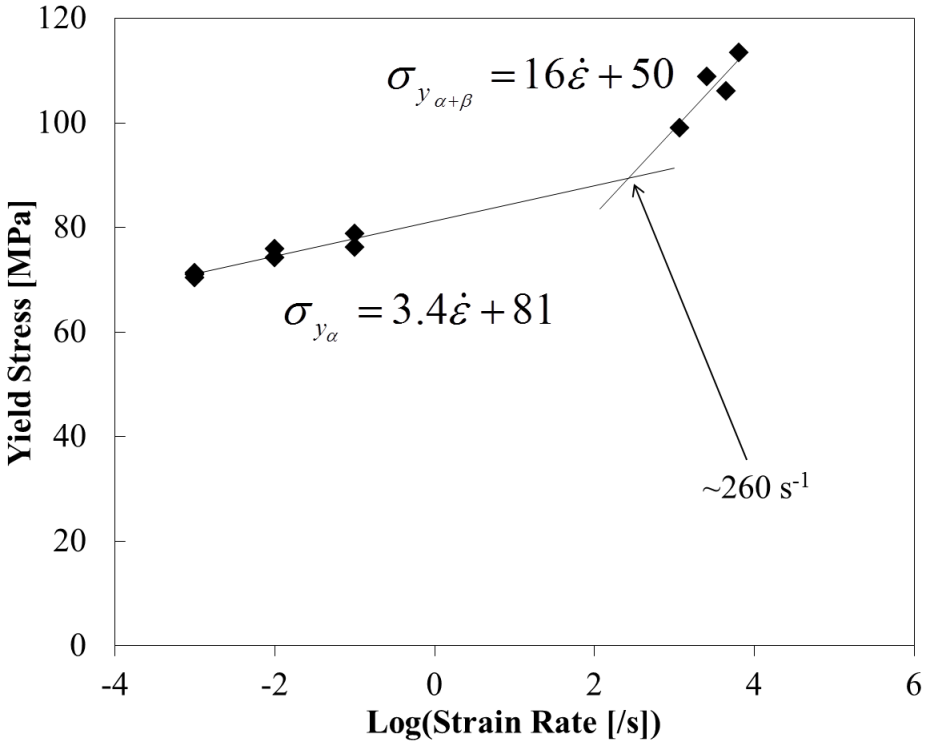


Figure 6-18: PC yield stress behavior as a function of (log) strain rate (10^{-3} s^{-1} – 6400 s^{-1}).

Instead, we see an increase in strain hardening when β-motions are restricted regardless of the observed adiabatic nature of PC at these high rates (discussed in the next section and presented in figure 6-22), this increase in strain hardening is understood to be a cause of a significant network stress or 'back stress' in PC (by using analysis seen in Hasan & Boyce, 1995). PC seems to be independent of the thermal softening that may affect other amorphous polymers such as PPVC-2 and PMMA. In the following section, the thesis investigates this behavior of PC further by applying the experimental simulation model (presented in previous section and Chapter 5).

6.2.3 Experimental Simulation Method

Table 6.4: PC thermal properties used for simulation method

PC		
Heat capacity	1250	J kg^{-1} K^{-1}
Density	1210	kg m^{-3}
Thermal diffusivity	0.144	mm^2 s^{-1}

Using the experimental data of this investigation, the experimental simulation method described in Chapter 5 is extended to capture PC behavior. The method has already been shown to capture the amorphous polymer true stress-true strain behavior of PPVC-2 and PMMA.

In this particular case, the experimental simulation method is applied to PC to predict the high rate true-stress and true-strain behavior up to a large true strain of ~50%. The result of a simulation test recreating PC behavior at a 2545 s^{-1} rate of deformation is presented in figure 6-19 (using thermal properties in table 6.4 to calculate the theoretical temperature rise experienced by PC during testing), 2545 s^{-1} chosen influenced by the β transition and the adiabatic temperature rise and also in the region which exhibits reduced post-yield strain softening. The elastic modulus, yield, and immediate post-yield strain softening is captured well at 0.001 s^{-1} starting the experiment at a temperature of -46 °C and applying a temperature rise equivalent to a β factor of 100%. The temperature rise continues with increasing strain at a rate of 67 °C/% true strain (seen in figure 6-19), however, the true stress-true strain behavior continues to strain soften and depart from the experimental (2545 s^{-1}) curve by nearly 30 MPa by the end of testing. It is known that PC strain hardens with increasing rate when β motions are restricted, and in parallel, undergoes adiabatic deformation where ~100% of the work is converted to heat during testing at these high rates (Mulliken, 2006). However, the experimental simulation presented in figure 6-19, shows the

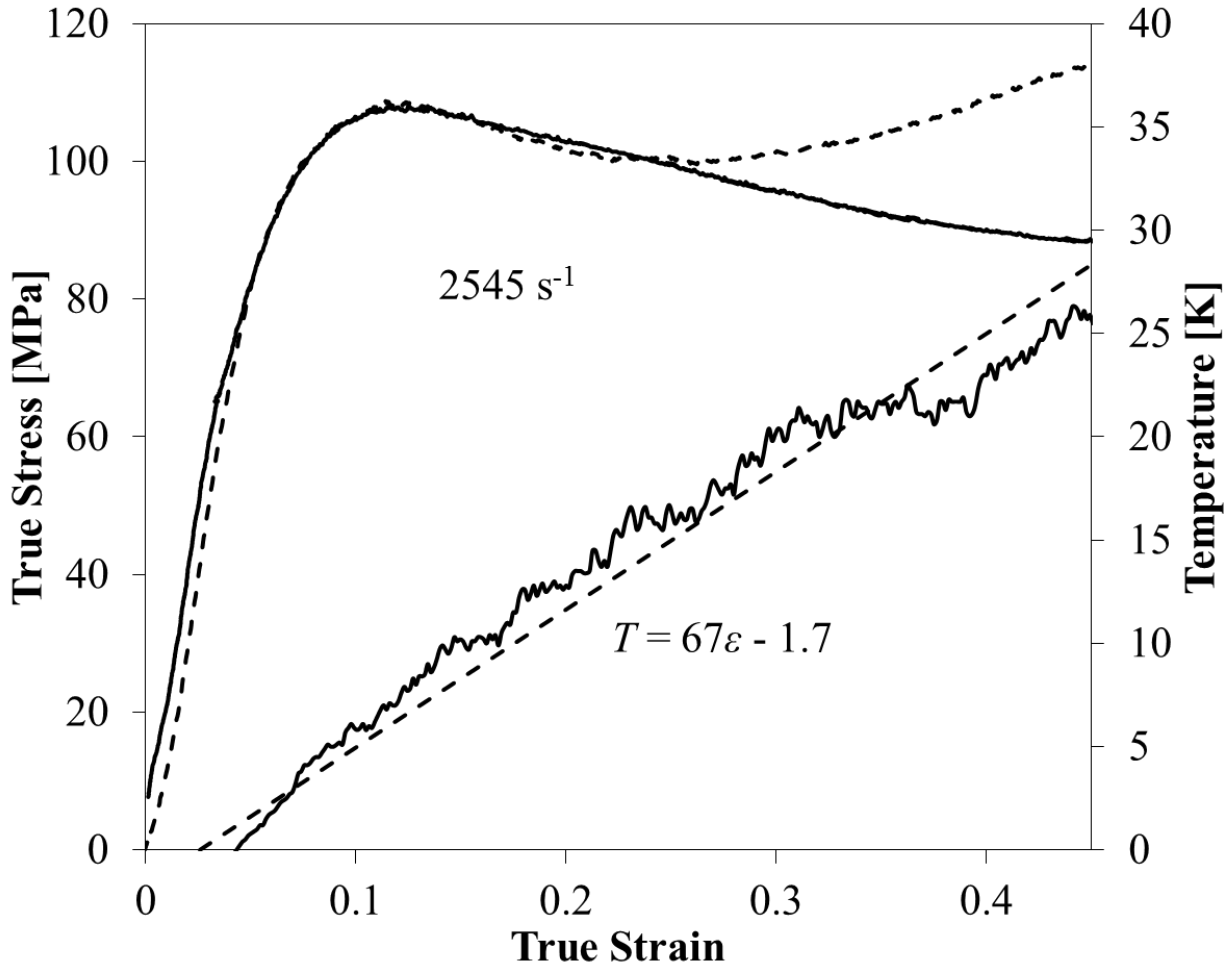


Figure 6-19: PC true stress-true strain behavior in uniaxial compression at 2545 s^{-1} (at 20 °C): experiment (dashed line) with its theoretical temperature rise from the model (dashed line) below, and experimental simulation model (solid line) and its temperature input during testing (solid line) in the lower half of the figure.

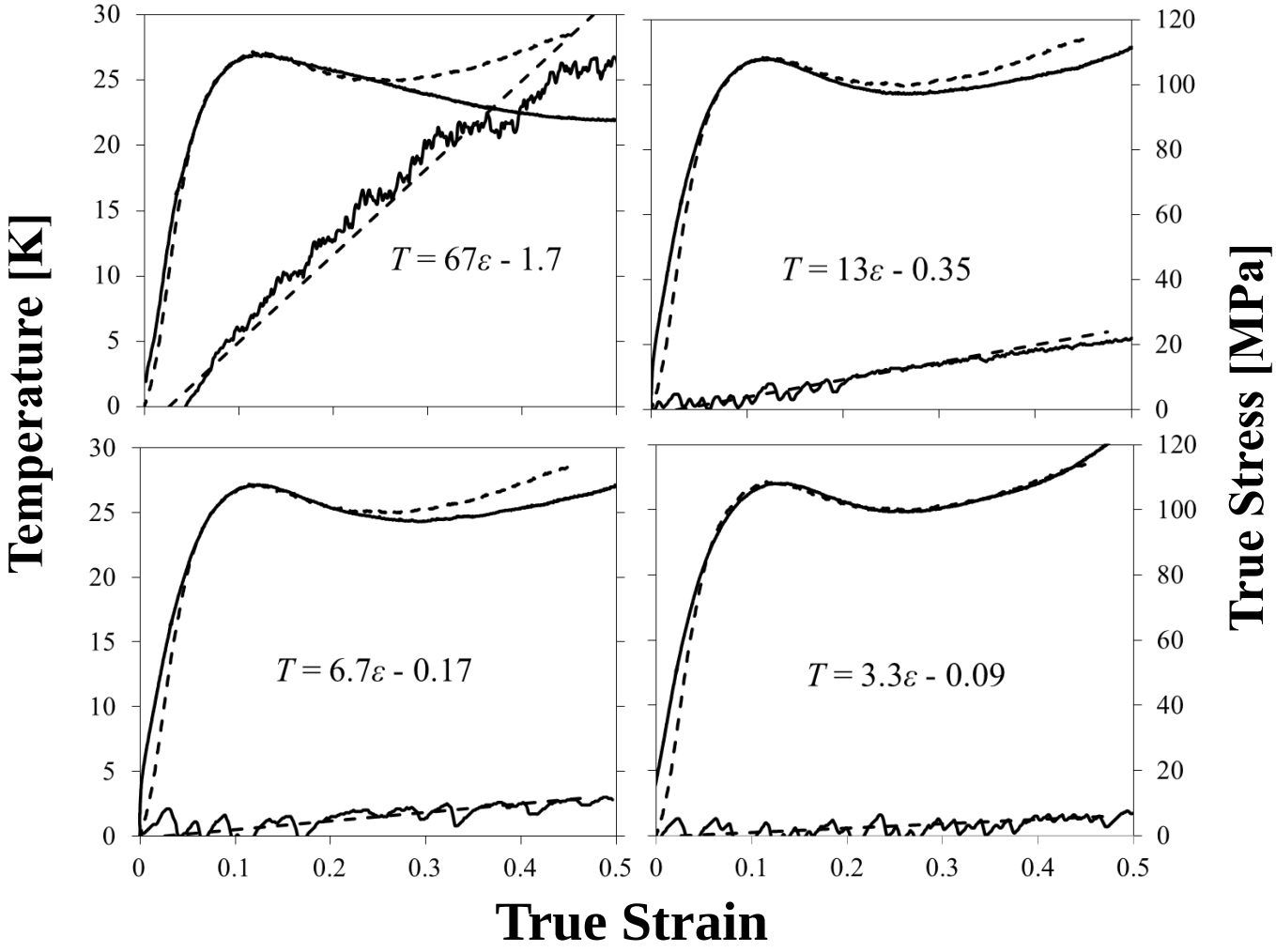


Figure 6-20: PC theoretical temperature rises (dashed lines) compared with the input temperature (solid lines) and its effect upon PC true stress-true strain behavior in uniaxial compression at 2545 s^{-1} (experimental behavior - dashed lines), at 20 °C, simulated (solid lines) assuming different amounts of work having been converted to heat (often referred to as 'β' or the 'β-factor'): (top-left) 100%, (top-right) 20%, (bottom-left) 10%, and (bottom-right) 5%. Please note: the temperature axis is the primary axis in this figure in order to emphasize the effects of temperature on PC.

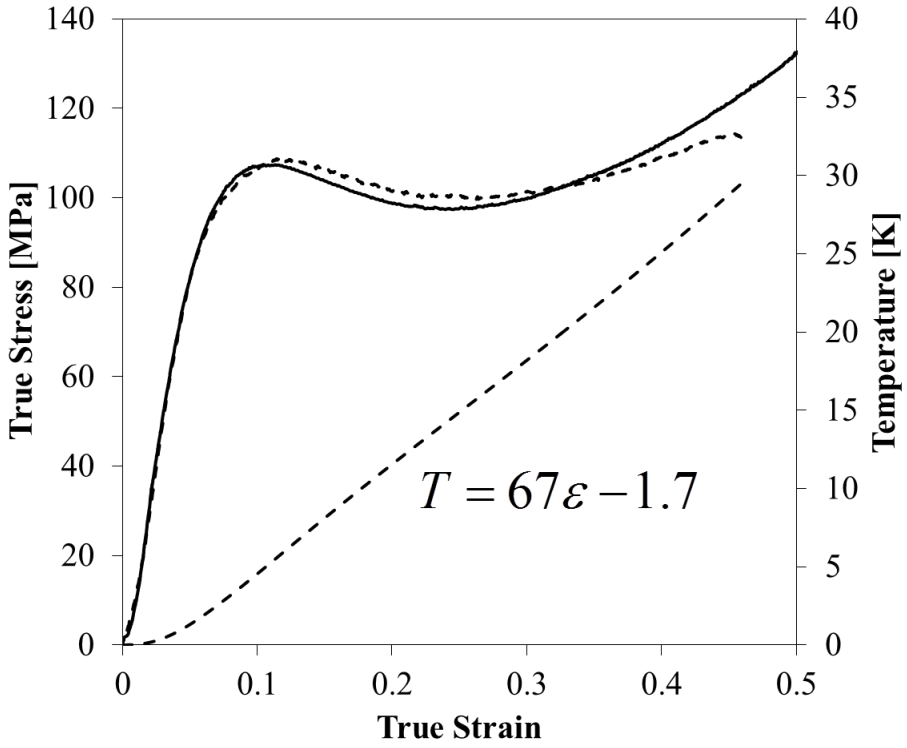


Figure 6-21: PC true stress-true strain behavior in uniaxial compression at 2545 s^{-1} (at 20 °C): experiment (dashed line) with its theoretical temperature rise from the model (dashed line) below, and a simulation test (-46 °C) with no temperature rise (solid line)

intrinsic behavior of the strain hardening PC at these high rates and PC's insensitivity to the adiabatic temperature rise at high rates (or the temperature insensitivity of the molecular movement involved in restriction of β motions at these high rates), clear sensitivity to temperature at low rates (observed in the strain softening in the low rate simulation test).

These observations were investigated further in figure 6-20 by performing simulation experiments with different applied temperature rises. After analyzing these behaviors, it is concluded that the post-yield strain hardening (and some softening) behavior of PC when β motions are restricted is nearly intrinsic – 5% of the PC post-yield behavior is caused by thermal softening (regardless of whether ~100% of the work is converted to heat), noted by the very good agreement between simulation and experiment of the behavior of PC at 2545 s^{-1}. Additionally, a 'dry run' was conducted at -46 °C and 0.001 s^{-1} for reference, with the result presented in figure 6-21.

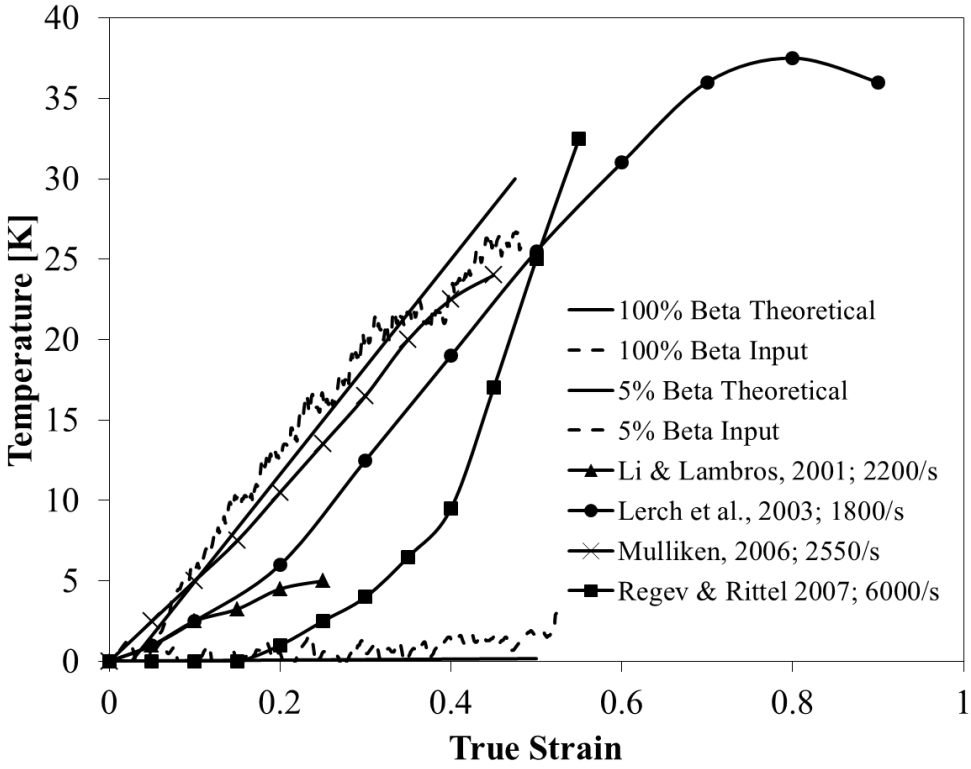


Figure 6-22: Theoretical temperature rises of PC (at 2545 s^{-1}) accompanied with the input temperature of simulation experiments (100% β-factor & 5% β–factor), compared with temperature rises of PC at high rates of deformation from literature.

Figure 6-22, adds the theoretical and the input (of the experimental simulation model) temperature rises to the comparison of experimentally measured temperature rises in PC at high rates of deformation. As noted previously, the temperature rise of PC at high strain rates measured by other authors is in agreement with the assumption that 100% of the work done at these high rates of strain is converted to heat. This assumption was implemented in our experimental simulation model, and is seen to be consistent with the measured temperature rise Mulliken measured in a high rate test at approximately the same rate (2545 s^{-1} versus 2550 s^{-1}). These large experimentally measured temperature rises are juxtaposed with the approximate rise in temperature which influences the strain hardening effects in PC – ~5% of the measured temperature rise is presumed to contribute to the (minimal amount of) thermal softening seen in PC at high rates. At high rates of deformation, when β-motions are restricted, the intrinsic softening in PC appears to decrease with increasing strain rate, and

seems to be very insensitive to the temperature rise which occurs inside the specimen at these rates.

A strategy to better understand the connections between β-motions, the back stress (or 'network stress' which causes strain hardening, e.g. PC at high rates), the effects of thermal softening, and the effects of strain energies (or Work, Heat, and Internal Energies) is needed to fully investigate these phenomena. A large number of amorphous polymers would need to be tested at rates and temperatures surrounding and inside of the β transition region, along with very close attention paid to the differences in these amorphous polymers' molecular influences.

6.2.4 Conclusion

The temperature- and rate-dependent behavior of PC was studied via uniaxial compression and DMTA testing. Rate-dependent true stress-true strain behavior showed no clear effects of adiabatic heating in that there was no apparent thermal softening in the behavior of PC at any of the rates tested (regardless of whether it is clear that heat would not have enough time to escape a specimen at these rates). A comparison of literature showed that there are clear temperature rises, or heat created, in PC at high strain rates (nearly 100% work is converted to heat at these rates). The experimental model presented in the fifth chapter was then applied to PC behavior at 2545 s^{-1} rate of deformation with good agreement between experimental versus model results in yield and the immediate strain softening, but poor agreement at higher strains when attempting to recreate the strain hardening that is seen in PC. Lastly, different theoretical temperature gradients were then applied to PC with the experimental simulation method, which garnered improved agreement between experiment and model once 5% of the work was assumed to be converted to heat. The better agreement was understood as the intrinsic strain hardening, understood to be caused by PC's intrinsic network stress, which

increases at higher rates and which stands alone from temperature effects (only 5% of the heat created inside the specimen during testing is shown to cause thermal softening at these rates).

Chapter 7

Simulating High Rate Composite Behavior in Tension & Compression:

Polymer Bonded Explosive Simulant

& Method for Soft Materials at High Rate

As detailed in the fifth chapter of this thesis, there are several benefits from having a low rate experimentation method which simulates high rate behavior. Composites frequently have large representative volume elements, which require large specimens, creating difficulties in high rate analysis: when measuring high rate properties of materials there is a requirement for dynamic equilibrium before the results of an experiment may be regarded as valid (Gray III, 2000). This requirement is more difficult to achieve in materials with a low sound speed and/or materials requiring greater length. In addition to this, because the Hopkinson bar technique uses forces and velocities calculated at the bar-specimen interface, average specimen properties are derived, so that until dynamic equilibrium is achieved, the forces

measured in the bars are not necessarily the same as those experienced by the specimen. Finally, there are diagnostic techniques which can be used in low rate testing, but cannot be applied to high rate experiments.

The fifth chapter of this thesis proposed a new experimental method which attempted to simulate the apparent elastic modulus, yield behavior, and post-yield amorphous polymer behavior observed at high rates of deformation, in such a way that is in accord with molecular and thermodynamic theory. Subsequently, the same method was applied to two additional amorphous polymers with contrasting behaviors: one, PMMA, which showed extreme strain softening and no strain hardening at high rates of deformation, and a second, PC, which demonstrated a decrease in strain softening and an increase in strain hardening.

In this chapter of the thesis, the experimental simulation method will be extended to simulate and predict the high rate behavior of a composite material, a polymer bonded explosive simulant, with a focus in tension tests (via Brazilian testing) during in-situ scanning electron microscope experiments. As in previous chapters, during this chapter, special attention will be paid to high rates of deformation and the adiabatic temperature rise which occurs at high deformation rates. In addition, this chapter presents a novel piezoelectric strain gage system developed for analyzing soft materials on Hopkinson bar apparatuses.

Although this chapter is mainly concerned with the use of PBSs as a model material for the simulation technique, a brief overview of their application is given in the following section.

7.1 Background

Polymer bonded explosives (PBXs) are seen in a wide range of applications, from the central explosive charge in standard armaments to rocket propellants. In armaments, PBXs typically contain 2-10% (by mass) of polymer, or up to 40% for rocket propellants – the polymer acts as a load mitigator to improve safety in in storage and handling and is typically a rubbery material (e.g. hydroxyl-terminated polybutadiene, HTPB and other polyurethane-based compositions). The second component of the PBXs typically consists of an explosive in the form of small crystals, such as cyclotetramethylene-tetranitramine (HMX), pentaerythritol-tetranitrate (PETN), cyclotrimethylenetrinitramine (RDX), or triamino-trinitrobenzene (TATB) (Palmer et al., 1993). For PBX simulants, such as the material used in this study, the explosive-substitute is typically a sugar crystal (mainly due to comparable particle-sizes and mechanical behavior).

Bowden and Yoffe (1952, 1958) were some of the first to study ignition mechanisms in explosives and concluded that explosive ignition reactions begin at localized 'hot spots.' Further investigations have offered insight into impact ignition (e.g. Field et al., 1982; Walley et al., 1992; Ho, 1996), and its two-step process: an initiation step and a propagation step (Ho & Fong, 1989; Field et al., 1992). The use of a binder suppresses both of these steps, and hence reduces the sensitivity of the explosive considerably.

Swallowe and Field (1982) studied the mechanical properties and sensitivity of polymer bonded explosives and found a wide range of differences depending on the characteristics of the polymer binder. Surface, thermal, and mechanical properties must all be considered when examining the choices for a binder material.

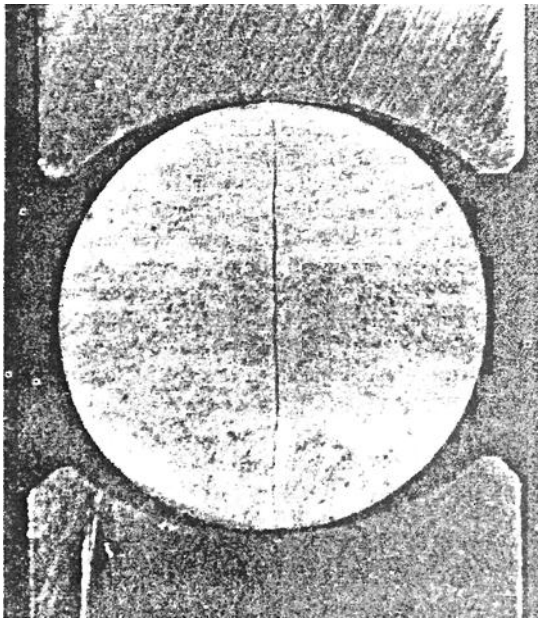


Figure 7-1: Brazilian test configuration where the tensile failure is seen at the center of the cylindrical specimen (marble) created from the compressive loading of curved anvils (Awaji & Sato, 1979).

Palmer et al. (1993) examined a wide range of PBXs with different compositions in tension at quasi-static strain rates, with the aim of studying the optimization of these materials. These authors found that compositions based on micronized crystals gave the best results in terms of brittle failure and debonding. Their analyses were conducted with an aim to optimize mechanical properties and maintain a low sensitivity and high explosiveness (e.g. material needs to be safe to manufacture, storage, and handle, but also react strongly to a prescribed stimulus). As will be presented later in this chapter, Palmer and colleagues used Brazilian tests (the 'indirect tensile test'), which were originally introduced by Carneiro and Barcellos (1949) (e.g. figure 7-1) to conduct tensile tests on their PBX specimens, and used optical techniques to measure the two-dimensional in-plane displacement fields. Advantages of this technique were cited as the relatively small specimens (e.g. cylindrical specimens of 10 mm diameter x 4 mm thickness), and that the complicated gripping methods required to perform tensile tests on composites were avoided. This experimental test method is described

in greater detail in section 2.8 of this thesis. The equation used to calculate tensile stress at the center of a test specimen is presented here:

$$\sigma = \frac{2P}{\pi D_s t_s}\left(1-\left(\frac{b}{R_s}\right)^2\right) \tag{7.1}$$

where P is the applied load, D_s and t_s the diameter and thickness of the specimen respectively, R_s is the radius of the specimen, and b is the width of the contact between the specimen and the anvils.

Over the past fifteen years, a wide range of insightful investigations of polymer bonded explosives (PBXs), and their simulants (PBSs), under high rates of deformation have been seen in literature (Gray III et al., 1998; Balzer et al., 2004; Cady et al., 2006; Siviour et al., 2008; Williamson et al., 2008; Zhou et al., 2012; Drodge et al., 2010; Williamson et al., 2010; Drodge et al., 2012; Thompson et al., 2012), and often use Brazilian testing as the test method when studying tension (e.g. Grantham et al., 2004; Williamson et al., 2009). These investigations found a clear rate-, and temperature-, dependency in the apparent elastic modulus, yield, and post-yield behavior. Williamson et al. (2008) and Thompson et al. (2012), both presented the mirrored nature of temperature and rate dependence by presenting successful time-temperature superposition results of PBX. Results such as these, and those presented in this section show how the experimental simulation method can be applied to a composite, in this case a polymer bonded sugar (PBS, a PBX simulant), in tension at high rates of deformation.

7.2 Experiments

Materials

The polymer bonded explosive simulant used in this chapter (DM076) consisted of 83% caster sugar, of both coarse (400-600 μm) and fine (10-110 μm) diameters, in a HTPB binder. The PBS and the HTPB binder were both studied in this chapter. Both materials were manufactured at the High Explosives Research and Development (HERD) facility of the Energetic Materials Branch of Air Force Research Laboratory, in Eglin, FL, USA. Tests specimens were all right cylinders 10 mm diameter x 4 mm thickness.

Dynamic Mechanical & Thermal Analysis

Dynamic mechanical and thermal analysis (DMTA) testing was conducted with a TA Instruments Q800 at the Department of Zoology. Tests were performed in dual cantilever configuration at 1, 10, 100 Hz, on PBS over the temperature range -150 °C (123 K) to 25 °C (298 K), and on HTPB over the temperature range -150 °C (123 K) to -15 °C (258 K), so that each material was taken well below their respective glass transition temperature. Rectangular samples were 60 mm long x 12.5 mm wide x 2.5 mm thick.

Compression Testing & Novel Piezoelectric SHPB Gage

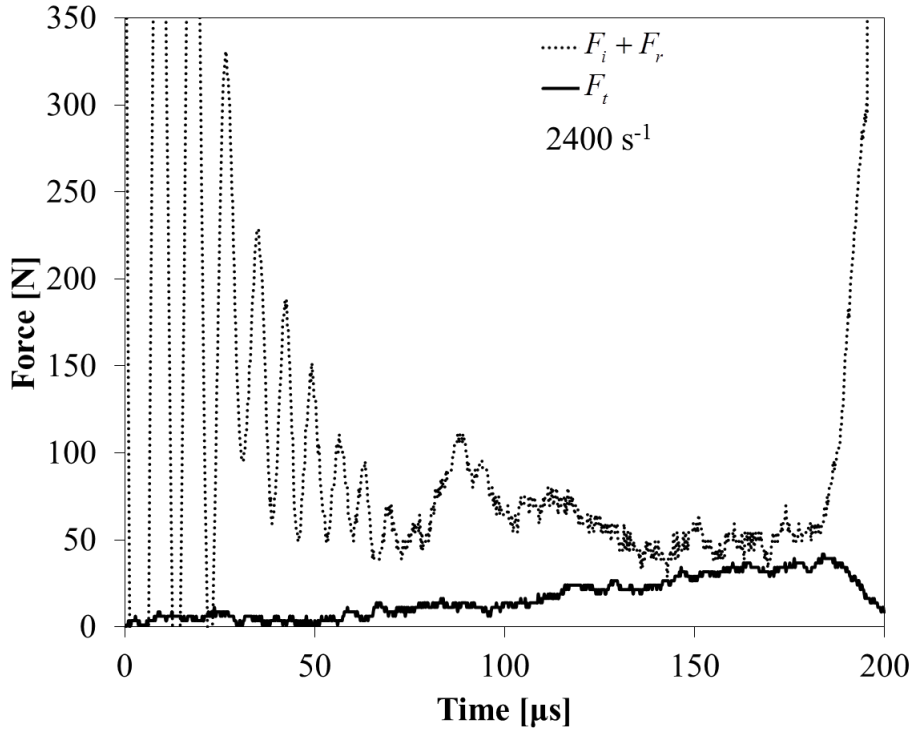


Figure 7-2: Representative force-time behavior of HTPB used to determine dynamic equilibrium during initial high rate testing using standard strain gages (or 'indirect surface strain gage method') on SHPB apparatus.

The uniaxial compression testing in this chapter was performed at temperatures from -110 °C to 20 °C at a strain rate of 10^{-2} s^{-1}, and rates from 10^{-3} to 4800 s^{-1} at an ambient temperature of 20 °C. Tests conducted for the experimental simulation testing to predict high rate behavior were also performed at 10^{-2} s^{-1}. The experimental method in uniaxial compression is the same as that described in the second and third chapters (e.g. section 3.3.2) of this thesis. Magnesium alloy (AZM) SHPB bars were used for high rate testing (~10^{3} s^{-1} rates of deformation and higher). In result of the very low forces observed by strain gages on the SHPB apparatus, it was very difficult to verify dynamic equilibrium during testing (figure 7-2). To improve the resolution of the force measurements, a novel stress gage method was developed and implemented, presented in figure 7-3. This method for testing soft materials at

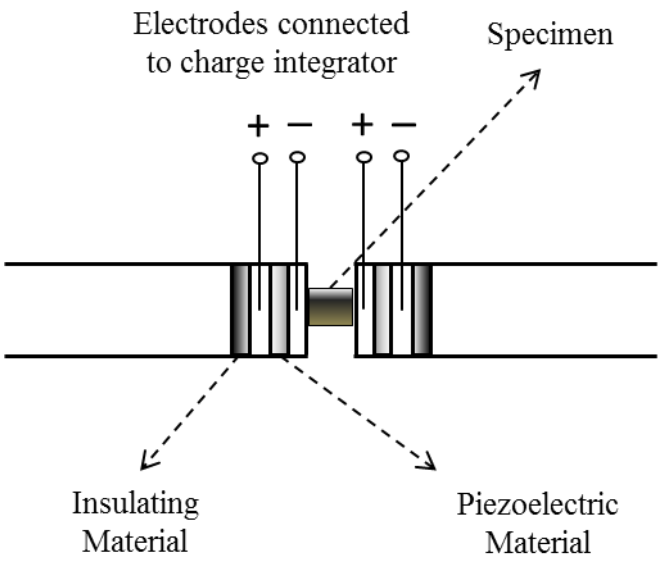


Figure 7-3: Novel piezoelectric strain gage system developed for analyzing soft materials on Hopkinson bar apparatuses. Note: the white portions of the SHPB setup represent the bar material of the relevant apparatus.

Table 7.1: Calibration factors for high sensitivity (SHPB) PZT gages.

	[V/N]	[V/True Strain]
Incident Bar	0.0079	115100
Transmission Bar	0.0171	249300

high rates of deformation is an improvement to the Quartz crystal methodology of Chen et al. (2000). The method presented here uses lead zirconium titanate (PZT)[10], a piezoelectric material which is approximately 100 times more sensitive. PZT's piezoelectric constant ranges between 290 – 630 x $10^{=12}$ C/N versus 2.3 x $10^{=12}$ C/N for Quartz-crystal, these materials also have equivalent strengths (in compression of $\geq$ 500 MPa)[11]. In addition to the improvement in the piezoelectric material, this method also improves upon the accuracy of measurement via the location of the piezoelectric gages: in the setup presented here, in figure 7-3, the gages are at the specimen-bar interface (versus a third of the length of the transmission bar away from the specimen-bar interface). Titanium alloy (Ti-6Al-4V) was

[10] PZT manufacturer was APC International Ltd., in Mackeyville, Pennsylvania, USA. The PZT used in this study has a piezoelectric constant of 400 x 10^{-12} C/N (or m/V), which was provided by manufacturer.
[11] PZT data was provided from the manufacturer; Quartz data is from Chen *et al.*, 2000.

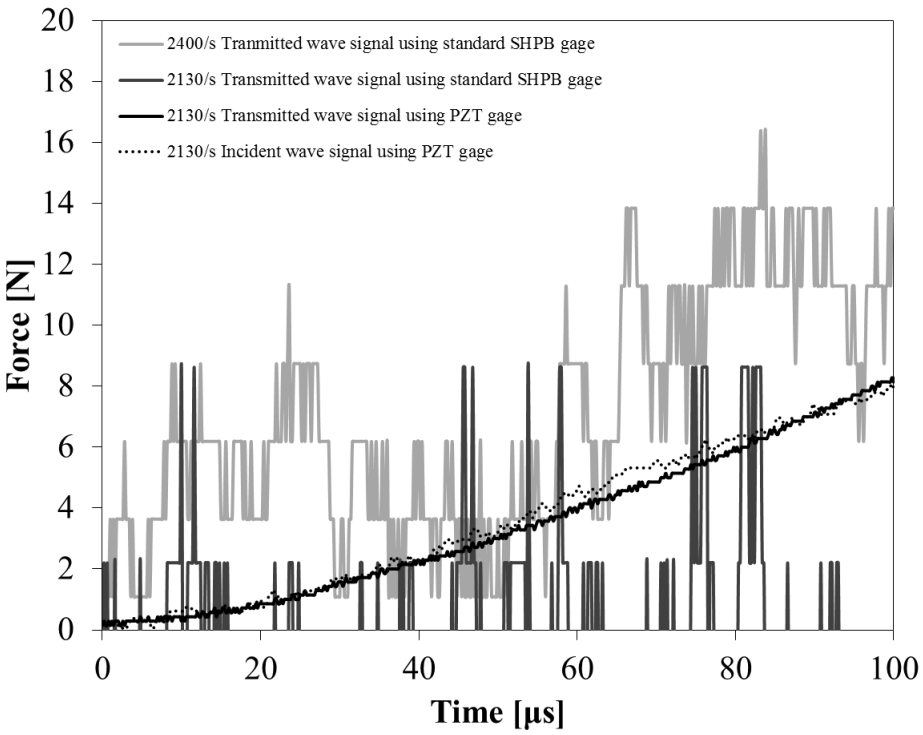


Figure 7-4: Representative force-time behavior of HTPB used to determine dynamic equilibrium during initial high rate testing using standard strain gages. Note: The standard gage 2400/s test shown here is the same as that conducted in figure 7-2.

used with (2 mm in width x 12.7 mm diameter; same diameter as SHPB bars) PZT endcaps and insulating layers made from biaxially-oriented polyethylene terephthalate (BoPET). The piezoelectric gage was connected to a charge integrator (designed in the Electronics Workshop of the Department of Engineering Science) in order to produce voltages to be read by a data acquisition system (presented in the second chapter, sections 2.4, and analyzed in Appendix A of this thesis). The calibration factors found with this setup are presented in table 7.2. The PZT gage method was advantageous for measuring the extremely low (compared to literature) temperature glass transition HTPB which was used in this thesis (seen in DMTA experiments presented in figure 7-5). Force-time plot comparison of the two strain gage methods (standard vs. PZT setup) is presented in figure 7-4. These data demonstrate dynamic equilibrium during testing, the large amount of noise observed in previous testing, and the inability of the standard strain gages to measure the low forces which were experienced by

the HTPB during testing (noting the 2130 s^{-1} standard stain gage transmitted wave signal). This setup avoids the use of polymer, or viscoelelastic bars, to test soft materials, and thus avoids the viscoelastic effects in a SHPB setup, that Zhao et al. (1997) has shown is consistently non-negligible (these advantages are described in additional detail in section 2.2.3).

Tension Testing via Brazilian Disc Tests

Table 7.2: Brazilian Test Parameters used to calculate the tensile stress at the center of the test specimen via equation 7.1.

Brazilian Test Parameter	
b [mm]	1.9
D_s [mm]	10
t_s [mm]	4.0
R_s [mm]	5.0
(b/R)	0.38

A Deben loading stage, with 660 N load cell and Peltier chip for heating and cooling specimens, from Deben UK Limited of West Sussex, UK, was configured for in-situ testing in accompaniment with an environmental electron scanning microscope (ESEM) made by Carl Zeiss AG, Oberkochen, Germany. Two sets of Brazilian compression platens were made in the Department of Engineering Science to a radius of 6 mm. In previous studies this combination of specimen and anvil dimensions has been shown to give b/R_S ratio greater than 0.27 in order to allow the tensile strength of the specimen to be independent of b/R_s: as presented in table 7.2, the ratio of compression platen contact width (b) and specimen radius (R_s) is calculated to be 0.38. Both sets of platens were manufactured from a Titanium alloy (Ti-6Al-4V): one set was used for Deben loading stage configuration, and the additional set was made to attach to the bars used for SHPB experiments (Titanium alloy bars). These platens were also used in quasi-static tests with the Instron testing machine and temperature

chamber (for additional detail please refer to Chapter 2). A Photron SA5 high speed camera was used to photograph Brazilian tests at high rates of strain, with an interframe time of 10 μs, triggered via the input bar's strain gage. The tensile strain in the Brazilian tests was calculated via Digital Image Correlation (DIC) methods with DaVis 7.2 DIC Software. The initial photograph of each test was used for calibration: two-point calibration (two ends of the specimen, i.e. the specimen diameter) was used. For calculating the strain on the surface of each specimen, a 64 x 64 pixel window size was used at the beginning of testing, and moving smaller to a 8 x 8 pixel window at the completion of testing (in order to follow the tensile stress concentrations at the center of the specimen). In addition to this, 75% overlap (between images) and 4 analytic passes (for each image) were found to give optimal results. A more detailed description of the DIC method may be found in the thesis of Siviour (2005). The Brazilian tension testing in this chapter presents two different data sets in temperature, one at -30 °C (conducted on a Deben rig) and another at -45°C at a strain rate of 10^{-2} s^{-1}, and rates from 10^{-3} to 4800 s^{-1} at an ambient temperature of 20 °C.

7.3 Results and Analysis

7.3.1 Dynamic Mechanical & Thermal Analysis

Table 7.3: Shift factors of HTPB and PBS viscoelastic transitions

	D_α [°C/ decade strain rate]	D_β [°C/ decade strain rate]
HTPB	6	20
PBS	10	-

HTPB and PBS DMTA test results are summarized in figures 7-5 and 7-6 – these figures are presented with the same axes in order for a direct comparison of the polymer binder and the composite. The shift factors calculated from these data sets are presented in table 7.3.

The α transition of HTPB is very low at approximately -85 °C, with the beginning of a very broad β transition being seen at approximately -100 °C (moving from high to low temperatures),in the 3.2 s^{-1} (or 100 Hz) curve. These measurements allow shift factors to be found: a 6 °C/decade strain rate for the α transition and a 20 °C/decade strain rate shift factor for the β transition. The α transition of the HTPB in this thesis is approximately 25 °C lower than that found in literature (-85 vs. -60 °C), and the α shift factor is ~4 °C/decade strain rate lower than that found in literature (6 vs. 10 °C/decade strain rate). In addition, the glass transition in the HTPB of this study spans approximately 25 °C, versus a range over 50 °C (Siviour et al., 2008). In conclusion, the HTPB in this study remains rubbery to lower temperatures, is less sensitive to strain rate once α processes are restricted, and is much more sensitive to temperature (or rate changes at very high rates) in the glass transition region.

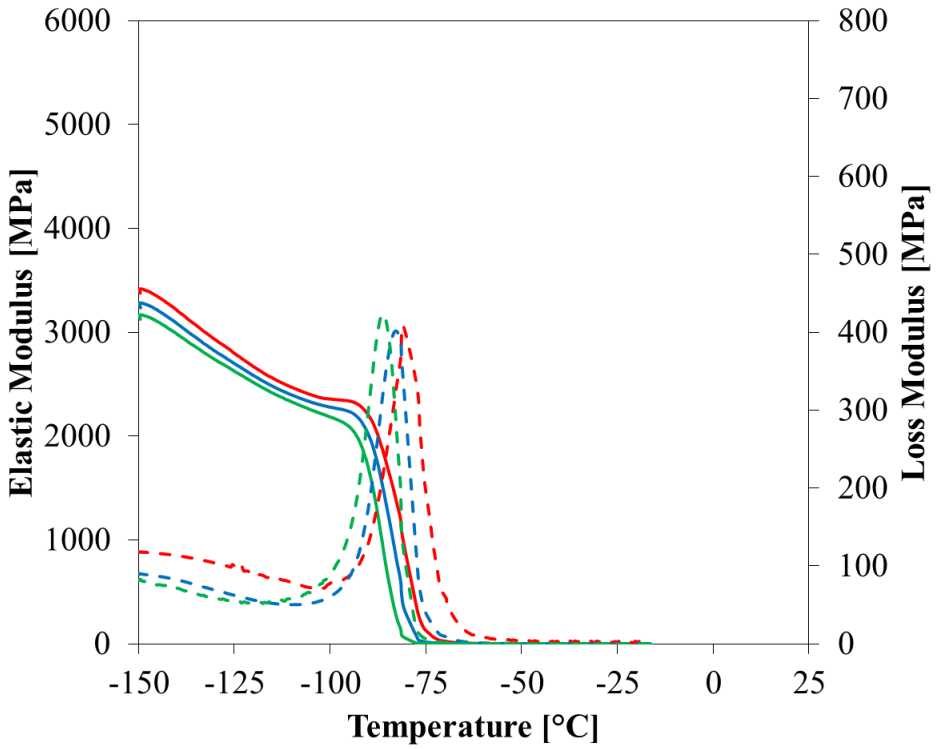


Figure 7-5: HTPB elastic modulus (solid lines) and loss modulus (dashed lines) as a function of temperature at 1 Hz (0.032 s^{-1}), 10 Hz (0.32 s^{-1}), and 100 Hz (3.2 s^{-1}).

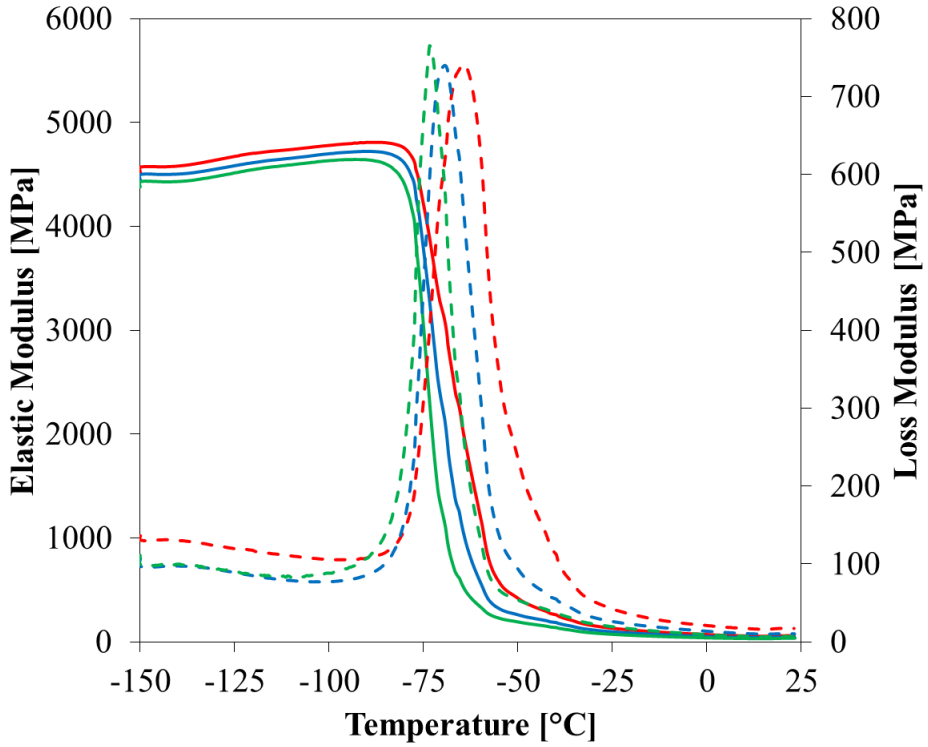


Figure 7-6: PBS elastic modulus (solid lines) and loss modulus (dashed lines) as a function of temperature at 1 Hz (0.032 s^{-1}), 10 Hz (0.32 s^{-1}), and 100 Hz (3.2 s^{-1}).

PBS also presents rubbery behavior with a sub-ambient α transition at approximately -70 °C, with the possibility of a β transition starting at approximately -150 °C, with a slight increase in elastic modulus seen in all curves. PBS has an α transition almost twice, or 5/3, larger compared to that of its binder, HTPB, demonstrating a comparatively much higher sensitivity to changes in strain rate. Comparing to literature (Siviour et al., 2008), from a 66% (vs. 83% in this study) caster sugar PBS, we see the α transition of the PBS in this thesis is approximately -60 °C lower than that found in literature (-70 vs. -10 °C), and the α shift factor is ~20 °C/decade strain rate lower than that found in literature (10 vs. 30 °C/decade strain rate). In addition, the glass transition in the PBS in this study spans approximately 45 °C, 20 °C larger than its binder, but over 55 °C less than that found in literature. In conclusion, the PBS in this study, due to the much more rubbery HTPB binder, is much more rubbery compared to equivalent PBXs with 83%, or even less, explosive material (or simulant, in this case). Regardless of the differences seen in the HTPB binder used in this study, the overall behavior of transitions broadening as a result of the added explosive or simulant, is consistent with observations in literature (e.g. Drodge et al., 2010; for additional references please refer to section 7.1).

7.3.2 Compression Testing

Uniaxial compression testing results are summarized in figures 7-7 – 7-14. During quasi-static temperature dependence testing, all HTPB specimens deformed in a rubbery manner at all tested temperatures (figures 7-7) above -90 °C, with a glassy region beginning sharply below this temperature. The behavior at -100 °C presents interesting characteristics: because these tests are centered around the glass transition temperature, slight changes in temperature bring about large changes in modulus, yield stress, and post-yield behavior; hence, even when testing at nominally the same temperature (-100 °C) a wide range of yield stresses is observed (figure 7-8) from roughly 10 MPa to just below 40 MPa. The HTPB true stress-true strain behavior demonstrates increasingly glassy polymer behavior when moving towards lower testing temperatures: a dramatic post-yield softening is visible at -110 °C where yield is measured at 77 MPa, and subsequently a softening in true stress is seen to continue for ~27 MPa. Comparing this behavior to that of PBS (figure 7-9), a maximum strain softening of 10 MPa is observed in true stress-true strain behavior at -80 °C. These contrasting behaviors demonstrate the large and de-localized chain motion which is seen in HTPB, and decrease in large-scale chain motion, and perhaps a slight restriction due to the explosive simulant.

The α transition in HTPB (figure 7-7) is between -90 °C and -100 °C (at 10^{-2} s^{-1}) which is consistent with DMTA data presented in figure 7-5 at 0.032 s^{-1}. Comparison between PBS data sets is slightly more interesting, in that there is what looks like glassy behavior shown in quasi-static compression data at room temperature (figure 7-11), although there is no apparent contribution of the glass transition at these rates and temperatures (20 °C) in DMTA data (figure 7-6) – this demonstrates that the observed behavior is most likely due to gradual debonding of the crystals from the binder.

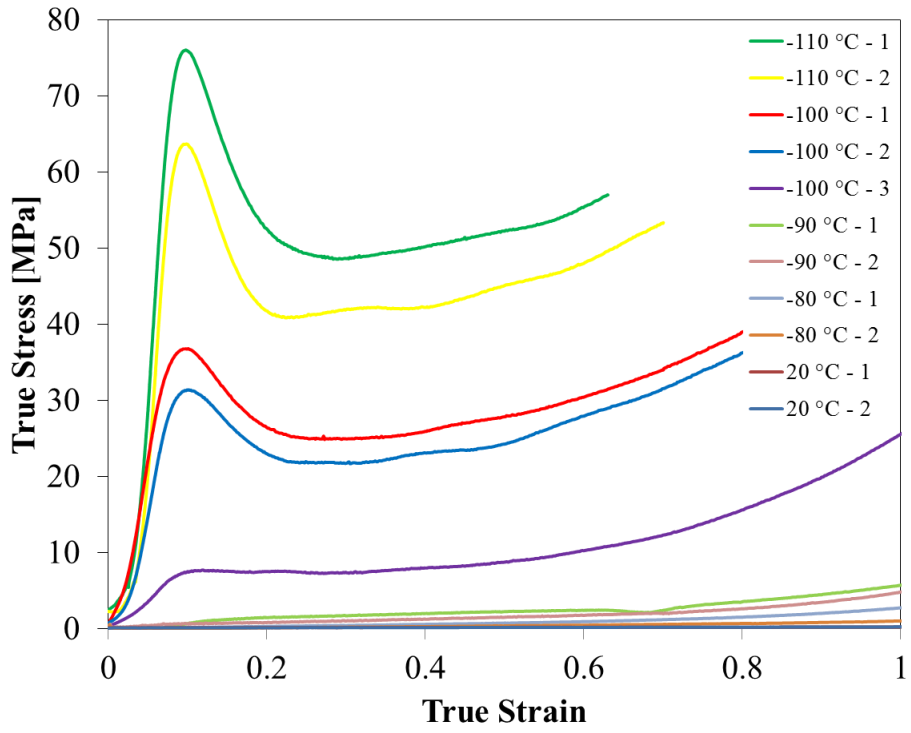


Figure 7-7: HTPB true stress-true strain behavior as a function of temperature (-110 – 20 °C) at a rate of 10^{-2} s^{-1}.

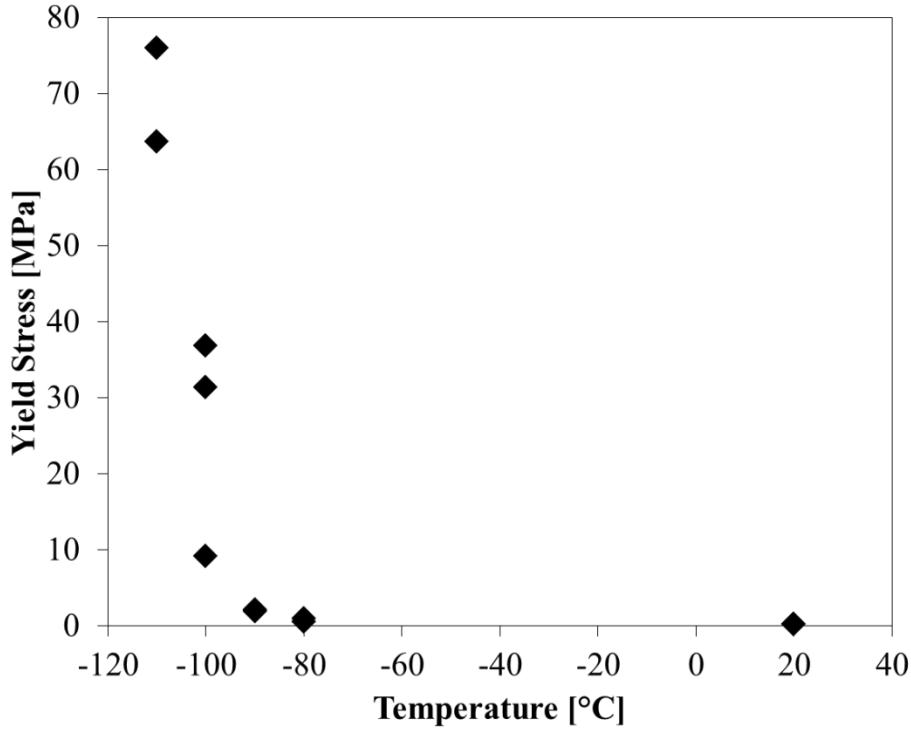


Figure 7-8: HTPB yield stress behavior as a function of temperature (-110 – 20 °C) at a rate of 10^{-2} s^{-1}. Note: stress at 0.1 true strain is reported for non-glassy behavior.

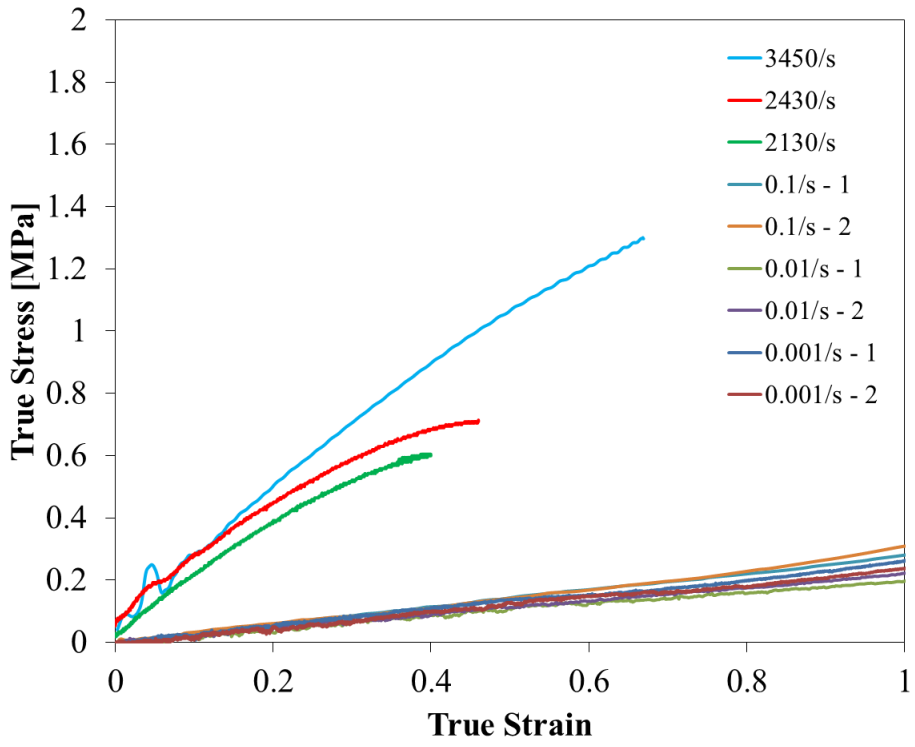


Figure 7-9: Representative true stress-true strain behavior of HTPB as a function of strain rate (10^{-3} – 3450 s^{-1}) at an ambient temperature of 20 °C. Note: High rate testing was conducted with the PZT gage system presented in figure 7-2.

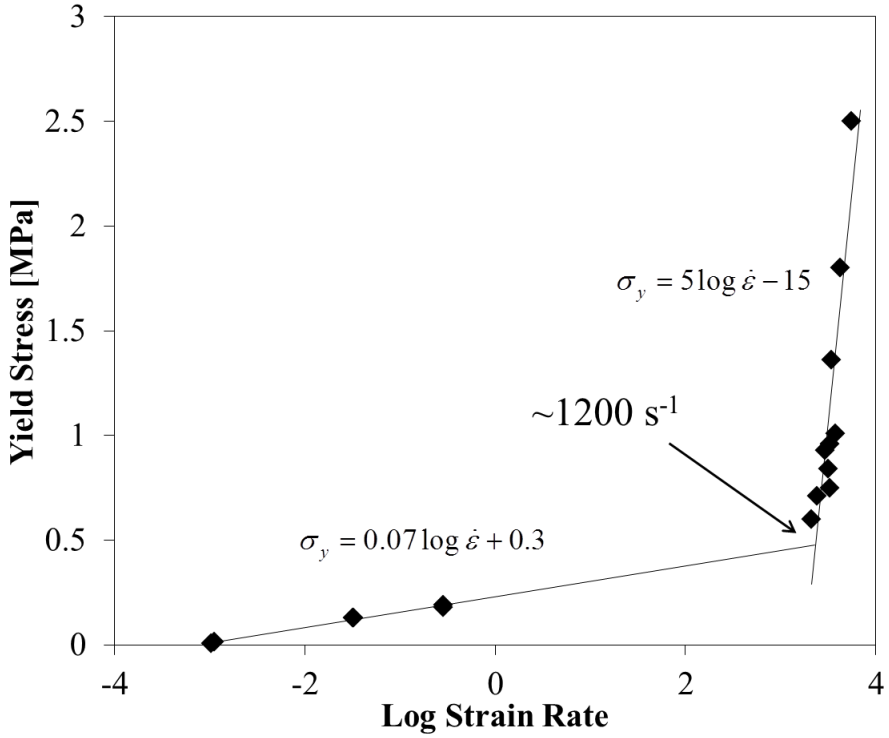


Figure 7-10: HTPB stress at 0.1 true strain as a function of strain rate (10^{-3} – 3450 s^{-1}).

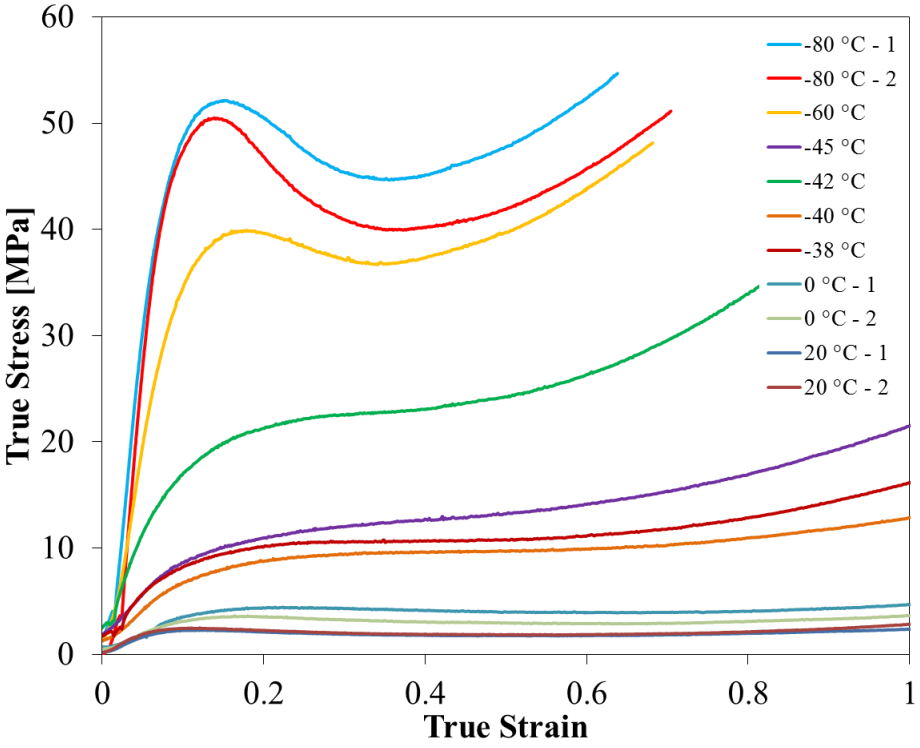


Figure 7-11: PBS true stress-true strain behavior as a function of temperature (-80 – +20 °C) at a rate of 10^{-2} s^{-1}.

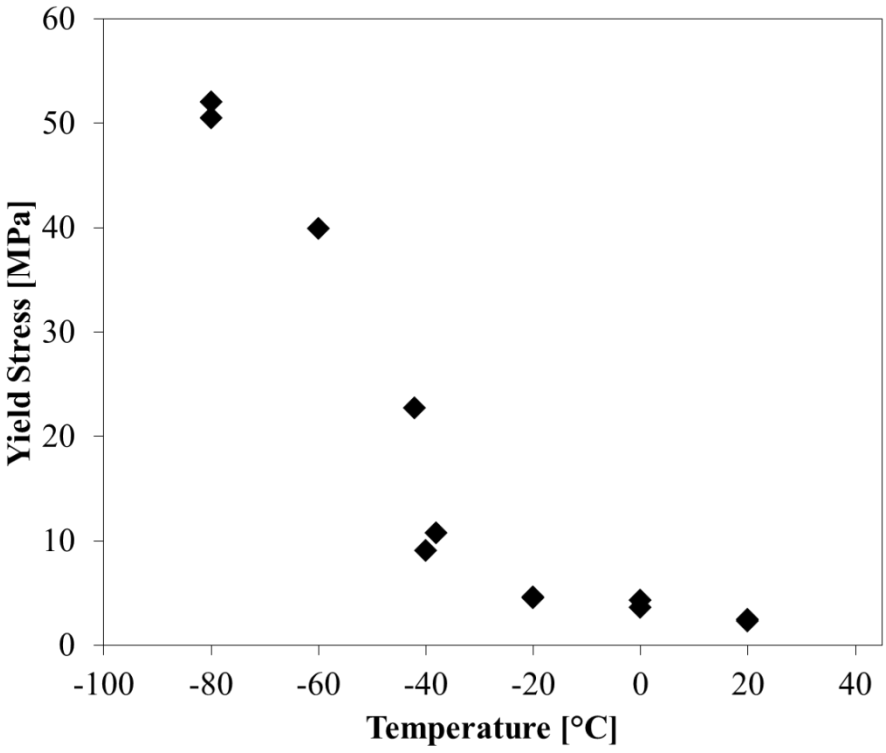


Figure 7-12: PBS yield stress behavior as a function of temperature (-80 – +20 °C) at a rate of 10^{-2} s^{-1}.

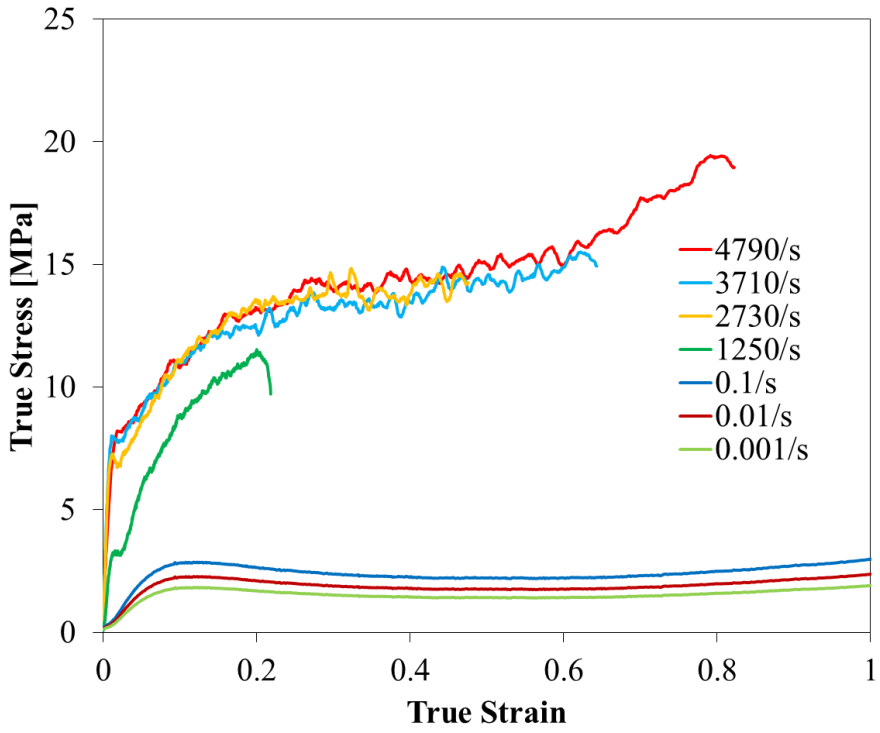


Figure 7-13: Representative true stress-true strain behavior of PBS as a function of strain rate (10^{-3} – 4790 s^{-1}).

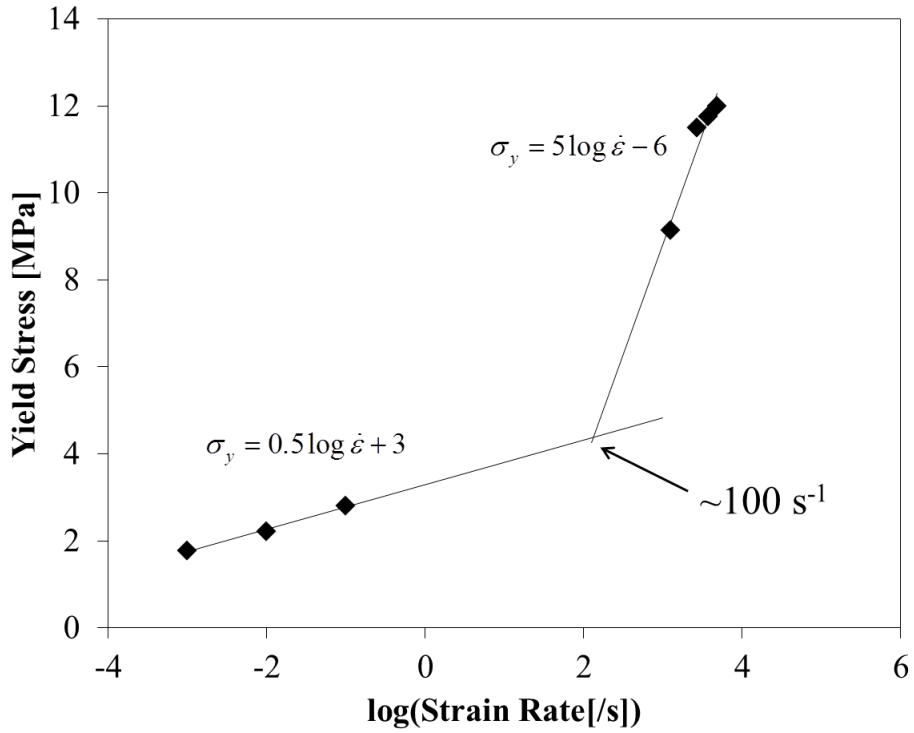


Figure 7-14: PBS yield stress behavior of as a function of strain rate (10^{-3} – 4790 s^{-1}).

In comparing rate dependencies of HTPB (figures 7-9) and PBS (figures 7-13), in PBS, glassy behavior is seen in all true stress-true strain rate dependent behavior, where in HTPB, the response continues to be rubbery even at high strain rates (up to 3450 s^{-1}). Examining the yield stress data (maximum stress at 10% true strain was used for rubbery behavior in both HTPB and PBS), we see a clear decrease in the rate at which the α transition is observed in the PBX as compared to the HTPB. (~100 vs. 1200 s^{-1}). This is to be expected from the difference in sensitivities to strain rate between the two materials seen earlier in the shift factors calculated from DMTA data (10 °C/decade strain rate for PBS vs. 6 °C/decade strain rate for HTPB), and the higher temperature of the transition in the PBS DMTA data.

7.3.4 Brazilian Testing on a Composite (PBS)

The preliminary results from Brazilian testing conducted on PBS are summarized in figures 7-15 – 7-16. The high rate behavior demonstrates an expected (pseudo-)glassy behavior, due to the system going through its alpha transition, and debonding of the polymer from the matrix, where an increase in yield stress is observed with increasing strain rate. In these experiments dynamic equilibrium was observed from about 20 μs after the start of testing, or 2% true strain.

After deciding to use the 6 m s^{-1} data seen in these figures, the DIC method was applied to the high speed video associated with this deformation. The high speed images captured during the Brazilian testing and used to calculate tensile true strain values (in order to have a data set to use for the simulation method) are presented in figures 7-17 – 7-19. These figures present

- High speed imagery
- Example images with displacement vectors found using a prescribed methodology in the DIC software
    - Alongside are the plots associated with these images used to calculate the tensile strain in each image
- The resultant true strain-time results from the test images, causing an 850 s^{-1} rate of deformation (in tension)

The combination of this tensile behavior is presented as true stress-true strain data, with its theoretical temperature rise, in figure 7-20.

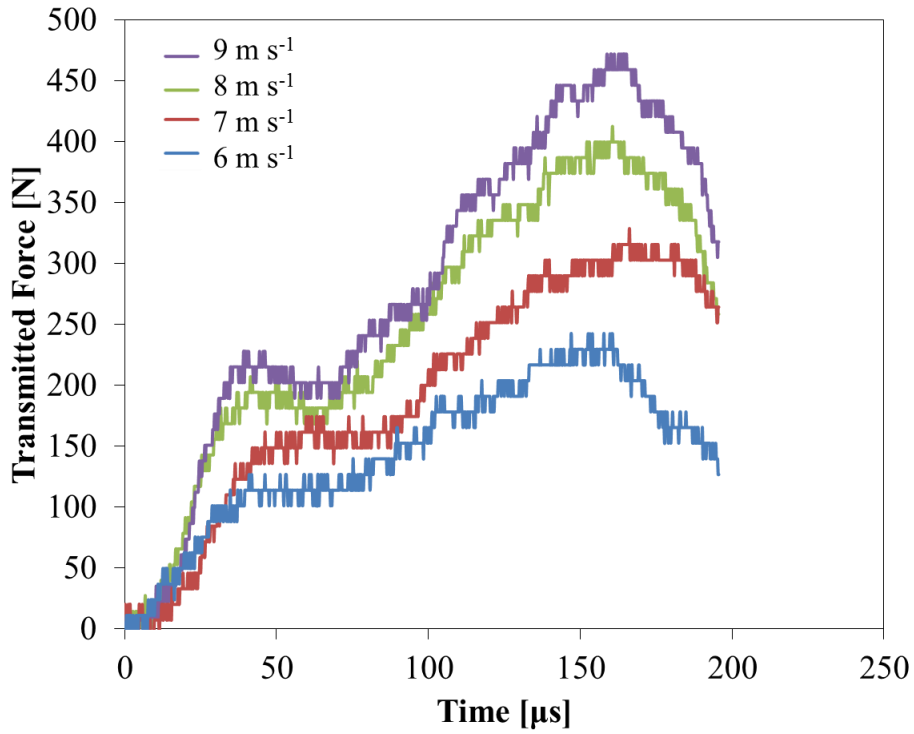


Figure 7-15: Force-time curves of PBS. Striker bar velocities of each curve are given in the upper left corner of the figure. The 6 m s^{-1} plot was chosen to simulate, and thus analyze using DIC to observe true stress-true strain behavior.

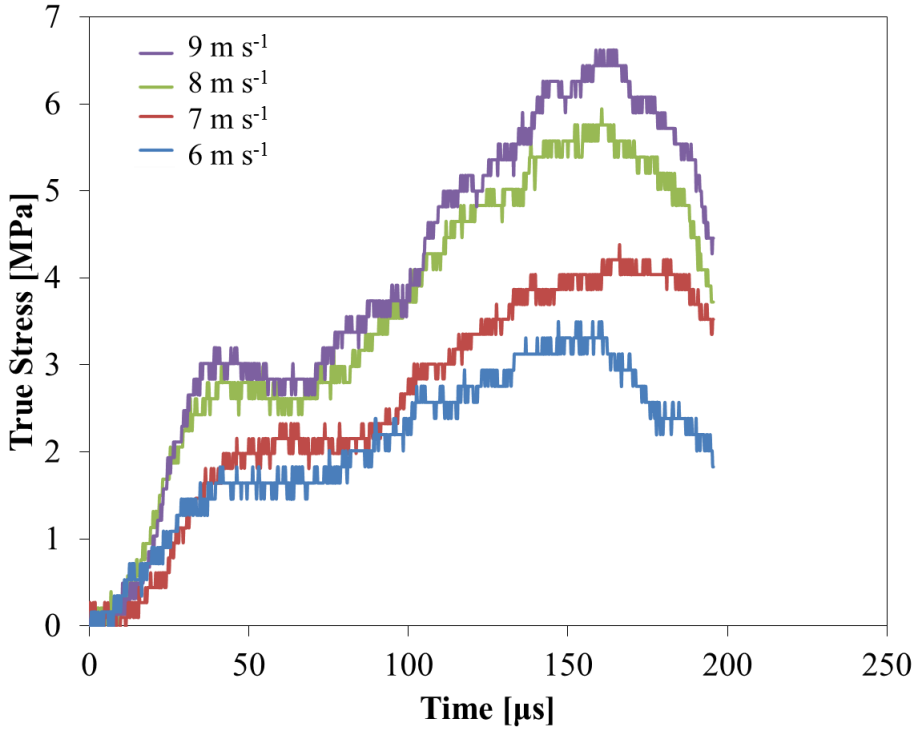


Figure 7-16: Tensile true stress-time curves of PBS. Tensile stress was calculated via equation 7.1 using parameters from table 7.2.

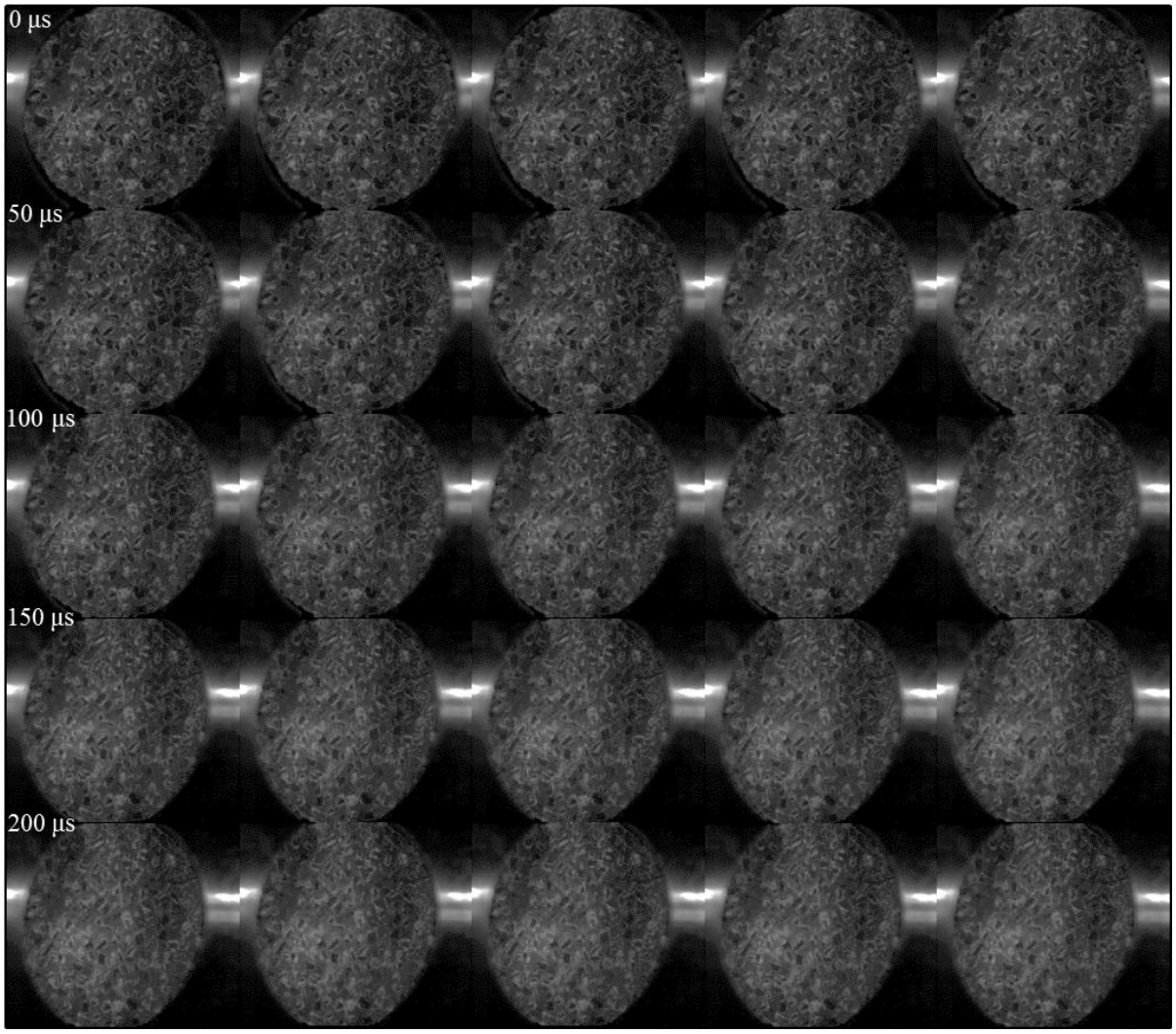


Figure 7-17: Initial high speed images during Brazilian tension testing of PBS (during the 6 m s^{-1} striker bar velocity curves seen in figures 7-15 and 7-16). In each row, the images increase in value by 10 µs reading left-to-right.

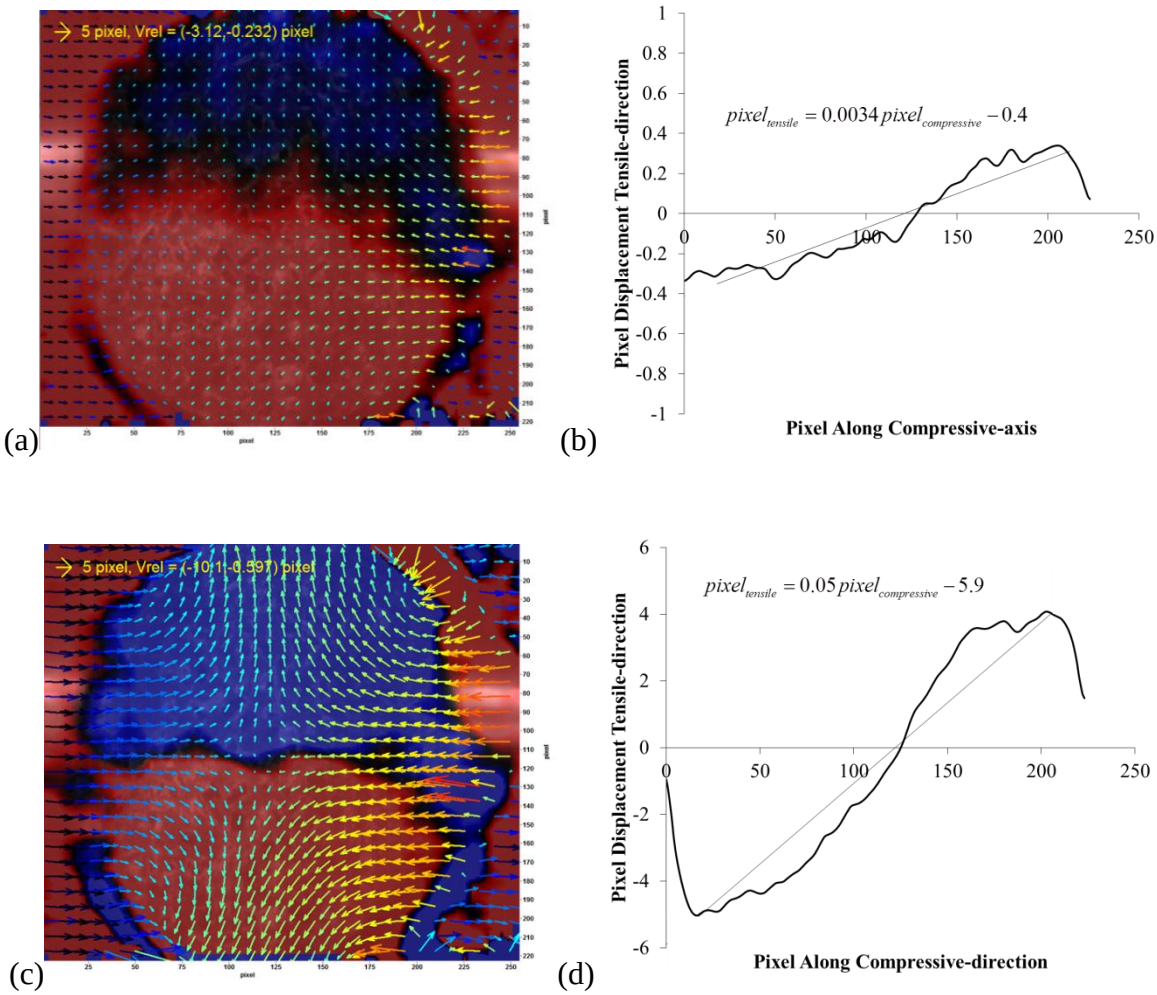


Figure 7-18: Representative (a & c) pixel displacement vectors (whose coloration depends on the magnitude and direction of the vector) and (b & d) their respective magnitudes plotted in order to determine the average true strain (the slope) calculated in each photograph at 50 (a & b) and 160 μs (c & d) during testing.

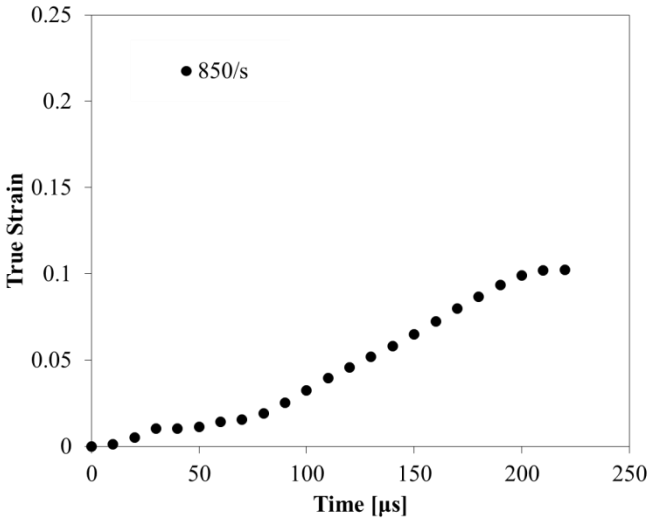


Figure 7-19: Resultant true stain-time curve demonstrating a tensile strain rate of approximately 850 s^{-1}. Each dot on the curve is a true strain value calculated from an image using the methodology presented in figure 7-18.

The true stress-true strain behavior and theoretical temperature rise are shown in figure 7-20. The theoretical temperature rise is very small, less than 1 K, even at very high rates of deformation[12]. This low temperature rise during deformation is considered a very desirable characteristic for PBX materials in their storage in order to ensure safety, in that this temperature rise may be the source of a 'hot spot' causing ignition. Four different places on the true stress-true strain behavior are presented photographically in figure 7-21:

- 1: Undeformed specimen
- 2: Specimen in dynamic equilibrium
- 3: Specimen during its first large debonding and yielding phase
- 4: End of testing

The first four photographs offer a clear representation of specimen deformation during high rate Brazilian testing. Comparison between image 1 and image 4 present a clear contrast in the fracturing of explosive simulant crystals (seen as the change of crystals from transparent to white in color) and the movement of the PBS along the axis perpendicular to the movement of the SHPB bars, or the compression axis. The fourth photograph is repeated in figure 7-22, but with an example of the displacements measured using the DIC software. These displacements are typical for Brazilian tests, with the clear tensile region in the center of the specimen shown by the direction and lengths of the displacement arrows.

[12] These were calculated using ρ_{HTPB} = 880 kg m^{-3} & C_{HTPB} = 2095 J kg^{-1} K^{-1}; ρ_{sugar} = 1586 kg m^{-3} & C_{sugar} = 1245 J kg^{-1} K^{-1}; giving (from the binder-crystal ratio) ρ_{PBS} = 1466 kg m^{-3} and C_{PBS} = 1390 J kg^{1} K^{-1}.

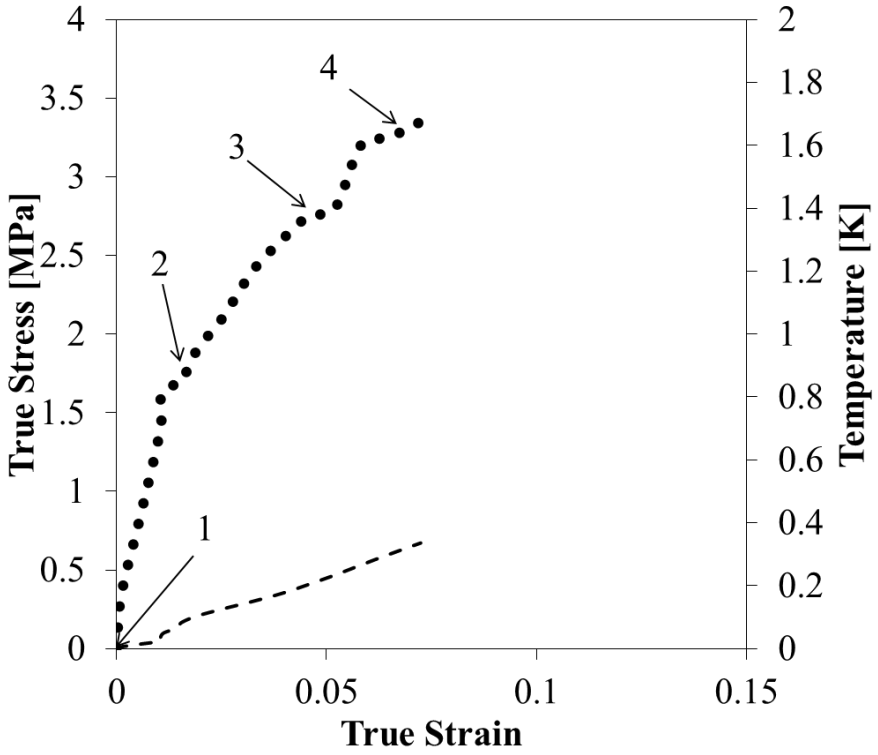


Figure 7-20: PBS true stress-true strain behavior and theoretical temperature rise in tension at a tension strain rate of 850 s^{-1}.

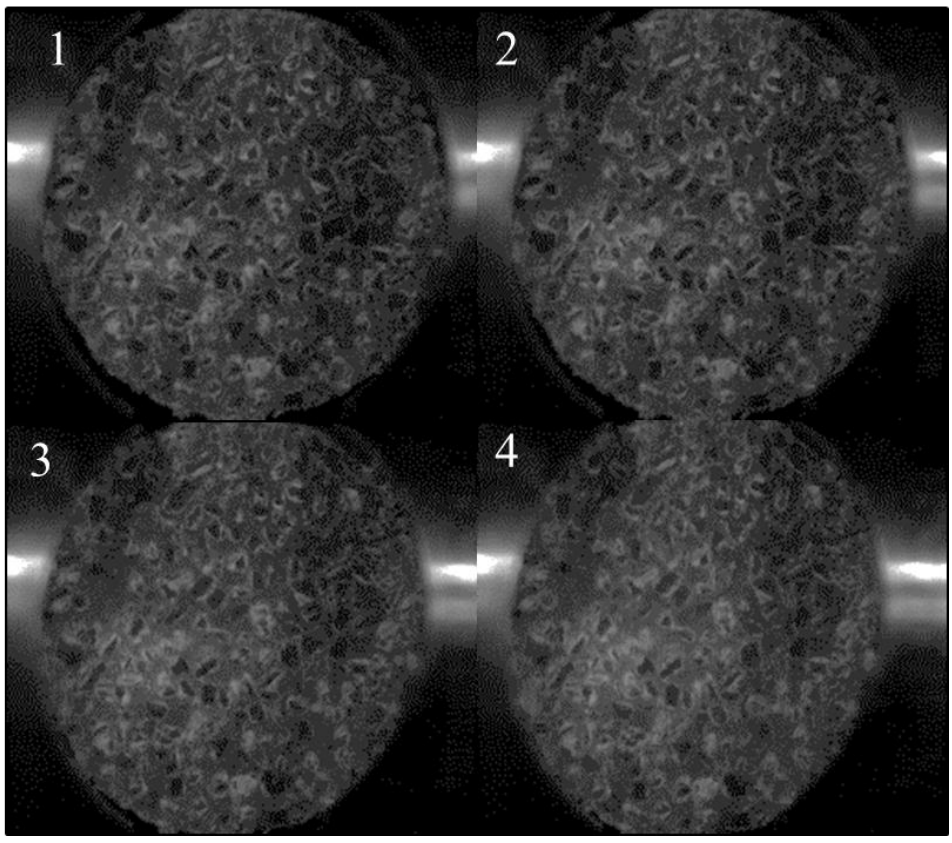


Figure 7-21: High speed photographs of PBS at of 850 s^{-1} corresponding to figure 7-20.

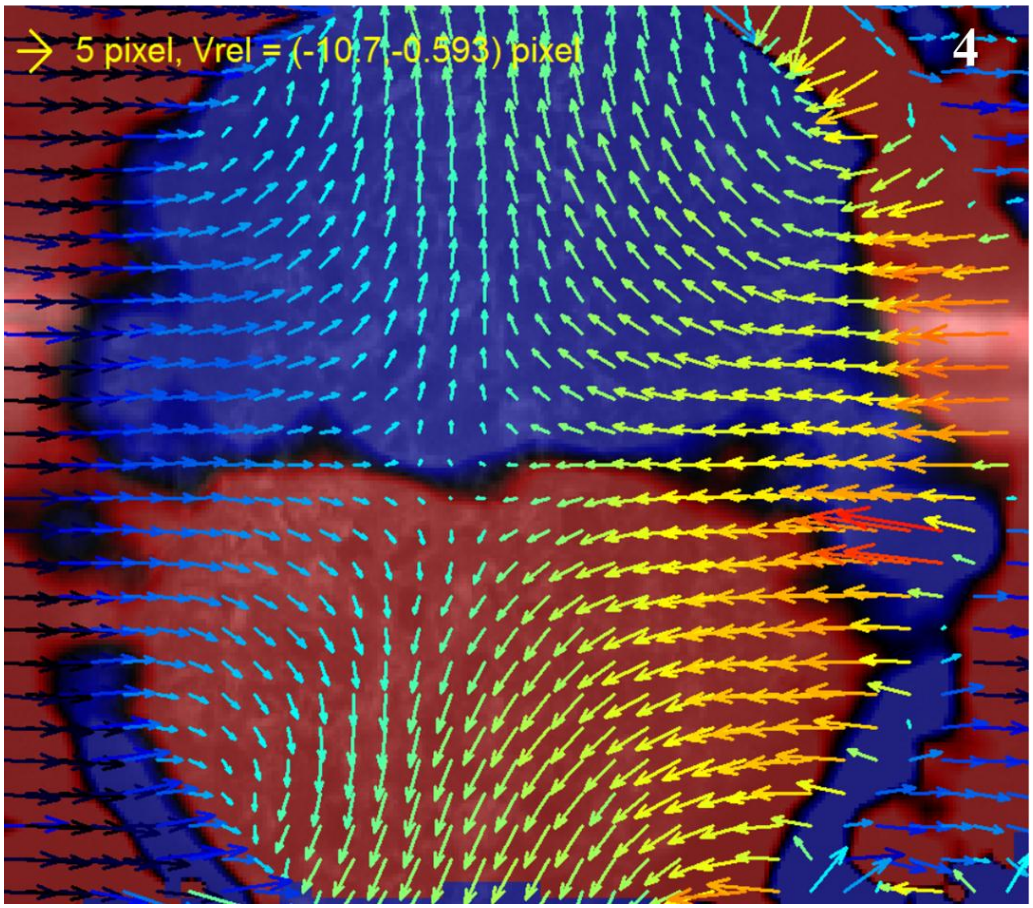


Figure 7-22: Dynamic photograph at approximately 7% strain with the associated DIC displacement vectors, whose coloration depending on the magnitude and direction of the vector. This image corresponds to the 850 s^{-1} true stress-true strain behavior presented in figure 7-20.

7.3.5 Predicting High Rate Composite Behavior in Tension

Using the experimental data from this investigation, the experimental simulation method described in Chapter 5 is extended to capture the PBSs high rate behavior in compression and tension. It should be noted that the theoretical temperature rises in these experiments are of the order 1 K, so no temperature rises were implemented.

The experimental simulation method was applied to predict the high rate true-stress and true-strain behavior in compression and tension, up to the final true strains in the high rate experiments (20% in compression; less than 10% in tension). In compression, the result of simulating the response at 1250 s^{-1} response is presented in figure 7-23. This rate was chosen because the influence of the α transition is readily observed. As seen in the figure, the simulation captures the high rate behavior extraordinarily well.

The simulation method applied to tension is summarized in figure 7-24. There is a clear drop in yield between tension data versus compression data to nearly a quarter of the value (approximately 12 MPa in compression versus 3 MPa in tension). It was noted that high rate data in compression and in tension of PBS were available at strain rates very close to one another (~10^3 s^{-1}), at which both saw the same effects of the α transition shifting to room temperature. This behavior was supported by the DMTA behavior where a shift factor for PBS was calculated at 10 °C / decade strain rate, and the effects of the glass transition were seen to begin between -40 °C and -50 °C at the relevant test rate (0.032 s^{-1}). In result, the same test temperature for simulation in compression, -45 °C, was used to predict 850 s^{-1} behavior in tension. As in the compression experiments, exceptionally good agreement between simulation and experiment was observed. The slight yielding in both results of ~3% true strain are understood to be mixtures of effects of debonding and yielding of the PBS.

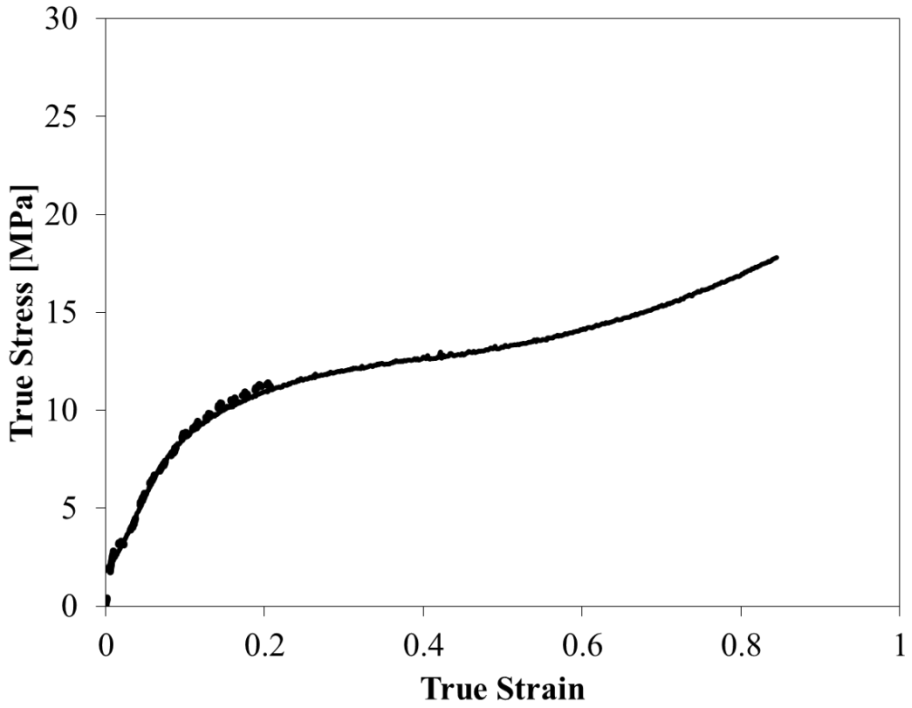


Figure 7-23: PBS true stress-true strain behavior in uniaxial compression at 1250 s^{-1} at 20 °C: experiment (dashed line) and experimental simulation model (solid line) which was conducted at -45 °C.

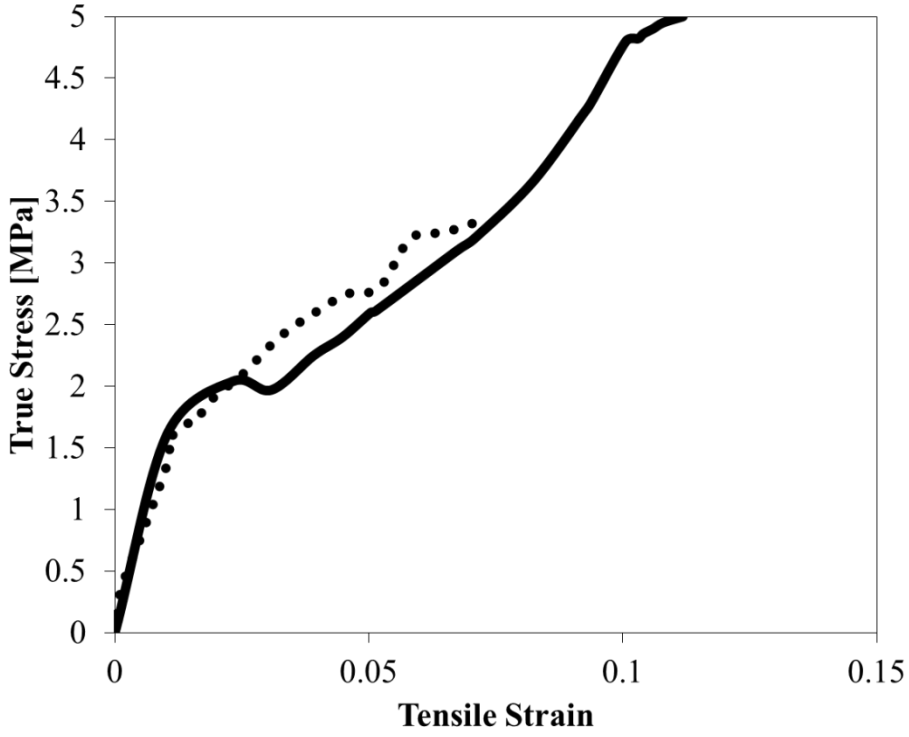


Figure 7-24: PBS true stress-true strain behavior in tension at 850 s^{-1} at 20 °C: experiment (dotted line) and experimental simulation model (solid line) which was conducted in tension at -45 °C.

By using -45 °C for the simulation-temperature, the α transition is seen in the same rate and temperature dependent location, regardless of testing in compression or tension. Lastly, as displayed in figure 7-24, the simulation method presents a very exciting result: the simulation method is shown to predict the high rate behavior of a polymer bonded explosive simulant in tension, as well as previously in compression. These results in several ways capture the objective of this thesis: to predict the high rate behavior of difficult-to-characterize materials (e.g. composites, in this case a composite using a binder with a very low T_g) via low rate deformation in order to allow for the use of micro-scale imaging tools (e.g. scanning electron microscopes (SEM) and X-ray tomography) to study and better understand these materials' high rate behavior. In the next section, a low rate Brazilian test of PBS, at -30 °C, is conducted inside an ESEM in order to better demonstrate opportunities in using the simulation method in accompaniment with ESEM-scale imaging for greater detail in high rate analysis.

ESEM In-Situ Analysis

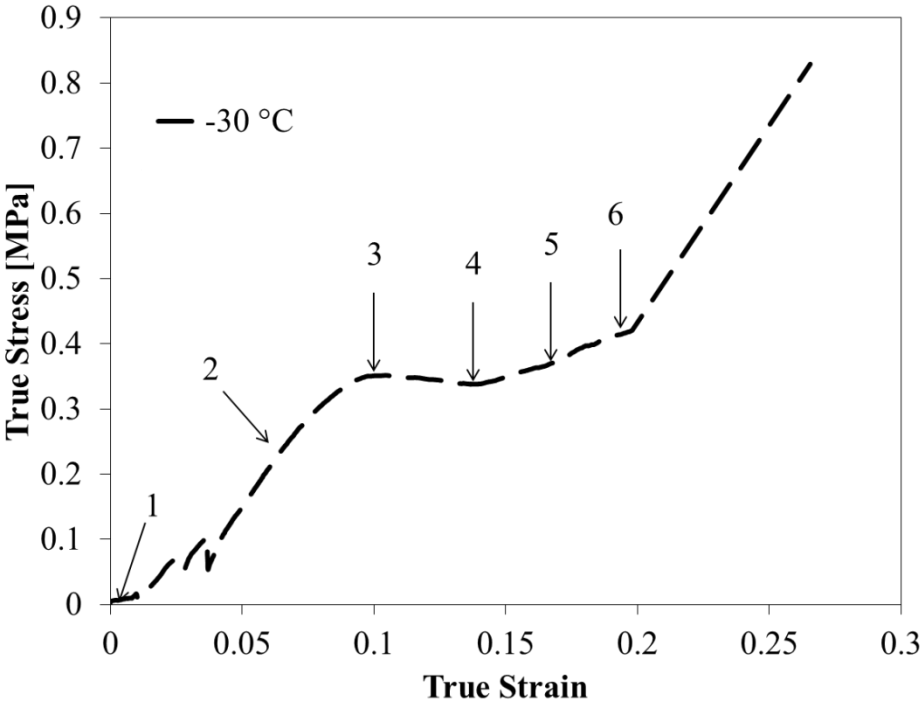


Figure 7-25: PBS true stress-true strain behavior in tension at -30 °C and a tensile strain rate of ~10^{-2} s^{-1}.

Additional testing was conducted on an Environmental Scanning Electron Microscope (ESEM) in order to present the capabilities of in-situ ESEM imaging which may readily be applied to the high rate simulation method presented in this thesis with the correct in-situ temperature control apparatus. The true stress-true strain behavior in tension at -30 °C (figure 7-25) demonstrates similar glassy behavior to that observed in compression below the glass transition, where the overall behavior is glassy but the yield and modulus are much smaller when compared to materials at, or lower in temperature to, the glass transition. This behavior is accompanied by ESEM photographs (figure 7-26) where a highlighted area is shown to debond during yield. At this point in testing, upon reaching -30 °C, the temperature stage in the ESEM was not capable of achieving the temperatures required to simulate the high rate behavior (-46 °C) and, therefore, the application of the simulation method was moved to the

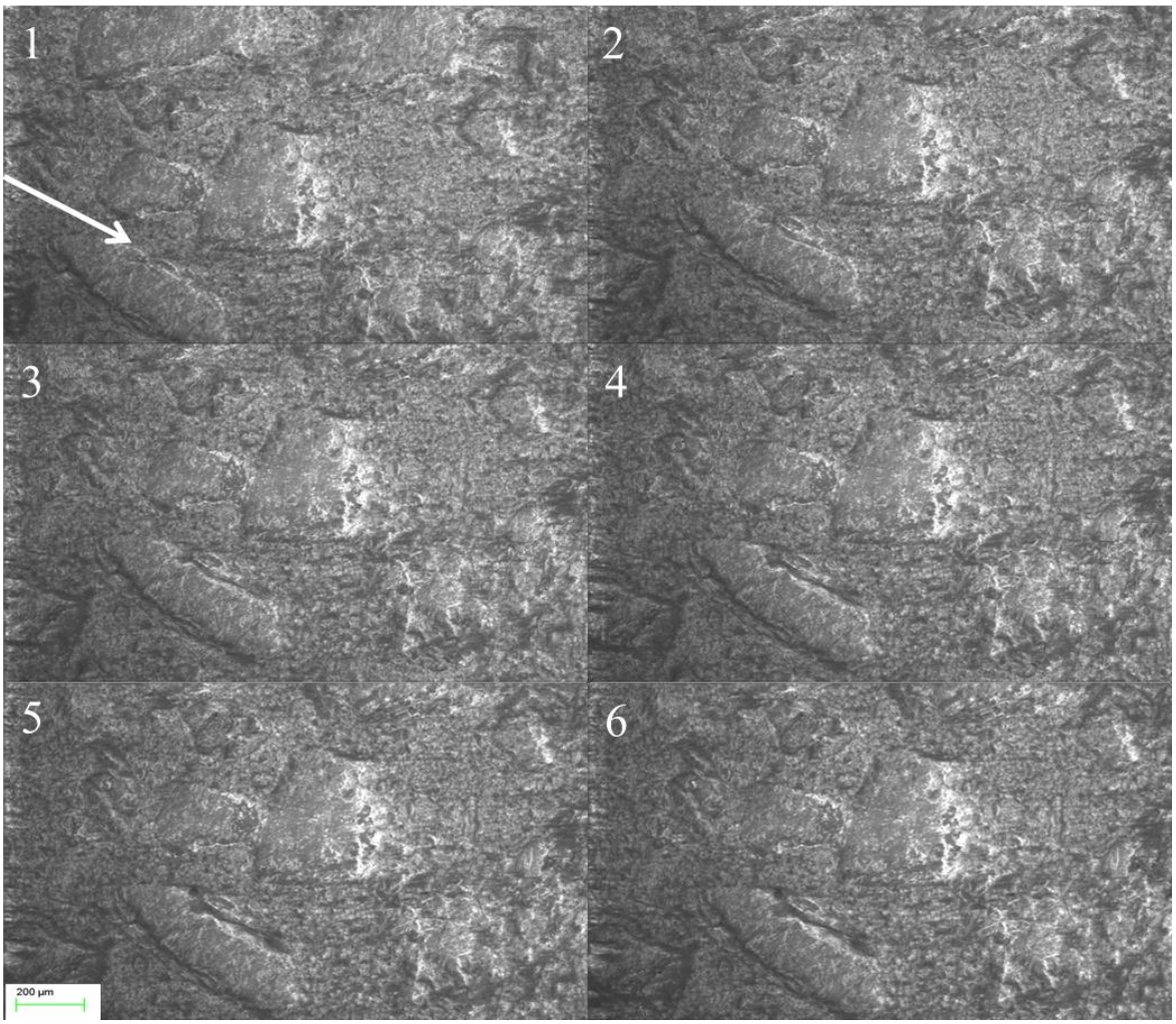


Figure 7-26: ESEM photographs of PBS at -30 °C corresponding to figure 7-25. The white arrow in frame 1 is a highlighted area of interest for these photographs: this region demonstrates the debonding which occurs during the yield of PBS. The debonding appears to gradually increase in each photo, with complete debonding between crystal and matrix seen in the last image, 6. Note: These photos were taken at the center of the test specimen.

quasi-static test machine with temperature chamber (made by Instron) in order to show that the bulk high rate behavior can be replicated in low rate experiments.

7.4 Conclusions

The temperature- and rate-dependent behavior of HTPB and PBS were studied via DMTA, compression, and tension testing using the Brazilian test method. From these investigations a novel piezoelectric (using PZT) SHPB strain measurement system was developed for testing soft materials at high rates of deformation. This piezoelectric method allowed for a large amount of experimental data to be accrued on a much more rubbery HTPB material, compared to those found in literature, at high rates. In addition to this, a new test method was learnt and applied to PBS, in order to study composites in tension at high rates. High rate deformation in tension was presented with photographs taken from a high speed camera, and also with DIC software analysis in demonstrating relevant displacements. ESEM photographs during low temperature testing at quasi-static rates were also presented to demonstrate the micro-scale debonding which occurs in PBS, while also illustrating the capability of using the simulation method in accompaniment with ESEM-scale imaging for greater detail in high rate analysis. In addition to this, the simulation method presented in Chapter 5 of this thesis was applied successfully to capture compression behavior and predict tension behavior at high rates of strain.

Chapter 8

Constitutive Modeling

Constitutive models aim to fully identify and predict how independent variables, such as stress, stress state, strain rate, strain, and temperature, fundamentally affect the mechanical behavior of a material (Buckley & Jones, 1995 and Gray III, 2000). A constitutive model is required to describe and predict the thermoplastic material response with respect to the effects of strain rate, temperature, and pressure. As stated by Shergold (2006), constitutive analyses of solids are often based upon a phenomenological or micromechanical approach. Within the current research, in order to fulfill the aim of predicting and simulating high rate response from low rate data, several models and interpretations have been studied in order to better develop and adopt a modeling approach for both rubbery and glassy polymers. The aim is to find an accurate and scientifically backed model that allows us to span the required strain rate and temperature regimes. Here constitutive models are reviewed and appropriate models are applied to PVC data and each of the PPVCs (PPVC-2, 4, & 6) data reported in Chapter 3.

8.1 Introduction to Processes in Polymers

8.1.1 Structural makeup

There is a wide range of classic literature which describes the material processes of polymers (e.g. Hill, 1950; Mark, 1999; Bicerano, 2002). Polymers are long chain macro-molecules made up of a series of repeating molecular units known as monomers. Most polymers have carbon backbones held together by strong covalent bonds within the chain, with individual chains typically being linked through secondary bonds such as van der Waals forces and hydrogen bonds. Molecular dipoles along a polymer chain construct the secondary bonds which hold together neighboring macromolecules that make up the polymer and determine a number of characteristics often involved in β-processes (e.g. high rate/low temperature elastic moduli and yield strength). Differences in bond strengths account for some of the differences between glassy and rubbery polymers; secondary bonds are often the cause of this, as these bonds are much weaker than primary bonds, which allow for lower melting temperatures, strength, and stiffness. Rubbery polymers often have the ability to undergo large and reversible elastic deformation. Additionally, incorporating plasticizers into polymers results in a reduction in viscosity and thus suggests an increase in local free volume[13] of the polymer (Mulliken & Boyce, 2006). Furthermore, polymers generally have very low coordination numbers compared to most glasses, ceramics, metals and intermetallics (Bicerano, 2002), which contributes to their low densities. Their low density is also a result of mostly consisting of light atoms such as carbon and hydrogen. In practical applications, polymers are typically poor thermal conductors and good electrical insulators because of the contained nature of their electrons.

[13] Commonly referred to as 'excluded volume' (Hill, 1986) which explains that two parts of a polymer chain cannot occupy the same space. Cases such as these ensure a polymer chain is additionally spaced apart compared to if no free volume existed.

Many thermoplastics have both amorphous regions and crystalline regions, depending on their degree of long-range three-dimensional order. Increasing crystallinity often leads to an increase in stiffness, yield strength, and tensile strength. Commonly, polymers are structurally amorphous in that they consist of a random arrangement of molecules, analogous to an entanglement, such as the thermoplastic tested here, poly(vinyl chloride) (PVC) (Matthews, 1996).

8.1.2 Glass (α) and β transitions

The glass transition is understood in polymers as the temperature range below which the cross-links (or secondary bonds, e.g. Van der Waal forces) occurring along the covalently bonded carbon chain are very stiff and contribute a large amount to the overall deformation response of the material (but contribute little to none of the overall modulus or stiffness). In most cases, this response includes the onset of microscopically visible non-uniform deformation zones, and often, the brittle facture of specimens. Above this temperature, the secondary bonds break apart (or melt if the temperature is high enough) – the material performs much how a rubber would respond (at room temperature and above) and the chains now slip over each other in areas where there are no cross-linked bonds (Ashby and Jones, 2005). Namely, this temperature range above the glass transition consists of the onset of permanent deformation due to the cooperative motions of sizable chain segments (Bicerano, 2002).

Amorphous[14] polymers are normally used near or below their glass transition temperature (T_g) in practical uses. Above the T_g the elastic modulus quickly decreases and creep effects are more pronounced, whereas below the T_g, amorphous polymers tend to be brittle and glassy (Weaver, 2000). Rubbery polymers have glass transitions below room

[14] After being cooled down from the melt, polymers form a disordered structure called the amorphous state.

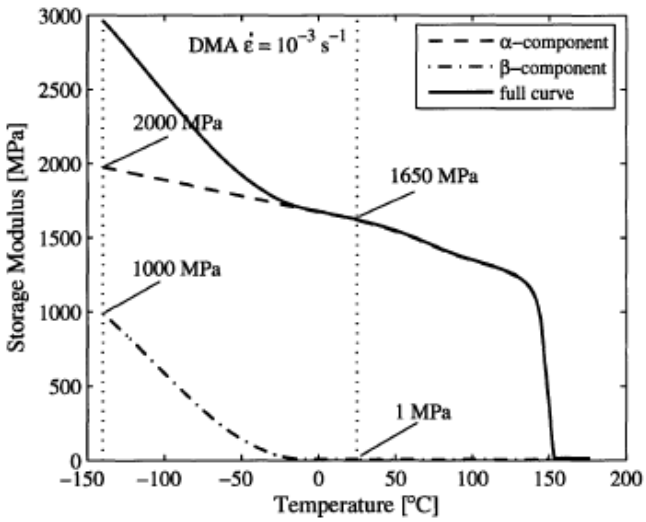


Figure 8-1: PC storage modulus components as a function of temperature. Vertical dashed lines mark the lowest temperature achieved in experiments (-140 °C) and room temperature (25 °C). (Mulliken, 2006).

temperature, which can be seen by lowering the temperature of the surroundings or increasing the rate of deformation of the material. Rubber-like polymers have a relatively low modulus at room temperature, while glass-like polymers have a high modulus at room temperature (Ward, 2004). These two types of polymer behavior depend on their current temperature with respect to their material-dependent and test-rate-dependent glass-rubber transition temperature.

As an example the temperature dependence of the storage modulus of PC is displayed in figure 8-1. The glass (α) transition is at approximately 115 °C, through which the storage modulus drops off by three orders of magnitude. The accepted analysis of the α-transition in a glassy polymer such as PC, is that the transition is associated with restricted rotations and translations of large segments of polymer main chains. The secondary viscoelastic transition (β-transition) is centered around -95 °C, which is clearly presented in the storage modulus versus temperature plot because of its considerable distance from the temperature of the α-transition peak. The molecular origins of the β-transition are not fully established (Jho & Yee, 1991; Xian & Yee, 1992; Floudas et al., 1993; Monnerie et al., 2005) but is generally

agreed that the restricted rotation of bulky side chain groups (e.g. phenyl rings and ester side groups) cause the increase in strength at low temperature or high strain rates; while at higher temperatures or lower strain rates the β motions are associated with cooperative intermolecular motion of the side groups and the main-chain units (Heijboer, 1964).

8.1.3 Relation between microstructure and macroscopic response

The relation between microstructure of polymers and their macroscopic constitutive response is theoretically understood, but has yet to be modeled to the point of prediction. The visco-elastic nature of amorphous rubbers comes from the mobility of the polymer chain, being rotations between molecular units on the atomic scale, or straightening of the chain between cross-links on the macroscopic scale (Ferry, 1970). Under applied stresses, polymer chains slide over one another and failure occurs by the separation or stretching or disentanglement of chains as opposed to breaking bonds along the main polymer chain. Many polymers have bulky side groups on their chains that alter alignment and inhibit inter-chain sliding (Weaver, 2000). Polymer sensitivity to, and dependence upon, strain rate depends on the timescale necessary for the mentioned chain re-orientations to occur. At low rates of strain the polymer chains have enough time to re-orientate themselves and the storage modulus is low. Contrasting this, at high rates of strain the polymer chain is limited to a believed bending and stretching of the chemical bonds, making the storage modulus of the polymer high and increasing by up to three orders of magnitude. Restriction of chain mobility at high strain rate is analogous to a rubbery polymer being cooled below its glass transition temperature, while greater chain motion at low rates is analogous to a polymer above its T_g, as seen in the DMTA data in figure 8-1. Crystallization of a polymer may also restrict chain motion and thus the constitutive behavior of a semi-crystalline polymer is mainly unaffected by strain rate (Bicerano, 2002). These restrictions which can be seen both at low temperatures and higher rates (or a lack of restrictions at low rates and high temperatures) in polymers

have been attempted to be modeled numerous times, and possibly the most familiar is the Williams-Landel-Ferry (WLF) formula which has been very effective in extrapolating small-strain deformations for a modest temperature range of T_g to T_g +100 °C in several amorphous polymers with hardly any or no changes to the coefficients in the model (Williams, Landel, and Ferry, 1955). Unfortunately, the WLF formula cannot capture the time-dependence of semi-crystalline polymers (which are similar to amorphous polymers) using the constants (Shergold, 2006), intended to be universal, which were obtained previously by William, Landel, and Ferry. In addition, viscoelastic studies such as these are limited to the low strain regime and have difficulty in predicting large strain deformations.

8.2 Rubber Elastic Materials

8.2.1 Introduction to Modeling of Rubbery Polymers

In literature, there is a small but well-established amount of research on the modeling of rubbers. A number of studies describe stress-strain phenomena by a set of parameters, and also plot relevant features of deformation as functions of temperature and strain rate. Often researchers plot data in order to better elucidate the strain rate and temperature effects on material properties, such as, the rapid increase in rate dependence at high rates as result of a shift in the glass transition and/or beta transition(s) to the test temperature.

Several phenomenological invariant-based models of rubber and soft material deformation with perspectives and have been developed by a number of researchers, e.g. Mooney (1940 & 1948), Treloar (1946), Rivlin (1948), Valanis and Landel (1967), Ogden (1972), Treloar (1979), Arruda and Boyce (1993), Wang and Arruda (2001), and Shim et al. (2004). The first statistical mechanics approach to describing the force on a deforming polymeric network assumed Gaussian statistics, that is, the chains never approached their fully extended length $r_L = lN$, where N is the number of statistical links of length l in the chain

between chemical crosslinks (Arruda & Boyce, 1993; Treloar, 1975), although several researchers have built networks from chain statistics to allow larger stretches than those allowed by Gaussian statistics. Gaussian statistics yields:

$$W = \frac{1}{2} G(\lambda_1^2 + \lambda_2^2 + \lambda_3^2 - 3),\ G = dk_B T \tag{8.1}$$

for the strain energy, W (also referred to as the 'entropic back stress' in other texts, e.g. Mulliken, 2006), where the λ_i are the principal stretch ratios (in a Cartesian reference frame) and the rubbery modulus G is a function of the chain density, d, Boltzmann's constant, k_B, and temperature, T. For an isotropic elastic solid, the strain energy depends on the strain only through the principal stretches λ_1, λ_2, and λ_3 relative to a "ground state" (where $\lambda_1\lambda_2\lambda_3 = 1$ because the volume of the material is constant) (Ogden, 1972). The mathematically refined approach by Ogden (1972) proposes for the strain energy function:

$$W = \sum_n \frac{\mu_n}{\alpha_n} (\lambda_1^{\alpha_n} + \lambda_2^{\alpha_n} + \lambda_3^{\alpha_n} - 3),\ G = \frac{2\mu}{\alpha} \tag{8.2}$$

where μ_n has the interpretation of the shear modulus under infinitesimal straining and the α_n is a strain hardening exponent; both are experimentally fitted constants. His model was intended for an incompressible, isotropic, hyper-elastic solid. Arruda and Boyce (1993) have argued that Ogden's model is primarily empirical, in that it makes no attempt to link the adjustable parameters to any physical deformation mechanism; additionally that the model requires more than one experiment to obtain the number of constants required to capture the detail of deformation dependence. In their study, Arruda and Boyce created an "eight chain constitutive model" in order to describe the behavior of rubbers and account for "the three-dimensional state of deformation dependence in networked solids." The "eight-chain model" is a rubber-elasticity model where the molecular network is represented with eight centrally connected non-Gaussian chains in a unit cube. In this model the strain energy is given by:

$$W = C_R \frac{\sqrt{N}}{3} L^{-1}\left(\frac{\lambda_{chain}}{\sqrt{N}}\right)\frac{(\lambda_i)^2 - \frac{1}{3}I_1}{\lambda_{chain}} \tag{8.3}$$

where C_R is the rubbery modulus (a function of temperature), where the chain stretch, $\lambda_{chain} = r_{chain} / r_0$, is the same in each chain and reduces to a function of I_1, where $\lambda_{chain} = \sqrt{\frac{I_1}{3}}$, and I_1 is the first stretch invariant (where $I_1 = \lambda_1^2 + \lambda_2^2 + \lambda_3^2$) . Furthermore, they summarized their model as providing a basis for including other aspects of rubber behavior such as swelling, the Mullins effect[15], and temperature dependence. In Arruda and Boyce's comparison of their model to data from Treloar (1944), the model did well in uniaxial and shear data, yet did poorly in fitting biaxial data. Wang and Arruda (2001) later improved on their model on performing experiments on plasticized PVC, finding two transitions involved in the material and modeling them fairly accurately. In the one-dimensional representation, the model included a nonlinear elastic spring with a viscoelastic-viscoplastic dashpot in parallel with non-Gaussian strain hardening spring. Their model was also accurate in measuring the loading and unloading of the specimen at low rates of strain, thus including the Mullins effect. In high rate data, their model did fairly well but had a sharp transition, lacking the representative curvature of the response at high strains.

[15] The Mullins effect is commonly observed in the mechanical response of rubbers: the unloading is below the loading curve, with the reloading curve in-between in the stress-strain response. Mostly studied at low rate, however Cheng and Chen (2003) have performed experiments at high rate by reloading EPDM rubber specimens and applying the Ogden and Roxburgh model (Ogden and Roxburgh, 1999) to explain the Mullins effect at high rates.

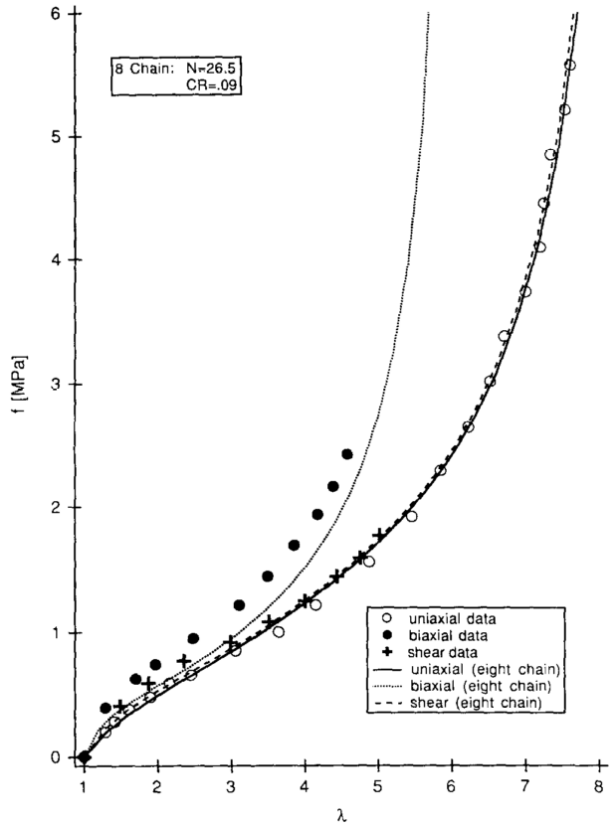


Figure 8-2: Arruda and Boyce (1993) results of simulations using their eight chain model versus data from Treloar (1955) in uniaxial extension, biaxial extension and shear.

All of these models have two physically based parameters in common: *G* the rubber modulus and λ_L the chain locking stretch, which becomes

$$\lambda_L = \frac{r_L}{r_0} = \sqrt{N} \tag{8.3}$$

where r_0 is the initial chain length given as $r_0 = l\sqrt{N}$, and r_L is the same as described earlier.

Another alternative model is the Mooney-Rivlin model, which is commonly used in describing rubber-like behavior. The Mooney-Rivlin model is presented as:

$$\varphi = C_1(\lambda_1^2 + \lambda_2^2 + \lambda_3^2 - 3) + C_2\left(\frac{1}{\lambda_1^2} + \frac{1}{\lambda_2^2} + \frac{1}{\lambda_3^2} - 3\right) \tag{8.4}$$

where φ is the strain energy density per undeformed unit volume, C_1 and C_2 are material constants (Mooney, 1940 and Rivlin, 1948). Shergold et al. (2006) (while testing pig skin

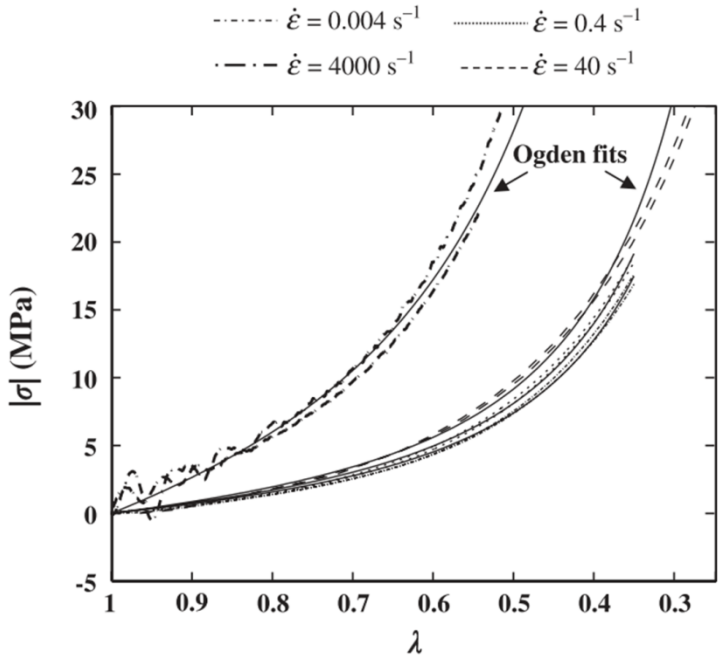


Figure 8-3: The engineering stress versus stretch ratio response of silicone rubber to uniaxial compression. (Shergold et al., 2006).

and silicone rubber) demonstrated that the Mooney-Rivlin model is inappropriate for describing rubber-like constitutive responses that have strong strain-hardening characteristics. Other studies by Jerrams et al. (1998) and Miller and Chinzei (2002) have found analogous results. Shergold et al. used a one-term Ogden model to fit data, which captured the uniaxial stress versus strain behavior of both the pig skin and the silicone rubber through a wide range of strain rates as seen in figure 8-3.

The Ogden model used by Shergold accurately described the constitutive behavior over a wide range of strain rates using only two parameters: the shear modulus μ and the strain hardening exponent α. To ensure accuracy of the shear moduli found, Shergold used large strain data in deriving the parameter, thus avoiding the often inaccurate small strain response in high rate experiments. The strain rate sensitivity was described accurately for multiple grades of silicone rubber and also for the pig skin tested (by changing the strain modulus component, μ). The model adequately described an increase in the modulus with increasing rate, while having no change in the strain hardening exponent (α) which is shown to be independent of strain rate for this material, thus validating the choice of model. The

convincing results presented by Ogden (1972) and confirmed by Shergold (2006), in addition to the relative simplicity of the mathematical formulation, encouraged application of the Ogden Model to the rubbery behavior seen in PVC, and PPVC-2, 4, & 6 in Chapter 3.

8.2.2 Results and Analysis

Using a one-term Ogden model to fit the rubbery uniaxial nominal stress versus nominal strain data[16] (please refer to chapter 3 for additional experimental information), all PVCs (PVC, PPVC-2, PPVC-4, & PPVC-6) were modeled at all temperatures (20 – 100 °C, at 10^{-2} s^{-1}), and strain rates (10^{-3} to 1 s^{-1}, at 20 °C) for PPVC-6, in which the materials showed rubbery behavior; these data are presented in the following pages in tables 8.1 and 8.2, and figures 8-4 and 8-5. The one term Ogden model, presented in equation 8.8, was manipulated to incorporate nominal stress. This model was attractive as it accurately describes the constitutive behavior of rubbery behavior in all of the materials tested. The model is as follows:

$$s_M = \frac{2\mu}{\alpha}\left(\lambda^{\alpha-1} - \lambda^{-1-\frac{\alpha}{2}}\right), G = \frac{2\mu}{\alpha} \tag{8.8}$$

where s_M is the nominal stress of the model and the stretch ratio $\lambda = l/l_0 = \exp(\varepsilon)$ and $e = \lambda + 1$ (Shergold et al., 2006). The equation is especially attractive as it only uses two parameters: the small strain modulus μ and the strain hardening exponent α. The parameters were fitted through an iterative approach implementing a least squares residual; parameters were varied both manually and automatically, via the 'Goal Seek' analysis on Excel, until the least squares residual was minimized. Having performed initial fits allowing both α and μ to vary freely, it became clear that the value of α was similar for all the materials, and the fits were

[16] These materials were fitted to nominal stress versus nominal strain data because the solution to whether a one- or two-term model is appropriate is much clearer. Take for example the PPVC-4 (figure 8-4c) 45 °C response: In true stress versus true strain an exponential response would be seen, where here we see a distinct yield at a very low strain ~1.5% - making it clear that a two-term (or 'glassy polymer') model would be more appropriate in describing the deformation response.

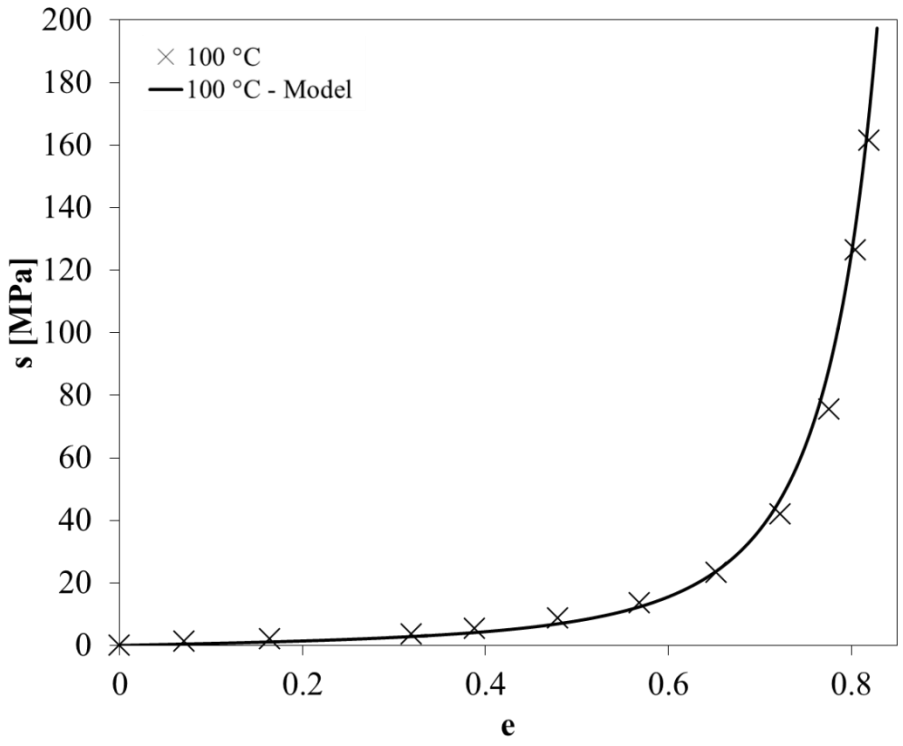
Table 8.1: Ogden model parameters used in order to capture PVC, PPVC-2, PPVC-4, PPVC-6 temperature dependent experimental data. T is the experimental temperature, μ is the strain modulus, α is the strain hardening constant, G is the shear modulus (described in equation 8.8).

	T [°C]	α	μ [MPa]	G [MPa]
PVC				
	100	4	1.8	0.9
PPVC-2				
	60	4	9.5	4.8
	80	4	4.5	2.3
	100	4	1.7	0.4
PPVC-4				
	45	4	7	3.5
	70	4	1.3	0.65
	100	4	0.3	0.15
PPVC-6				
	20	4	9	4.5
	40	4	7.5	3.8
	60	4	3.8	1.9
	80	4	1.2	0.6

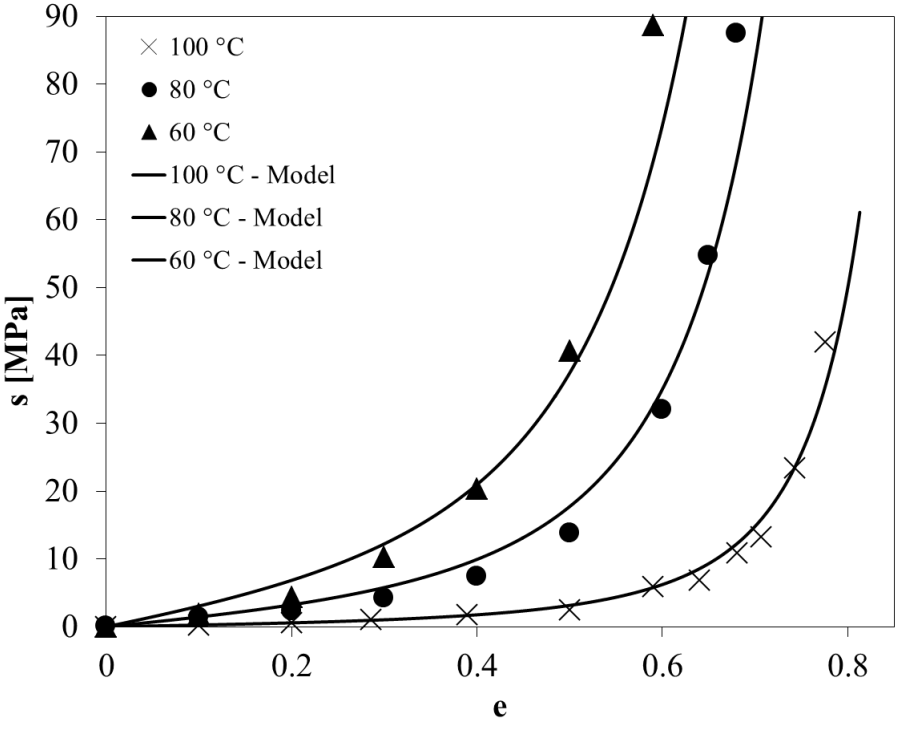
Table 8.2: Ogden model parameters used in order to capture PPVC-4 and PPVC-6 rate dependent experimental data. $\dot{\varepsilon}$ is the experimental strain rate, μ is the strain modulus, α is the strain hardening constant, G is the shear modulus (described in equation 8.8).

	$\dot{\varepsilon}$ [s^{-1}]	α	μ [MPa]	G [MPa]
PPVC-6				
	1	4	14	7
	0.1	4	13	6.5
	0.01	4	9	4.5
	0.001	4	7.3	3.7

repeated using a constant value of α = 4 (tables 8.1 and 8.2). The largest change in least squares residual resulting from this decision was 7.5%. To ensure accuracy of the shear moduli found, large strain data were used in deriving both parameters, thus avoiding the probable inaccuracy of small strain response. The rubbery behavior of the temperature dependent data (table 8.1 and figure 8-4) and the rate dependent data (table 8.2 and figure

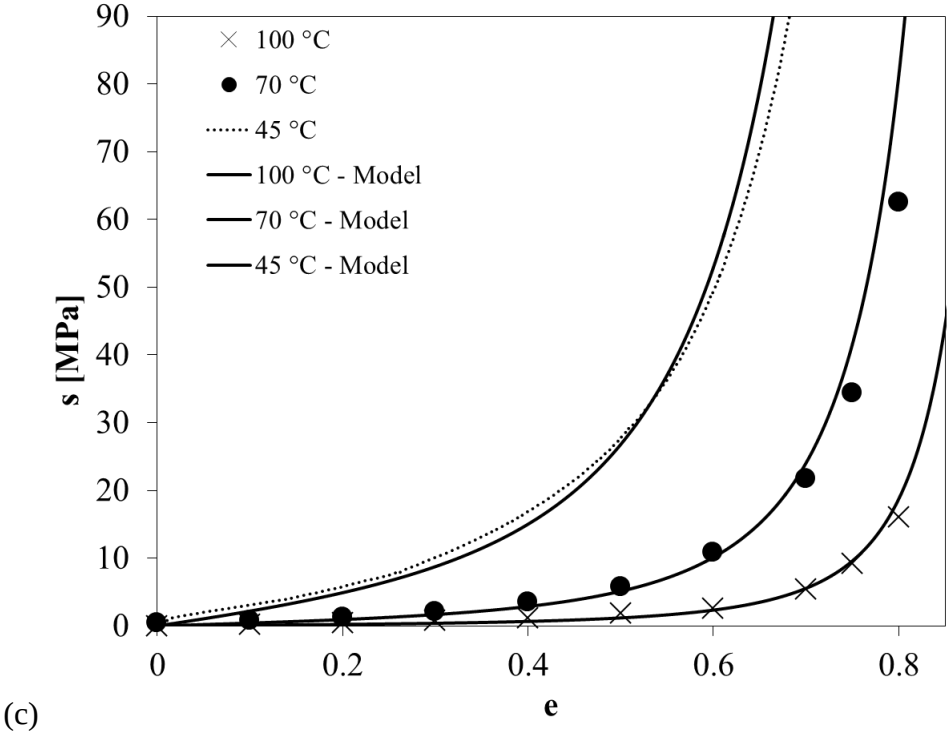


(a)

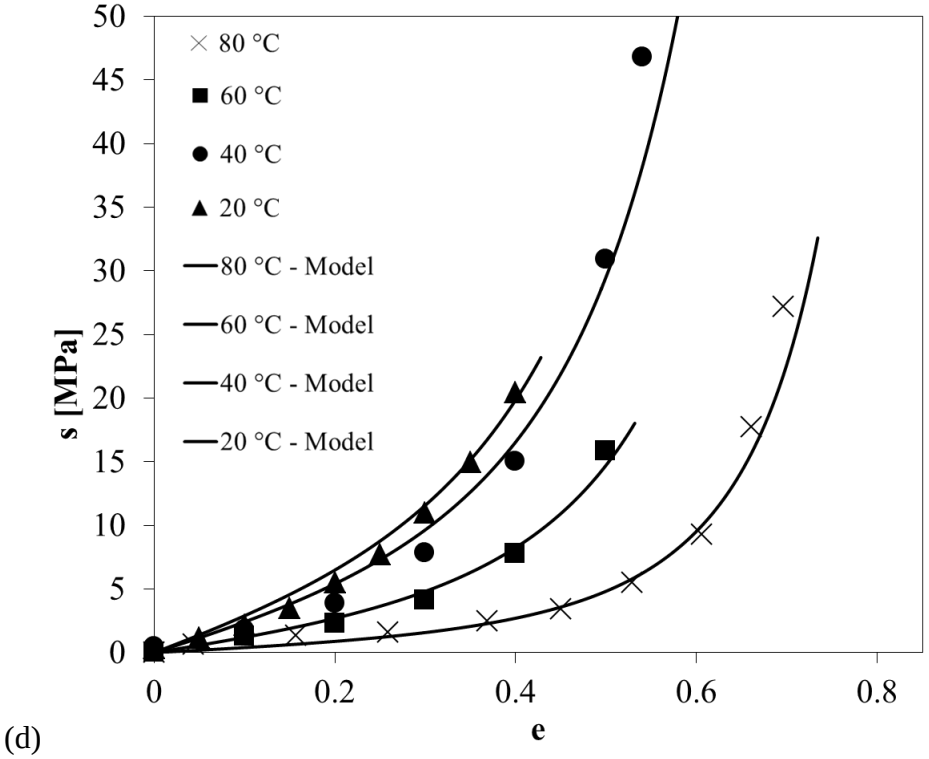


(b)

Figure 8-4: The temperature dependent nominal stress versus strain response of (a) PVC, (b) PPVC-2, (c) PPVC-4, and (d) PPVC-6 to uniaxial compression at 10^{-2} s^{-1} strain rate fit to the Ogden model.



(c)



(d)

Figure 8-4: The temperature dependent nominal stress versus strain response of (a) PVC, (b) PPVC-2, (c) PPVC-4, and (d) PPVC-6 to uniaxial compression at 10^{-2} s^{-1} strain rate fit to the Ogden model.

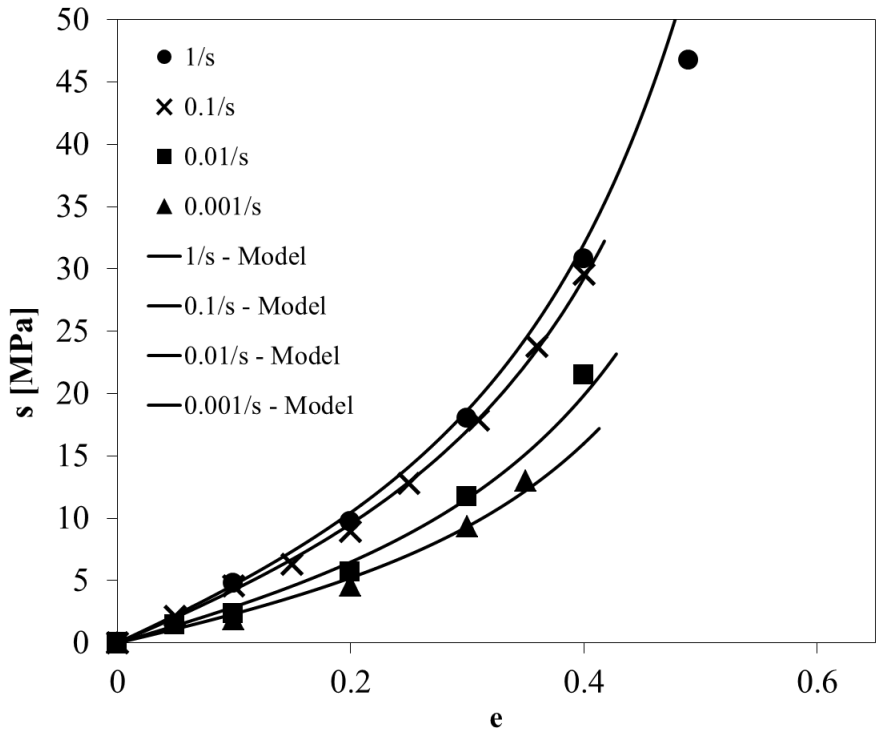
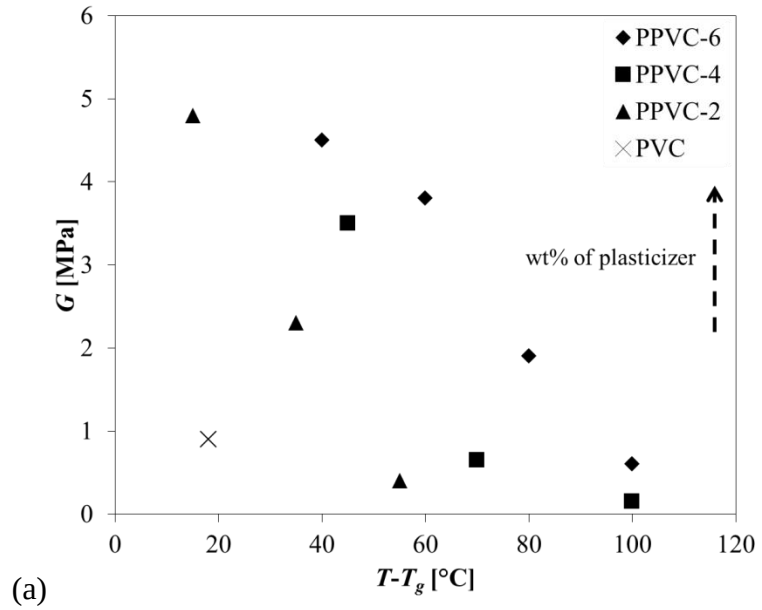


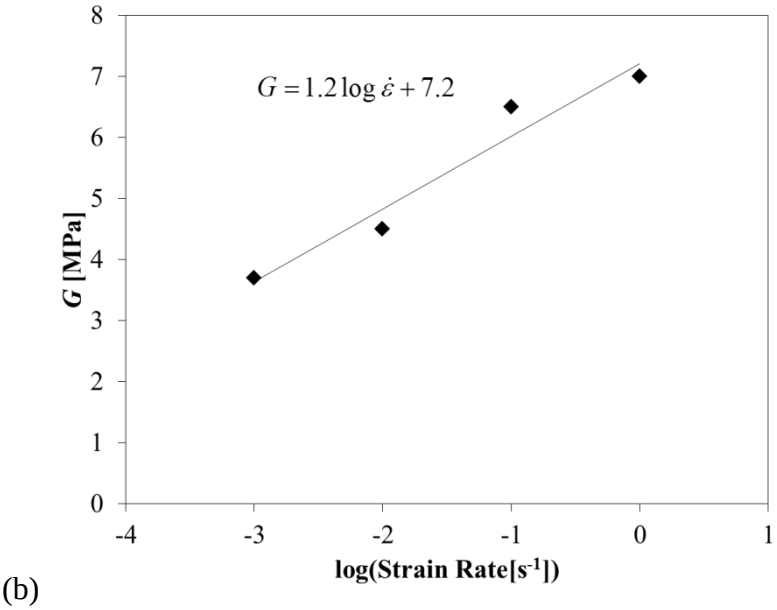
Figure 8-5: The rate dependent nominal stress versus strain response of PPVC-6 to uniaxial compression at 20 °C fit to the one-term model. Note: PPVC-2 was the only material tested which displayed rubbery behavior at room temperature or 20 °C.

8-5) were described accurately by the model for all specimens at the test temperatures (20 – 100 °C) and for PPVC-6 at test strain rates (10^{-3} to 1 s^{-1}).

As seen in table 8.1 and 8.2, and figures 8-4 and 8-5, the model adequately described an increase in the shear modulus with decreasing temperature and increasing strain rate for all PVCs tested (regardless of plasticizer content), while having no change in the strain hardening exponent α (which is thought of as independent of strain rate; Ogden, 1972) over temperature and/or strain rate or material type. These data validate the appropriateness of the model and present a clear connection between the material mechanisms controlling temperature- and rate-dependent deformation responses of PVC above T_g. Close to T_g, the shear modulus is strongly dependent on temperature, showing a gradual decrease as the temperature increases. Figure 8-6a presents the shear modulus dependence upon corrected temperature, or the amount of temperature above the glass transition temperature, for all



(a)



(b)

Figure 8-6: Shear modulus analysis (a) with respect to corrected temperature ($T - T_g$) for all PVCs and (b) with respect to log strain rate for PPVC-6. Note: the corrected temperature is equivalently the number of degrees above the glass transition temperature.

materials. Interestingly, this plot shows that with the increase of plasticizer content in PVC the shear modulus also increases (at the same corrected temperature values). Namely, when the PVCs are compared to each other at temperature values above their glass transition, it is clear that the shear modulus is much larger in the more rubbery (at ambient temperature)

polymers (PPVC-4 & PPVC-6) when compared to the glassy behaving (at ambient temperature) polymers (PVC & PPVC-2).

This data also lends insight into the changes of material properties dependent upon plasticizer – the strain hardening exponent, α, appears to be dependent upon the base polymer of PVC but independent of the amount of plasticizer. This shows that the majority of the deformation demonstrated by each material's rubbery behavior is due to the main polymer chain – the most rigid polymer chain within the polymer due to its primary bonds. These primary bonds are being compressed, and therefore stretched, to their maximum length scale to cause the strain hardening observed (plesae refer to the following paragraph for additional discussion on this topic). The strain modulus, μ, alternatively, is more challenging in its analysis. Firstly, this parameter was very dependent upon the effects of plasticizer content – decreasing by approximately 39% (or ~0.95 MPa) per 20wt% increase of plasticizer content (calculated by using each materials temperature dependent data, table 8.1 and figure 8-4). Further to this, in analyzing the rate-dependent data in figure 8-5, an average of a 22% increase in shear (or strain) modulus (or ~1 MPa) per decade of increasing strain rate was calculated.

The 45 °C response of PPVC-4 (figure 8-4c) is utilized to demonstrate the deviation from a single-term model (to a two-term model being more appropriate), and the beginning of the glass transition (where the polymer begins to yield in the temperature dependent deformation response). This transition designates the deviation from the one-term model exponential behavior which constitutes a rubbery model. Rubber models are used to describe what is referred to as the 'network back stress', 'strain energy', 'Langevin stress', or 'Langevin spring' (in rheological interpretations of constitutive models, which can be seen in the next section 8.3.1, figure 8-8). Although termed differently by several authors (Arruda et al., 1993; Mulliken et al., 2006; Jordan et al., 2008), each describes the same entropic

resistance to chain alignment in the deformation response. This is often understood as the strain-hardening seen in polymer stress-strain behavior. This process is understood as being distinct from α or β motions – which can be more readily interpreted by observing that this behavior/process is only seen alone once the tested rates and temperatures are above each polymers glass transition temperature (the reader is asked to please refer to chapter 3 for the experimental DMTA data which observes and further discusses these material transitions). The observation in the start of PPVC-4's glass transition illustrates not only the shift toward amorphous polymer behavior, but also a shift to an amorphous polymer model being more appropriate to describe the constitutive behavior. This deviation describes the change in a one-term model being more appropriate to predict and describe experimental data versus a two-term (or *n*-term) model.

8.3 Amorphous Polymers

8.3.1 Introduction to the Constitutive Modeling of Polymers

Most models for describing the deformation and yield behavior for polymers can be traced back to the activated viscosity model of Eyring (1936) and Ree and Eyring (1955), where viscous flow occurs through a process of molecules in a material overcoming a potential energy barrier by a combination of thermal and mechanical energy. Eyring's theory recognized shear stress as a driving force behind an unspecified activation process which allows polymer chains to change into new, plastically deformed configurations, and delivered a model for the shear strain rate as a function of shear stress:

$$\dot{\gamma} = \dot{\gamma}_0 \exp\left(-\frac{\Delta H}{RT}\right)\sinh\left(\frac{\Omega\tau}{RT}\right) \tag{8.4}$$

where $\dot{\gamma}_0$ is a frequency parameter, ΔH is the activation energy required for one transition, Ω is the activation volume (the result of multiplying a local activation volume and a local shear strain), and R is the universal gas constant. The model uses the variables $\dot{\gamma}, \tau$, and T, which are the shear strain rate, the shear stress, and the absolute temperature respectively. A simplification ($\sinh^{-1}(x) \simeq \ln 2x$) of equation 8.4 may be made, which gives an equation for the shear stress as a function of strain rate:

$$\frac{\tau}{T} = A\left[\ln(2C\dot{\gamma}) + \frac{\Delta H}{RT}\right] \tag{8.5}$$

and thus predicting a linear relationship between shear yield stress and the logarithm of shear strain rate. This was later re-written by Bauwens-Crowet et al. (1969) in order to express tensile yield stress σ_y as a function of strain rate:

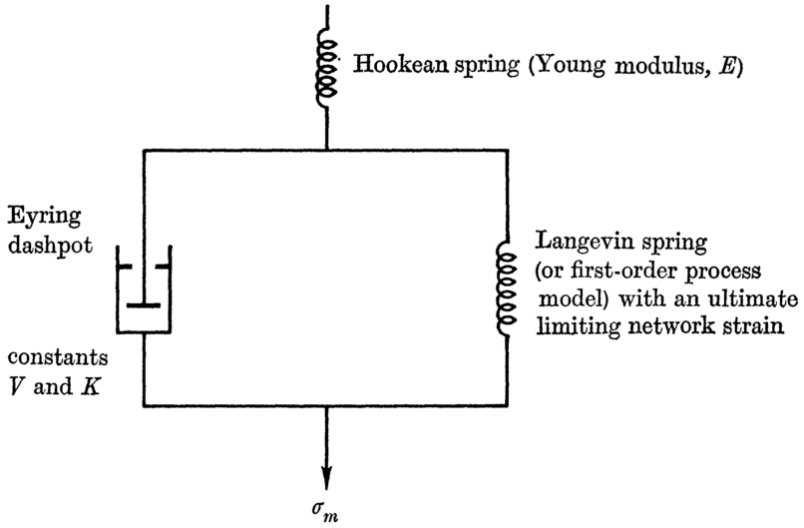


Figure 8-7: Haward and Thackray (1968) representation of their glassy polymer model which consisted of three simplified process: a constant Hookean modulus, an Eyring viscosity (a high internal viscosity), and the Langevin formula which is used to describe the elastic extension and/or compression of rubbers.

$$\frac{\sigma_y}{T} = A'\left[\ln(2C'\dot{\varepsilon}) + \frac{\Delta H}{RT}\right] \tag{8.6}$$

where A' and C' are grouped parameters (different to A and C, by a factor of $\sqrt{3}$ due to true versus shear values, in equation 8.5). These parameters are described in detail in Bauwens et al. (1969) and Bauwens-Crowet et al. (1969).

In 1968, in order to simplify stress-strain curve analysis into a small number of distinct processes, Haward and Thackray developed the commonly seen spring-dashpot representation of time dependent polymer models. Since their initial implementation of the Hookean spring, 'Eyring dashpot', and Langevin spring in this format, these components and representations are now customary in presenting polymer constitutive models (see figure 8-7).

The Eyring model, and subsequent modifications (i.e. Ree-Eyring model), were applied to modeling the yield stress of polymers in tension in studies from Bauwens-Crowet and Homès (1964) and by Roetling (1965a&b, 1966). The Ree-Eyring theory is essentially a modification to a more general form of the original Eyring theory, allowing for multiple rate-

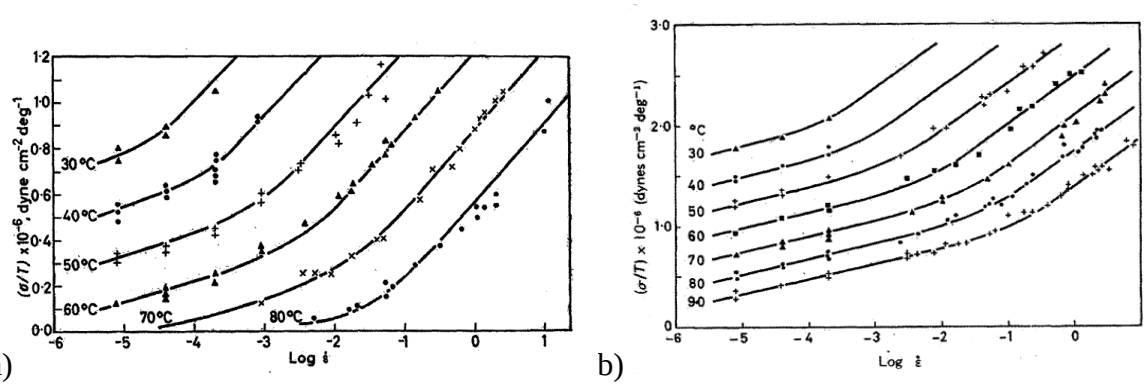
activated processes (termed α, β, γ) to be acting at once, rather than only one activated process as in the original Eyring theory. When the model is expressed in terms of polymer yield stress (equation 8.7) it is unambiguous how each process in a polymer adds another element to the yield stress (Mulliken, 2006):

$$\frac{\sigma_y}{T} = \sum_i \frac{1}{A_i} \sinh^{-1}\left[\frac{C_i \dot{\varepsilon}}{T} \exp\left(\frac{\Delta H_i}{RT}\right)\right] \tag{8.7}$$

Bauwens et al. (1969) developed a two-process version of this equation in their studies:

$$\frac{\sigma_y}{T} = \frac{\sigma_\alpha}{T} + \frac{\sigma_\beta}{T} = A_\alpha \left[\ln(2C_\alpha \dot{\varepsilon}) + \frac{\Delta H_\alpha}{RT}\right] + A_\beta \sinh^{-1}\left[C_\beta \dot{\varepsilon} \exp\left(\frac{\Delta H_\beta}{RT}\right)\right] \tag{8.8}$$

where the approximation $\sinh^{-1}(x) \cong \ln(2x)$ is made on the first term in regards to the α-process of the equation, because the α-process is considered to be in a high stress state over the entire range of interest. Under the Ree-Eyring framework, the processes of plastic flow in polymers (i.e. α, β, γ) are typically associated with particular degrees of freedom of the polymer chain. The specific polymers Roetling used in testing and modeling were poly(propylene) (PP), poly(ethyl methacrylate) PEMA, and poly(methyl methacrylate) (PMMA); PMMA was also used in the work by Bauwens-Crowet and Homès. Yield data by Roetling fit with the Ree-Eyring model for PMMA and PEMA are shown in figure 8-8a & b, indicating a good level of agreement. Roetling (1965b) fit the two-process Ree-Eyring yield model to PMMA data (figure 8-8b) by assuming that the contribution of stress by the lower energy activation process, or β-process, was negligible at the lowest strain rates and highest



a) b)

Figure 8-8 a&b: a) Roetling PEMA yield data fit with the Ree-Eyring model (Roetling, 1965a). b) Roetling PMMA yield data fit with the Ree-Eyring model (Roetling, 1965b).

temperatures, where at lower temperatures, and at higher strain rates both α and β processes required a contribution of stress for activation.

Bauwens-Crowet et al. (1969) included poly(vinyl chloride) (PVC) and polycarbonate (PC) in studying the tensile yield stress behavior and updating their model, while focusing on the two relaxation processes seen in the materials. In analyzing PC, Bauwens-Crowet (1972) found a strong correspondence between their calculated β-process activation energy and the activation energy measured by dielectric techniques (40.2 kJ mol^{-1} vs 33.5 kJ mol^{-1}). Similarly, both authors drew the conclusion that restrictions on the same molecular movements control both the increased strengthening at low temperatures and that at high rates, by observing the increased rate-sensitivity of yield, and the secondary (β) transition in the viscoelastic behavior. Bauwens-Crowet (1973) then studied the yield behavior of PMMA in compression over a wide range of temperatures and strain rates, and modeled the viscoelastic behavior with a parallel spring and dashpot combination in series with another spring. The models demonstrated yield with the transition from a glassy high elastic modulus to a viscoelastic state, which is equivalent to the thermally induced α-transition (glass transition). Inaccuracy at low yield stresses and high temperatures near T_g is a weakness in the model; this can be attributed to the use of an Arrhenius activation function (single-parameter or linear formula) for rate-temperature transformations through T_g,

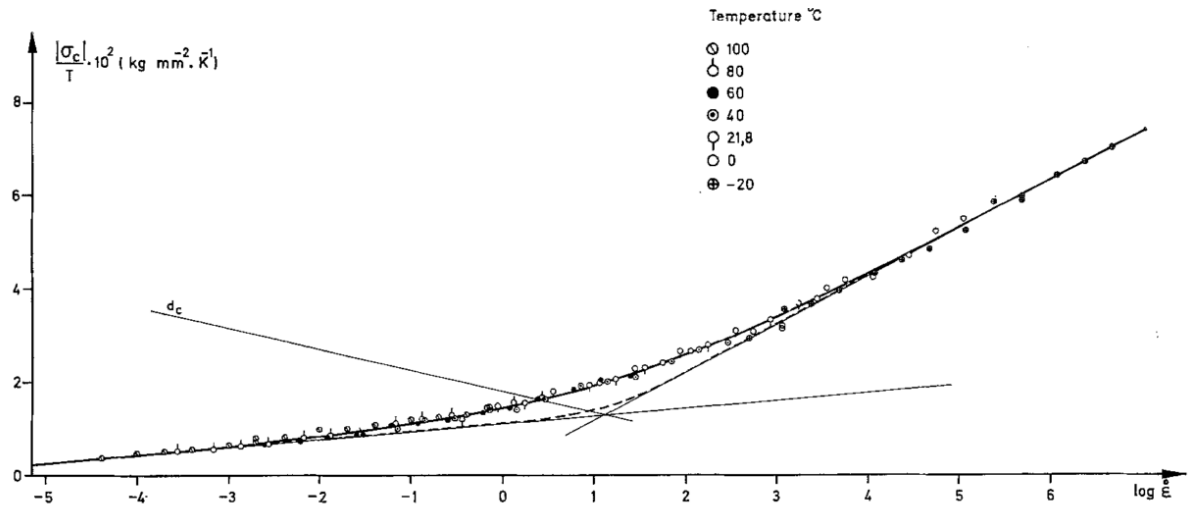


Figure 8-9: PMMA yield data as a function of temperature mapped onto strain rate yield data to create master curves at 100 °C in uniaxial compression. The dashed curve is calculated from the Ree-Eyring equation (8.8). (Bauwens-Crowet et al., 1973).

rather than the Williams-Landel-Ferry (WLF) or Vogel-Fulcher-Tammann (VFT) model (multiple-parameter and non-linear) description which covers a wider temperature range (Williams et al., 1955). The authors also created a master compression yield stress curve at 100 °C which was the first of its kind (figure 8-9). The master curve spanned strain rates ranging from 10^{-5} to 10^{6} using a time temperature superposition method; the experimental data ranged in strain rate from 10^{-4} to 10^{0} s^{-1} and temperatures ranging from -20 to 100 °C (at each rate). Lomellini in 1992 studied the differences between the two functions with polystyrene (PS), concluding that the WLF equation clearly obeyed the entire temperature range tested while no Arrhenius-like behavior was found at the highest temperatures.

In 1988, Argon and Boyce used a model based upon molecular structure of a glassy polymer while studying inelastic deformation at large strains, using restrictions on intermolecular movement to govern the deformation characteristics below yield and T_g, and entropic resistance directing the viscoelasticity above yield stress and T_g. At the time, their model was fitted to a fairly low upper strain rate limit at ~1 s^{-1}. The parameters were quantified by fitting the model to experimental data and utilizing thermodynamic relations.

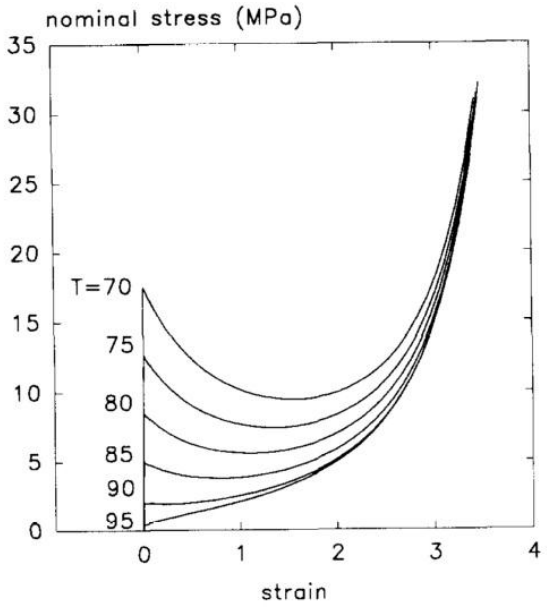


Figure 8-10: PET nominal stress versus nominal strain behavior simulated via the Buckley and Jones model over temperatures (70 to 95 °C in increments of 5 °C).

Buckley and Jones (1995), created a three-dimensional constitutive model in order to capture the characteristic behavior of amorphous polymers via simulation of glassy polymer behavior over a range of temperatures near the glass transition region (70 to 90 °C) of poly(ethylene terephthalate) (PET) under quasi-static loading (10^{-2} s^{-1}). The model describes glassy polymer behavior up to large strains, while also presenting a sharp yield region (see figure 8-10). No comparison of experimental results to the proposed model were presented in the 1995 paper, although future papers demonstrated that capturing the glassy-polymer yield behavior was not the main focus of the polymer model, but rather hot-drawing behavior, which is more associated with rubbery polymer behavior.

Zerilli and Armstrong (2007) have modeled the behavior of polymers using a "shear activation volume" and a molecular basis to make time-temperature-stress transformations, while using a large number of parallel spring-dashpot combinations to increase accuracy when compared to experimental data. These parallel combinations contribute to a large number of parameters needed for model implementation: a model such as this was less favorable when deciding upon a model for application to this thesis's research.

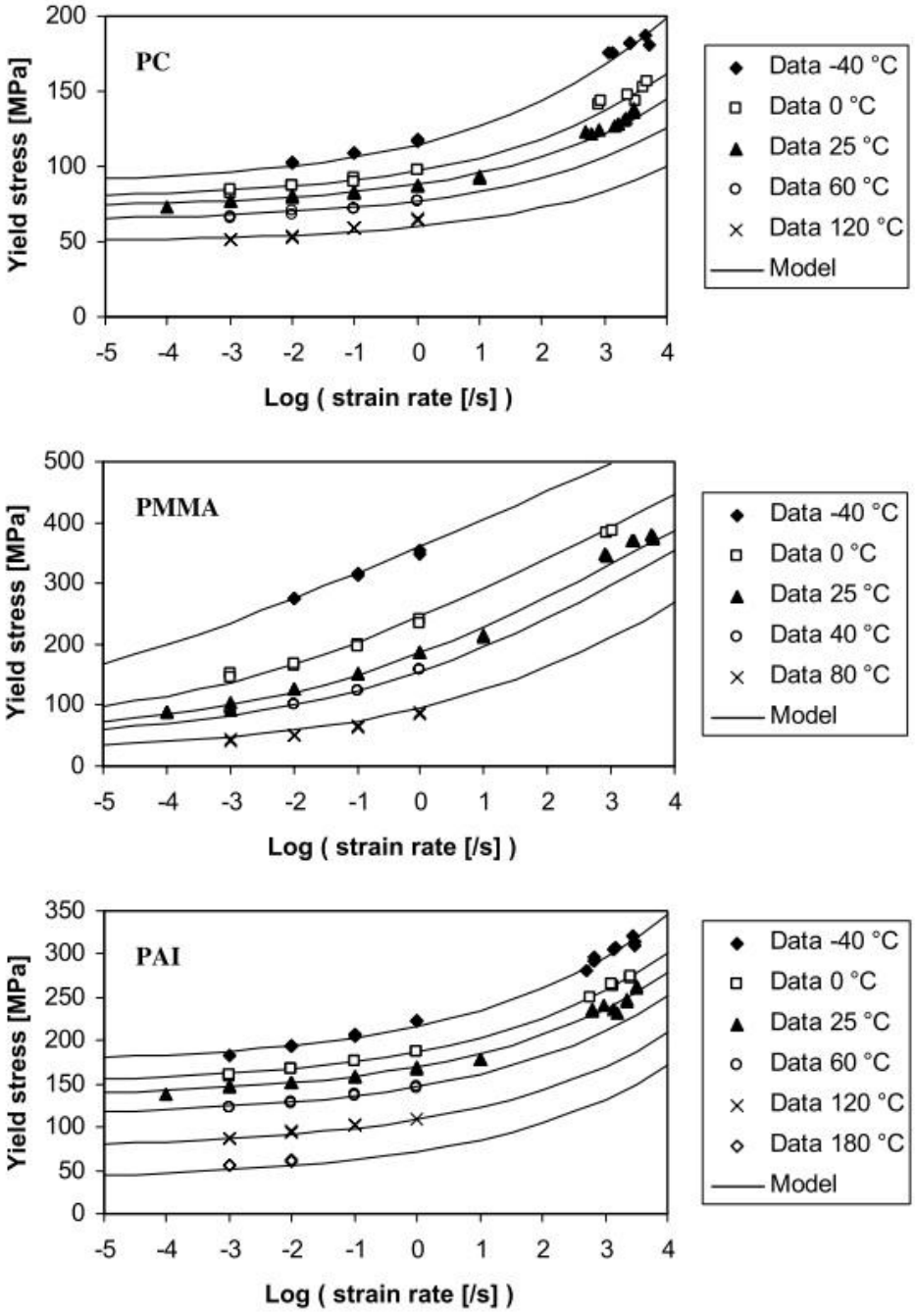


Figure 8-11: Strain rate dependence of the compression yield stress for PC, PMMA, and PAI, over a large temperature range (-40 to 180 °C). (Richeton et al., 2007).

Richeton, Ahzi, and co-workers (Richeton et al., 2005, 2006, and 2007), created a cooperative yield model which assumes that plastic flow will occur only when *n* identical chain segments simultaneously transition from one energy state to another, via stress-assisted activation, thereby requiring a cooperative relaxation motion of polymer segments (figure 8-11). Richeton et al. (2005) also incorporates the thermal history of a polymer as an internal stress, providing additional resistance to yielding. His model was able to reproduce experimental yield data on a range of polymers at high rates while using a thermodynamic approach.

Focusing on modeling high rate behavior, Mulliken and Boyce (2006) and Soong, Mulliken, Boyce, and Cohen (2006) performed compression experiments on PC, PMMA, and PVC, while modeling these polymers using a large amount of DMTA data. They showed that the rate dependence of the α-transition and β-transition loss modulus peaks and storage modulus curve can be used to model the shifts in modulus and yield as a function of temperature and rate (also shown by Siviour et al., 2005, see section 2.4). In the phenomenological one-dimensional approach in their model, they employed a pair of parallel springs and dashpots to demonstrate the α- and β-processes and a nonlinear parallel spring for the limiting elastic behavior (figure 8-12). The model again assumes that there are multiple rate-activated processes involved in yield, and that each of these processes is associated with a unique molecular motion of a specific length scale. In contrast to the Richeton-Ahzi cooperative model, the Mulliken-Boyce model "never assumes that the molecular motions of these processes are not cooperative, only that they are distinct and that they are restricted under unique rate, temperature, and pressure conditions" (Mulliken thesis, 2006). Publications for both models (Richeton-Ahzi and Mulliken-Boyce) have demonstrated an ability to describe the rate- and temperature-dependent yield behavior of various polymers in

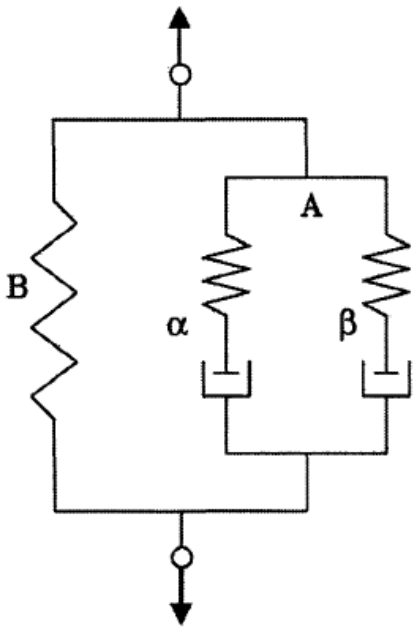


Figure 8-12: A one-dimensional rheological interpretation of the Mulliken-Boyce constitutive model for rate-dependent thermoplastic behavior. (Mulliken et al., 2006).

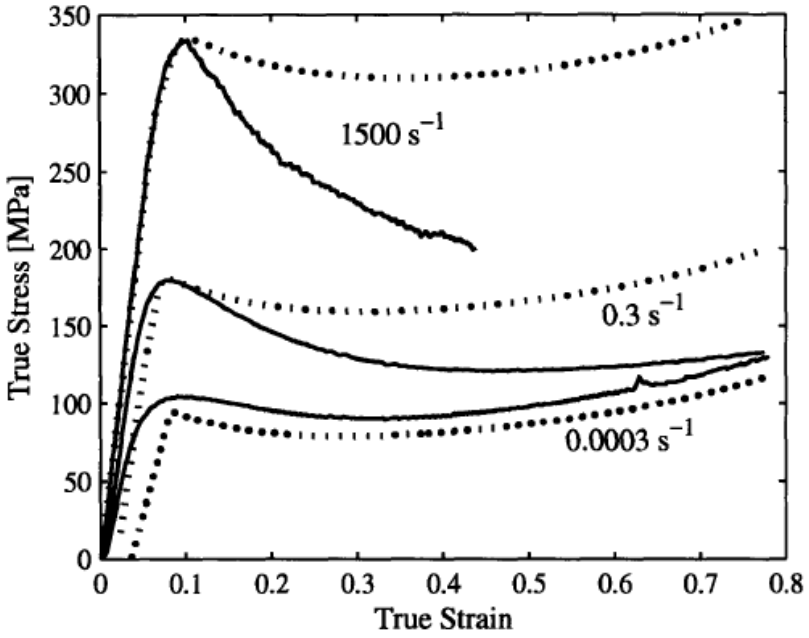
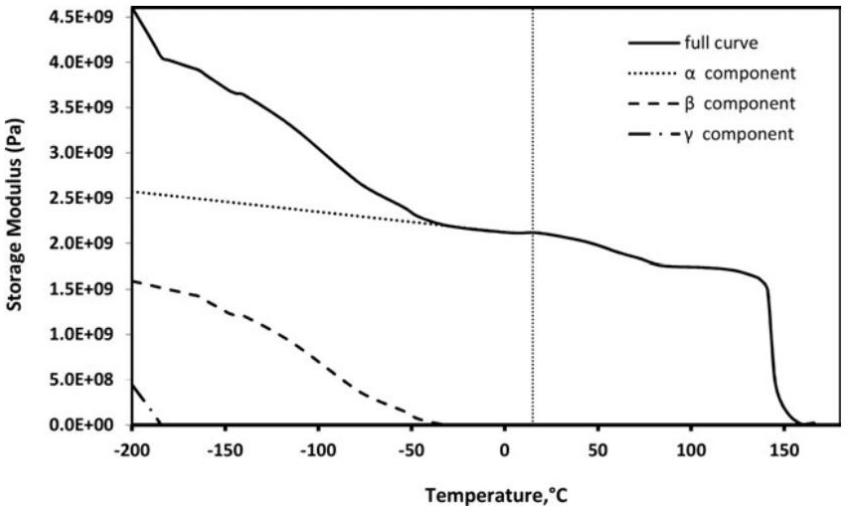
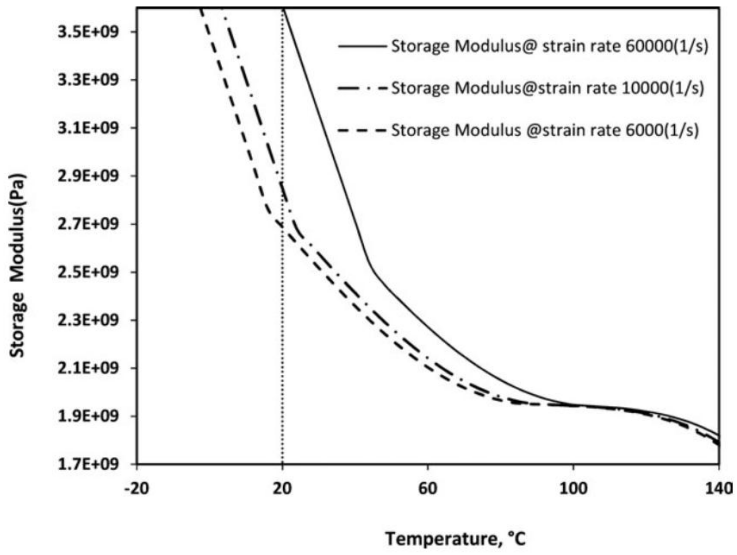


Figure 8-13: PMMA true stress-true strain behavior in uniaxial compression at low, moderate, and high strain rates: model prediction (dashed lines) and experiment (solid lines). (Mulliken et al., 2006)



(a)



(b)

Figure 8-14: (a) PC experimental DMTA storage modulus curve separated into α, β, and γ components. (b)DMTA data reconstructed in order to capture material transitions, in this case the beginning of PC's γ transition, being shifted to room temperature at rates 6000, 10000, and 60000 s^{-1}. (Safari et al., 2013).

engineering applications, garnering similar accuracy in results, yet the foundations and mathematical formulations are distinct. The Mulliken-Boyce model has gathered a large amount of attention (Jordan et al., 2008; Porter and Gould, 2009; Shim and Mohr, 2009), yet has had difficulties in modeling the distributed nature and curvature of yield in polymers as illustrated in figure 8-13 (note the sharp yield behavior of the model which is most apparent at 0.0003 s^{-1}).

Recently, Safari and coauthors (2013) used experimental SHPB data and DMTA data, spanning a wide range of temperatures from -200 °C to just over 150 °C, to create a constitutive model which was broken up into three rate-activated processes (α, β, and γ), rather than the commonly seen two component constitutive model (α and β processes). Safari used Boyce and coauthors (2000) previous work in three-dimensional constitutive modeling of glassy polymers to form the basis of their work resulting in similar model versus experimental results to Boyce's previous work. Interestingly, the authors were also able to confirm influences from the γ rate activated process at ~6000 s^{-1} from a Deconstruct Shift Reconstruct (DSR) method, also developed by Boyce and other authors (2006). The method involves shifting each of the transitions to reconstruct a DMTA curve at 6000 s^{-1}, where the beginning of the γ transition is seen at room temperature, as presented in figure 8-14. The γ transition of PC, which occurs at extremely low temperatures (approximately -190 to -220 °C, at 1 Hz – see in the authors' experimental DMTA data), or equivalently high strain rates exceeding 10^5 s^{-1}, is unlikely to occur in most applications, making the investigation largely academic. Strain rates surpassing 10^5 s^{-1} must also take into account compressibility and shock wave phenomena, and thus a revision of the model would be necessary to be scientifically accurate in predicting such a response.

Other modeling methods which focus much more on a 'ground up' approach have also been developed. These models focused more on the chemical and mechanical contributions to deformation behavior, using chemical properties as a way to describe molecular mechanics and dynamics. Contributions to atomistic modeling were made by Theodorou and Suter (1985 and 1986) where they developed methods to attempt to predict elastic constants of glass polymers by small-strain deformation of microscopically detailed model structures. They concluded that elastic constants may be obtained from changes in the total potential energy of these small-strain deformations and predicted elastic constants

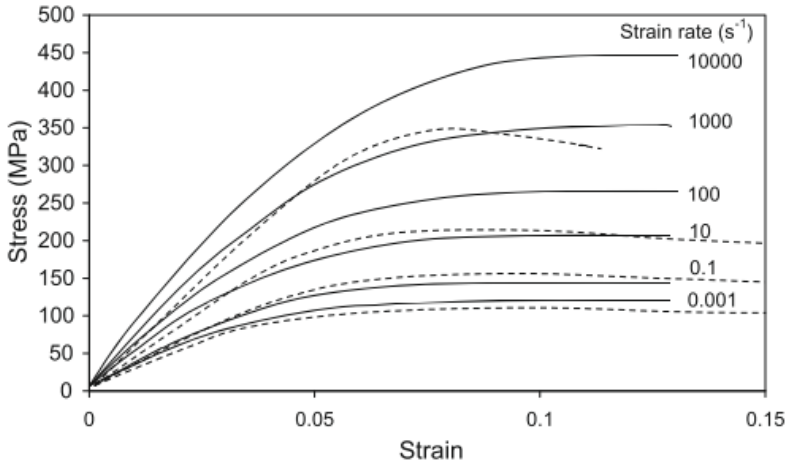


Figure 8-15: Stress-strain predictions for PMMA at T_0 = 300 K (solid lines) compared with experimental data of Richeton (dashed lines; Richeton et al., 2007) at a wide range of strain rates as labeled. (Porter and Gould, 2009).

within 15% of the experimental values, giving detailed explanations in molecular mechanisms, thus helping the understanding of mechanical properties in polymers. Several molecular modeling methods have become a standard for calculating polymer properties, but it has been argued that such 'black box' methods of numerical simulations of large groups of atoms are not easily adapted into an analytical understanding of dynamic mechanical properties for polymer design and application, as well as time-temperature scales not easily being applied to these difficult dynamic engineering problems (Porter, 2009).

Porter and Gould (2009) attempted to combine the approaches which described mechanical behavior with a more chemistry-based approach by using quantitative structure-property relations to relate polymer properties directly to their chemical composition and morphology. They used a group interaction modeling method, which highlights the understanding of different structural aspects and their roles in the polymer's behavior. The model is based on mechanical properties being directly connected to the energy stored and energy dissipated at the molecular level, due to interactions between groups of atoms in a polymer during deformation of a material. Namely, these interactions are used to predict DMTA data (e.g. storage and loss moduli as functions of temperature and strain rate), which

are then used to predict the mechanical response of amorphous polymers. They compared their model to PMMA stress-strain data from Richeton et al. (2007) as seen in figure 8-15. Their modeling method reproduces the general trend between rates but does not capture the subtleties of the behavior. However, it attempts to be a completely predictive model.

Bouvard et al. (2010 and 2013) departed from the commonly seen spring-dashpot representation of time dependent polymer models (developed by Haward and Thackray, 1968), where a large deformation kinematics and thermodynamics framework was implemented. Earlier modeling within the kinematic and thermodynamic framework was seen by Coleman and Gurtin in 1967, modeling metals, and seen by Bouvard adapting the model to the response of amorphous polymers. More conclusively, a lack of model data at higher strain rates and inaccurate predictions in post-yield temperature rise at relevant rates provides little insight into relevant areas of this research.

8.3.2 Model Application

The Mulliken et al. (2006) constitutive model builds on previous work originating from practical applications of the Ree-Eyring yield theory (as seen in work by Bauwens et al., 1967, 1969, 1971 & 1972), and follows the original structure developed by Haward and Thackray (1968). This model improved upon the Eyring-based constitutive model by focusing on capturing the underlying components of high rate polymer behavior (please refer to the previous section's literature review for additional information): implementing a two process model which considers the primary (α) and secondary process (β) of the deformation response of an amorphous polymer (see figure 8-12 for a rheological interpretation of the model) while also considering the effects of adiabatic heating at higher rates of deformation. Please refer to section 3.3.3 for the experimental data used in this section.

The finite strain kinematic framework is consistent with that presented in Boyce et al. (1998, 2000 & 2001), with the main difference being developed by Mulliken et al. (2006),

which duplicates each intermolecular resistance relationship (α and β). The underlying deformation behavior acts on three main components of the model which include the elastic-viscoplastic component which has α and β processes, as well as an entropic hardening component. The kinematic framework is fairly general, with the material specific modeling constitutive laws connecting the plastic stretching with the stress in the material response. The derivations of the kinematics can be found in detail in the articles mentioned earlier in this paragraph.

A main component of the constitutive model as described in the previous paragraph is the intermolecular contribution or elastic-viscoplastic component, which is broken up into two processes. Building upon the Eyring equation (8.4) and the work of Bauwens and Bauwens-Crowet (equations 8.6 and 8.8), presented in the previous section (8.3.1), α and β viscoplastic processes are described by the following constitutive laws

$$\dot{\gamma}_{\alpha}^{p} = 2\dot{\gamma}_{0,\alpha}^{p} \exp\left(-\frac{\Delta H_{\alpha}}{kT}\right) \sinh\left(\frac{\tau_{\alpha}\left(\frac{\Delta H_{\alpha}}{s_{\alpha} + \alpha_{p,\alpha} p}\right)}{kT}\right) \tag{8.9}$$

$$\dot{\gamma}_{\beta}^{p} = 2\dot{\gamma}_{0,\beta}^{p} \exp\left(-\frac{\Delta H_{\beta}}{kT}\right) \sinh\left(\frac{\tau_{\beta}\left(\frac{\Delta H_{\beta}}{s_{\beta} + \alpha_{p,\beta} p}\right)}{kT}\right) \tag{8.10}$$

where $\dot{\gamma}_{0,i}^{p}$ ($i = \alpha, \beta$) is the pre-exponential factor proportional to the attempt frequency, ΔH_i is the activation energy, p is the pressure, $\alpha_{p,i}$ is the pressure coefficient and s_i is represents a shear resistance dependent upon the process-specific shear moduli (found from DMTA data, or Young's modulus data). The entropic hardening component, or the network back stress

due to entropic resistance, is understood as deviatoric and was developed in Arruda & Boyce's (1993) 8-chain approximation:

$$\mathbf{T}_B = \frac{C_R}{3}\frac{\sqrt{N}}{\lambda_{chain}^p} L^{-1}\left(\frac{\lambda_{chain}^p}{\sqrt{N}}\right)\bar{\mathbf{B}}' \tag{8.11}$$

where $\lambda_{chain}^p = \sqrt{\text{trace}(\bar{\mathbf{B}})/3}$ is the stretch on a chain in the eight-chain network, L is the Langevin function defined by $L(\beta) \equiv \coth\beta - \frac{1}{\beta}$, $\bar{\mathbf{B}}'$ is the deviatoric part of the isochoric left Cauchy-Green tensor $\bar{\mathbf{B}}=(\det\mathbf{F})^{-2/3}\mathbf{F}\mathbf{F}^T$, $\sqrt{N}$ is the limiting chain extensibility, and $C_R \equiv nkT$ is the rubbery modulus where *n* is the number of chains per unit volume, *k* is Boltzmann's constant, and *T* is the absolute temperature. The effects of energy storage and dissipation under adiabatic deformation are also incorporated into the model, where the work of the entropic back stress is stored, and the inelastic work associated with the viscoelastic dashpot is 100% dissipative, or 100% converted into heat that does not have enough time to escape the material in high rate experiments (making these tests adiabatic in nature). To describe the dissipative nature of high rate experiments an equation was used which has foundations in first law of thermodynamics and the work of Boyce et al. (1992b) and Arruda et al. (1995), and further developed by Mulliken et al. (2006). Under adiabatic conditions, the rate of temperature change in the material is described as

$$\dot{T} = \frac{\text{trace}(\mathbf{T}_{A_\alpha}\tilde{\mathbf{D}}_{A_\alpha}^p)}{\rho c_p} + \frac{\text{trace}(\mathbf{T}_{A_\beta}\tilde{\mathbf{D}}_{A_\beta}^p)}{\rho c_p} \tag{8.12}$$

where $\tilde{\mathbf{D}}_{A_\alpha}^p$ and $\tilde{\mathbf{D}}_{A_\beta}^p$ are the rates of viscoplastic stretching (which are products of a direction tensor for each α & β process and a magnitude of the plastic strain rate $\dot{\gamma}_\alpha^p$ or $\dot{\gamma}_\beta^p$), and $\mathbf{T}_{A_\alpha}$ and $\mathbf{T}_{A_\beta}$ are the true stress tensors acting on the α and β elements of the model and are related to the deformation by the constitutive laws from linear elastic springs:

$$\mathbf{T}_{A_\alpha} = \frac{1}{J_\alpha} L_\alpha^e [\ln \mathbf{V}_{A_\alpha}^e] \tag{8.13}$$

$$\mathbf{T}_{A_\beta} = \frac{1}{J_\alpha} L_\beta^e [\ln \mathbf{V}_{A_\beta}^e] \tag{8.14}$$

where $\mathbf{T}_{A_i}$ ($i = \alpha, \beta$) is the Cauchy (true) stress, L_i^e is the fourth order modulus tensor, $\ln \mathbf{V}_{A_i}^e$ is the Hencky strain, and $J_i = \det \mathbf{F}_{A_i}^e$ is the elastic volume change. The assumption is made that the material is initially in an isotropic state, and additionally that the elastic behavior of the material may be decomposed into α and β components. Any two element-specific elastic constants, such as the shear modulus (μ) and bulk modulus (κ) can derive the modulus tensors, L_i^e, where elastic constants are assumed to be functions of both strain rate and temperature. Additional detail on the mathematics involved in this model and the material constants described in this section may be found in the work of Bauwens et al. (1969), Arruda and Boyce (1993), Arruda et al. (1995), and Mulliken et al. (2006).

The constitutive model summarized in the previous paragraphs was initially implemented (in 1-D) by Jason Foley (of the Air Force Research Laboratory, Eglin AFB, Florida, USA) into a numerical computing environment and programming language (MATLAB, or matrix laboratory) developed by MathWorks, and subsequently edited by the author in order for more tailored analysis. Using the model involves knowledge of 12 material constants to define several elements of the model:

Viscoelastic dashpots

$\dot{\gamma}_{0,\alpha}^{p}$	$\dot{\gamma}_{0,\beta}^{p}$	pre-exponential factors
ΔH_{α}	ΔH_{β}	activation energies
$\alpha_{p,\alpha}$	$\alpha_{p,\beta}$	pressure coefficients
h_{α}	–	softening slope
$s_{ss,\alpha}$	–	preferred state of athermal shear strength

Langevin spring, or backbone stress

$\sqrt{N}$	limiting chain extensibility
C_R	rubbery modulus

Rate and temperature dependent elastic springs

$E_{\alpha}(T,\dot{\varepsilon})$	$E_{\beta}(T,\dot{\varepsilon})$	elastic moduli as functions of strain rate and temperature

Elastic Moduli

The elastic moduli as functions of strain rate and temperature were found experimentally from the DMTA data of PVC (presented in section 3.4.2). In order to better understand and describe DMTA data, the DMTA information was converted into a continuous function via a manipulation of a probability distribution, known as the Weibull distribution. It was found that the elastic moduli in most applications may be described as

$$E = E_{\alpha} + E_{\beta} \tag{8.15}$$

α-components

$$E_{\alpha} = \left(E_{0,\alpha} + E_{lin}\right)\exp\left[\left(-\frac{T}{T_{0,\alpha}}\right)^{m_{\alpha}}\right] \tag{8.16}$$

$$T_{0,\alpha_i} = T_{0,\alpha_{ref}} + D_{\alpha}\left[\log(\dot{\varepsilon}_i) - \log(\dot{\varepsilon}_{ref})\right] \tag{8.17}$$

$$E_{lin} = \left(T_{0,\alpha} - T\right)E_{lin,0_i} \tag{8.18}$$

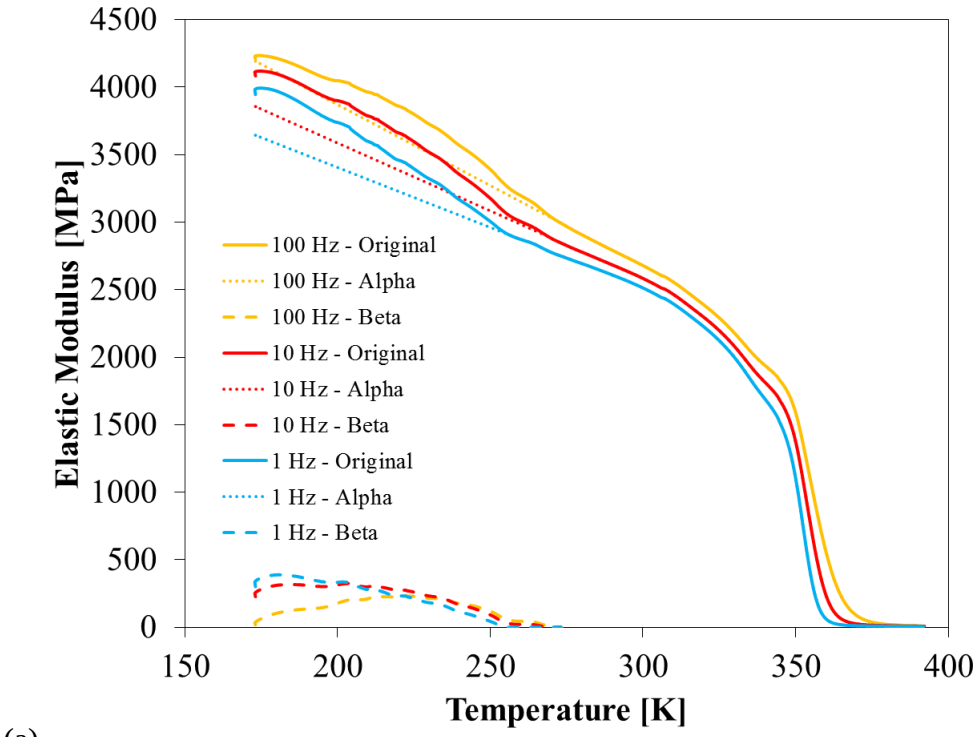
$$E_{lin,0_i} = E_{lin,ref} + A_{lin}\left[\log(\dot{\varepsilon}_i) - \log(\dot{\varepsilon}_{ref})\right] \tag{8.19}$$

β-components

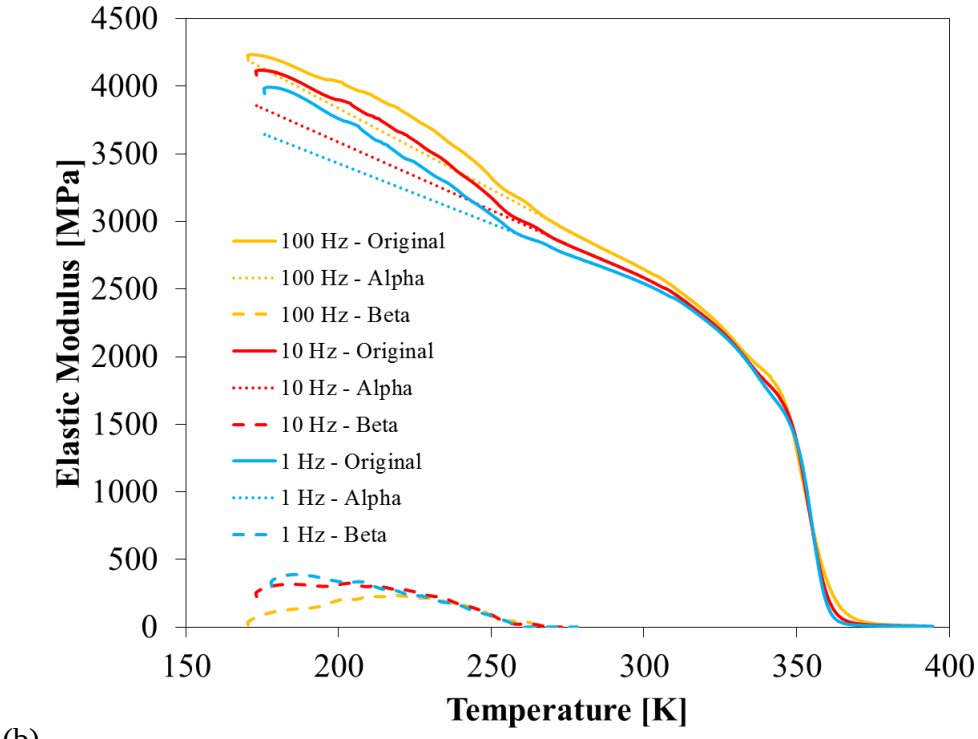
$$E_{\beta} = E_{0,\beta} \exp\left[\left(-\frac{T}{T_{0,\beta}}\right)^{m_\beta}\right] \tag{8.20}$$

$$T_{0,\beta_i} = T_{0,\beta_{ref}} + D_{\beta}\left[\log(\dot{\varepsilon}_i) - \log(\dot{\varepsilon}_{ref})\right] \tag{8.21}$$

where $E_{0,j}$ ($j = \alpha, \beta$) is a fitted constant (rate independent) which determines the intercept of the elastic modulus curve pertaining to the j process, T_{0,j_i} is a material constant dependent upon strain rate which decides the temperature location of the j transition at rate i, m_j is empirically fitted and dimensionless material constant which determines the slope of the j transition, D_j is the shift factor – a rate independent material constant found from elastic modulus data (found from decomposing data into α and β contributions, see figure 8-16), E_{lin} is a rate dependent parameter which provides another component of the gradient pertaining to the α contribution of the modulus, $E_{lin,0_i}$ (rate dependent) and $E_{lin,ref}$ (constant fitted to empirical reference data) provide a pivot for modulus at temperatures lower than T_g, $\dot{\varepsilon}_{ref}$ is the strain rate (converted from the DMTA test frequency as described in equation 3.1 in section 3.4.3) which pertains to the DMTA reference data, $\dot{\varepsilon}_i$ is the strain rate user input, T is the temperature data for the reference curve, A_{lin} is the shift factor for E_{lin}. The formula described by these equations was able to successfully capture the detail of the PVC temperature and rate dependent elastic modulus, which is presented in figure 8-17.



(a)



(b)

Figure 8-16: (a) Example of PVC modulus data (at 1, 10, and 100 Hz or 0.032, 0.32, and 3.2 s^{-1}) decomposed into α and β components. (b) The rate-dependent moduli shifted onto a reference moduli (in this case 10 Hz or 0.35 s^{-1}) in order to find the shift factor, D_j (D_α = 5.3 K/decade strain rate & D_β = 11.8 K/decade strain rate – the experimentally found shift factors seen in chapter 4).

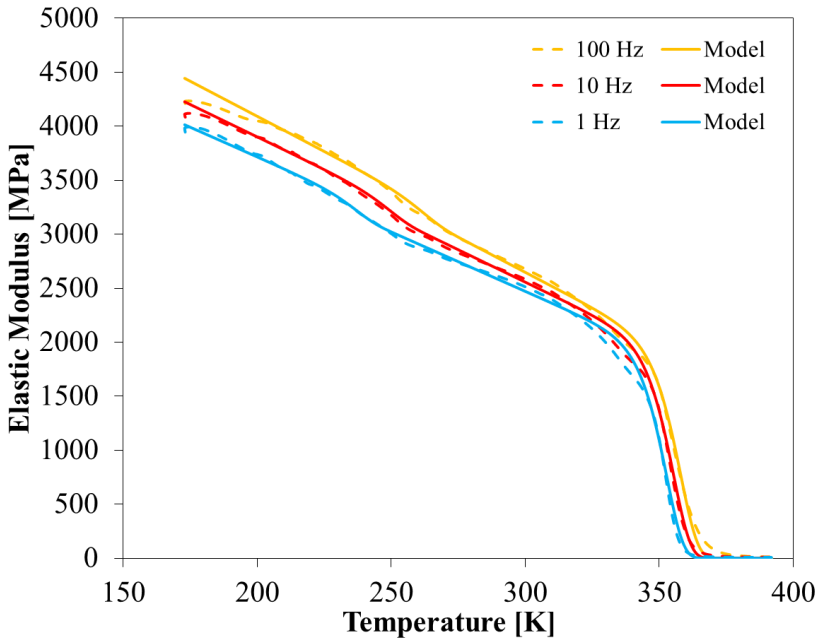


Figure 8-17: PVC elastic moduli modeled (at 1, 10, and 100 Hz or 0.032, 0.32, and 3.2 s^{-1}) with the probability distribution as described in equations 8.15 – 8.21.

Table 8.3: PVC parameters for the probability distribution model used to capture experimental moduli.

$E_{0,\alpha}$	1885 MPa
$T_{0,\alpha_{ref}}$	356 K
D_α	5.3 K/decade strain rate
$E_{0,\beta}$	145 MPa
$T_{0,\beta_{ref}}$	250 K
D_β	11.8 K/decade strain rate
$\dot{\varepsilon}_{ref}$	0.32 s^{-1}
m_α	60
m_β	30
$E_{lin,ref}$	12
A_{lin}	1

Model vs. Experiment

Low, Medium, & High Strain Rates

Upon implementing the continuous function (equations 8.14 – 8.17) to describe the DMTA data within the material parameters of the constitutive model previously described earlier in this section (and in equations 8.8 – 8.13). The model was implemented with constant strain rates in order for a more consistent and direct comparison between rates, and with the material parameters presented in table 8.4 at the end of this chapter.

Looking at model versus experiment data in figure 8-18, there is good agreement in yield stress was found from low to moderate rates (0.001 to 10 s^{-1}). At higher rates (50 and 2400 s^{-1}), where the beta transition can be seen at room temperature, the model had a more difficult time describing the large increase in yield stress (or higher sensitivity to strain rate) which occurs at higher rates in experimental data. Both of these β influenced rates present a ~10 MPa difference in true yield stress (135 MPa model vs 145 MPa experimental at 2400 s^{-1}; 111 MPa model vs 121 MPa experimental at 50 s^{-1}). This difference is consistent with Mulliken's (2006) implementation of the model to an unplasticized PVC, where he found a ~10 MPa difference between his model and experimental yield stresses at a deformation rate of 1750 s^{-1} (160 MPa model vs 170 MPa experimental yield stress). The driving parameters of the rate dependence of yield stress in this model are $\Delta H_j, \dot{\gamma}_{0,j}^{p}$, $E_j(T, \dot{\varepsilon})$, and $\alpha_{p,j}$ ($j = \alpha, \beta$). Succeeding the decomposition of the yield data (technique originally developed by Ree-Eyring, 1958), ΔH_j and $\dot{\gamma}_{0,j}^{p}$ are found by simultaneously solving the equations 8.9 (for $j = \alpha$) and 8.10 (for $j = \beta$) via numerical methods (and using two different strain rates and yield stresses from experimental uniaxial compression data for the additional parameters). The

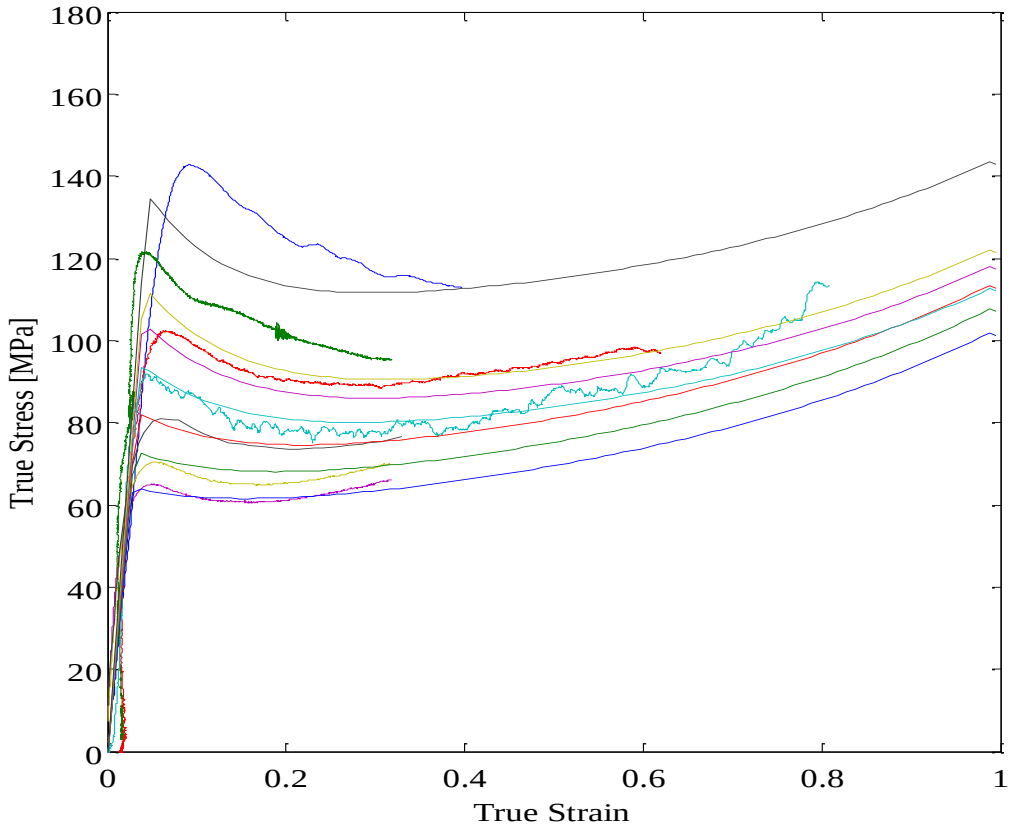


Figure 8-18: PVC true stress-true strain behavior in uniaxial compression over a span of strain rates (0.001, 0.01, 0.1, 1, 10, 50, and 2400 s^{-1}) and model prediction with adiabatic heating turned on for higher rates (1 s^{-1} or greater) and turned off for lower rates (0.1 s^{-1} or less).

$\alpha_{p,j}$, or pressure coefficient, is found experimentally. The $\alpha_{p,j}$ values used in this research are the same used by Mulliken et al. (2006) for unplasticized PVC (with approximately the same T_g and T_β as the 'PVC' used in this research (within 0.5 K)).

Yield stress is very sensitive to any changes in ΔH_j (an ΔH_α increase of the order of 0.1 x 10^{-19} J relates to a 5 MPa increase in the α-component of yield stress), and $\dot{\gamma}^p_{0,j}$ (a 1 x 10^{19} J increase in $\dot{\gamma}^p_{0,\alpha}$ relates to a 0.89 MPa increase in yield stress). Although, the sensitivity of these two parameters increase or decrease depending on the value of $E_j(T,\dot{\varepsilon})$. Thus making it difficult to fit parameters such as $\dot{\gamma}^p_{0,\beta}$ when $E_\beta(T,\dot{\varepsilon})$ is on the order of 100 MPa (for a material such as the PVC used in this study). Materials such as PC and PMMA have 5 and 15 times the amount of β influence in elastic modulus (500 MPa and 1500 MPa) when seen at room temperature at strain rates of ~10^3 s^{-1}.

This difficulty in describing the larger increase in yield can be attributed to the β transition not being large enough – which implies that the β shift factor may increase with increasing strain rate, thus becoming more sensitive to strain rates at higher strain rates. Or perhaps the formulas involving the β influence in the model need to be reevaluated. This reevaluation will be investigated in future work.

The shape of the yield, primarily the post-yield strain softening, is determined by both the $s_{ss,\alpha}$ and h_α (with the shape of the yield being more sensitive to $s_{ss,\alpha}$ versus h_α), and adiabatic heating which occurs at higher rates of strain (this is investigated at the end of this section). These parameters are both determined by fitting the model to empirical data. Medium to high rates (specifically 0.1 to 2400 s^{-1}) were described better by these parameters compared to the low rates (0.001 and 0.01 s^{-1}). Note: the higher rates' yield stresses for the model were shifted temporarily to the experimental values in order for easier comparison. These variables allow for the temperature dependence of the yield stress to replicate the

temperature dependence of the elastic shear moduli (for more detail please refer to Argon, 1973, and Mulliken et al., 2006).

Strain hardening seen by the model may be manipulated by N and C_R which both largely affect the network 'back stress', Langevin stress, or 'strain energy' W (seen in the previous section 8.2.1 describing rubbery models). N is not very sensitive to changes although C_R changes the final stress value at the end of testing (this implementation of the model was set to a final test value of '1.2' true strain) by ~7 MPa in true stress per 1 MPa in changing C_R. C_R is an empirically fitted parameter, and was fitted to the PVC experimental data with relative good agreement in medium rate curves (0.1 to 10 s^{-1}) and less good agreement in lower rate curves (particularly 0.01 and 0.001 s^{-1}). It is difficult to judge the efficacy of the C_R value for 2400 and 50 s^{-1} curves, because of their relatively low final strain values, which do not show strain hardening in their responses. Although, the efficacy of C_R is proven at high rates when fitted to 4355 s^{-1} in the next paragraph.

Adiabatic Temperature Rise

Figure 8-19 presents a very good agreement between high rate experimental data (4355 s^{-1}) and the model. In this case, much larger (~1000 MPa seen at lower temperatures) and constant E_β was used to better study the effects of adiabatic heating. Specifically, the effects of adiabatic heating (equation 8.12) was turned on at higher rates to capture the additional post-yield thermal strain softening which occurs at these rates. The effects of adiabatic heating have been explored in greater detail, theoretically and experimentally, in Chapters 5, 6, and 9. The model equation describes adiabatic heating with very good agreement, lowering the true stress values by ~20 MPa at higher strains (>0.5) to accommodate the heat that is created at 4355 s^{-1} strain rate, or strain rates of the order of 10^3 s^{-1}.

Importantly, this data provided a clear window into the effect of adiabatic heating in our high rate tests on our different PVC materials, namely providing a theoretically isothermal high rate curve versus an adiabatic high rate curve. This development allowed for comparisons to low rate and low temperature data which were found to be very similar, which is presented in figure 8-20, and which provided encouragement to pursue a low rate simulation method to capture the high rate response seen in polymers.

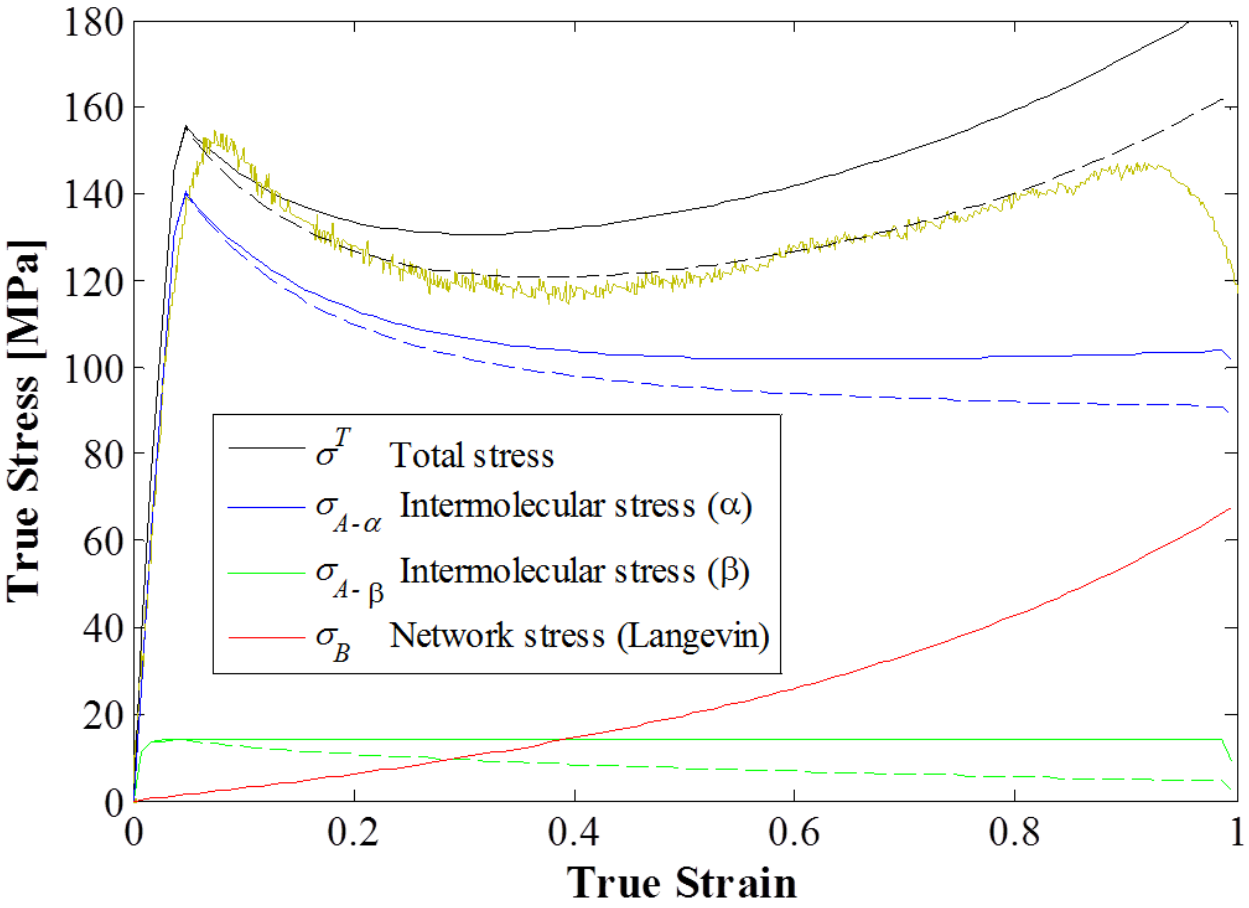


Figure 8-19: PVC true stress-true strain behavior in uniaxial compression at a high rate of 4355 s^{-1} (an olive green color) and model prediction with adiabatic heating turned on (dashed lines) and turned off (solid lines) split into the constitutive components of the model.

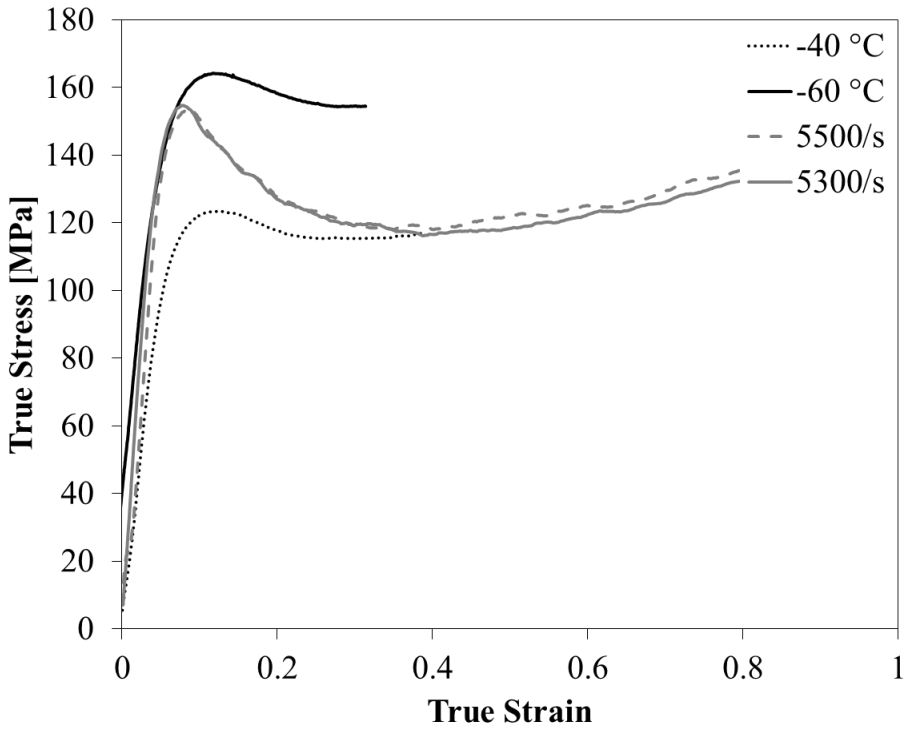


Figure 8-20: Comparison of the observed true stress-true strain behavior of low temperature experiments conducted at 10^{-2} s^{-1} and high rate experiments conducted at room temperature (20 °C). Note the similarity between isothermal -40 °C stress-strain behavior and the 'isothermal' high rate response (solid black line) in figure 8-19.

8.4 Conclusions

Two thorough literature reviews of rubbery and amorphous polymer models were carried out in order to better understand the significant research which has been conducted in constitutive modeling, and importantly, the constitutive models which developed from these investigations and their underlying theories. After the review, two models were decided upon for application: the Ogden model for rubbers and a Ree-Eyring based-model which has recently been built upon by Mulliken and Boyce. Rubbery behavior of two amorphous polymers at elevated temperatures (PVC and PPVC-2), and materials with sub-room temperature glass transition temperatures (PPVC-4 and PPVC-6), were successfully modeled using the Ogden model, presenting very good model versus experiment agreement in both temperature dependence (all PVC materials) and rate dependence (PPVC-6). The effects of the shear modulus were additionally investigated in its (corrected) temperature dependent and

rate dependent effects. The differences between the application of a one-term and two-term model were also noted in the rubbery polymer investigation. PVC true stress-true strain behavior in uniaxial compression was captured using an implementation and manipulation of the Ree-Eyring equation by Mulliken and Boyce (2006). A probability distribution was developed in order to generate a continuous function to describe DMTA data for the amorphous polymer model which was used. The Mulliken and Boyce model (with the continuous DMTA function implemented) captured the yield stresses of low to moderate rates (and had difficulty at higher rates). The model also captured the effects of adiabatic heating seen in the strain softening which occurs at higher strain rates of deformation. Within this investigation, an 'isothermal' high rate stress-strain curve was produced and compared to isothermal low temperature quasi-static behavior with encouraging results with respect to simulation method application. The model is unable to capture the detail, or curvature, of the yield stress in each comparison of model vs. experiment. An understanding of the effects of material parameters (table 8.4) were better understood from the modeling conducted, and thus a better understanding of the drivers of PVC's constitutive response – the results of this understanding and sensitivities to each material parameter were described and quantified in evaluating the model versus experiment results for low, medium, and high rates of PVC.

Table 8.4: PVC model parameters

$E_\alpha(T,\dot{\varepsilon})$	DMTA data/model data
$E_\beta(T,\dot{\varepsilon})$	DMTA data/model data
c_v	3.146 x 10^6 $Jm^{-3}K^{-1}$
$\dot{\gamma}^p_{0,\alpha}$	1e19 s^{-1}
$\dot{\gamma}^p_{0,\beta}$	8.26 x 10^6 s^{-1}
ΔH_α	4.7 x 10^{-19} J
ΔH_β	9.2 x 10^{-20} J
$\alpha_{p,\alpha}$	0.22
$\alpha_{p,\beta}$	0.22
h_α	450 MPa
$s_{ss,\alpha}$	100 MPa
$\sqrt{N}$	2.24
C_R	6 MPa

Chapter 9

Thermodynamic Investigations & Novel Temperature Measurement Method

In the fifth chapter of this thesis, a new experimental model was proposed in an effort to describe observed thermal softening behaviors which occur at high rates of deformation, in a way that corresponds with thermodynamic and molecular theory. It was suggested that the elastic, yield, and post-yield amorphous polymer behavior at moderate to high strain rates may be captured by low temperature quasi static behavior, with a subsequent temperature rise to capture the post-yield strain softening understood to be caused by adiabatic heating at higher rates of strain. An experimental model was presented and successfully applied to the rate dependent behavior of a prototypical amorphous polymer PPVC-2 (PVC with 20wt% DINP plasticizer).

In the sixth of this thesis, the experimental model was applied to two additional amorphous polymers with complementary constitutive behaviors: PC and PMMA. PC demonstrated characteristic increases in strain hardening (or decreases in strain softening) with increasing strain rate, while PMMA revealed the opposite by its vivid change from isothermal to adiabatic heating ($0.01\ s^{-1} \rightarrow 0.1\ s^{-1}$) at low strain rates and its increases in strain softening (or thermal softening) with increasing strain rate, which masked any

orientation-induced strain hardening at larger strains (this has also been observed by other authors, e.g. Arruda et al., 1995 & Mulliken, 2006). The experimental model application was expanded in the seventh chapter in testing a composite material, a polymer bonded explosive simulant (PBS), in tension (via Brazilian testing). During the research presented in these chapters, special attention has been paid to high rates of deformation and the adiabatic temperature rise which occurs at these rates.

In this chapter, the thermodynamic foundation of the experimental model presented in the fifth chapter, and additionally studied in the subsequent chapters, of this thesis is investigated via high and moderate rate temperature measurement of two amorphous polymers, PPVC-2 and PMMA, in parallel with investigations of strain energy. The effectiveness of and differences between methods for temperature measurement were studied as a result of the previously described investigations, and are presented in detail in this chapter.

9.1 Background

The material responses of both PPVC-2 and PMMA have shown dramatic transitions, where the rate dependent responses have transitioned from approximately isothermal, full heat transfer, to approximately adiabatic, no heat transfer. This thermodynamic transition region has been shown in PPVC-2 between 0.1 s^{-1} and 1 s^{-1}, and in PMMA between 0.01 s^{-1} and 0.1 s^{-1}. This transition is dependent upon the polymer's thermal properties, as well as the specimen geometry of the polymer (Arruda et al., 1995). This thermomechanical transition is not under consideration at higher strain rates, where the material response is understood to be fully adiabatic, where all heat generated (from plastic work) stays within the specimen. This affected behavior of amorphous polymers due to thermal softening has been examined using different temperature measurement methods in a number of experimental studies.

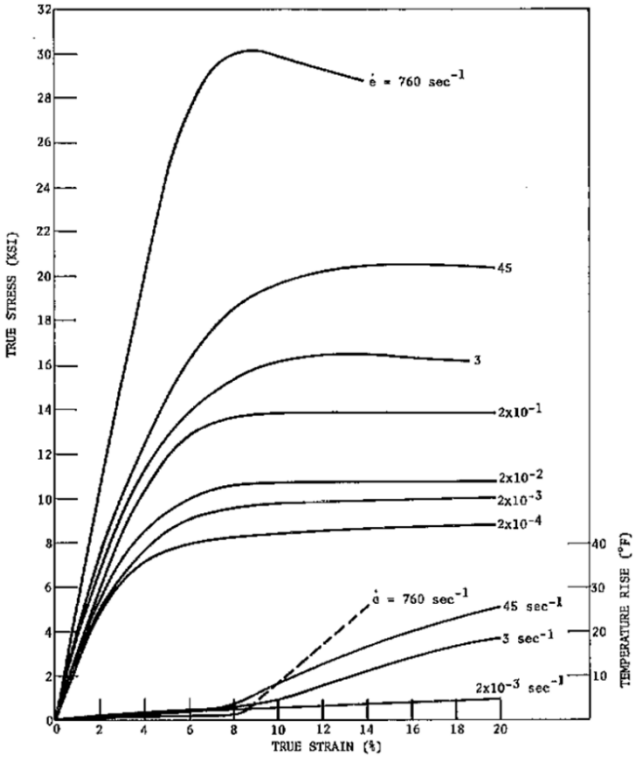


Figure 9-1: PMMA temperature rises and true stress-true strain behaviors reported by Chou et al. (1973) using embedded thermocouples from low to high rates of deformation (2×10^{-3} s^{-1} → 760 s^{-1}).

Chou and co-workers (1973) were among the first to measure the temperature rise of polymers from low to high strain rates. Chou et al. used embedded thermocouples to measure temperature rise in several different polymers including PMMA, cellulose acetate butyrate (CAB), polypropylene (PP), and nylon 6-6 under low to high rates of deformation. In order to verify the efficacy of their temperature method, the authors employed the equation[17]:

$$\tau = \frac{V\rho C}{hA} \tag{9.1}$$

where τ is the response time of the thermocouple, V is the volume of the thermocouple, ρ is the density, C the specific heat, h the coefficient of heat transfer, and A the surface area. The rate dependent

[17] The authors further determined the validity of their thermocouple method experimentally by observing whether there was a time-lag in data.

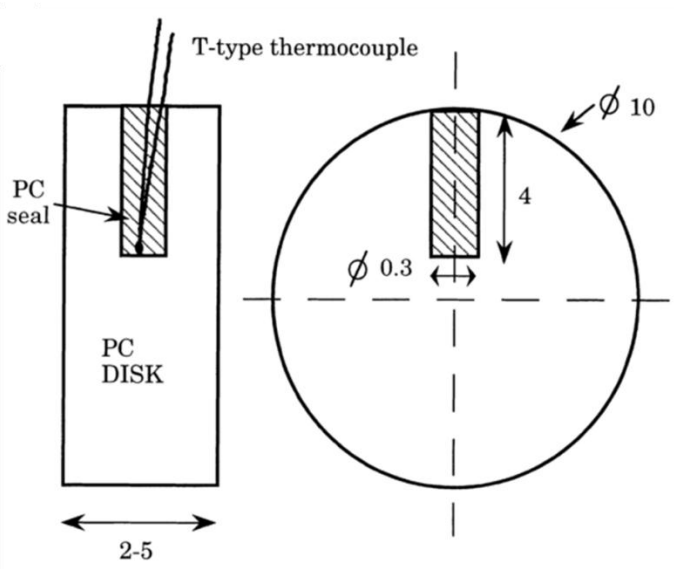


Figure 9-2: Experimental setup used by Rittel (1999) in order to study the high rate temperature response of PC, and also used by the author (2000) in order to measure the temperature rise of PMMA in moderate rate tests.

temperature rise and true stress-true strain behaviors of PMMA reported by the authors are presented in figure 9-1. Rittel (1999 & 2000) implemented this same embedded-thermocouple technique in investigating the temperature rises of PC and PMMA during moderate[18] and high rates of deformation. Figure 9-2 presents the experimental setup used by Rittel in these investigations. Prior to these investigations, Rabin & Rittel (1999) developed a sophisticated analysis of the time response of solid-embedded thermocouples and concluded that the thermal diffusivity of the thermocouple is required to be at least one order of magnitude higher than that of the measured body in order to obtain useful results[19], and that the transient response time is governed by the radius of the thermocouple and the thermal diffusivity of the material being measured. Using the results of this analysis, Rittel and colleagues have produced a large amount of research on using thermocouples in high

[18] The thermodynamic effects of PMMA are most commonly studied at low to moderate rates of deformation because of its brittle failure observed at higher strain rates ($\sim 10^3\ s^{-1}$).

[19] This study utilizes a thermocouple diffusivity which is 4 orders of magnitude larger than the measured domain ($\alpha_{PVC} = 0.144 \times 10^{-6}\ m^2s^{-1}$ and $\alpha_{K\text{-}Type} \approx 1 \times 10^{-4}\ m^2s^{-1}$). Accuracy was confirmed during experiment after observing no lag time of the temperature signal (as it was consistent in time with the transmission bar wave signal), and additionally, the thermocouples used in this study were of much smaller diameter compared to that of previously successful works in high rate thermocouple temperature measurement (e.g. Rittel, 2000)

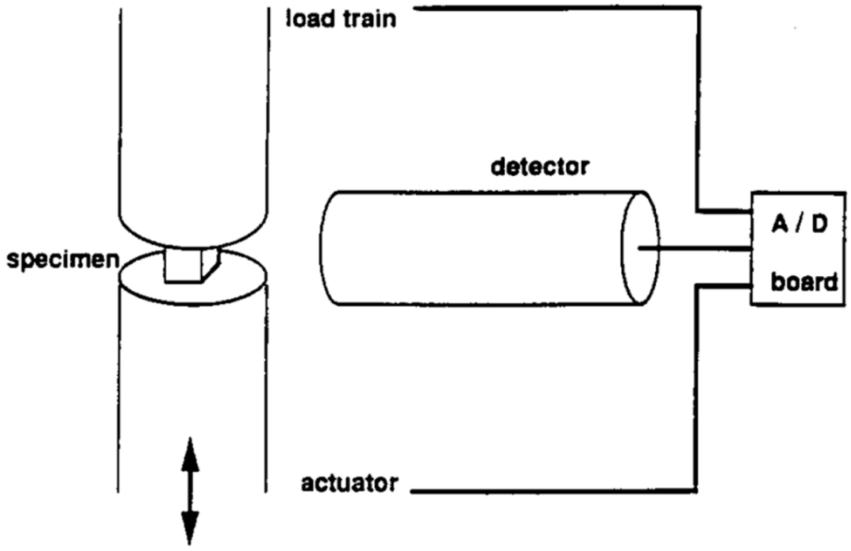


Figure 9-3: Experimental setup used by Arruda et al. (1995) in order to study the low to moderate rate temperature response of PMMA.

strain rate applications investigating the temperature rise which occurs in amorphous polymers.

Infrared (IR) detection techniques have also been used to investigate the temperature rises which occur in polymer specimens at low to high rates of deformation. Arruda et al. (1995) studied the temperature rise which occurs in PMMA from low to moderate rates using an IR method, with the experimental setup presented in figure 9-3. In this method, focusing optics are arranged around the specimen to direct surface radiation onto a photovoltaic detector (approximately 100 μm x 100 μm). The detector is then calibrated to measure the voltage output associated with the correct temperature rise of the specimen. This technique has also been used by several other authors to study the adiabatic heating which occurs in polymeric materials at high strain rates (e.g. Buckley et al.; Li & Lambros, 2001; Lerch et al., 2003; Mulliken, 2006; Garg et al., 2008; Regev & Rittel, 2008).

Results reported from literature of the two different temperature measurement methods are presented in figures 9-4 and 9-5. These data sets have very subtle differences,

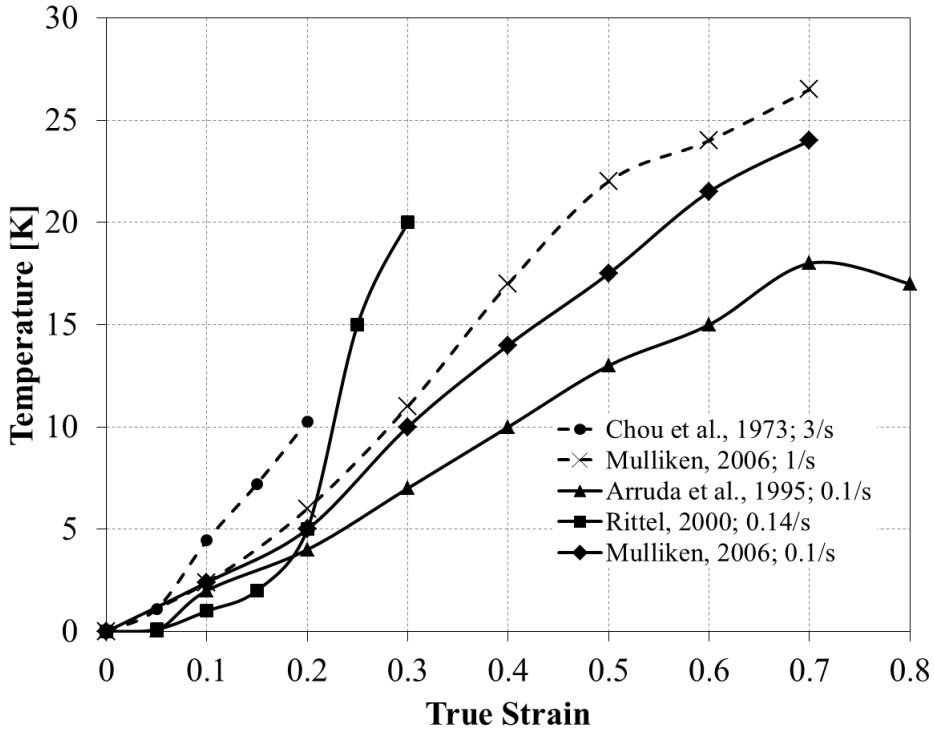


Figure 9-4: Data on the temperature rise in PMMA during uniaxial compression at 0.1 s^{-1} as specified in literature. The dashed lines present data at ~1 s^{-1} and the solid lines present data at ~0.1 s^{-1}.

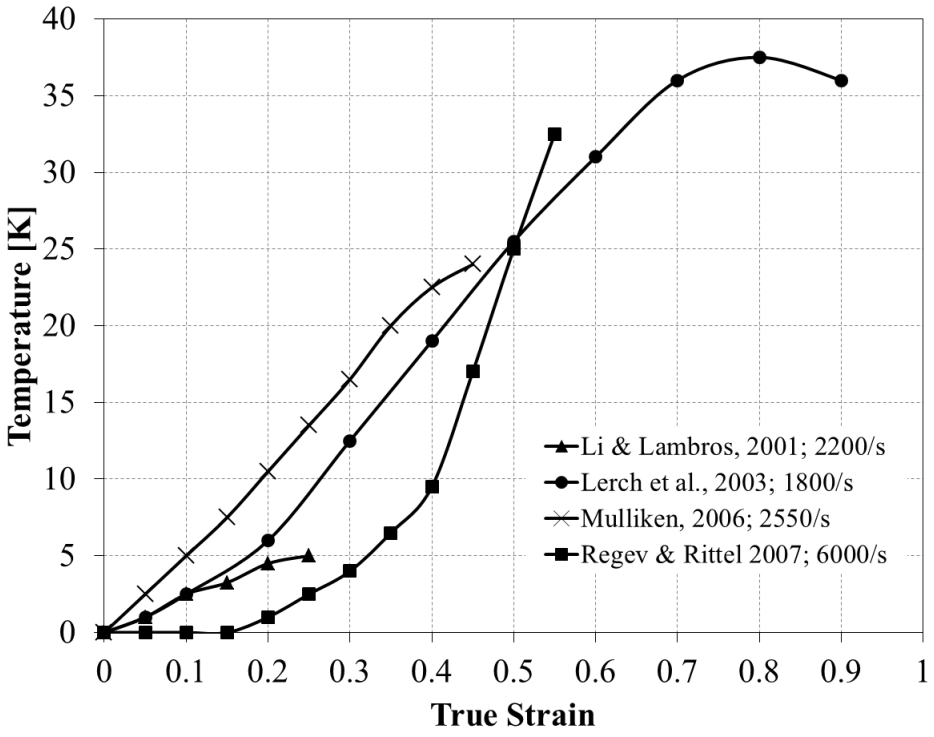


Figure 9-5: Data on the temperature rise in PC during uniaxial compression on the SHPB at as specified in literature.

and are nearly consistent when acknowledging the differences in materials used for each study and the arbitrary nature (if the data acquisition trigger is not set in agreement with all data acquisition devices) of deciding the initial strain associated with the observed temperature increase. A difference in polymeric materials is made clear by considering the example of comparing the PMMA in Arruda et al. (1995) versus the PMMA in Mulliken (2006). Observing figure 9-4 it is noted that the temperature measurement at 40% true strain the PMMA temperature rise is 4 K less in Arruda et al.'s data when compared to Mulliken's data. Looking at the true stress-true strain behavior associated with these temperature rises, Arruda et al.'s PMMA specimens demonstrated a true stress of 100 MPa at 40% true strain, versus a ~130 MPa true stress seen by Mulliken at the same strain. These differences substantiate the observed differences in temperature rises between PMMA specimens, while also demonstrating a consistency in temperature measurement studies.

There are subtle differences in behavior between the data sets presented in figures 9-4 and 9-5, particularly the slightly exponential nature of Rittel et al.'s temperature measurements versus the more linear response reported in other literature. In confirming the observed temperature measurements made by the author, Regev and Rittel (2008) conducted an additional temperature measurement study on PC implementing both IR and embedded thermocouple techniques at high strain rates (3000, 6000, and 8000 s^{-1}). The authors found no difference in results between the two techniques until a rate of 8000 s^{-1}. At this rate, after a true strain of 50% was reached, it was noted that the field of view of the IR detector was hidden by the SHPB bars used in testing. A thermocouple method appeared encouraging after observing this good agreement between techniques. Walley and colleagues (2000) have also conducted similar tests in comparing thermocouples and IR temperature measurements at high strain rates in comparing metals (e.g. iron and copper)). In this study, the authors also presented an insightful review of the different techniques available in measuring rapid

temperature changes, including their strengths and weaknesses. In the review, some of the advantages of thermocouples included: being well calibrated over a wide temperature range, and monitoring temperature inside a body

Alternatively, some of the disadvantages included their invasive nature, which may alter the observed specimen response, and the fact that heat takes a certain amount of time to diffuse into the thermocouple even if the two mediums are in good thermal contact with one another. Walley et al. found that the thermocouples measurements were within a range of 3 °C of the IR method when studying copper, with a slightly higher difference of 8 °C in iron. In comparing these data to theoretical data, they found that the thermocouples gave temperature values to within 1 °C of their theoretical temperature rise (calculated with the same equation used in the simulation method seen in the fifth chapter), demonstrating that all of the plastic mechanical work performed on the specimens was converted to heat[20].

Lastly, the results of the two different temperature measurement methods are consistent in showing that 75 – ~100% of the plastic work is converted to heat during moderate to high rates of deformation, which is consistent with the assumptions used in the simulation method proposed in Chapter 5.

In the following section, the thermodynamic foundation of the experimental model in earlier chapters of this thesis is investigated via high and moderate rate temperature measurement of two amorphous polymers, PPVC-2 and PMMA, in parallel with investigations of strain energy. An experimental and analytical investigation between methods for temperature measurement (e.g. IR, various thermocouple methods) during

[20] This particular evidence of 100% of plastic work being converted to heat does not support the simulation method in this thesis which is meant for polymers, yet this study was helpful in comparing the advantages of the IR and thermocouple temperature measurement methods.

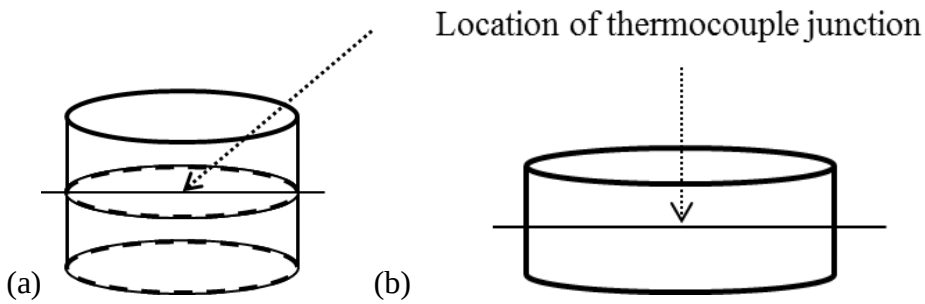


Figure 9-6: (a) Illustration of a 'sandwiched' thermocouple method initially used for temperature measurement (before the novel version of this method presented in the following section) and (b) the 'threaded' thermocouple method, a thermocouple is threaded (like a needle) through a hole drilled through the diameter of the specimen. The center of the specimen is denoted in order to illustrate the location of the thermocouple junction used in each experiment. (~0.1 mm hole drilled in each specimen with a ~0.08 mm diameter thermocouple used).

deformation is presented, with a goal to better understand and perhaps optimize current methods.

9.2 Materials & Temperature Measurement Equipment

PPVC-2 temperature measurements in compression were conducted on 2.5 mm length x 5.0 mm diameter cylindrical specimens. During 'sandwiched' temperature measurement tests (described in the following section) two cylindrical specimens of the same dimensions were used (creating ~5 mm length x 5 mm diameter specimens). PMMA temperature measurements, also in compression, were conducted on 8 mm length x 8 mm diameter, and for 'sandwiched' temperature measurement tests were conducted on two 4 mm length x 8 mm diameter cylindrical specimens. All K-type thermocouple tests were conducted with OMEGA Fine Gage Thermocouples, from Omega Engineering, Inc., Stamford, Connecticut, USA. These thermocouples were 0.075 mm in diameter and 30.5 cm in length. In addition, the PMMA tests employed T-Type thermocouples, using copper and constantan (Cu55/Ni45) foil (0.05 mm thick) and wires (0.125 mm diameter) from Goodfellow Cambridge Ltd., Huntingdon, UK. The thermal camera employed was a FLIR T640 Model from FLIR

Systems, Inc from Kent, UK. This model creates MPEG-4 video which has capabilities of capturing more than 5 images per second – a frame rate more than fast enough for its use in this thesis.

9.3 Experimental Setup

High Rate: PPVC-2

Each temperature measurement on PPVC-2 was performed on the split-Hopkinson bar. Two different methods of temperature measurement were employed in studying PPVC-2: 'sandwiched' and 'threaded' thermocouple methods. These methods are illustrated in figure 9-6. Both methods employ a thermocouple-placement which differentiates itself from the literature: in this study the thermocouple wire is fixed along the axis normal to the axis of compression. This placement is used in order to create a more symmetric or 'uniform' alteration in material properties, compared to the more often used setup seen in figure 9-2. A quick-response thermocouple amplifier, with a response time of 5 K μs^{-1}, was employed in order to ensure that the only limiting factor of the thermocouples was the heat of diffusion into the thermocouple junction (described in further detail in section 9.1). The amplifier in this study was found to have a calibration factor of 0.0113 ± 0.0003 V K^{-1}. The data acquisition system is the same used for other SHPB experiments (described in Chapter 2).

Moderate Rate: PMMA

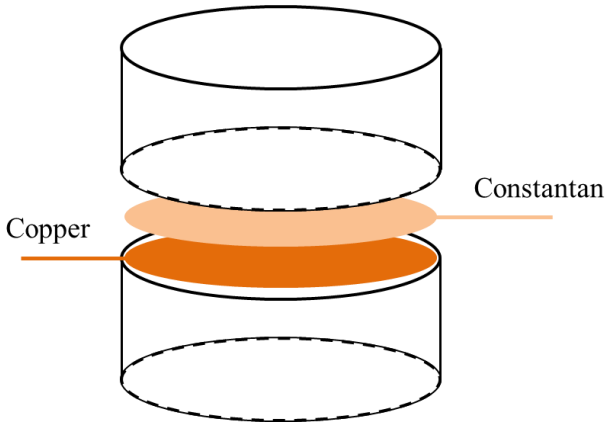


Figure 9-7: Novel moderate rate copper-constantan thermocouple temperature measurement method.

Moderate rate temperature measurements (0.1 s^{-1}) conducted on PMMA followed a similar experimental setup to high rate PPVC-2 tests. The 'threaded' thermocouple method (figure 9-6b) was used in combination with a novel thermocouple method using the 'sandwiching' of copper and constantan (Cu55/Ni45) foil in order to create a T-Type thermocouple junction, presented in figure 9-7. In preparing each specimen, each foil was welded with its respective wire, and the foils created a thermocouple junction via contact. The grouping of materials was held together with rubber glue. The same high speed thermocouple amplifier was used and a 100 MS s^{-1} Tektronix oscilloscope was used in combination with the Instron quasi-static machine and temperature chamber described in Chapter 2.

9.4 Results and Discussion

High Rate

Experimental results from testing at high strain rates are summarized in figures 9-8 – 9-9. For PPVC-2, temperature measurements were useful in observing the adiabatic conditions which resulted from high rate testing, as well as confirming that approximately all of the plastic work in testing is converted to heat (presented in figure 9-9). In addition, these experiments were helpful in observing the sensitivity of the specimens to alterations, e.g. drilled holes for thermocouples, in their material behavior (figure 9-8).

In both the 1250 and 1470 s^{-1} tests, the thermal softening seen in PPVC-2's behavior was confirmed to be a result of the adiabatic nature of testing and the near 100% of conversion of plastic work to heat. These data also confirm that the work converted to heat fluctuates during testing, which has also been observed in literature from polymeric material and metal experiments (Macdougall, 2000). The curves in figure 9-8 result in gradients of approximately 78 K/% true strain (both theoretical curves), 69 K/% true strain (both 1250 and 1470 s^{-1}). These comparisons were then extended to studying the energies of deformation, by using 1250 s^{-1} as representative behavior of PPVC-2 under uniaxial compression at rates at approximately 10^3 s^{-1}. Approximately 100% of the plastic work is converted to heat, which is seen clearly at true strain values above 15%, and is assumed to continue past the final true strain of testing (~23%). This value is consistent with the 80-100% range seen in high rate tests in literature (please refer to sections 9.1 and 6.1.1 for further discussion). Looking at figure 9-9, the internal energy decreases from 3 kJ/kg, to values near 0 kJ/kg as the true strain increases.

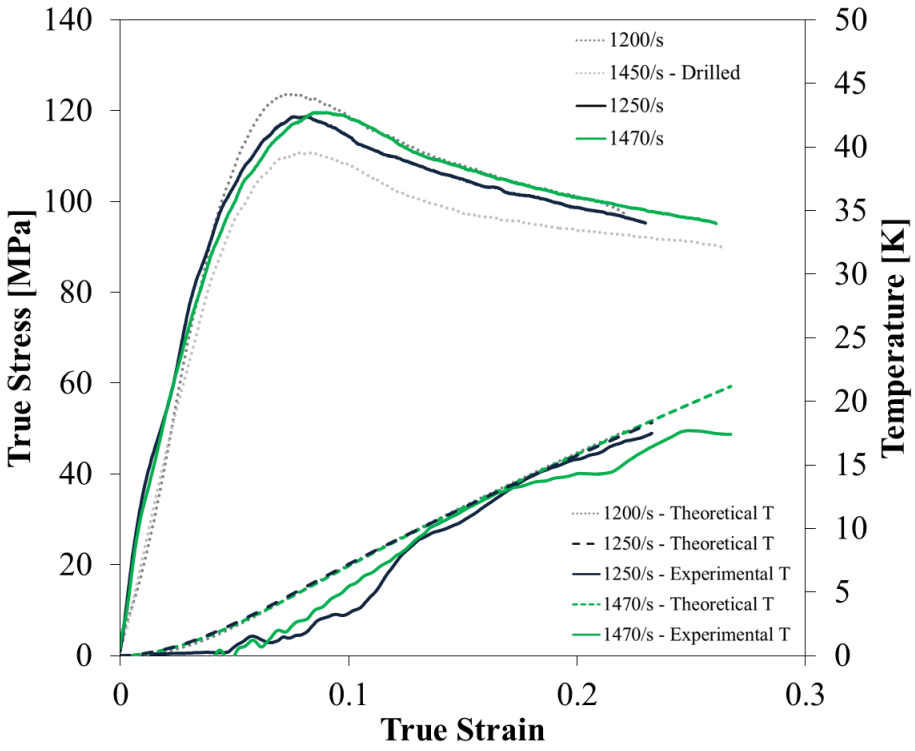


Figure 9-8: PPVC-2 true stress-true strain behavior and corresponding temperature rise under uniaxial compression at rates of 1250 s^{-1} (black) and 1470 s^{-1} (green), and relevant theoretical temperature rises. Representative true stress-true strain behaviors of a non-intruded PPVC-2 specimen and PPVC-2 'threaded' specimen (hole drilled into specimen, although without thermocouples) at rates of 1200 and 1450 s^{-1} are also presented for comparison. Temperature rises were measured using the threaded thermocouple method (figure 9-6b).

Figure 9-8 demonstrates representative behavior of PPVC-2 where a clear decrease in yield stresses is visible as a result of the holes placed in the specimens used for high rate testing. 1470 s^{-1} strain rates of a drilled temperature measurement specimen, allow for yield stresses slightly lower than what is found in representative 1200 s^{-1} true stress-true strain behavior for PPVC-2. Representative 1400 s^{-1} true stress-true strain behavior produces yield stresses at approximately 130 MPa, thus the drilled holes and thermocouple insertions demonstrate a drop in yield stress of approximately 10 MPa, and we see that without thermocouple insertion, this value increases two times the amount, to 20 MPa. Additional literature (Rittel, 1999) has been used to investigate whether strain concentrations are caused by the inserted thermocouples in amorphous polymers (PC, in this case), and have shown that shear localization in the vicinity of the thermocouple does not exist. Thus, regardless of the

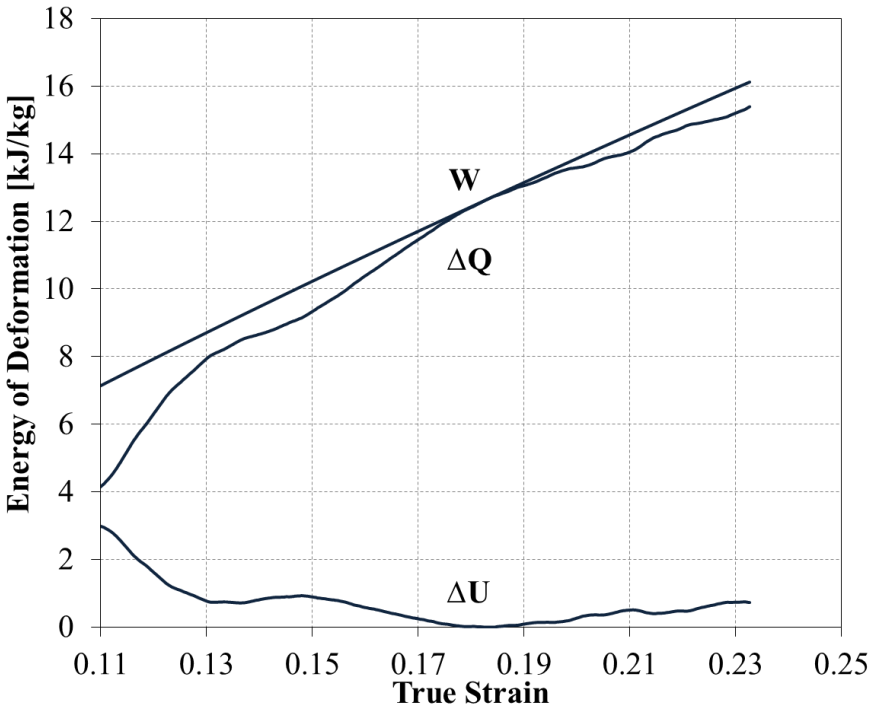


Figure 9-9: PPVC-2 energies of deformation at 1250 s^{-1} strain rate in uniaxial compression starting at 11% true strain to allow for a more clear comparison of the deformation energies: total work (W), heat of deformation (ΔQ), and internal or 'stored' energy (ΔU).

marked change in yield stress with respect to the insertion of thermocouples, the overall behavior is relatively consistent with unhampered specimens. Although these results were considered successful, the results still demonstrated a need for improvement in obtaining a better agreement between polymer behavior and polymer-thermocouple behavior. The idea of sandwiching a thermocouple between two cylindrical specimens was encouraging after the changes in material behavior were revealed. The results of the sandwich method are presented in figure 9-10. The sandwich method proved promising, in that the temperature rise results were similarly successful in measuring the temperature rise of PPVC-2 at high strain rates, garnering nearly equivalent results: ~100% of the plastic work is shown to be converted to heat and contribute to the specimen temperature rise. The more telling result of this study is the good agreement between true stress-true strain behavior at 2100 s^{-1}, of the sandwiched specimen, and 2000 s^{-1}, of PPVC-2 without modification. The yield stresses of the two specimens are nearly identical at 140 MPa, and the post yield softening increases only

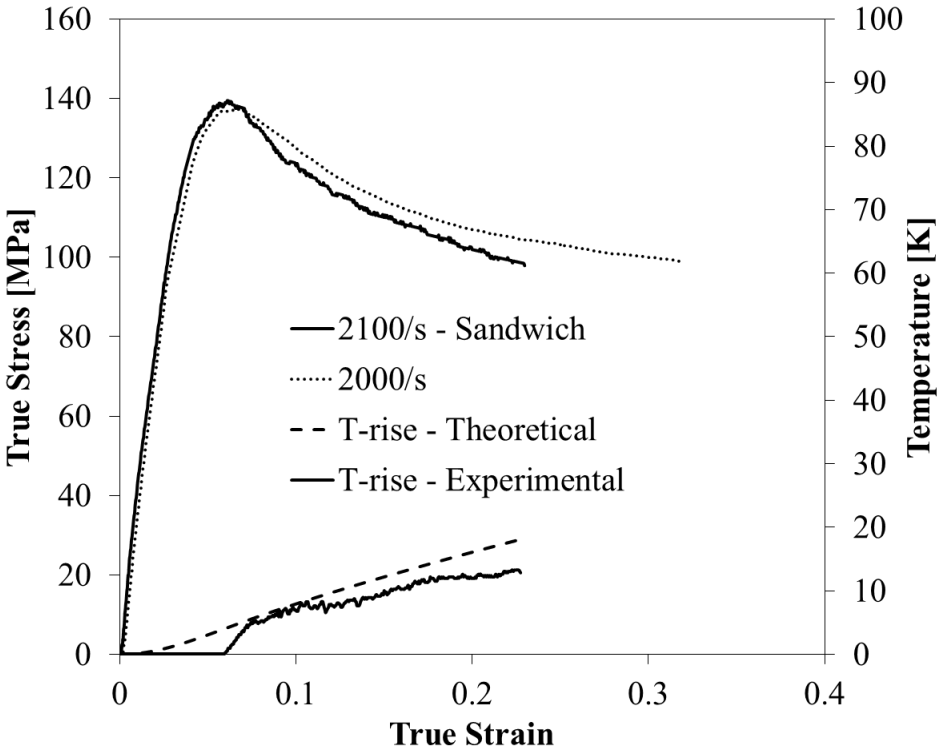


Figure 9-10: PPVC-2 representative true stress-true strain behavior and corresponding temperature rise under uniaxial compression at a rate of 2100 s^{-1}, and the relevant theoretical temperature rise. Representative true stress-true strain behavior of a non-intruded PPVC-2 specimen at 2000 s^{-1} is included for comparison. Temperature rises were measured using the sandwich thermocouple method (figure 9-6a). Note: the rapid increase in temperature at yield is consistent with observations in the literature, e.g. Chou et al., 1973.

slightly, by less than 1%. In addition, post-mortem analysis proved useful for further observations: the drilled PPVC-2 specimens tended to fracture (after post-test reloading on the Hopkinson bar) and sandwiched specimens did not fracture (which is consistent with PPVC-2 unmodified specimen response). This improved agreement in true stress-true strain behavior, and the consistency in the measured temperature rise between results, demonstrates the advantages in using a 'sandwich' method as opposed to the more intrusive method involved with drilling a hole in a specimen.

Moderate Rate

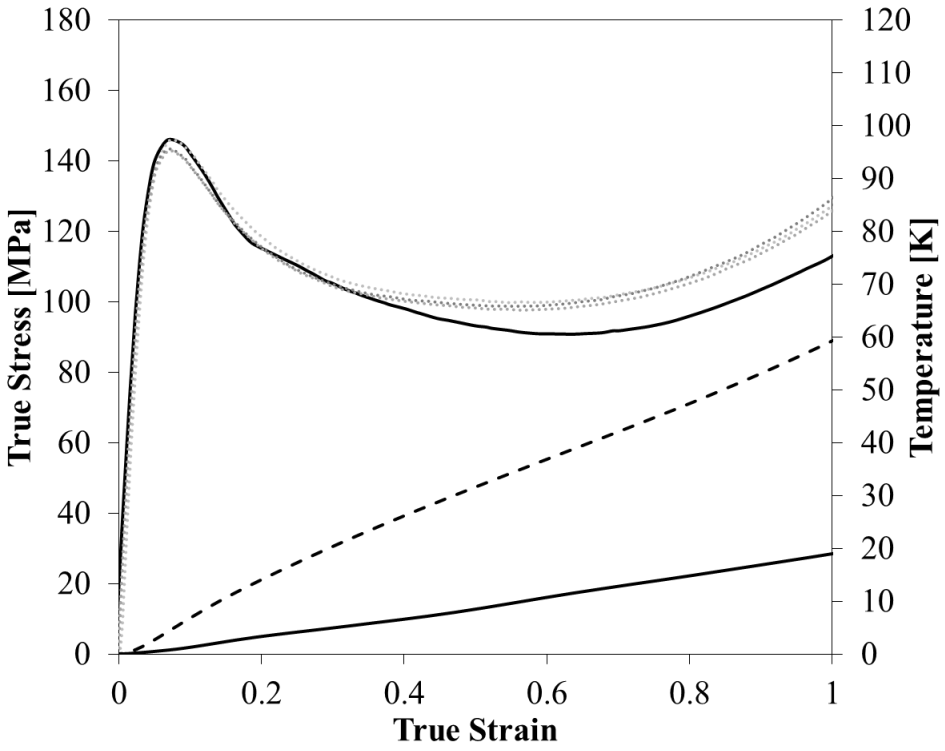
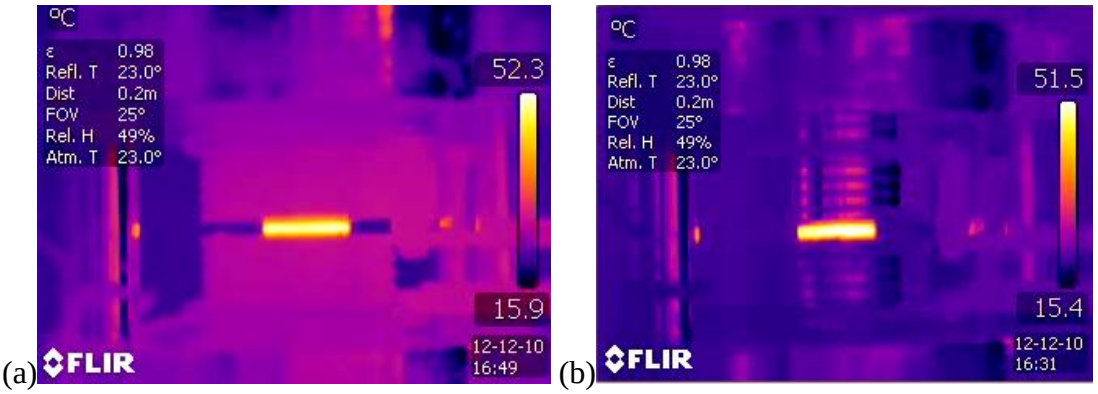
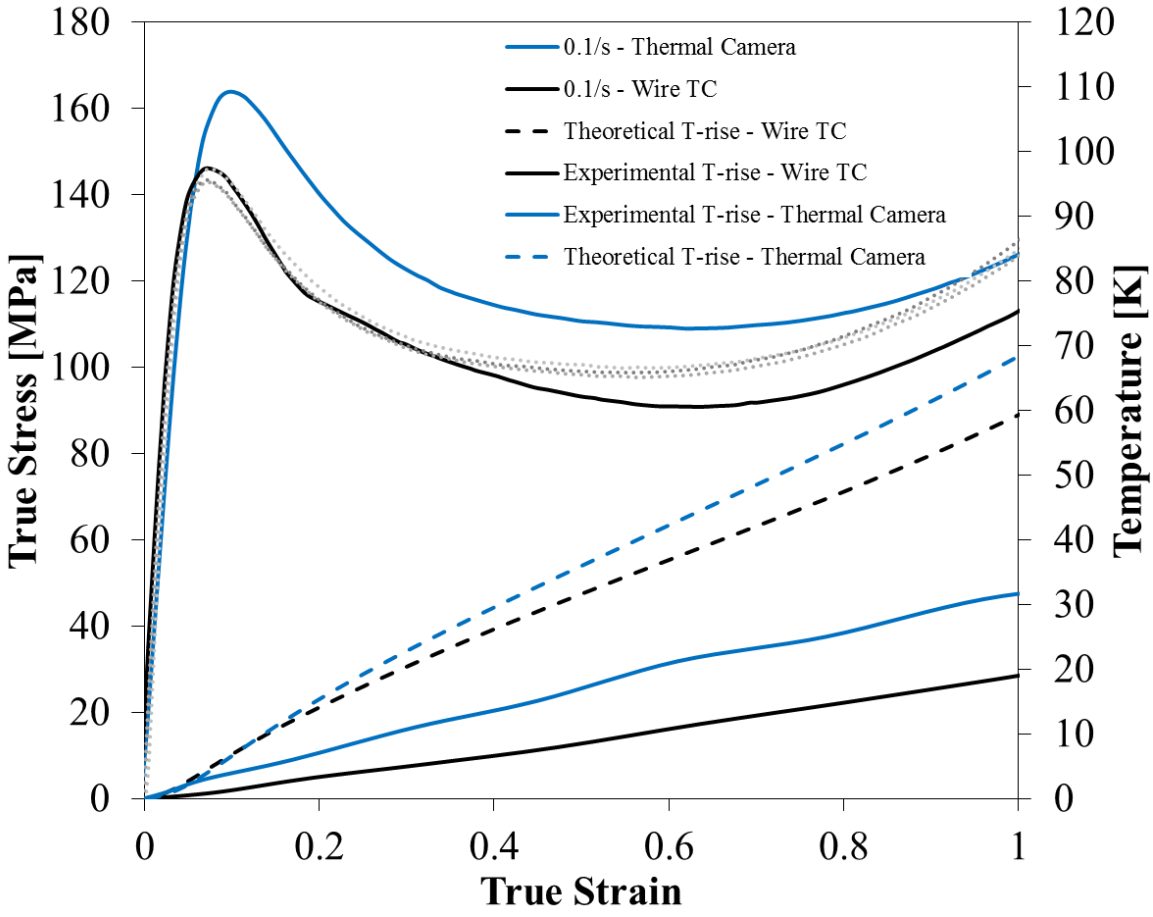


Figure 9-11: PMMA true stress-true strain behavior and corresponding temperature rise (solid lines) under uniaxial compression at a rate of 0.1 s^{-1}, and the theoretical temperature rise (dashed line). Representative true stress-true strain behaviors of unmodified PMMA specimens at the 0.1 s^{-1} are included for comparison (grey dotted lines). Temperature rises were measured using the threaded thermocouple method.

Experimental results from moderate rate temperature measurement methods were similar to the high rate results in that a sandwich specimen was sought after following the unwelcome changes in true stress-strain behavior which resulted from the drilled-hole and threaded thermocouple technique. Figure 9-11 presents a comparison between unmodified PMMA specimen behavior and the threaded thermocouple technique, as well as its measured temperature rise compared with the theoretical temperature rise. The true stress-strain behavior of the drilled specimen veers of the unmodified PMMA behavior by approximately 10-15 MPa starting at 50% true strain and increasing in value. The temperature rise in figure 9-11 was not convincing. The temperature rise measured was far less than that assumed in the initial simulation experiment, as well as in literature, which initially had been attributed to the



(a) (b)



(c)

Figure 9-12: Thermal camera image (a) at just above 95% true strain during insulating platen testing and (b) just below 95% true strain during metal platen testing. (c) PMMA true stress-true strain behavior and corresponding temperature rise (solid lines) via thermal camera (blue) and threaded thermocouple methods (wire) under uniaxial compression at a rate of 0.1 s^{-1}.

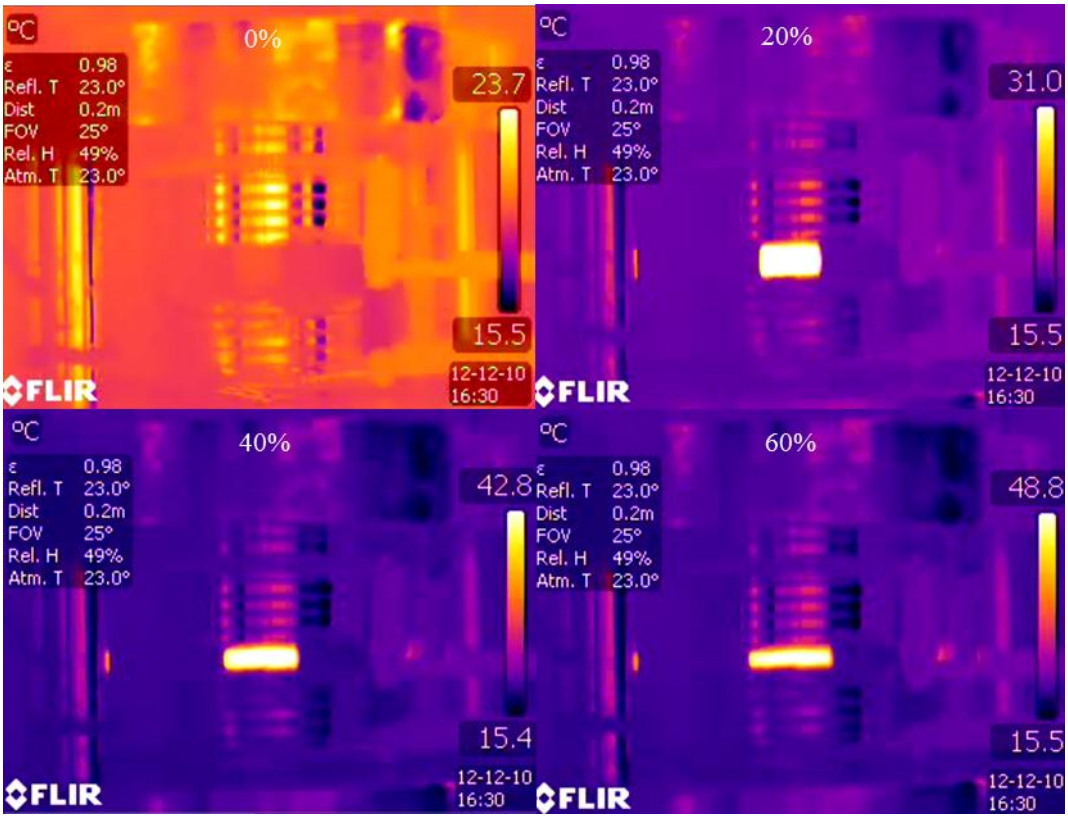


Figure 9-13: Photographs from PMMA deformation during thermal camera testing at 0, 20, 40, and 60% true strain. The thermal camera uniaxial compression test presented here is the same as that presented in figure 9-12.

β factor being less than 1, or the conditions not being fully adiabatic. Further investigations were performed using a thermal camera to look for temperature gradients in the specimen, none were observed (see figure 9-12), and replacing the steel anvils with more insulating, plastic, ones, which made no difference to the measured stress-strain response. Although these experiments are not wholly conclusive, they indicated that the experimental conditions were in fact adiabatic, and therefore that either the β factor (the fraction of plastic work converted to heat) is less than 1 or the heat capacity changes when the specimen yields. The rate at which a material transitions from isothermal to adiabatic deformation can also theoretically be calculated using the method presented in Chapter 5: PMMA's transition is calculated as 0.07 s^{-1}, which agrees well with the transition between 0.01 s^{-1} and 0.1 s^{-1} seen in its rate dependent true stress-true strain behavior (presented in Chapter 6).

In addition, the temperature rise measured by the thermal camera presented a higher experimental temperature rise observing a beta factor of 43%, versus a beta factor of 32% for the specimen with embedded thermocouple wires, (this ratio inherently considers the larger yield stress of the specimens used in these experiments[21]), which is presented in figure 9-12c. The temperature rise from the threaded temperature measurement technique is not only lower than thermal camera measurement, but also lower to what is expected from comparisons to literature. Referring back to figure 9-4, at 70% true strain, we see values surround 25 K, where in figure 9-12 we see a PMMA temperature rise approximately 10 K lower at the same strain.

Non-intrusive methods were sought to reach a better agreement between true stress-true strain behaviors seen in high rate testing using PPVC-2 (figure 9-10). Sandwich techniques were reviewed and the copper constantan thermocouple method, presented in figure 9-7, took shape. The experimental results of this technique are presented in section 6.1.3, and here in figure 9-14 for completeness, with the experimentally measured and theoretically calculated temperature rises compared to each other. These curves result in gradients of approximately 0.68 K/% true strain (theoretical) and 0.52 K/% true strain (experimental). This comparison was then extended to studying the energies of deformation during a 0.1 s^{-1} rate of uniaxial compression (figure 9-15). Approximately 75% of the work was converted into heat (commonly the 'β-factor') during 0.1 s^{-1} testing. This value is consistent with the 45-100% range seen in literature, which was also seen experimentally in the previous section testing PPVC-2 (please refer to sections 9.1 & 6.1.1 for further discussion). It is noted that at 0.1 s^{-1} testing of PMMA, deformation has recently become

[21] Two different PMMA extruded rods were used in creating test specimens. A rod provided by the USAFRL resulted in specimens having yield stresses of ~140 MPa at 0.1 s^{-1}, and the rod provided by the Department of Engineering Science resulted in specimens having a 20 MPa higher yield stress. Both specimens followed the same gradients of yield stress dependence upon rate and temperature.

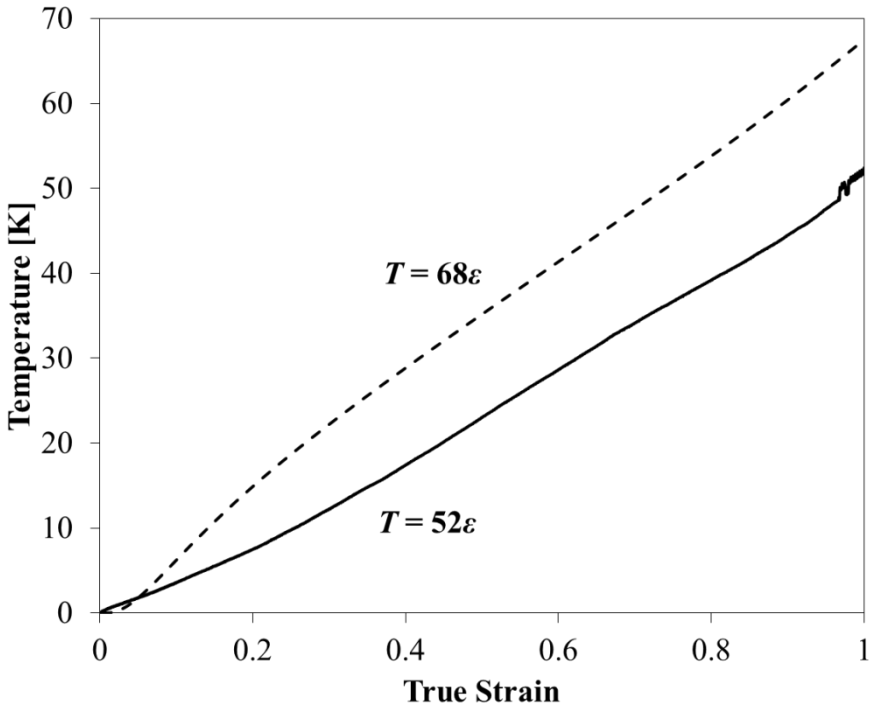


Figure 9-14: PMMA experimentally measured temperature rise (solid line) and theoretical temperature rise (dashed line) during uniaxial compression at 0.1 s^{-1}.

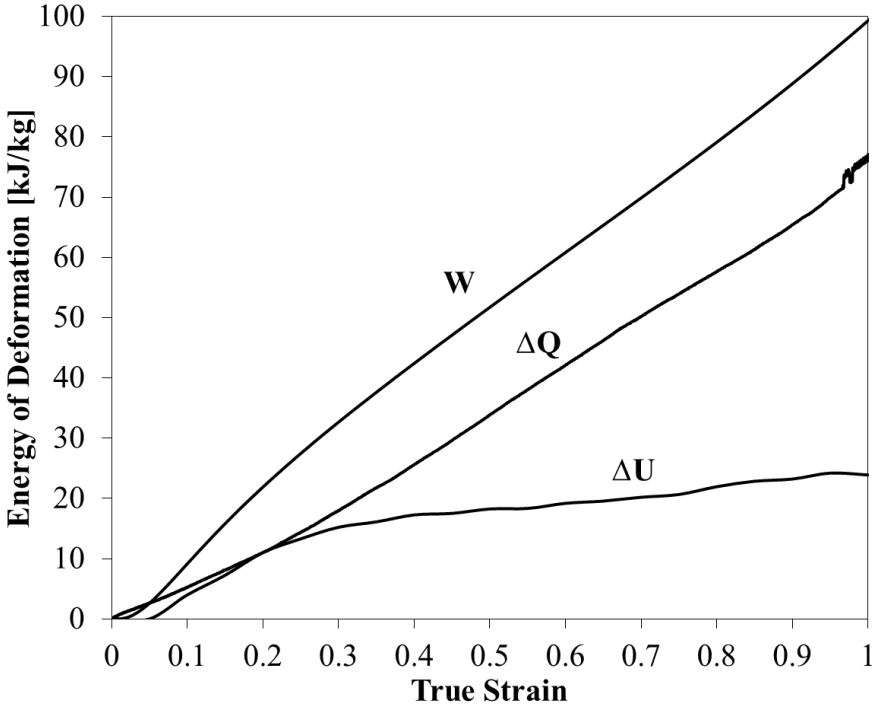


Figure 9-15: PMMA energies of deformation at 0.1 s^{-1} strain rate in uniaxial compression: total work (W), heat of deformation (ΔQ), and internal or 'stored' energy (ΔU). Mechanical work and heat of deformation during testing are calculated from the theoretical and experimentally measured temperature rises in figure 9-11; internal energy is calculated as the difference between the two.

adiabatic in nature with 0.07 s^{-1} being calculated as the characteristic strain rate in adiabatic heating. Looking at figure 9-15, the internal energy (or 'stored energy') marginally increases with increased strain, but more specifically, plateaus with increasing strain, staying between ~15-19 kJ/kg from 30% true strain until the end of testing, which is also an effect which has been seen by other authors in amorphous polymers (see section 6.1.1).

The effectiveness of this novel temperature measurement method is presented in figures 9-16 and 9-17. Namely, good agreement between unmodified and thermocouple specimens are presented in figure 9-16, and the premature fracturing of the threaded specimens compared to the ductile response of PMMA (consistent with unmodified specimens after 0.1 s^{-1} testing) using the T-type sandwich method in figure 9-17. Figure 9-17b presents a clear concentration of fracturing surrounding the drilled hole used for the thermocouple and also an inner circular fracture, approximately 2 mm from the outer edge of the specimen. Figure 9-17a depicts a radially uniform deformation of the thermocouple materials between the two transparent specimen, and no fracturing along the circumference of the specimen.

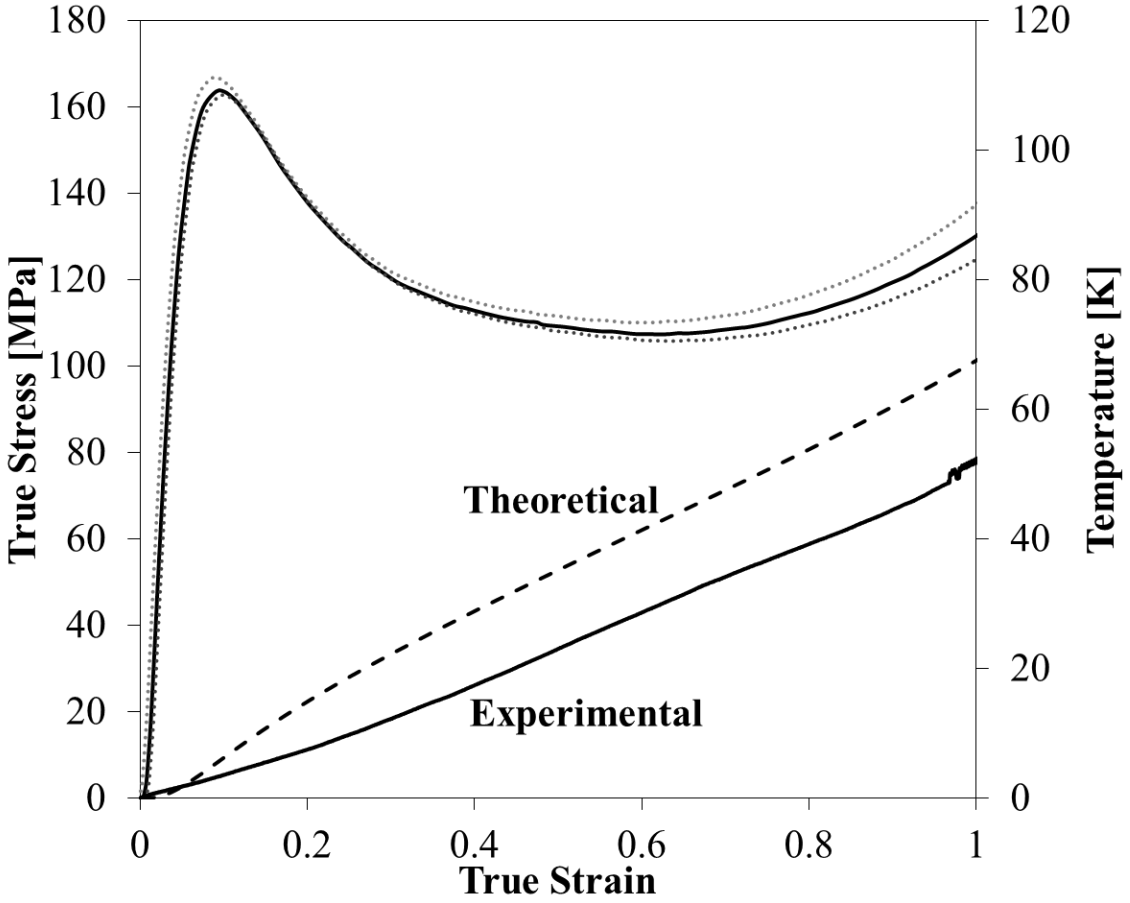
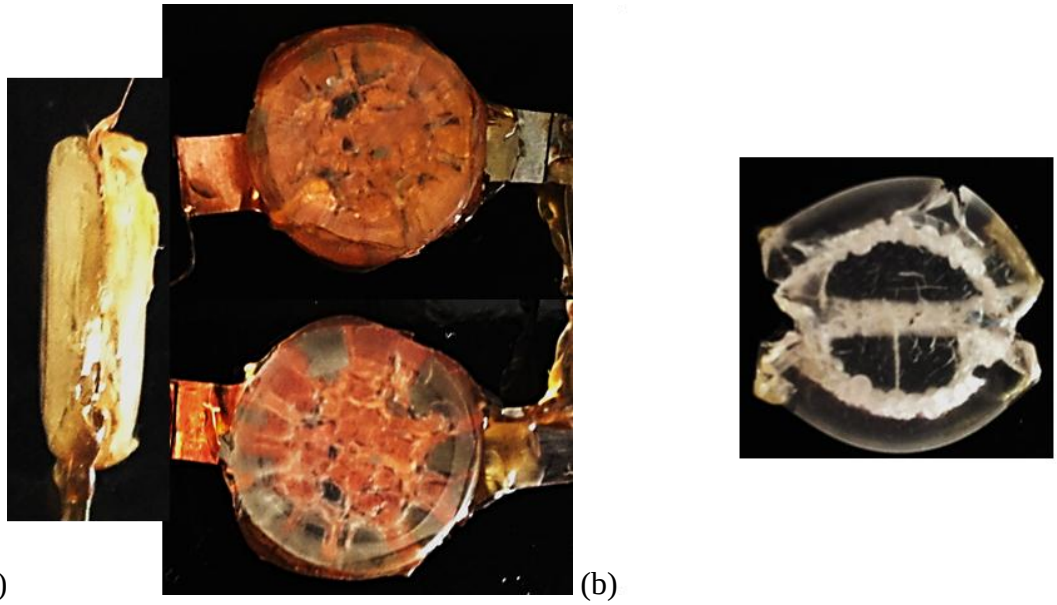


Figure 9-16: PMMA true stress-true strain behavior and a comparison of temperature rises (theoretical versus measured) under uniaxial compression at a rate of 0.1 s^{-1}. Representative true stress-true strain behaviors of PMMA at 0.1 s^{-1} are included for comparison (grey dots).



(a) (b)

Figure 9-17: Representative PMMA post-mortem photographs of (a) the copper-constantan thermocouple method and (b) the threaded thermocouple method.

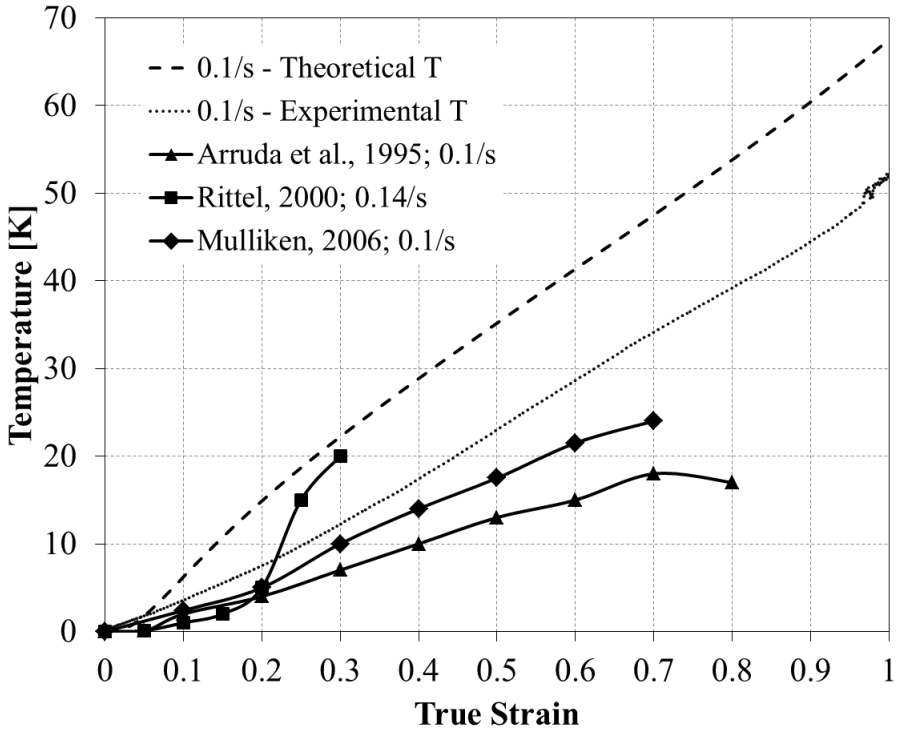


Figure 9-18: Data on the temperature rise in PMMA during uniaxial compression at 0.1 s^{-1} as specified in literature compared to temperature rise data from this thesis (figure 9-14).

Figure 9-18 compares data for the temperature rise of PMMA in the literature to the experimental results found with the novel sandwich-thermocouple temperature measurement method for low to moderate strain rates. The measured temperature rise is in very good agreement to that of Mulliken (2006), which was achieved via IR temperature measurement techniques. These comparisons also present the clear advantage of the novel temperature measurement method in measuring higher strains of deformation. IR techniques are difficult to measure high strains because of the decreased field of view of the specimen which is a result of the platens or bars coming closer together towards the end of compression testing. In addition, as noted by Mulliken (2006), there is no uniformity in the set up and technique for the IR experiment (e.g. differences in the photovoltaic detector, focusing optics), and in addition, there is a lack of consistency in calibration methods, and difficulties in the calibration itself.

9.5 Conclusions

Different temperature measurement methods were reviewed and employed in order to find the most true deformation and temperature rise of the material being studied. In these experiments it was revealed that drilled holes in specimens, used for thermocouples to measure in-situ temperature rises in specimens, were found to decrease the yield stress substantially for PPVC-2, and were found to cause large changes in post-yield behavior and fracturing for PMMA. Temperature measurement results were presented which demonstrated nearly 100% conversion of plastic work was converted to heat at high rates: this confirms the assumption used to apply the simulation method presented in Chapter 5. In addition, a β-factor of approximately 75% was seen in testing PMMA at moderate rates. Both moderate and high rate results were further investigated in analyzing their strain energies of deformation. All temperature results were presented in accompaniment with the true stress-true strain behaviors of the test materials.

In the moderate rate temperature measurement investigation, a novel temperature method was developed for low to moderate strain rates, and found to:

- Give a more accurate temperature measurement than an IR camera or a threaded thermocouple
- Measure temperatures to much higher strains than IR methods
- Provide a nearly identical true stress-true strain response to unmodified specimens
- Avoid premature fracturing seen from embedded thermocouples (in materials which are pseudo-brittle such as PMMA)

Lastly, temperature measurements made here for PMMA were compared with those found in literature at the same strain rate. These consisted of both IR and thermocouple techniques in measuring the temperature rise during deformation.

Chapter 10

Concluding Remarks

This thesis project has been motivated by a desire to achieve a better understanding of the interplay between temperature and strain rate using a model polymer: PVC. The ultimate goal was to be able to predict high rate polymer response by performing experiments at low strain rates. In Chapter 1, the problems inherent in the high rate testing of complex and low impedance materials was introduced, along with the lack of testing machines which spanned impact rates for engineering components (in e.g. medical, aerospace, automotive, and military industries).

In second chapter of this thesis, the significant amount of research in the field of polymer mechanics was reviewed, along with the test methods used to conduct the research, which date back to over sixty years ago. Moreover, this review was coupled with a review of the research in polymer mechanics at high rates of deformation.

Summary of Accomplishments

Rate & Temperature Dependence, & Time-Temperature Equivalence

The third chapter of this thesis presents the outset of the experimental work put forth in this thesis. A sincere and notable accomplishment in this thesis is the large amount of experimental data which has been developed. To note, several materials which do not have DMTA data in literature were presented in this thesis (e.g. PVC materials with high amounts of plasticizer, a new and much more rubbery HTPB material). Moreover, the test methods used in previous research were applied to four different PVC materials, ranging in plasticizer content, with a variety of constitutive behaviors. The materials were chosen with the aim of investigating the rate dependence of different materials which could readily be compared. While performing the experiments and analyses in yield and true stress-true stain behavior, additional analyses were conducted resulting in supplementary investigations (e.g. fractures in high rate behavior, high speed photography, and the complexities of strain rate profiles).

In the fourth chapter, the literature of time-temperature equivalence was reviewed and three different time-temperature equivalence methods were explored over a large temperature range. Building upon the linear formulation of linear time-temperature equivalence by Siviour, a novel methodology of time-temperature equivalence was created in order to separate the β and α influence in high rate and low temperature data. This time-temperature equivalence methodology's significance was underlined when using it to predict the yield and modulus of high rate behavior in the simulation method presented in subsequent chapters.

Modeling & Temperature Measurement

Two literature reviews of rubbery and amorphous polymer models were carried out in order to better understand the significant research which has been conducted in constitutive modeling, and importantly, the constitutive models which developed from these investigations and their underlying theories. After the review, two models were applied to

experimental data presented previously in Chapter 3 of this thesis: the Ogden model for rubbers and a Ree-Eyring based-model which has recently been built upon by Mulliken and Boyce. Ogden model fitted all rubbery PVC and PPVC data with exceptional agreement by capturing the subtleties of the effects of the network back stress. The effects of the shear modulus were additionally investigated in its (corrected) temperature dependent and rate dependent effects. The differences between the application of a one-term and two-term model were also noted in the rubbery polymer investigation. Unplasticized PVC true stress-true strain behavior in uniaxial compression was captured by using the model presented in Mulliken and Boyce (2006). A probability distribution was developed in order to generate a continuous function to describe DMTA data for the amorphous polymer model which was used. The model was unable to capture the detail, or curvature, of the yield stress in each comparison of model vs. experiment, which is a consideration for future work. Within this investigation, an 'isothermal' high rate stress-strain curve was produced and compared to isothermal low temperature quasi-static behavior with encouraging results with respect to simulation method application.

In Chapter 9, different temperature methods were reviewed and applied to high rate behavior in PPVC-2 and moderate behavior in PMMA. Emerging from this investigation was a novel temperature measurement method for moderate rates of deformation. This method found to: give more accurate temperature measurements than an IR camera or a threaded thermocouple, measure temperatures to much higher strains than IR methods, provide a nearly identical true stress-true strain response to unmodified specimens, and avoid premature fracturing seen from embedded thermocouples (in materials which are pseudo-brittle such as PMMA). In this chapter, PMMA temperature measurements measured experimentally were compared with those found in literature at the same strain rate. These consisted of both IR

and thermocouple techniques in measuring the temperature rise during deformation, which made clear the large-strain advantages of the novel temperature measurement method.

Simulation & Prediction of High Rate Deformation

An experimental method for simulating behavior spanning from low to high rates of deformation was proposed and applied to polyvinyl chloride with 20wt% DINP plasticizer content in Chapter 5. This method simulated all behaviors with exceptionally good agreement, and demonstrated the benefits of avoiding physical complications inherent in high rate testing while gathering critical constitutive information without the need for changing the material testing technique. High rate and moderate rate behavior of two contrasting polymers were simulated in Chapters 6: PC – increases in strain hardening and decreases in strain softening with increasing rate, while being insensitive to temperature changes; and PMMA – increases in strain softening and decreases in strain softening, while being very sensitive to changes in temperature. In this study the simulation method agreed incredibly well with PMMA data, in assuming 100% of the plastic work was converted to heat, and PC the opposite effect was observed, in that regardless of a measured temperature rise which demonstrated 100% dissipation of heat, post-yield behavior did not agree well with this temperature rise implemented in simulation. Importantly, the effects in the theoretical amount of plastic work converted to heat were further investigated in PC, with a beta value of 5% capturing high rate behavior, and a novel temperature measurement method was created in studying the thermodynamic effects of PMMA, presented in Chapter 9, which included a study in the energies of deformation. This temperature measurement allowed for an application of the experimental temperature rise to the simulation of PMMA's moderate rate behavior, although the measured value of 75% conversion of work to heat produced to large of a stress for the post-yield response. It was concluded, that in PMMA all of the mechanical

work must be replicated by heat in order to capture the strain softening (which only a percentage of is caused by thermal softening) at these rates.

In the seventh chapter of this thesis, the temperature- and rate-dependent behavior of HTPB and PBS were studied via DMTA, compression, and tension testing using the Brazilian test method. From these investigations a novel piezoelectric SHPB strain measurement system was developed for testing soft materials at high rates of deformation. This piezoelectric method employed the advantageous PZT as the piezoelectric material, and allowed for a large amount of experimental data to be accrued on a much more rubbery HTPB material, compared to those found in literature, at high rates. In addition to this, the Brazilian test method was learnt and applied to PBS, in order to study composites in tension at high rates. High rate deformation in tension was presented with photographs taken from a high speed camera, and also with DIC software analysis in demonstrating relevant displacements. Importantly, ESEM photographs during low temperature testing at quasi-static rates were presented to demonstrate the micro-scale debonding which occurs in PBS, while also illustrating the capability of using the simulation method in accompaniment with ESEM-scale imaging for greater detail in high rate analysis. In addition to this, the simulation method presented in Chapter 5 of this thesis was applied successfully to capture compression behavior and predict tension behavior at high rates of strain. Most importantly, the results presented in Chapter 7 of this thesis successfully achieve the goal of this thesis: to predict the high rate behavior of difficult-to-characterize materials (e.g. composites, in this case a composite using a binder with a very low T_g) via low rate deformation in order to allow for the use of micro-scale imaging tools (e.g. scanning electron microscopes (SEM) and X-ray tomography) to study and better understand these materials' high rate behavior.

References

Al-Maliky, N., Fernandez, J., & Parry, D. (1998). Drops in the flow stress of semi-crystalline polymers at very high rates of strain. *Journal of materials science letters*, *17*, 1141–1143.

Al-Maliky, N., & Parry, D. (1996). A freely expanding ring technique for measuring the tensile properties of polymers. *Measurement Science and Technology*, *7*, 746–752.

Arruda, E., & Boyce, M. (1993). Evolution of plastic anisotropy in amorphous polymers during finite straining. *International Journal of Plasticity*, 697–720.

Arruda, E. M., & Boyce, M. C. (1993). A three-dimensional constitutive model for the large stretch behavior of rubber elastic materials. *Journal of the Mechanics and Physics of Solids*, *41*, 389–412.

Arruda, E. M., Boyce, M. C., & Jayachandran, R. (1995). Effects of strain rate, temperature and thermomechanical coupling on the finite strain deformation of glassy polymers. *Mechanics of Materials*, *19*, 193–212.

Arruda, E. M., Boyce, M. C., & Quintus-Bosz, H. (1993). Effects of initial anisotropy on the finite strain deformation behavior of glassy polymers. *International Journal of Plasticity*, *9*, 783–811.

Ashby, M. F., & Jones, D. R. (2005). *Engineering Materials 1: An Introduction to Properties, Applications and Design* (Third.). Oxford, UK: Elsevier Butterworth-Heinemann.

Awaji, H., & Sato, S. (n.d.). Diametral Compressive Testing Method. *Journal of Engineering Materials and Technology*, *101*, 139–147.

Balzer, J. E., Siviour, C. R., Walley, S. M., Proud, W. G., & Field, J. E. (2004). Behaviour of ammonium perchlorate-based propellants and a polymer-bonded explosive under impact loading. *Proceedings of the Royal Society A: Mathematical, Physical and Engineering Sciences*, *460*, 781–806.

Baragar, D. L. (1987). The high temperature and high strain-rate behaviour of a plain carbon and an HSLA steel. *Journal of Mechanical Working Technology*, *14*, 295–307.

Bauwens, J. C. (1967). Déformation plastique des hauts polymères vitreux soumis á un système de contraintes quelconque. *Journal of Polymer Science Part A-2: Polymer Physics*, *5*, 1145–1156.

Bauwens, J. C. (1971). Relation between the compression yield stress of poly(vinyl chloride) and the loss peak in the beta-transition range. *J. Polymer Sci.: Part C*, *133*, 123–133.

Bauwens, J. C. (1972). Relation between the compression yield stress and the mechanical loss peak of bisphenol-A-polycarbonate in the Beta transition range. *Journal of Materials Science*, *7*, 577–584.

Bauwens, J. C. (1980). Attempt to correlate the formation of free volume and the plastic deformation process in glassy polymers. *Polymer*, *21*, 699–705.

Bauwens, J. C., Bauwens-Crowet, C., & Homès, G. (1969). Tensile yield- • stress behavior of poly (vinyl chloride) and polycarbonate in the glass transition region. *Journal of Polymer Science: Part A-2*, *7*, 1745–1754.

Bauwens-Crowet, C. (1973). The compression yield behaviour of polymethyl methacrylate over a wide range of temperatures and strain-rates. *Journal of Materials Science*, *8*, 968–979.

Bauwens-Crowet, C., Bauwens, J. C., & Homès, G. (1969). Tensile yield-stress behavior of glassy polymers. *Journal of Polymer Science: Part A-2*, *7*, 735–742.

Bauwens-Crowet, C., Bauwens, J. C., & Homès, G. (1972). The temperature dependence of yield of polycarbonate in uniaxial compression and tensile tests. *Journal of Materials Science*, *7*, 176–183.

Bicerano, J. (2002). *Prediction of Polymer Properties* (Third.). New York, USA: Marcel Dekker.

Blumenthal, W. R., Cady, C., Lopez, M., Gray III, G., & Idar, D. (2002). Influence of Temperature and Strain Rate on the Compressive Behavior of PMMA and Polycarbonate Polymers. *AIP Conference Proceedings*, *620*, 665–668.

Bouvard, J. L., Francis, D. K., Tschopp, M. a., Marin, E. B., Bammann, D. J., & Horstemeyer, M. F. (2013). An internal state variable material model for predicting the time, thermomechanical, and stress state dependence of amorphous glassy polymers under large deformation. *International Journal of Plasticity*, *42*, 168–193.

Bouvard, J. L., Ward, D. K., Hossain, D., Marin, E. B., Bammann, D. J., & Horstemeyer, M. F. (2010). A general inelastic internal state variable model for amorphous glassy polymers. *Acta Mechanica*, *213*, 71–96.

Bowden, F., & Yoffe, A. (1952). *Initiation and growth of explosion in liquids and solids*. Cambridge, UK: Cambridge Univ Press.

Bowden, F., & Yoffe, A. (1958). *Fast reactions in solids*. London, UK: Butterworth.

Bowden, P. (1973). The Yield Behaviour of Glassy Polymers. In R. N. Haward (Ed.), *The Physics of Glassy Polymers* (pp. 279–280). London: Applied Science Publishers Ltd.

Boyce, M., & Arruda, E. (1990). An experimental and analytical investigation of the large strain compressive and tensile response of glassy polymers. *Polymer Engineering & Science*, *30*, 1288-1298.

Brown, E. N., Willms, R. B., Gray, G. T., Rae, P. J., Cady, C. M., Vecchio, K. S., Martinez, M. Y. (2007). Influence of Molecular Conformation on the Constitutive Response of Polyethylene: A Comparison of HDPE, UHMWPE, and PEX. *Experimental Mechanics*, *47*, 381–393.

Brown, R. (1999). Dynamic mechanical (thermal) analysis. In *Handbook of Polymer Testing - Physical Methods* (pp. 501–530). Marcel Dekker.

Buckley, C. P., & Jones, D. C. (1995). Glass-rubber constitutive model for amorphous polymers near the glass transition. *Polymer*, *36*, 3301–3312.

Cady, C. M., Blumenthal, W., Gray III, G., & Idar, D. (2003). Determining the constitutive response of polymeric materials as a function of temperature and strain rate. In *Journal de Physique IV (Proceedings)* (Vol. 110, pp. 27–32).

Cady, C. M., Blumenthal, W. R., & Gray III, G. (2006). Mechanical Properties of Plastic-Bonded Explosive Binder Materials as a Function of Strain-Rate and Temperature. *Polymer Engineering and Science*, *46*, 812–819.

Cai, J., Walley, S. M., Hunt, R., Proud, W. G., Nesterenko, V., & Meyers, M. (2008). High-strain, high-strain-rate flow and failure in PTFE/Al/W granular composites. *Materials Science and Engineering: A*, *472*, 308–315.

Calvert, F. C., & Johnson, R. (1859). On the hardness of metals and alloys. *Philos. Mag.*, *17*(4th Ser.), 114–121.

Carneiro, F., & Barcellos, A. (1949). Résistance à la traction des bétons. *RILEM Bull.*, *13*, 98–125.

Chen, W., Zhang, B., & Forrestal, M. J. (1999). A Split Hopkinson Bar technique for low-impedance materials. *Experimental Mechanics*, *39*, 81–85.

Chen, W., Lu, F., & Zhou, B. (2000). A quartz-crystal-embedded split Hopkinson pressure bar for soft materials. *Experimental Mechanics*, *40*, 1–6.

Chou, S., Roberston, K., & Rainey, J. (1973). The Effect of Strain Rate and Heat Developed During Deformation on the Stress-Strain Curve Of Plastics. *Experimental Mechanics*, *13*, 422–432.

Chree, C. (1889). The Equations of an Isotropic Elastic Solid in Polar and Cylindrical Co-ordinates. *Tran. Cambridge Phil Soc.*, *14*, 250–369.

Coleman, B. D. (1967). Thermodynamics with Internal State Variables. *The Journal of Chemical Physics*, *47*, 597.

Davies, E., & Hunter, S. (1963). The dynamic compression testing of solids by the method of the split Hopkinson pressure bar. *Jounal of the Mechanics and Physics of Solids*, *I*, 155–179.

Dioh, N., & Ivankovic, A. (1994). The high strain rate behaviour of polymers. *Le Journal de Physique IV*, *4*, C8–119 – C8–124.

Dioh, N. N., Leevers, P. ., & Williams, J. . (1993). Thickness effects in split Hopkinson pressure bar tests. *Polymer*, *34*, 4230–4234.

Drodge, D. R., Williamson, D. M., Palmer, S. J. P., Proud, W. G., & Govier, R. K. (2010). The mechanical response of a PBX and binder: combining results across the strain-rate and frequency domains. *Journal of Physics D: Applied Physics*, *43*, 1–7.

Field, J. E., Swallowe, G. M., & Heavens, S. N. (1982). Ignition Mechanisms of Explosives during Mechanical Deformation. *Proceedings of the Royal Society A: Mathematical, Physical and Engineering Sciences*, *382*, 231–244.

Field, J. E., Walley, S. M., Bourne, N. K., & Huntley, J. M. (1994). Experimental methods at high rates of strain. *Le Journal de Physique IV*, *04*, C8–3–C8–22.

Field, John E, Walley, S. M., Proud, W. G., Goldrein, H. T., & Siviour, C. R. (2004). Review of experimental techniques for high rate deformation and shock studies. *International Journal of Impact Engineering*, *30*, 725–775.

Foot, J. S., Truss, R. W., Ward, I. M., & Duckett, R. a. (1987). The yield behaviour of amorphous polyethylene terephthalate: An activated rate theory approach. *Journal of Materials Science*, *22*, 1437–1442.

Furmanski, J., Brown, E. N., Clements, B., Cady, C. M., & Gray, G. T. (2012). Large-strain time-temperature equivalence in high density polyethylene for prediction of extreme deformation and damage. *EPJ Web of Conferences*, *26*, 01057.

Furmanski, J., Cady, C. M., & Brown, E. N. (2013). Time-temperature equivalence and adiabatic heating at large strains in high density polyethylene and ultrahigh molecular weight polyethylene. *Polymer*, *54*, 381–390.

Furmanski, J., Trujillo, C. P., Martinez, D. T., Gray, G. T., & Brown, E. N. (2012). Dynamic-Tensile-Extrusion for investigating large strain and high strain rate behavior of polymers. *Polymer Testing*, *31*, 1031–1037.

Garg, M., Mulliken, a. D., & Boyce, M. C. (2008). Temperature Rise in Polymeric Materials During High Rate Deformation. *Journal of Applied Mechanics*, *75*, 011009.

Gerlach, R., Siviour, C. R., Petrinic, N., & Wiegand, J. (2008). Experimental characterisation and constitutive modelling of RTM-6 resin under impact loading. *Polymer*, *49*, 2728–2737.

Gerlach, R., Siviour, C. R., Wiegand, J., & Petrinic, N. (2012). In-plane and through-thickness properties, failure modes, damage and delamination in 3D woven carbon fibre composites subjected to impact loading. *Composites Science and Technology*, *72*, 397–411.

Glasstone, S., Laidler, K., & Eyring, H. (1941). *The theory of rate processes: the kinetics of chemical reactions, viscosity, diffusion and electrochemical phenomena*. (McGraw-Hill, Ed.). New York, USA.

Gorham, D. (1989). Specimen inertia in high strain-rate compression. *Journal of Physics D: Applied Physics*, *22*, 1888–1893.

Grantham, S. G., Siviour, C. R., Proud, W. G., Field, J. E., & Road, M. (2004). High-strain rate Brazilian testing of an explosive simulant using speckle metrology. *Measurement Science and Technology*, *15*, 1–4.

Gray, G. T., Idar, D., Blumenthal, W., Cady, C., & Peterson, P. D. (1998). High-and low-strain rate compression properties of several energetic material composites as a function of strain rate and temperature. In *Proceedings of the eleventh international detonation symposium.* (pp. 76–84). Boston, USA.

Gray III, G. (2000). Classic split-Hopkinson pressure bar testing. In H. Kuhn & D. Medlin (Eds.), *ASM Handbook - Mechanical Testing and Evaluation, vol. 8* (pp. 462–476). Materials Park, OH: ASM International.

Gray III, G., & Blumenthal, W. (2000). Split-Hopkinson pressure bar testing of soft materials. In H. Kuhn & D. Medlin (Eds.), *ASM Handbook - Mechanical Testing and Evaluation, vol. 8* (pp. 488–96). Materials Park, OH: ASM International.

Gueguen, O., Richeton, J., Ahzi, S., & Makradi, a. (2008). Micromechanically based formulation of the cooperative model for the yield behavior of semi-crystalline polymers. *Acta Materialia*, *56*, 1650–1655.

Hamdan, S., & Swallowe, G. M. (1996a). A crossbow system for high-strain-rate mechanical testing. *Measurement Science and Technology*, *7*, 1068–1072.

Hamdan, S., & Swallowe, G. M. (1996b). The strain-rate and temperature dependence of the mechanical properties of polyetherketone and polyetheretherketone. *Journal of Materials Science*, *31*, 1415–1423.

Hasan, O., & Boyce, M. (1995). A constitutive model for the nonlinear viscoelastic viscoplastic behavior of glassy polymers. *Polymer Engineering & Science*, *35*.

Haward, R., & Thackray, G. (1968). The use of a mathematical model to describe isothermal stress-strain curves in glassy thermoplastics. *Roy. Soc. A. Mathematical and Physical Sciences*, *302*, 453–472.

Heijboer, J. (1964). *Physics of Non-Crystalline Solids*. (J. A. Prins, Ed.) (p. 231). Amsterdam: North Holland.

Hill. (1950). *The Mathematical Theory of Plasticity*. Oxford, UK: Oxford University Press.

Hillmansen, S., & Haward, R. N. (2001). Adiabatic failure in polyethylene. *Polymer*, *42*, 9301–9312.

Hillmansen, S., & Hobeika, S. (2000). The effect of strain rate, temperature, and molecular mass on the tensile deformation of polyethylene. *Polymer Engineering and Science*, *40*, 481–489.

Ho, S. Y. (1992). Impact ignition mechanisms of rocket propellants. *Combustion and Flame*, *91*, 131–142.

Hockett, J., & Lindsay, N. (1971). Cam plastometer data acquisition system. *Journal of Physics E: Scientific Instruments*, *4*, 520.

Hopkinson, B. (1905). The Effects of Momentary Stresses in Metals. *Proc. R. Soc. (London) A*, *74*, 498.

Hopkinson, B. (1914). A Method of Measuring the Pressure Produced in the Detonation of High Explosives or by the Impact of Bullets. *Philos. Transactions of the Royal Society London A*, *212*, 437–456.

Hopkinson, J. (1901). *Original paers by J. Hopkinson*. *Cambridge Univ. Press* (pp. 316–324). Cambridge, UK: Cambridge Univ Press.

Illers, Kilian, & Kosfeld. (1961). Physical Properties of High Polymers. *Annual Review of Physical Chemistry*, *12*, 49–82.

Jordan, J. L., Foley, J. R., & Siviour, C. R. (2008). Mechanical properties of Epon 826/DEA epoxy. *Mechanics of Time-Dependent Materials*, *12*, 249–272.

Jordan, J. L., Siviour, C. R., & Woodworth, B. (2012). High strain rate mechanical properties of glassy polymers, *191*, 191–194.

Jordan, J. L., Spowart, J., Siviour, C. R., Woodworth, B. T., & Kendall, M. J. (2013). Mechanics of Particulate Composites with Glassy Polymer Binders in Compression. *Submitted to the Royal Society (Special Issue)*.

Kendall, M. J., & Siviour, C. R. (2012). Strain rate dependence in plasticized and un-plasticized PVC. *EPJ Web of Conferences*, *26*, 02009.

Kendall, M. J., & Siviour, C. R. (2013a). Strain Rate and Temperature Dependence in PVC. In *SEM 2013 Annual Conference* (p. 526).

Kendall, M. J., & Siviour, C. R. (2013b). Experimentally simulating adiabatic conditions: Approximating high rate polymer behavior using low rate experiments with temperature profiles. *Polymer*, *54*, 5058–5063.

Kendall, M. J., & Siviour, C. R. (2013c). Experimentally Simulating High Rate Behaviour: Rate and Temperature Effects in Polycarbonate and PMMA. *Proceedings of the Royal Society*, (Special Issue).

Kendall, M. J., Froud, R. F., & Siviour, C. R. (2013d). Novel Temperature Measurement Method & Thermodynamic Investigations for Amorphous Polymers during High Rate Deformation. *Measurement Science and Technology, Submitted*.

Kirkaldy, D. (1862). *Results of an Experimental Enquiry into the Comparitive Tensile Strength and Other Properties of Various Kinds of Wrought Irons and Steel etc.* Glasgow, UK: Bell & Bain.

Koerber, H., Xavier, J., & Camanho, P. P. (2010). High strain rate characterisation of unidirectional carbon-epoxy IM7-8552 in transverse compression and in-plane shear using digital image correlation. *Mechanics of Materials*, *42*, 1004–1019.

Kolsky, H. (1949). An investigation into the mechanical properties of materials at very high rates of loading. *Proceedings of the Physical Society. Section B*, *62*, 676–701.

Kuhn. (2000). Tension, Compression, Bend, and Shear Testing. In H. Kuhn & D. Medlin (Eds.), *ASM Handbook - Mechanical Testing and Evaluation*. Materials Park, OH: ASM International.

Labibes, K., Wang, L., Azari, Z., & Pluvinage, G. (1994). Generalization of Split Hopkinson Bar Technique to use Viscoelastic Bars. *Int. J. Impact Engng*, *15*, 669–686.

Lomellini, P. (1992). Williams-Landel-Ferry versus Arrhenius behaviour: polystyrene melt viscoelasticity revised. *Polymer*, *33*, 4983–4989.

Mark, J. (Ed.). (1999). *Polymer Data Handbook*. Oxford, UK: Oxford University Press.

Matthews, G. (1996). Properties of vinyl chloride polymers and copolymers. In *PVC: Production, Properties, and Uses* (p. 52). London, UK: The Institue of Materials.

Mooney, M. (1940). A Theory of Large Elastic Deformation. *J. Appl. Phys.*, *11*, 582.

Mooney, M. (1948). The Thermodynamics of a Strained Elastomer. I. General Analysis. *Journal of Applied Physics*, *19*, 434–444.

Mulliken, a. D., Soong, S., Boyce, M., & Cohen, R. (2006). High-rate thermomechanical behavior of poly (vinyl chloride) and plasticized poly (vinyl chloride). In *Journal de Physique IV (Proceedings)* (Vol. 134, pp. 217–223).

Mulliken, A. D. (2006). *Mechanics of Amorphous Polymers and Polymer Nanocomposites during High Rate Deformation*. Massachussetts Institute of Technology.

Mulliken, A. D., & Boyce, M. C. (2006). Mechanics of the rate-dependent elastic-plastic deformation of glassy polymers from low to high strain rates. *International journal of solids and structures*, *43*, 1331–1356.

Nie, X., Song, B., Ge, Y., Chen, W. W., & Weerasooriya, T. (2009). Dynamic Tensile Testing of Soft Materials. *Experimental Mechanics*, *49*, 451–458.

Ogden, R. W. (1972a). Large Deformation Isotropic Elasticity - On the Correlation of Theory and Experiment for Incompressible Rubberlike Solids. *Proceedings of the Royal Society A: Mathematical, Physical and Engineering Sciences*, *326*, 565–584.

Ogden, R. W. (1972b). Compressible Rubberlike Solids Large deformation isotropic elasticity : on the correlation of theory and experiment for compressible rubberlike solids. *Proceedings of the Royal Society of London. Series A, Mathematical and Physical Sciences*, *328*, 567–583.

Okereke, M. I., Buckley, C. P., & Siviour, C. R. (2012). Compression of polypropylene across a wide range of strain rates. *Mechanics of Time-Dependent Materials*, *16*, 361–379.

Palmer, S. J. P., Field, J., & Huntley, J. (1993). Deformation, strengths and strains to failure of polymer bonded explosives. *Proceedings of the Royal Society of London A*, *440*, 399–419.

Pochhammer. (1876). Uber die fortpflanzungsgeschwindigkeiten kleiner schwingungen in einem unbegrentzen isotropen kreiszylinder. *J. Reine. Angew. Math.*, *81*, 324–336.

Porter, D., & Gould, P. J. (2009). Predictive nonlinear constitutive relations in polymers through loss history. *International Journal of Solids and Structures*, *46*, 1981–1993.

Porter, D., Vollrath, F., & Shao, Z. (2005). Predicting the mechanical properties of spider silk as a model nanostructured polymer. *The European physical journal. E, Soft matter*, *16*, 199–206.

Quintavalla, S. J., & Johnson, S. H. (2004). Extension of the Bergstrom-Boyce Model to High Strain Rates. *Rubber Chemistry and Technology*, *77*, 972–981.

Rabin, Y., & Rittel, D. (1999). A model for the time response of solid-embedded thermocouples. *Experimental Mechanics*, *39*, 132–136.

Rae, P. J., Goldrein, H. T., Palmer, S. J. P., Field, J. E., & Lewis, A. L. (2002). Quasi-static studies of the deformation and failure of / 3-HMX based polymer bonded explosives. *The Royal Society; Proceedings: Mathematical, Physical and Engineering Sciences*, *458*, 743–762.

Regev, A., & Rittel, D. (2008). Simultaneous Transient Temperature Sensing of Impacted Polymers Using Infrared Detectors and Thermocouples. *Experimental Mechanics*, *48*, 675–682.

Richeton, J., Ahzi, S., & Daridon, L. (2007). Thermodynamic investigation of yield-stress models for amorphous polymers. *Philosophical Magazine*, *87*, 3629–3643.

Richeton, J., Ahzi, S., Daridon, L., & Rémond, Y. (2003). Modeling of strain rates and temperature effects on the yield behavior of amorphous polymers. In *Journal de Physique IV (Proceedings)* (Vol. 110, pp. 39–44).

Richeton, J., Ahzi, S., Daridon, L., & Rémond, Y. (2005). A formulation of the cooperative model for the yield stress of amorphous polymers for a wide range of strain rates and temperatures. *Polymer*, *46*, 6035–6043.

Richeton, J., Ahzi, S., Vecchio, K., Jiang, F., & Adharapurapu, R. (2006). Influence of temperature and strain rate on the mechanical behavior of three amorphous polymers: Characterization and modeling of the compressive yield stress. *International Journal of Solids and Structures*, *43*, 2318–2335.

Rietsch, F., & Bouette, B. (1990). The compression yield behaviour of polycarbonate over a wide range of strain rates and temperatures. *European Polymer Journal*, *26*, 1071–1075.

Rinde, J. a., & Hoge, K. G. (1971). Time and temperature dependence of the mechanical properties of polystyrene bead foam. *Journal of Applied Polymer Science*, *15*, 1377–1395.

Rittel, D. (1999). On the conversion of plastic work to heat during high strain rate deformation of glassy polymers. *Mechanics of Materials*, *31*, 131–139.

Rittel, D. (2000). An investigation of the heat generated during cyclic loading of two glassy polymers. Part I: Experimental. *Mechanics of Materials*, *32*, 131–147.

Rivlin, R. S. (1948). Large Elastic Deformations of Isotropic Materials, IV, Further Developments of the General Theory. *Phil. Trans. Roy. Soc. Lond., Series A*, 379.

Roetling, J. (1965). Yield stress behaviour of poly (ethyl methacrylate) in the glass transition region. *Polymer*, *6*, 615–619.

Roland, C. M., Twigg, J. N., Vu, Y., & Mott, P. H. (2007). High strain rate mechanical behavior of polyurea. *Polymer*, *48*(2), 574–578.

Safari, K., Zamani, J., Ferreira, F., & Guedes, R. (2013). Constitutive modeling of polycarbonate during high strain rate deformation. *Polymer Engineering & Science*, *53*, 752–761.

Shergold, O. A., Fleck, N. A., & Radford, D. (2006). The uniaxial stress versus strain response of pig skin and silicone rubber at low and high strain rates. *International journal of impact engineering*, *32*, 1384–1402.

Shim, V. P. W., Yang, L. M., Lim, C. T., & Law, P. H. (2004). A visco-hyperelastic constitutive model to characterize both tensile and compressive behavior of rubber. *Journal of Applied Polymer Science*, *92*, 523–531.

Silva, F. D. A., Butler, M., Mechtcherine, V., Zhu, D., & Mobasher, B. (2011). Strain rate effect on the tensile behaviour of textile-reinforced concrete under static and dynamic loading. *Materials Science and Engineering: A*, *528*, 1727–1734.

Siviour, C. R. (2005). *High strain rate properties of materials using Hopkinson bar techniques*. University of Cambridge.

Siviour, C. R., Laity, P. R., Proud, W. G., Field, J. E., Porter, D., Church, P. D., … Huntingdon-Thresher, W. (2008). High strain rate properties of a polymer-bonded sugar: their dependence on applied and internal constraints. *Proceedings of the Royal Society A: Mathematical, Physical and Engineering Sciences*, *464*, 1229–1255.

Siviour, C. R., Walley, S. M., Proud, W., & Field, J. (2006a). Mechanical behaviour of polymers at high rates of strain. In *Journal de Physique IV (Proceedings)* (Vol. 134, pp. 949–955).

Siviour, C. R., Walley, S. M., Proud, W. G., & Field, J. E. (2005). The high strain rate compressive behaviour of polycarbonate and polyvinylidene difluoride. *Polymer*, *46*, 12546–12555.

Siviour, C. R., Walley, S. M., Proud, W. G., & Field, J. E. (2006b). Mechanical behaviour of polymers at high rates of strain. *J. Phys. IV France*, *134*, 949–955.

Soong, S., Cohen, R. E., Boyce, M. C., & Mulliken, a. D. (2006). Rate-Dependent Deformation Behavior of POSS-Filled and Plasticized Poly(vinyl chloride). *Macromolecules*, *39*, 2900–2908.

Swallowe, G., & Lee, S. (2003). A study of the mechanical properties of PMMA and PS at strain rates of 10 to 10 over the temperature range 293–363 K. In *Journal de Physique IV (Proceedings)* (Vol. 110, pp. 33–38).

Swallowe, G. M., & Field, J. E. (1982). The Ignition of a Thin Layer of Explosive by Impact; the Effect of Polymer Particles. *Proceedings of the Royal Society A: Mathematical, Physical and Engineering Sciences*, *379*, 389–408.

Taylor, G. (1946). The testing of materials at high rates of loading. *J. Inst. Civil Eng*, *26*, 486–519.

Taylor, G., & Davies, R. M. (1958). The mechanical properties of cordite during impact stressing. In G. Batchelor (Ed.), *The Scientific Papers of Sir Geoffrey Ingram Taylor* (Vol. 1: Mechani, pp. 480–495). Cambridge, UK: Cambridge Univ Press.

Theodorou, D.N., & Suter, U. W. (1986). Atomistic modeling of mechanical properties of polymeric glasses. *Macromolecules*, *19*, 139–154.

Theodorou, Doros N., & Suter, U. W. (1985). Detailed molecular structure of a vinyl polymer glass. *Macromolecules*, *18*, 1467–1478.

Thiruppukuzhi, S. V., & Sun, C. T. (1998). Testing and modeling high strain rate behavior of polymeric composites. *Composites Part B: Engineering*, *29*, 535–546.

Thompson, D., DeLuca, R., & Wright, W. J. (2012). Time-temperature superposition applied to PBX mechanical properties, *657*, 657–660.

Trautmann, A., Siviour, C. R., Walley, S. M., & Field, J. E. (2005). Lubrication of polycarbonate at cryogenic temperatures in the split Hopkinson pressure bar. *International Journal of Impact Engineering*, *31*, 523–544.

Treloar, L. (1946a). The elasticity of a network of long-chain molecules.-III. *Trans. Faraday Soc.*, *42*, 83–94.

Treloar, L. (1946b). The statistical length of long-chain molecules. *Trans. Faraday Soc.*, *42*, 77–82.

Treloar, L. R. G., & Riding, G. (1979). A Non-Gaussian Theory for Rubber in Biaxial Strain. I. Mechanical Properties. *Proceedings of the Royal Society of London. Series A, Mathematical and Physical Sciences*, *369*, 261–280.

Valanis, K. C., & Landel, R. F. (1967). The Strain Energy Function of a Hyperelastic Material in Terms of the Extension Ratios. *Journal of Applied Physics*, *38*, 2997.

Volterra, E. (1948). Alcuni resultati di prove dinamiche sui materiali (Some results on the dynamic testing of materials). *Rivista Nuovo Cimento*, *4*, 1–28.

Wade, W. (1856). Hardness of metals. In H. K. Craig (Ed.), *Reports on Experiments on the Strength and Other Properties of Metals for Cannon with a Description of the Machines for Testing Metals, and if the Classification of Cannon in Service* (pp. 259–275, 313–314). Philadelphia, USA: Henry Carey Baird.

Walley, S. M., & Field, J. E. (1994). Strain Rate Sensitivity of Polymers in Compression from Low to High Rates. *Dymat Journal*, *1*, 211–227.

Walley, S. M., Field, J. E., & Palmer, S. J. P. (1992). Impact sensitivity of propellants. *Proceedings of the Royal Society*, *438*, 571–583.

Walley, S. M., Field, J. E., Pope, P., & Safford, N. A. (1989). A Study of the Rapid Deformation Behaviour of a Range of Polymers. *Philosophical Transactions of the Royal Society of London. Series A, Mathematical and Physical Sciences*, *328*, 1–33.

Walley, S. M., Field, J. E., Pope, P., & Safford, N. A. (1991). The rapid deformation behaviour of various polymers. *J. Phys. III France*, *1*, 1889–1925.

Walley, S. M., Proud, W. G., Rae, P. J., & Field, J. E. (2000). Comparison of two methods of measuring the rapid temperature rises in split Hopkinson bar specimens. *Review of Scientific Instruments*, *71*, 1766.

Wang, Y., & Arruda, E. M. (2001). Characterization and constitutive modeling of a plasticized poly (vinyl chloride) for a broad range of strain rates. *Rubber chemistry and technology*, *74*, 560–574.

Williams, M. L., Landel, R. F., & Ferry, J. D. (1955). The Temperature Dependence of Relaxation Mechanisms in Amorphous Polymers and Other Glass-forming Liquids. *Journal of the American Chemical Society*, *77*, 3701–3707.

Williamson, D., Palmer, S. J. P., Proud, W. G., & Govier, R. (2009). Brazilian Disc Testing of a UK PBX Approaching the Glass Transition Condition. *AIP Conference Shock Compression of Condensed Matter*, 981–984.

Wu, J. J., Buckley, C. P., & O'Connor, J. J. (2002). Mechanical integrity of compression-moulded ultra-high molecular weight polyethylene: effects of varying process conditions. *Biomaterials*, *23*, 3773–83.

Zerilli, F. J., & Armstrong, R. W. (2007). A constitutive equation for the dynamic deformation behavior of polymers. *Journal of Materials Science*, *42*, 4562–4574.

Zhao, H., Gary, G., & Klepaczko, J. (1997). On the use of a viscoelastic split hopkinson pressure bar. *International Journal of Impact Engineering*, *19*, 319–330.

Zhao, & Lampmann. (2000). Tension, Compression, Bend, and Shear Testing. In Kuhn & Medlin (Eds.), *ASM Handbook - Mechanical Testing and Evaluation*. Materials Park, OH.

Zhou, Z., Chen, P., Duan, Z., & Huang, F. (2012). Study on Fracture Behaviour of a Polymer-Bonded Explosive Simulant Subjected to Uniaxial Compression Using Digital Image Correlation Method. *Strain*, *48*, 326–332.